2-16-2022 11:30 AM

Behavior of Hybrid and Monopile Foundation Systems for OWT: Centrifuge testing and Numerical Modelling

Yazeed A. Alsharedah, *The University of Western Ontario*

Supervisor: M. Hesham El Naggar, *The University of Western Ontario*
Co-Supervisor: Timothy Newson, *The University of Western Ontario*
Co-Supervisor: Jonathan A. Black, *University of Sheffield*
A thesis submitted in partial fulfillment of the requirements for the Doctor of Philosophy degree in Civil and Environmental Engineering

Abstract:

Offshore foundation systems are constantly evolving to meet the needs of new developments in energy sector. Moving into ever deeper water for hydrocarbon recovery or creating foundation systems for renewable energy sources, such as offshore wind turbine (OWT) farms, creates specific challenges. Large fixed vertical tower structures are typically used to support OWT inducing complex loading on foundations as a result of combined wind, wave and self-weight loading effects, all of which must be accommodated within very small rotation envelopes and natural frequency band to allow the turbines to operate effectively. In this thesis, a hybrid foundation (H.F) comprising a plate with a diameter (W) fitted with a pile with a length (L_p) at the center is proposed as an alternative to monopiles (MP) with aim of reducing needed pile diameter and penetration. This type of foundation system can benefit OWTs since the turbine are subjected to high overturning moments. Since there is no guidance available regarding the performance of this system to support OWTs, the objective of this research is to evaluate the behavior of this system and the typically used monopile in various clay profiles and examine the effects of various parameters on their performance.

The research methodology includes three aspects: (i) developing a calibrated and verified 3D finite element model (FEM) (ii) conducting a detailed FE modelling on the behavior of a 5MW wind turbine supported by hybrid foundation and monopiles considering various pile/monopile length to plate width/diameter to characterise their lateral ultimate capacity, compare their structural response under serviceability loading, establish their stiffness properties and study their dynamic response (iii) performing a series of geotechnical centrifuge tests on scaled models representing a

monopile and a hybrid foundation to investigate the benefits of the proposed system and compare it to monopiles.

Results of this research indicated adding a plate to monopile improves the relative lateral ultimate capacity, whilst enabling a reduction of monopile penetration depth and diameter. Specifically, when the hybrid foundation was used in stiff clay sites, similar lateral capacity was reached for the hybrid foundations as that of a 30m depth monopile well as comparable stiffness response. Reduction of bending moment and tower tip displacement of 30-45%, 4-7% were recorded. Soil compliance reduced the 1st natural frequency compared to the equivalent fixed base by 52-10% and 40-0% for the monopile and the hybrid foundation, respectively. Formulae considering foundation geometry and soil profiles are proposed to (i) estimate the lateral ultimate capacity of both systems under loading eccentricity representative of medium depth water (ii) evaluate the three spring stiffness values (iii) estimate the 1st natural frequency. Centrifuge testing results indicated the performance of the proposed hybrid foundation system was similar to that of monopile in stiff clay profiles indicating potential use.

Keywords;

Offshore wind turbines, gravity base, monopile, centrifuge, green energy, renewable energy.

Summary for lay audience

Offshore foundation systems are constantly evolving to meet the needs of new developments in energy sector. Moving into ever deeper water for hydrocarbon recovery or creating foundation systems for renewable energy sources, such as offshore wind Turbines (OWT) farms, creates specific challenges. Large fixed vertical tower structures are typically used to support OWT inducing complex loading on foundations as a result of combined wind, wave and self-weight loading effects, all of which must be accommodated within very small rotation envelopes and natural frequency band to allow the turbines to operate effectively. In this thesis, a hybrid foundation (H.F) comprising a plate with a diameter (W) fitted with a pile with a length (L_p) at the center is proposed as an alternative to monopiles (MP) with aim of reducing needed pile diameter and penetration. This type of foundation system can benefit OWT since the turbine are subjected to high overturning moments. Since there is no guidance available regarding the performance of this system to support OWTs, the objective of this research is to evaluate the behavior of this system and the typically used monopile in various clay profiles and examine the effects of various parameters on their performance.

Acknowlegement

First and foremost, I begin by thanking Allah for all what He has bestowed on me. I would like to thank my mother, Norah, my father, Abdullah, my wife Mashael and my family in Saudi Arabia for their endless love, support and motivation. I would like to also thank my children, Abdullah and Rania for bringing joy to my life. I would like to express my gratitude to Dr. M. Hesham El Naggar and Dr. Timothy Newson for their constructive comments and moral support throughout the past 5 years. Indeed, their insights, help, communications, and positive outlook were of significance to completing my thesis. Special thanks to Dr. Jonathan Black from University of Sheffield for hosting me to conduct my centrifuge tests and for his team at the machine shop, his warm welcome and support was enormous and had significant positive impact on my studies. I also thank Dr. Aly Ahmed for his support, motivation, and guidance.

My thanks are extended to Qassim University in Saudi Arabia and Saudi Cultural Bureau for funding my Ph.D study. Special thanks to Dr. Ahmed Alnuaim and Dr. Ahmed Taha who helped me during my research and gave lot of valuable comments. I wish to thank my colleagues at the GRC for their friendship and discussions. Last but not least, thanks to the University of Western Ontario for being such a wonderful place for study and research.

Co-Authorship statement

This thesis work has been done by the candidate himself except where mentioned. The thesis methodology and scope of work is developed by the candidate with help from Dr. M.H El Naggar and Dr. Timothy Newson. Planning for parameter FE analyses and data interpretations and presentation is solely done by the candidate. The scaling of laboratory tests models was done by the candidate himself under supervision of Prof. Timothy Newson and Dr. Jonathan Black. All data calibration and test planning were done by candidate with under supervision of Dr. Jonathan Black and Dr. Timothy Newson. Dr. Jonathan carried out much of the rest of lab work because of Covid-19 impact on labs. The candidate is indebted to and thankful for his supervisors for their kindness, courtesy, positive impact, thoughtful constructive discussions which had significant positive impact on the candidate progress and academic achievements.

Glossary

C_u: Undrained shear strength of the soil

c': Cohesion intercept of shear strength

D& r_o: Pile's diameter and radius

E_s: Young's modulus of the soil

E_{50}^{ref}: Devatoric stiffness of soil at 50% of ultimate at reference pressure

E_{oed}^{ref}: Oedmeter stiffness of the soil at reference pressure

E_p: Young's modulus of the pile's cross section

E_c: Young's modulus of the concrete

F_n: First natural frequency of the system

$F_{F.B.}$: Fixed base natural frequency

H_u: Maximum horizontal load capacity

H: Tower height (m)

k_0: coefficient of at rest earth pressure

K_L: Lateral spring stiffness

K_{LR}/K_{RL}: Coupling spring stiffness

K_R: Rotational spring stiffness

K_t: Lateral stiffness of the turbine tower

L_p: Pile's length

M_u: Maximum moment load capacity

m: An exponent describing variation of soil stiffness with overburden

M: Mass of the tower

M_{eff}: Equivalent mass giving same base shear and moment to distributed mass at tower tip

P: soil resistance

P^{ref}: Reference pressure

$P_{res.}$: large strain soil resistance after a number of cycles of loading

P_u: large strain soil resistance for first cycle of loading

Q_c: cone tip resistance

N_c: cone tip bearing capacity factor

V_u: Maximum vertical load capacity

W_L: liquid limit

W_P: plastic limit

y: pile lateral deflection

W: Width of the shallow foundation/wheel/plate

1P: rotational speed

3P: Blade passing frequency

G.S: Ground surface

M.L: Mud line

m_{RNA}: Mass of rotor and nacelle assembly

M.S.L: Mean sea level

ULS: Ultimate limit state

SLS: Serviceability limit states

Φ': Soil friction angle

γ_s: Soil unit weight

γ_c: Concrete unit weight

σ_1': Major effective stress at certain depth below G.S

σ_3': Minor effective stress at certain depth below G.S

σ: Total stress

θ_1: rotation at mudline for first cycle

θ_N: rotation at mudline after N cycles

Contents

Table of Figures

Table of Tables

Chapter 1: Introduction and Research Objectives

1.1 Introduction

Fossil fuel powered electricity plants produce CO_2 emissions in the atmosphere and are being replaced by green energy sources. The Paris Accord in 2015 emphasized the need to reduce these emissions by 2050 in order to avoid the catastrophic results of CO_2 on our climate. At the same time, Cambridge Energy Research Associates (CERA) estimate the world oil reserves at 3.74 trillion barrels and Lamb (2010) predicts that our globe will run out of fossil oil within the coming 100 years. Therefore, renewable resources of energy are critically needed. Efficient alternatives include biomass fueled powerplants, hydropower, wind powered turbines and solar panels. Of these, wind turbines produce the most suitable option for electricity with no by-products such as ashes from coal and biomass combustion that require further recycling or disposal. Wind farms as green energy technology are being expanded to harvest clean and sustainable electricity for future needs. Hence, onshore and offshore wind turbines farms have been introduced to service since the late 20^{th} century.

Offshore wind farms numbers have been on the rise. For instance, Westwood (2004) reported that the capacity of offshore wind turbines initiated in 2003 was more than the capacity of all previous years combined (Wind Europe, 2016; Westwood, 2004). Figure 1-1 shows the growth of annual installed capacity of Europe offshore wind farms for the period 2000-2016. Figure 1-1 clearly shows the exponential growth of offshore energy output.

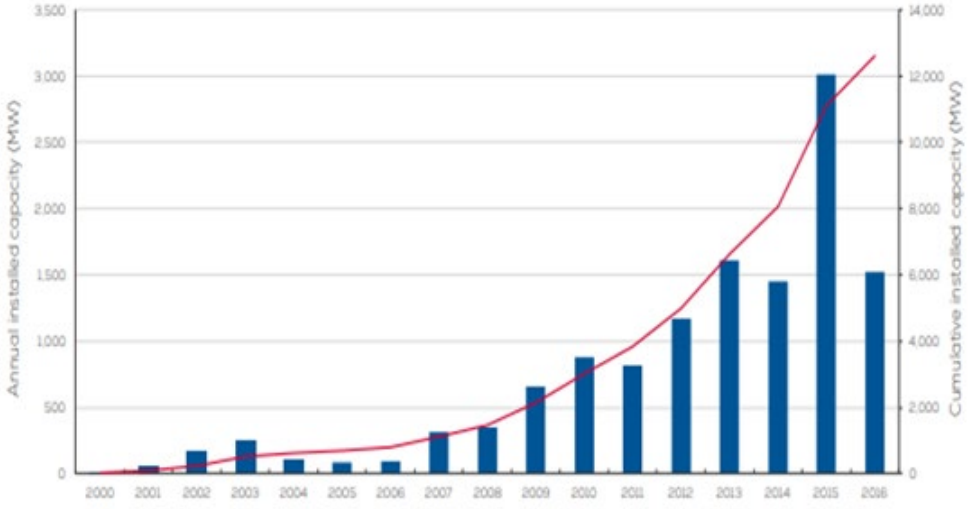

Figure 1-1 Capacity of wind farms installed in Europe (Wind Europe, 2016)

Table 1-1 shows the installed wind farms in different parts of the world between 2004 and 2008 and their associated cost. The average initial cost per MW is $1.6M. A 5 MW wind turbine, which has been used as a standard unit for comparison in design codes in OC3 task by NREL (NREL 5MW) costs between $2.7-7.1 M U.S dollars. It is reported that the cost of foundation systems for these wind turbines can constitute around 25-40 % of the total cost (Wang et al., 2018). Typical cost of foundation is therefore expected to be between $ 1-2.8 M depending on the manufacturer (unit cost), water depth (and therefore wave and wind loads) and soil conditions.

Table 1-1 World market summary 2004-2008 (Westwood, 2004).

Country	Projects	MW	Turbines	Capex$	$Millions/unit[1]
Belgium	2	316	110	777	7.064
Canada	1	700	350	960	2.743
Denmark	5	1625	630	2280	3.619
Finland	2	257	89	424	4.764
France	3	160	57	229	4.018
Germany	30	6437	1679	11796	7.026
Ireland	10	1374	375	1849	4.931
Netherlands	2	219	96	462	4.813
Spain	4	263	107	396	3.701
Sweden	14	1979	598	3014	5.040
UK	21	3112	923	4648	5.036
USA	14	891	278	1438	5.173
Total	108	17333	5292	28273	4.827

[1]**Cost is dependent** on the wind turbine cost, foundation cost
*Foundation cost is dependent on water level and therefore applied forces and soil stratigraphy

The size of large capacity wind turbines requires massive areas for their installation, which limits their use in densely populated areas. On the other hand, offshore wind farms offer vast area availability and better environmental factors (stronger and uninterrupted wind speed). Nonetheless, offshore wind turbines are challenged by soil conditions and water depth, which

imposes very high moment and lateral loads compared to vertical loads. Being installed further from shorelines to utilize better wind conditions, up to 30-45 km, at such distance the average depth of water ranges between 10-50 meters. Figure 1-2 provide a schematic representation of the exerted loads on an OWT including environmental loads that act on an offshore wind turbine. These complex loading conditions represent a challenge for design and require massive and costly foundation systems.

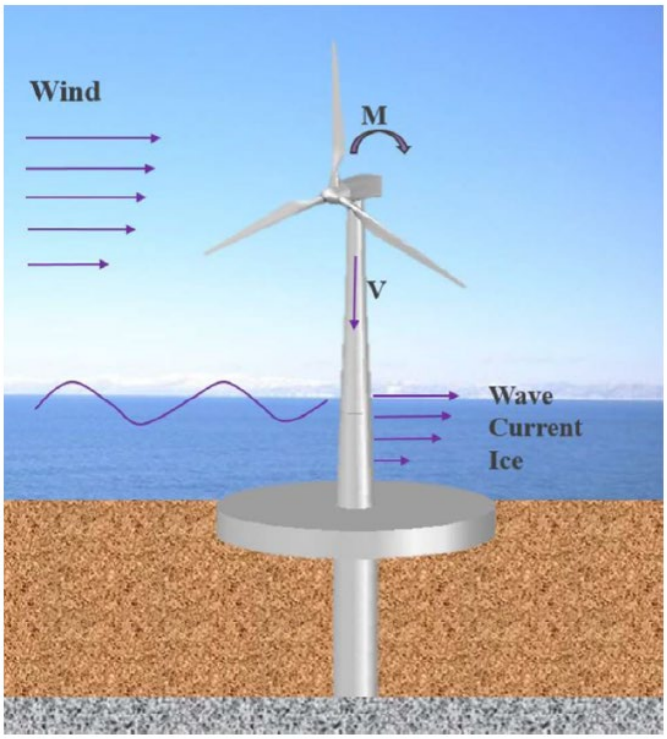

Figure 1-2 Loadings imposed on a wind turbine (Wang et al., 2018)

Design practice and experience in offshore wind turbine foundations emanate from offshore oil platforms. However, the ratio of lateral load to vertical load varies significantly between the two, which would impact the design with more focus on the lateral resistance and performance for wind turbines. Figure 1-3 compares the loading magnitudes for a wind turbine and an offshore platform. It can be clearly seen that the ratio of horizontal loads to vertical loads in wind turbines is way

higher than those of oil platforms. Additionally, offshore oil rigs are typically supported by more than one foundation system which provides redundancy to moments resulting from wind/wave horizonal forces and therefore reducing rotation of members and the associated variable stress distribution underneath/besides foundation members and leading to a reduction of cost of the foundation system.

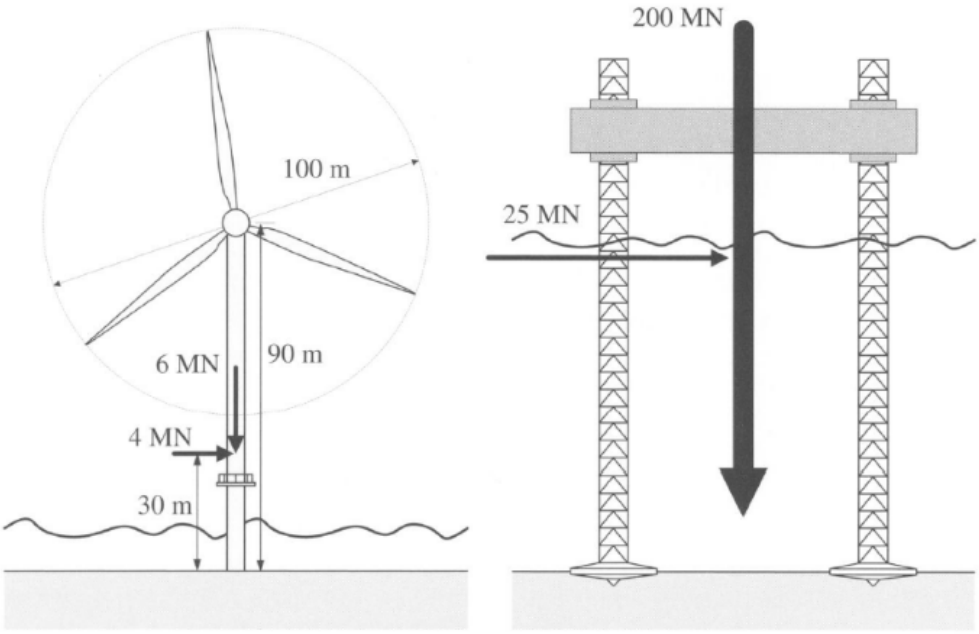

Figure 1-3 Offshore wind turbine and a jack-up rig drawn to same scale showing typical loads (Byrne and Houlsby, 2003)

Different foundation systems are employed to support wind turbines. For onshore wind turbines, they can be fixed on a steel jacket and supported by monopiles, a raft foundation, or a gravity base. For offshore wind turbines, the foundation systems used include gravity base foundations (GBF), monopiles (MP), tripod structures, and jacket and buoyant fixed structures (El-Marrassi, 2011). Typically, MP foundations are utilized as the main foundation system. The monopiles used can be drilled shaft concrete, driven concrete piles and open-ended steel pipe. The

diameter of such monopiles ranges between 3-7.5 m (Wang et al., 2018). Figure 1-4 shows the available foundation systems for OWT.

Being installed in ever deeper water and bounded by strict tolerable displacement and rotation envelopes, contemporary research indicates monopile size will continue to increase up to 10 m in diameter. As the monopile is typically extended above the mudline and connected with the transition piece, the load from waves will increase, demanding larger monopiles further away from shorelines, where newer developments are expected. This can lead to substantial increase in foundation cost and can hinder development of new farms. As such, innovative foundation systems and improved designs are needed.

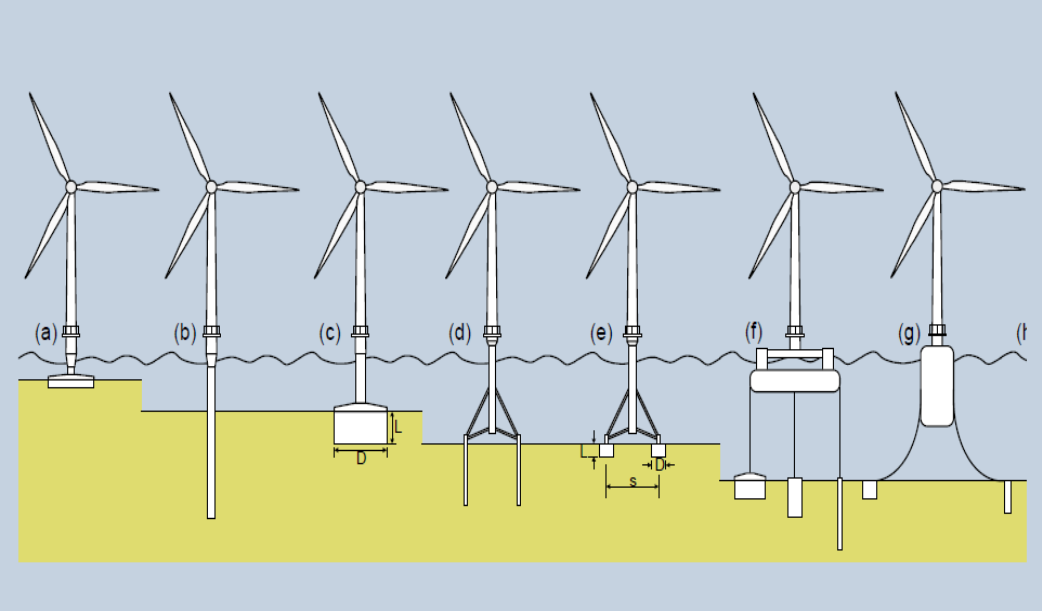

Figure 1-4 Available foundation options for offshore wind turbines (a) GBF (b) monopile (c) suction caisson (d) tripod/tetrapod piles (e) tripod/tetrapod suction caissons (f) multiple foundation options (h) guys with anchors (Byrne, 2003)

In this thesis, hybrid foundation system is proposed to support new generation of offshore wind turbines (OWTs) installed in clayey sediments. The system is comprised of a plate of a diameter

(W) fitted with a monopile with a diameter and length (D_p, and L_p). Calibrated and validated FE models are used to study the system performance when used to support a typical 5MW turbine in different clayey beds and conduct a parameter study to define system lateral ultimate capacity, estimate the three spring stiffness parameters, compare the system performance to monopiles and propose closed form equations describing its first natural frequency variation in different soil beds. This is followed by a centrifuge testing suite to compare the proposed hybrid foundation system against the typically used monopile in an over-consolidated clay bed under monotonic lateral loads. Models are fabricated representing a monopile and a hybrid foundation and tested at the centrifuge facility of the University of Sheffield. The results of this investigation are then summarized in the following chapters of this research.

1.2 Hybrid Foundation system for wind turbine

The proposed hybrid system is composed of a monopile with a plate at the mudline. This system was first proposed by Carder et al. (1993) and later investigated by many (Wang et al., 2018; Wang et al., 2017; Abdelkader, 2016; Cherchia, 2014; Lehane et al., 2014; Elmarassi, 2011; Stone et al., 2007). However, no one to the author's knowledge has attempted to investigate its behavior in clayey beds. Therefore, the objective of this study is to close this gap in the literature by providing a comprehensive study of various effects pertaining to its utilization in soft (Gulf of Mexico) and stiff (North Sea) clayey beds (Byrne et al., 2015a). Figure 1-5 shows the proposed foundation system.

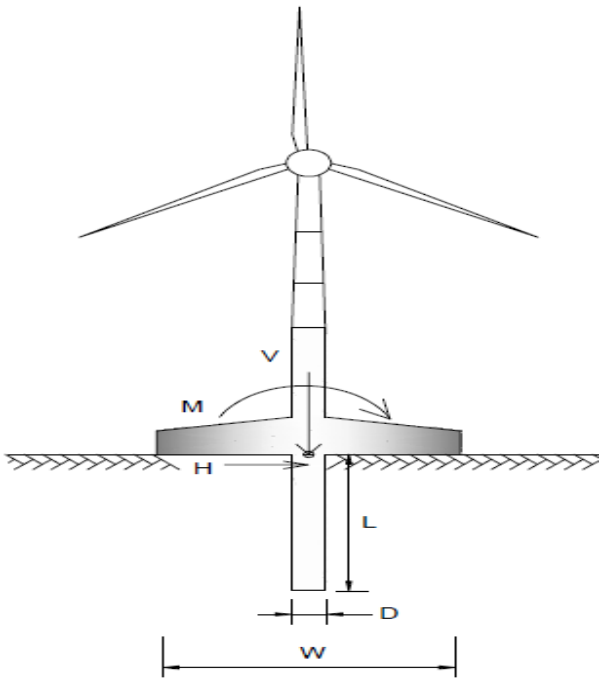

Figure 1-5 Proposed foundation system (El Marassi, 2011)

The proof-of-concept study will include studying the effects of monotonic and cyclic properties of the proposed system in clayey soil medium to establish the static and dynamic response characteristics of the system. To achieve this objective, an in-depth literature review was done to summarize areas of importance, establish geometry of model tests and define gaps for improvement. This was followed by a detailed FE program to study the system lateral ultimate capacity under eccentric loading similar to that expected in medium depth water, compare its performance with monopiles under service loading, establish the three spring stiffness parameters and investigate the system dynamic characteristics. This was followed by centrifuge testing. Two models were constructed, a monopile (MP) and a hybrid foundation (H.F) with L_p/W, where L_p is length of pile and W is the diameter of plate, of 2. These models were fabricated from acrylic material at the Machine shop of UWO according to centrifuge scaling laws. Four tests in total were conducted. These tests were done in an OC clayey bed prepared using inflight consolidation. Both models were tested under monotonic lateral loading. The lateral loads were applied at eccentricity,

e, to diameter ratio (e/d) of 3.63-4.1 for MP/H.F, respectively, in centrifuge tests and at 6.83 at all FEM. This will ensure that the effects of load eccentricity are considered (Wang 2017).

Generally, for a 5MW OWT installed in medium depth water (20-40m depth) the moment arm is between 6-13 m for wave loading which account for about 60% of the capacity of the lateral loads. Wind loads, on the other hand, are typically applied at the hub height of the wind turbine. This is typically around 40-90 meters above mean sea level (M.S.L.) These values translate into around 41 m eccentricity of the horizontal load for the considered 5MW wind turbine. With a typical 6 m diameter monopile, the max anticipated loading eccentricity is 6.83. Table 1-2 presents the proposed centrifuge study plan. Models' vertical capacities were established based on FE models prior to centrifuge tests. The applied vertical loads on the foundations were about 20% of the ultimate capacity (V_u).

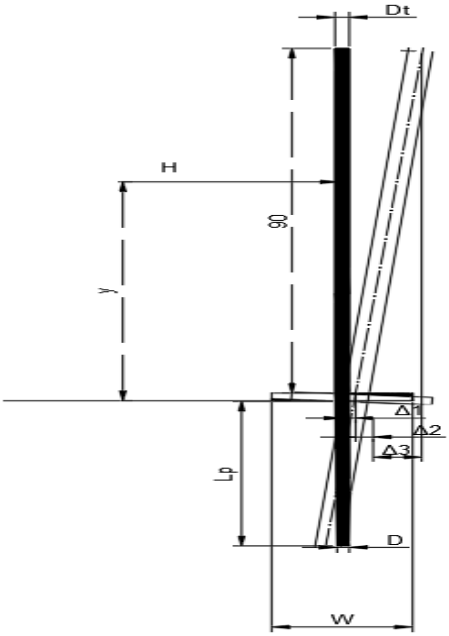

Figure 1-6 Deflected shape of wind turbine tower components.

1.3 Scope of research

The goal of this study is to:

A. Establish a FEM calibrated and validated using a case study to:

1. Analyze the effect of L_p/W on the horizontal load capacity (H_u)
2. Characterise and quantify the effects of L_p/W ratio on the lateral load behavior under monotonic loads in the studied clay medium
3. Propose a set of equations describing the lateral ultimate capacity of the monopiles and the hybrid foundations in medium depth water for preliminary analyses
4. Define three spring stiffness parameters describing foundation compliance
5. Propose correlations describing the first natural frequency of the MP and HF from basic soil and foundation parameters

B. Conduct centrifuge testing of scaled models of MP and HF to

1- Compare the lateral ultimate capacity of the MP and the proposed hybrid foundation (HF) in an OC clay bed

2- Compare the stiffness properties of the MP and the proposed hybrid foundation (HF) in an OC clay bed

3- Compare the two systems behavior when laterally loaded

4- Provide geotechnical community with a high-quality data that can be used for further research

5- Use results to conduct further parameter analyses

1.4 Methodology

To achieve the set-up goals, a case study involving a driven open ended 2.2m diameter monopile was installed offshore China and was subjected to lateral monotonic and cyclic loading was used to calibrate and validate the FE model parameters. A series of 3D finite element models (FEMs) were carried out to conduct a parametric study of the effects of L_p/W(L/D) ratio on the foundation response in several clayey soil profiles to quantify the response of the proposed foundation system. Since few studies exist on the hybrid foundations, it was found that there is a lack of tools to characterise their lateral ultimate capacity. Hence, chapter 3 is dedicated to address this issue to study the mechanism of the lateral load improvement provided by the hybrid foundation. A three-spring stiffness is typically used to characterize the foundation response especially when modelling the eigen frequency of superstructure while incorporating the soil compliance. Hence, three spring stiffness values were established for the proposed system in chapter 4. Because OWTs are dynamically sensitive structures, chapter 5 investigates the effects

of the system geometry and the soil profile on the natural frequency response and links these effects to the three spring stiffness values through fitting equations. Finally, model testing is a reliable tool to judge the system performance. Since the clay response is effective stress dependent, the model tests were carried out in a centrifuge environment. A series of laboratory testing was carried out by testing the clay to be used in the centrifuge by conducting lab tests to characterise the physical and strength/stiffness properties. The models were instrumented with half bridge strain gauges to help interpret their behavior when laterally loaded. Laser sensors were used to detect the lateral response and a load sensor was used to measure the applied lateral load. The clay slurry was poured in a strong box which was then loaded to the centrifuge frame and inflight consolidated at 70g with a sand surcharge. The centrifuge was spun down after reaching 100% primary consolidation and the models were inserted at 1g one at a time for testing. Table 1-2 displays the tests that were carried out.

1.5 Thesis Organization

Chapter 1 Discusses the general nature of the problem and the gap existing in research and addresses the scope of research and the methodology

Chapter 2 Presents a literature review summary of previous work and relevant information required to conduct the current research. The different foundation types for OWTs are presented and the progress made to date is discussed, and relevant research studies undertaken are summarized. Soil behavior and constitutive modelling is presented and discussed.

Chapter 3 Presents FEM validation work and parametric studies conducted to define ULS of the MP and H.F systems in various clayey mediums. Predictive equations are proposed for preliminary analysis based on the FE results. A serviceability limit state (SLS) comparison was

done towards the end of the chapter to compare the response of the hybrid foundation to a 30 m length monopile. Findings and discussion are presented towards the end of the chapter.

Chapter 4 Present three spring stiffness parameters of the proposed system in different clay mediums. Based on the FE results, formulae for computing the three spring stiffness parameters based on foundation geometry and soil profile are presented and discussed.

Chapter 5 Discusses dynamics characteristics of a 5MW OWT founded on the considered foundation systems. Best fit equations are produced to provide easy to use expression for 1st natural frequency estimation by practicing engineers.

Chapter 6 Introduces centrifuge modelling and centrifuge laws and discusses the testing programme and the research facility. Model construction and instrumentation are summarized, and soil properties are discussed.

Chapter 7 Presents centrifuge tests results and comparison between MP and Hybrid foundation

Chapter 8 Summarizes the research programme undertaken and gives recommendation for future researchs

1.6 Thesis Original Contributions

This thesis explores a hybrid foundation system for offshore wind turbines in clayey soils. The system has been studied in sand and no one attempted studying its behaviour in clayey soil. The contributions of this research are listed below:

1- The foundation system lateral ultimate capacity is investigated under eccentric loading considering medium depth water in several clayey profiles from soft (s_{uo}=4 kPa) to hard

clay (S_{uo}=354kPa). The effects of plate and pile diameters on the lateral ultimate capacity of the hybrid foundation plate have been evaluated.

2- The effect of L_p/W ratio on the hybrid foundation lateral ultimate capacity was evaluated for different soil profiles.

3- Equations are proposed to predict the lateral ultimate capacity of the hybrid foundation and monopiles in medium depth water (e/Dt = 6.83).

4- The performance of the hybrid system was compared to a monopile of 30 m penetration and 6 m diameter under lateral service loading.

5- A three-spring model at soil mudline is proposed to simulate the stiffness properties of the hybrid foundation. Normalized stiffness values are proposed, and best fit equations are derived, which can be used to calculate the tower displacement and rotation for preliminary studies

6- Dynamics characteristics of the hybrid foundation and the monopile are investigated, predictive equations are derived for estimating the 1st natural frequency

7- A centrifuge study was conducted to compare the performance of hybrid foundation and monopiles in over consolidated clay.

Chapter 2: Literature Review

2.1 Introduction

Sustainable energy sources such as wind, hydro and solar are essential to meet the world energy demands, but they are still under utilized. Global warming and increasing CO_2 emissions in the atmosphere and the associated increased frequency and severity of natural disasters have accelerated efforts to cultivate more energy from these renewable energy sources in a bid to reduce the dependency on fossil fuels. Specifically, exponential growth of wind energy has been achieved from onshore and offshore wind farms with offshore wind turbines (OWT) reaching a capacity of 14MW already available in the market. This increase in the capacity is realized by using heavier and taller turbines, often leading to very large foundation systems, which can represent up to 40% of the OWT total cost.

Humans have used some form of wind energy for thousands of years, mainly for transportation. Typically, a wind turbine is comprised of a two or three blades system connected to a generator fixed on a mast. The wind turbine size has grown tremendously to harvest more energy by converting the mechanical movements of the generator into electricity. This increase in size has resulted in an increase in required area for their installation, aesthetic problems, and an increase in weight and exposure to lateral loads from wind requiring large and heavy foundation systems. In addition, wind turbines are installed in various ground conditions that can pose significant challenges for their foundation design. The first two issues were the driving factors for moving to offshore installations, therefore exacerbating issues pertaining to increased weight and lateral loading.

Although installed in a harsh environment, number of offshore wind farms has been on the rise taking advantage of better wind conditions and avoiding logistic problems related to installations

in urbanized locations. For instance, Westwood (2004) reported that capacity of offshore wind turbines initiated in 2003 was more than the capacity of all previous years combined (Wind Europe, 2016, Westwood, 2004). According to Wang et al. (2018), the electricity output of offshore wind turbines was expected to be almost 3 times the onshore wind turbines by the end of 2018. Figure 2-1 presents the growth of annual installed capacity of European offshore wind farms for the period 2000-2016, which demonstrates the exponential growth of offshore energy output.

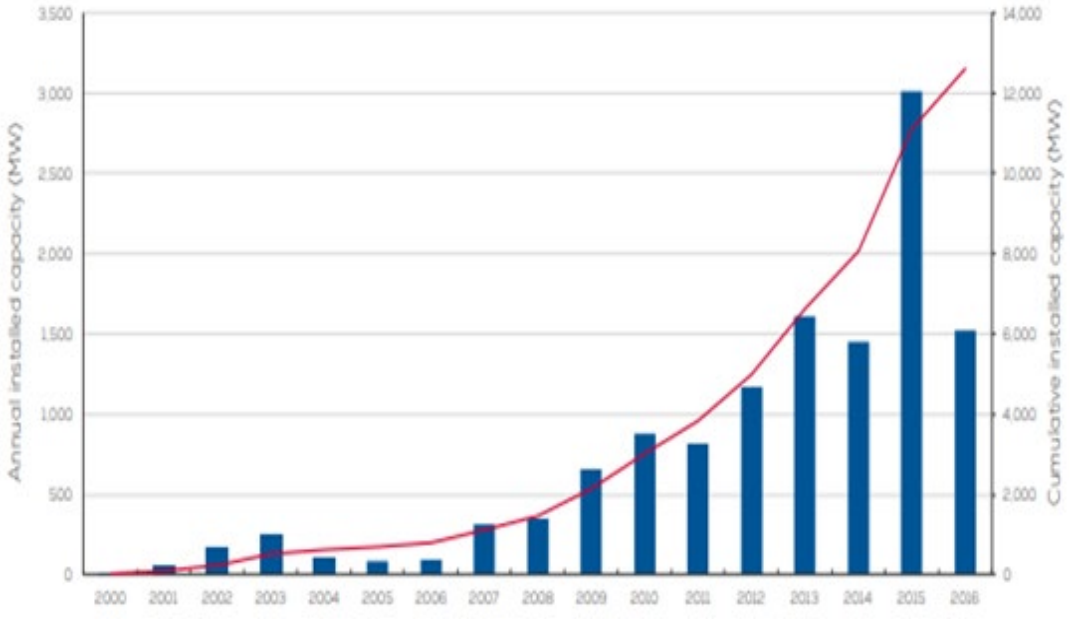

Figure 2-1 Capacity of wind farms installed in Europe (Wind Europe, 2016)

Table 2-1 shows the installed wind farms in different parts of the world between 2004-2008 and their associated cost. The average initial cost per MW is $1.6M. A 5 MW wind turbine, which has been used as a standard unit for comparison in design codes in OC3 task by NREL (NREL 5MW) costs between $M 2.7-7.1 U.S dollars. Byrne and Houlsby (2003) provided similar estimates of OWT costs. The cost of foundation system can constitute around 25-40 % of the total cost (Wang et al., 2018), i.e., typical cost of foundation is expected to be $1-2.8M depending on

the manufacturer (unit cost), water depth (and therefore wave and wind loads), installation cost and soil conditions.

Table 2-1 World market summary 2004-2008 (Westwood, 2004).

Country	Projects	MW	Turbines	Capex$	$Millions/unit[1]
Belgium	2	316	110	777	7.064
Canada	1	700	350	960	2.743
Denmark	5	1625	630	2280	3.619
Finland	2	257	89	424	4.764
France	3	160	57	229	4.018
Germany	30	6437	1679	11796	7.026
Ireland	10	1374	375	1849	4.931
Netherlands	2	219	96	462	4.813
Spain	4	263	107	396	3.701
Sweden	14	1979	598	3014	5.040
UK	21	3112	923	4648	5.036
USA	14	891	278	1438	5.173
Total	108	17333	5292	28273	4.827

[1]**Cost is dependent** on the wind turbine cost, foundation cost
*Foundation cost is dependent on water level and therefore applied forces and soil stratigraphy

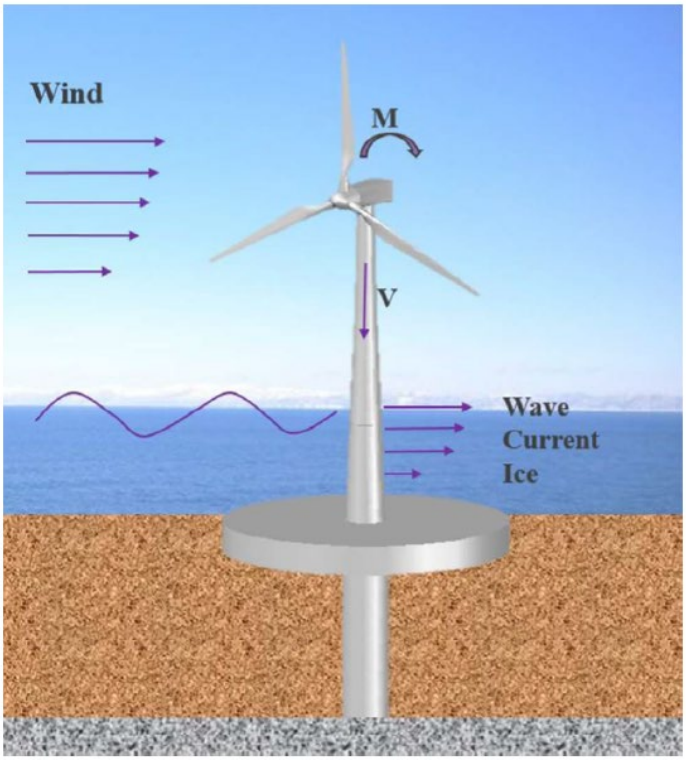

Figure 2-2 Loadings imposed on a wind turbine (Wang et al., 2018)

The depth of water at offshore wind turbine farms ranges between 10 and 50 meters. Such water depths can be challenging for the design of OWT's foundations due to high lateral loads and associated moments from waves and wind. Additionally, these loads are cyclic in nature imposing other problems on the foundations such as fatigue and excessive deformation and rotations. Besides, the OWTs are dynamically sensitive structures due to their slenderness, which requires due consideration when choosing their foundation option to avoid resonance. Resonance happens when the forcing frequency is similar to the structure natural frequency thereby increasing the dynamic magnification factor (DMF). Figures 2-2 and 2-4 provide a schematic representation and the range of the gravitational and typical values of environmental loads that act on a 3-5 MW capacity offshore wind turbine.

These complex loading conditions represent a challenge for design and require large and costly foundation system, which motivated researchers and industry to investigate different foundation options of offshore wind turbines. Design codes provisions and methodology used for the design of offshore wind turbine foundations originated from offshore oil platforms design experience. However, the ratio of lateral load to vertical load varies significantly between the two systems, which should impact the design with more focus on the lateral resistance and performance for wind turbines. Figure 2-4 compares the loading magnitudes for a wind turbine and an offshore platform. It can be clearly seen that the ratio of horizontal loads to vertical loads in wind turbines is way higher than those of onshore wind turbines. Additionally, offshore oil rigs are typically supported by more than one foundation systems which provides redundancy to moments resulting from wind/wave horizonal forces unlike OWT which typically relies on one foundation element.

Different foundation systems are employed to support wind turbines such as fixed Gravity Base Foundations (GBF), tripod structures, jackets, suction caissons, monopiles (MP), buoyant fixed structures, rafts on monopiles and pile groups, Figure 2-3 (Abdelkader, 2016; El-Marassi, 2011; Byrne and Houlsby, 2003). In most cases, monopile foundations are utilized as the main foundation system. Monopiles used can be drilled concrete shaft and open-ended steel pipe. The diameter of such monopiles ranges from 3 to 7.5 m (Wang et al., 2018).

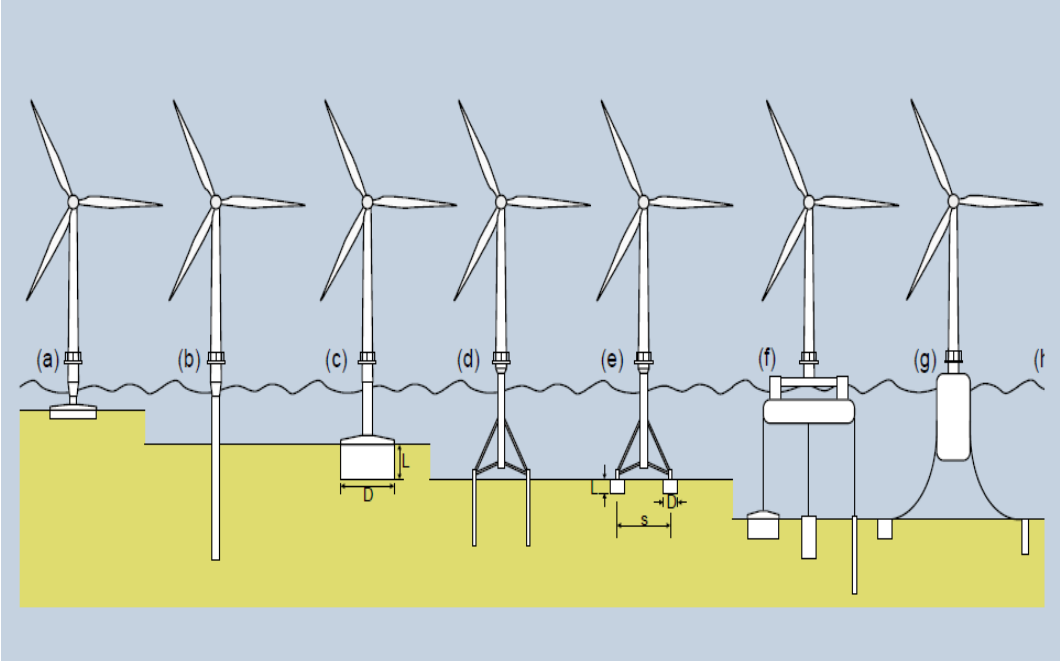

Figure 2-3 Available foundation options for offshore wind turbines (a) GBF (b) monopile (c) suction caisson (d) tripod/tetrapod piles (e) tripod/tetrapod suction caissons (f) multiple foundation options (h) guys with anchors (Byrne, 2003)

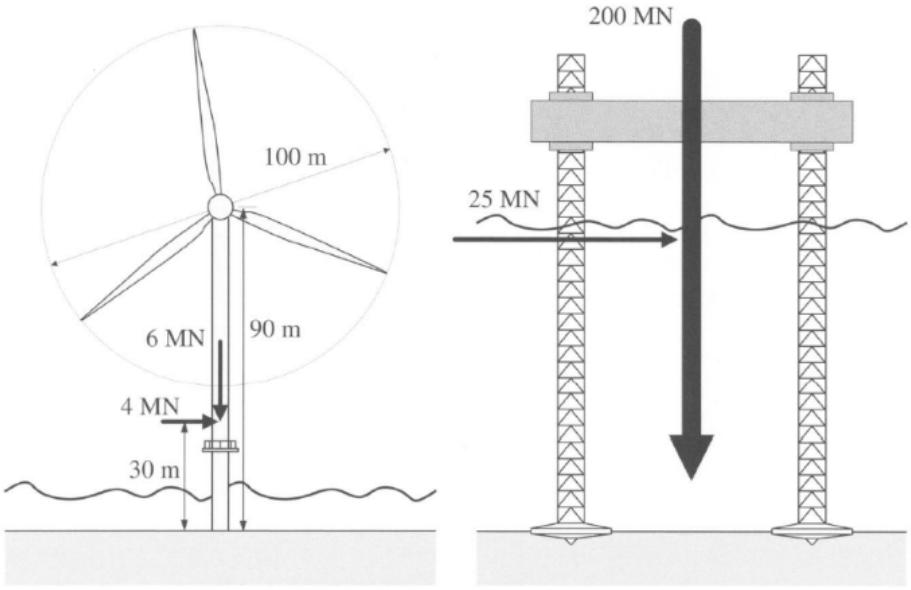

Figure 2-4 Offshore wind turbine and a jack-up rig drawn to same scale showing typical loads (Bryne and Houlsby, 2003)

2.2 Types of wind turbine foundations

Different foundation systems are employed to support wind turbines. For onshore wind turbines, they can be supported by monopiles, a raft resting directly on the soil or on a pile group. For offshore wind turbines, foundation systems used include gravity base foundations (GBF), tripod structures, jackets, suction caissons, monopiles (MP) and buoyant fixed structures (El-Marrassi, 2011). The selection of foundation system depends on many factors including location and type of structure, subsurface conditions, magnitudes of loads and their distribution, adjacent structures, local experience and availability of materials, durability and cost (Poulos, 2016).

2.2.1 *Gravity base foundation system*

This foundation system derives its resistance by its own weight to counter sliding and overturning. Thus, very large dimensions are used depending on the loading condition and water depth. At certain limit, GBF may not be practical and becomes costly. Typical water depth for GBF ranges from 0 to 20 m (shallow). The reported diameters installed offshore range from 12 m to 35 meters (Abdelkader, 2016).

2.2.1 *Monopile*

Monopile foundation is suitable for intermediate water depth. Wang et al. (2018) stated that MP option accounts for almost 80% of the installed wind turbines. Typically, a pile is extended from the transition piece of the tower to a suitable penetration depth determined based on established limit for lateral deflection and rotation as well as vertical geotechnical capacity. Open ended steel pipe of diameter between 3 and 7.5 m are used in practice. Typical depth of installation is from 16 to 50 while typical diameters are 5-6m (Abdelkader. 2016). Typically, pile length is determined based on serviceability limits imposed against rotation and lateral deflection. Wang et

al. (2018) stated that the lateral rotation limit for OWT is 0.004 radians and Wang et al. (2017) reported that ground level rotation for wind turbine monopiles should not exceed 0.5°. The monopile wall thickness shall be selected to fulfill vertical, lateral and driving forces. As a guideline, thickness (t_p) to resist applied stresses during driving can be estimated as stated in American Petroleum institute (API, 2005):

$$t_p, \text{mm} = 6.25 + (\frac{D_p(mm)}{100}) \quad (2\text{-}1)$$

2.2.2 *Tripod*

Increased water depth can lead to substantial increase of the lateral load and moment at the mudline, which results in significant increase in the required weight of the structure. Therefore, GBF and MP become expensive. Tripod structures are 3 legs structures founded on either spudcans/suction caissons or piles. Under each leg, monopiles are fed through the steel legs and are driven into the seabed. Where necessary, pile groups can be used to resist higher loads.

2.2.3 *Jacket*

Jacket structure is a space frame structure of 4 legs that is used in deep water for supporting a deck where oil extraction operation is conducted in offshore oil industry. It is a compliant structure (i.e., has natural frequency lower than the environmental loading) and therefore dissipate more energy through its movement with exciting wave/current/wind loads. Further, it is easy to relocate and be used in another oil extraction. However, it is not suited for wind turbines since the weight of these wind turbines is far less than the offshore platforms and hence its use has not been reported for offshore wind turbine installation.

2.2.4 *Suctions Buckets*

The suction caisson is an inverted bucket, which is lowered to the seabed until touch down is established at its tip. Afterwards, water contained within the bucket is sucked by pumps creating suction that pulls it down penetrating the seabed. Suction caissons are easy to install and could be recycled by reversing the installation procedure. Byrne and Houlsby (2003) studied this system extensively and provided in depth review of its behavior. As offshore wind farms (OWF) are being installed far from shoreline with further developments, the depth of water increases significantly. Largest reported OWF depth of water is 40m. As water depth increases, the wave and wind loads increase, therefore renders monopiles not feasible. A prototype suction caisson was first used at Frederikshaven in 2002 for a 3MW OWT only with half steel weight needed if using a monopile (Oh et al. 2018).

2.3 Loads

Offshore wind turbine foundations are subjected to dead loads (own weight) and environmental loads (periodic) and can be subjected to transient loads from impact by ships. The dead load component emanates from the turbine own weight, blades, generator and tower. Environmental loads are caused by wind, current, waves, rotor imbalance, aerodynamic loads and seismic loads. These are random in nature and typically are the governing factor in the design of OWT's (Elmarassi, 2011, Abdelkader, 2016).

2.3.1 *Dead loads*

Dead load comes from own weight of the structural elements plus operation machines and other utilities required for the structure to perform its intended purpose. Table 2-2 shows the dead load component for 5MW NREL (NREL, 2016).

Table 2-2 NREL 5MW wind turbine properties (Abdelkader, 2016).

Parameter	Value
Rating	5 MW
Rotor Orientation, Configuration Upwind	3 Blades
Control Variable Speed	Collective Pitch
Drivetrain High Speed	Multiple-Stage Gearbox
Rotor, Hub Diameter	126 m, 3 m
Hub Height	90 m
Cut-In, Rated, Cut-Out Wind Speed	3 m/s, 11.4 m/s, 25 m/s
Cut-In, Rated Rotor Speed	6.9 rpm, 12.1 rpm
Rated Tip Speed	80 m/s
Overhang, Shaft Tilt, Precone	5 m, 5º, 2.5º
Rotor Mass	110,000 kg
Nacelle Mass	240,000 kg
Tower Mass	347,460 kg

2.3.2 *Wind loads*

Wind loading is stochastic in nature. In the research project OC3 conducted by NREL (National Renewable Energy Laboratory) from 2004-2010, participants from governments and industry investigated the differences in their design assumptions and highlighted the importance of wind loading (Jonkman, 2010). Wind loads can be categorised based on the wind speed and duration. Wind gust velocity is the velocity of wind in a duration of less than 10 minutes, while sustained wind load is the load of passing wind of average speed measured at 10 minutes period. Wind loads can be expressed as forces given by (DNV, 2014):

$$F_w = (1/2)\,\rho\, V^2\, C_s\, A \tag{2-2}$$

Where: F_w: static wind force (force unit); V: wind speed (length/time); A: projected area perpendicular to wind direction (length^2); ρ: air density (usually taken as 1.25 kg/m^3 at 20 ºC); C_s: shape coefficient (s = 0.5 for cylindrical sections & Cs = 1.0 for total projected area of offshore platform).

Wind speed is usually reported at reference depth and to get the speed profile with height, power law can be used (Davenport, 1963).

2.3.3 *Current and waves loads*

Current and waves exert substantial lateral loading components on wind turbine shaft. The load is dependent on the wavelength and frequency and the structure dimension. Morrison's equation is used for high H/D structures (H is structure height and D is projected breadth perpendicular to wave action), where inertia and dynamic loadings govern. For low H/D (bulky structures), diffraction theory is used to obtain the lateral loads. Equation 2-3 gives the lateral force for inertia and drag components for high H/D structures while Equation 2-4 produces the lateral forces based on diffraction theory. For wind turbines, H/D ratio is typically large and therefore Morrison's equation is used to calculate the lateral loads (Rahman, 1984).

$$\text{F (lateral force)} = \rho \frac{D^2}{4} C_m a + \frac{1}{2} \rho D C_d V^2 \tag{2-3}$$

Where,

ρ: Fluid (water) density; D: Diameter of structure perpendicular to fluid motion; C_m&C_d: inertia and drag coefficient; a: acceleration; V: velocity

$$\frac{F_{max}}{\rho * g * D^3} = 2\left(\frac{\pi}{8}\right)\frac{\left(\frac{H}{L}\right)}{\left(\frac{D}{L}\right)} \tanh(k * h) \tag{2-4}$$

where, K (wave number) = $\frac{2\pi}{L}$, and L is the crest-to-crest wavelength. H and D are height of wave from M.S.L and D is the diameter of the obstructing structure.

2.3.4 *Other forms of loads*

Wind turbines may exist in seismic areas, and consequently the foundation system can be subjected to seismic loads due to kinematic (movement of the foundation relative to the supporting soil) and inertial (due to superstructure relative vibration) interactions. These forces generate a demand on the soil that is dissipated through rocking and yielding of the foundation soil and through lateral translation. The seismic loads are a function of the local site effects that can cause amplification or attenuation. Sites are classified based on their shear wave velocity, V_{s30}, or according to their topography (slopes and exposed cuts) (Jackson, 2016; Kramer, 1996).

Impact loads from ship collision and slope moving soil mass due to lateral spreading might also occur and therefore allowance for these loads is very important to preserve the wind turbine from collapse or damage. These loads are very sophisticated to measure, and a separate study should be undertaken to quantify their magnitude. DNV (2014) states that the ship impact can be taken as 5 MN in case of lack of information about the size of expected ships and speed of impact.

2.4 Limit states

All geotechnical structures must be designed to meet two criteria: ultimate limit state (ULS), and serviceability limit state (SLS). The ultimate limit state ensures sufficient reserves of capacity and limit structural and geotechnical failure while serviceability limit states prevents certain threshold of deformation and rotation to be reach to ensure functionality of the structure is not impacted. Typically for OWTs the serviceability limit states (SLS) controls the design. Sections below summarise research findings regarding these limits for GBF, MP and Hybrid foundations.

2.4.1 *Vertical Capacity*

2.4.1.1 Bearing capacity of shallow foundations

The general bearing capacity (vertical) of shallow foundation (square/rectangular) is of the following form (Vesic, 1973);

$$Q_u = c' N_c S_c d_c i_c b_c g_c + \gamma' D N_q S_q d_q i_q b_q g_c + 0.5 \gamma_1' N_\gamma S_\gamma d_\gamma i_\gamma b_\gamma g_\gamma \quad (2\text{-}5)$$

Where;

s_c, s_q, s_γ = Shape factors; d_c, d_q, d_γ = Depth factors ;i_c, i_q, i_γ = Load inclination; b_c, b_q, b_γ = Base inclination factors; g_c, g_q, g_γ = Ground inclination factors; c' = Cohesion; N_c, N_q, and N_γ = Bearing capacity factors and are all dependent on the friction angle, φ'; γ'= Bulk unit weight above foundation level (F.L); γ_1'= Unit weight of the soil up to B below F.L. Its value is determined based on the ground water table level (G.W.T).

2.4.1.2 Bearing capacity of piled foundations

For piled foundation, the ultimate vertical capacity, $Q_{u,c}$, (compression) and uplift, $Q_{u,t}$, (tension) are of the form (Bowels, 1996).

$$Q_{u,c} = Q_s + Qt - W \quad (2\text{-}6)$$

$$Q_{u,t} = Q_s + W \quad (2\text{-}7)$$

Ultimate capacity is typically determined based on Alpha method (undrained) for clay and Beta (drained) method for sand (CFEM, 2006). For pile groups, assumption is made weather block failure or individual summation of vertical capacity is made, after applying reduction factors, typically taking the lowest value as the ultimate capacity.

2.4.1.2.1.1 α method:

$$Q_s = \int_{G.S}^{L} C \propto C_u \, d\ell \quad (2\text{-}8)$$

$$Q_t = C_u * N_c * A_t \quad (2\text{-}9)$$

2.4.1.2.1.2 β method:

$$Q_s = \int_{G.S}^{L} C * \sigma' * ks\ tan(\delta) d\ell \quad (2\text{-}10)$$

$$Q_t = \sigma' * N_q * A_t \quad (2\text{-}11)$$

Where;

$Q_{u,c}$: Compression capacity, $Q_{u,t}$: Tension capacity , Q_s: Shaft friction, Q_t: Tip resistance, W: Weight of the pile, G.S: Ground surface, C: Pile circumference, $\propto$: Strength reduction factor, β: Shaft resistance factor depending on the soil stress history and pile installation method $= ks\ tan(\delta), ks$: In-situ lateral/vertical stress ratio which depends on pile installation method and soil structure; δ: Soil-pile interface friction angle commonly taken between 1/3-2/3 ϕ', ϕ': Soil friction angle; N_q& N_c: Bearing capacity factor; l:pile's length, A_t: pile's tip area

2.4.1.3 Hybrid Foundation

Abdelkader (2016) studied the effects of added plate on the vertical capacity of hybrid foundation system for OWT in sand, his results indicated the vertical capacity of such system exceeds that of monopile and can be expressed in the form:

$$Q_u = 2.48\ Q_{u,monopile} + 0.4\ (D_{pl}/L)\ Q_{u,Plate} \quad (2\text{-}12)$$

For horizontal capacity, scarce research has been taken to characterize the lateral ultimate capacity of the hybrid foundations. Charts have been proposed by Elmarassi (2011) can be used as a guidance for preliminary analysis.

2.4.2 *Horizontal capacity*

For shallow foundations, the sliding capacity has the form:

$$H_u\ (\text{sliding capacity}) = V \tan\left(\frac{2}{3}\phi'\right) * A + \frac{2}{3} k_p * (\gamma * h^2 * 0.5) * B + Cu \propto * A \quad (2\text{-}13)$$

Where;

V: Vertical applied load, K_p: Passive earth pressure coefficient, B: Foundation breadth, A: area of foundation

Several authors provided analytical solutions for ultimate capacity of laterally loaded piles (Heytani, 1946; Broms, 1964, Reese, 1975, Poulos and Davis, 1980; Brown, 1999, Gerolymos et al., 2019). Monopiles lateral ultimate capacity is determined through the Beam on Nonlinear Winkler Foundation (BNWF) method (commonly referred to as p-y approach), sophisticated FEM or Brom's approach. The p-y approach is commonly used in the offshore industry where soil is simulated by independent springs characterized by load-displacement curve. It was first validated by Matlock (1970) for the case of slender pile in soft soil and then by Reese (1975) who added p-y formulae for stiff soil. Nevertheless, the p-y approach suffered some limitations when it was applied to monopile foundation for offshore wind turbines. Firstly, the p-y curves are developed through testing slender piles in soft soil with diameter of 0.32m and length of 12.8m making L/D ratio of 39.5; however, MPs are rigid and have diameters of 3-7.8 and length of 20-80 m making L/D = 2.5-26. Numerous researchers pointed out the diameter effect on the accuracy of the method for MPs (Lai et al., 2020; Zhu et al., 2017, Byrne et al, 2015a; Byrne et al., 2015b; Lau, 2015). Secondly, the tested pile has only experienced 20 cycles of loading whereas OWT foundations experience load cycles in the order of 10^7 over its lifetime. Finally, the effects of cyclic loading are treated uniformly across pile depth with a reduction factor A = 0.9 irrespective of load level (Haigh, 2014). Improved p-y formulae have since been focused on closing these gaps in literature (Murph and Hamilton, 1993; Jeanjean, 2009, Byrne et al., 2015; Byrne et al., 2015; Zhu et al., 2017). Figures 2-5 and 2-6 show the different modes of failure adopted in Brom's method for long and short piles with different fixity conditions (Broms,1964). Figure 2-7 shows the p-y approach which can be used to obtain both the stiffness and the lateral ultimate capacity of piles. It displays the slope/moment, shear and lateral loads (Heyer and Reese, 1979).

The soil ultimate soil bearing pressure, Pu, for laterally loaded piles can be estimated by:

$$P_u = 3\ C_u\ d + \gamma\ x\ d + J\ c_u\ x \text{ or } Pu = 9\ c_u \quad (2\text{-}14)$$

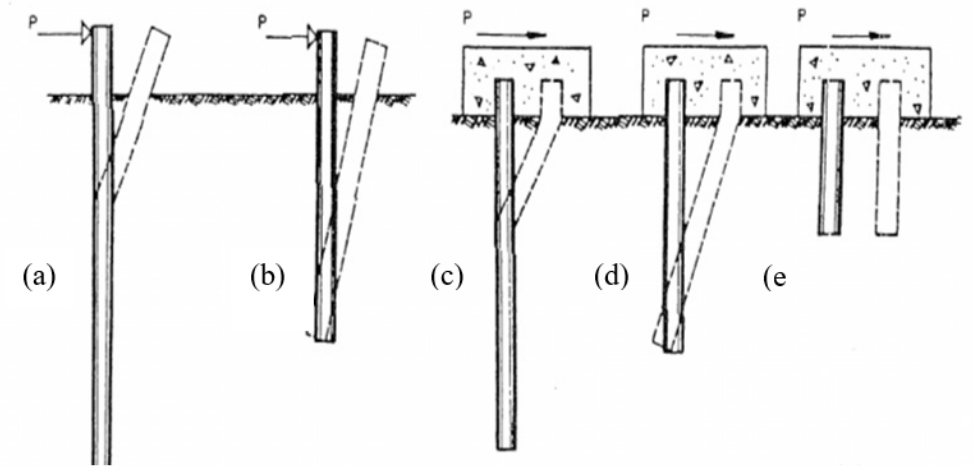

Figure 2-5 Laterally loaded piles a and b represent free head condition for long and short piles while c, d and e represent fixed head long, short conditions (Broms, 1964)

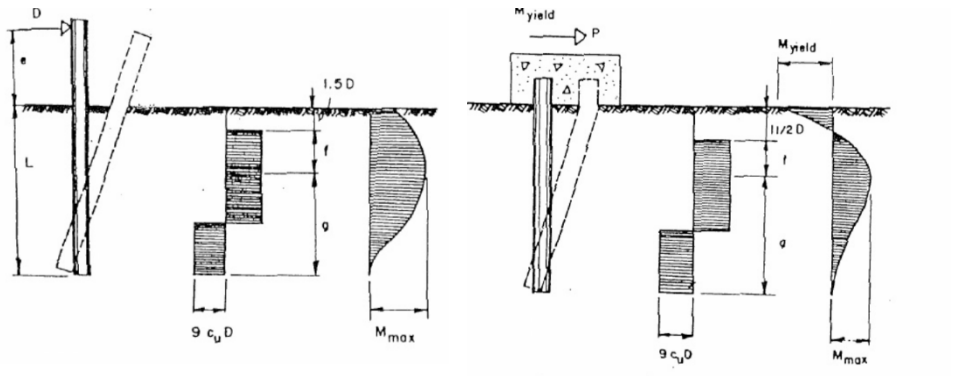

Figure 2-6 Pressure distribution for (a)free-head and (b) fixed head laterally loaded piles in clay (Broms, 1964)

Elmarassi (2011) studied the ultimate lateral capacity of hybrid foundation system using 2D and 3D finite element modelling and centrifuge testing and concluded that the ultimate lateral capacity can be substantially increased if a shallow foundation is supported by a monopile (Hybrid) for L_p/W ratio from 0.25-1. Normalized curves were provided for h versus v where h and v are normalized lateral capacity and vertical capacity, respectively.

2.4.3 *Stiffness*

Numerous researchers valuated the axial, rotational and lateral stiffness of shallow and deep foundations. This section summarizes the available information on this aspect of design.

2.4.3.1 Shallow foundations

For shallow foundations, the rocking, lateral and vertical elastic stiffness under undrained behavior can be obtained as (Davis, 1974);

$$\theta = \frac{3(1-\nu^2)}{4ER^3} M \tag{2-15}$$

$$y = \frac{(7-8\nu)(1+\nu)}{16(1-\nu)ER} H \tag{2-16}$$

$$x = \frac{(1-\nu^2)}{2ER} V \tag{2-17}$$

2.4.3.2 Piled foundations

Randolph (1992) proposed to calculate the axial pile stiffness by:

$$K_p = G_{sl} * D_p * \frac{\frac{2\eta}{(1-\nu)\xi} + \frac{2\pi\rho}{\zeta} * \frac{\tanh(\mu L)}{\mu L} * \frac{L_p}{D_p}}{1 + [\frac{8\eta}{\pi\lambda(1-\nu_p)\xi} * \frac{tanh(\mu L_p)}{\mu L_p} * \frac{L_p}{D_p}}} \tag{2-18}$$

where: r_o = pile radius; D_p = pile diameter; $\zeta = \ln(r_m/r_o)$; $r_m = 2.5\rho(1-\nu)L_p$; $\xi = E_{sl}/E_{sb}$; $\rho = E_{sav}/E_{sl}$; $\mu L = (2/(\zeta\lambda))^{0.5} * (L/r_o)$; $\lambda = E_p/G_{sl}$; $\eta = r_b/r_o$; L_p = pile length; E_{sl} = soil Young's modulus at pile toe level; E_{sb} = soil Young's modulus below pile toe; E_{sav} = average soil Young's modulus along pile shaft; ν = soil Poisson's ratio; G_{sl} = soil shear modulus at the pile toe level; and E_p = pile material Young's modulus (Fleming et al., 2009).

Novak (1974) investigated the vertical, lateral stiffness and coupling stiffness for piles (frequency independent), and proposed the following equations for their evaluation:

$$K_v = \frac{E_p I}{A} * fv \tag{2-19}$$

$$K_L = \frac{E_p I}{R^3} * fu \tag{2-20}$$

$$K_{RL} = \frac{E_p I}{R^2} * fc \tag{2-21}$$

$$K_R = \frac{E_p I}{R} * fy \tag{2-22}$$

where: Fv, fu, fc and fy are, Ep = pile Young's modulus, I = moment of inertia, R = radius or equivalent radius of foundation

Poulos and Davis (1978) and Poulos and Hull (1989) proposed elastic solutions to obtain the lateral stiffness of piles. Beam on elastic/Nonlinear subgrade/beam of Winkler Foundation (BWF/BNWF) are also used. Typically, p-y approach is used to obtain the deflected shape and stiffness of piles. The theoretical solution for piles deformation under static lateral loading may be given by:

$$EI \frac{d_y^4}{d_x^4} + P_x \frac{d_y^2}{d_x^2} + E_s y = 0 \tag{2-23}$$

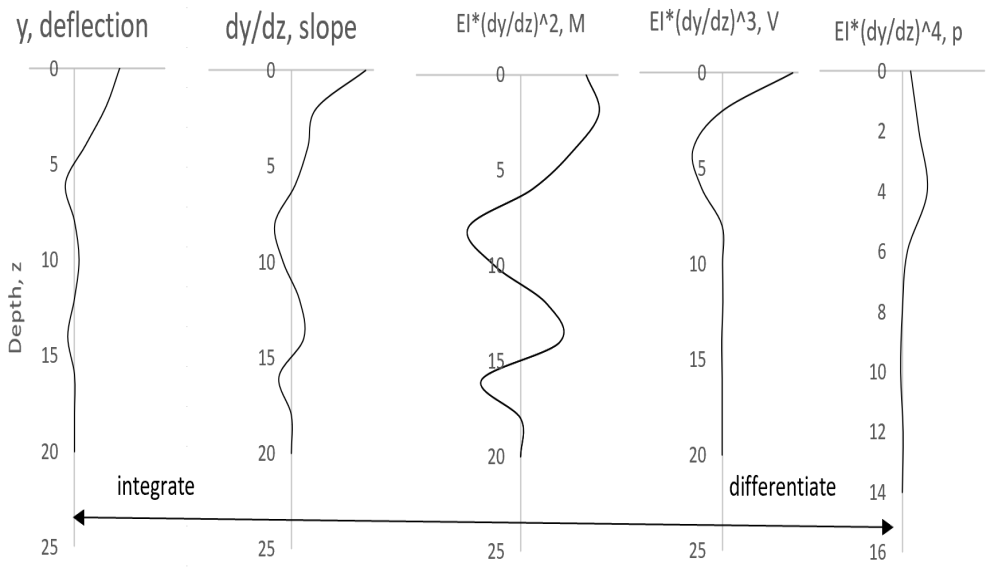

Figure 2-7 Diagrams of slope/moment, shear and lateral loads for laterally loaded piles

The BNWF assumes that the soil can be replaced by springs with the pile element modeled as beam elements resting on elastic spring. El Naggar (1998) provided a BNWF model for laterally loaded piles under cyclic loadings. El Naggar and Bentley (2002) extended this approach to model gapping and slippage of cohesive soils and verified their solution with field data. The strain wedge (SW) approach is an analytical solution proposed by Ashour (1998) to solve for deflection of laterally loaded piles, which accounts for side friction on the pile. Other methods for solution of laterally loaded piles' stiffness properties include FEM approach and continuum approach.

2.4.1 *Moment resistance:*

The resisting moment of shallow foundation should be more than 1.5 overturning moment, i.e.

$$M_r = V * \frac{W}{2} \geq M_o = P * e \tag{2-24}$$

where: M_r: resisting moment (restoring moment), M_o: overturning moment (destabilizing moment) P: any lateral load applied above G.S

For pile foundations, the equation describing the moment resistance is obtained as follows (Shrestha et al., 2018):

$$M_{r(block)} = \alpha * D_p * P_u * L_p^2 \tag{2-25}$$

where: α = factor for effective depth depending on distribution of lateral pressure on pile, D_p = diameter of pile, P_u: ultimate lateral load, L_p = length of pile

For Hybrid foundation, M_r is composed of two components, one coming from weight of the plate and from the soil structure interaction including passive resistance against pile and shear resistances underneath the plate.

2.4.2 *V-H-M failure envelope*

Offshore structures are subjected to complex regime of loads and their design must consider their combined effects. This may be accomplished through checking the overall stress ratio against a failure criterion. Such criterion may have the following form (Bhudu, 2008):

$$\frac{V}{V_{max}} + \left(\frac{H}{H_{max}} + \frac{M}{M_{max}}\right)^{0.5} = 1 \qquad (2\text{-}26)$$

2.5 Clay *behavior*

2.5.1 *Behavior of clay under monotonic loading*

Clay behavior under monotonic loading is dependent on its stress history and fabric. Generally, normally consolidated clays will strain harden when sheared until reaching a plateau (S_u) while over-consolidated clays will attain a peak (S_u) followed by a reduction in stress, a phenomenon called strain softening, until a plateau is reached (termed residual shear strength; $S_{u,res.}$).

2.5.2 *Behavior of clay* under *cyclic loading*

Under cyclic loading, clay behaviour depends on several factors including: loading intensity, duration, frequency and number of cycles, as well as clay stress history and drainage condition. For low amplitude and low frequency loading with short drainage path, the shearing can be considered drained. This will cause normally consolidated specimen to contract and therefore attain higher shear strength (strain hardening with expansion of yield locus in q-p' space) while in over-consolidated clays the shearing will induce dilation with collapse of yield locus (strain softening). If the loading intensity is high and/or the duration is short, the excess pore pressure may not have sufficient time to dissipate. Under such conditions, the normally consolidated clays will tend to contract developing a positive excess pore water pressure and hence reducing the effective stress and the soil strength. This is typically accompanied with significant straining after shearing has ceased. For over-consolidated clays, the undrained cyclic loading will generate negative excess pore water pressure and therefore higher strength is attained for such materials.

2.6 Numerical Modelling

Extensive parametric study will be performed to investigate the effects of parameters that are difficult to be covered thoroughly using physical model owing to cost/time limitations. Two foundation options will be investigated: monopiles (MP) and hybrid foundation (HF) at different geometric properties and soil conditions. To obtain accurate results, a fine mesh should be established, and appropriate boundaries should be implemented and should be placed far enough such that they do not affect the calculated response. In addition, reliable and validated material constitutive models should be used. Some of the main features of good finite element models are discussed below.

2.6.1 *Mesh size and boundaries*

The mesh size should be selected based on optimization approach to produce optimum results with minimum run time. There are various element types available such as 15 node triangular, tetrahedron and prism elements. The selection of soil element shape and size should consider the necessary degrees of freedom and the accuracy of integration method. Further, the soil to structure interaction should be modelled with interface elements with shear strength related to that of neighbouring soil. As a rule of thumb for foundation design under static loadings, the x and y (vertical) boundaries from structure center lines should be placed at distance at least five times the foundation width and the horizontal (bottom) boundary should be at 2 to 3 times the foundation/pile width/diameter. For dynamic loading the element size is controlled by shear wave velocity (V_s) of the soil medium and diameter of the foundation. Absorbent boundaries are placed at bottom and vertical boundaries.

2.6.2 *Constitutive behavior*

There are numerous constitutive models available in literature which have been implemented readily in most FE packages such as elastic perfectly plastic Mohr-Coulomb (MC), elastoplastic Hs and Hs small (Hss) and Modified Cam Clay (MCC). The current study adopted the Hs and Hss models that are incorporated in the commercial FE code Plaxis 3D. They were selected because their parameters can be obtained by routine geotechnical lab testing and can generally capture small strain behavior of soil thus providing high quality data for establishing natural frequency of structures.

2.6.2.1 Hs model

In this study, use of Hs was implemented for all monotonic parametric studies. For dynamic calculations for free vibrations, Hss was used to model hysteretic damping of clay. Hs model is advanced model where the behaviour of both soft and stiff soils can be modelled. It was first proposed by Schanz (1998) as a second order model. Hs model differs from first order models such as MC in that the stress dependency of stiffness can be modeled, plastic straining due to deviatoric and primary compression loading can be obtained, and that unloading stiffness is higher than loading stiffness giving plastic straining before reaching failure. In Hs model, the clay the behavior accounted for effects of two strain hardening; namely volumetric hardening (cap) and shear hardening (Figures 2-14 and 2-15) where contraction and densification cause the yield surface to expand.

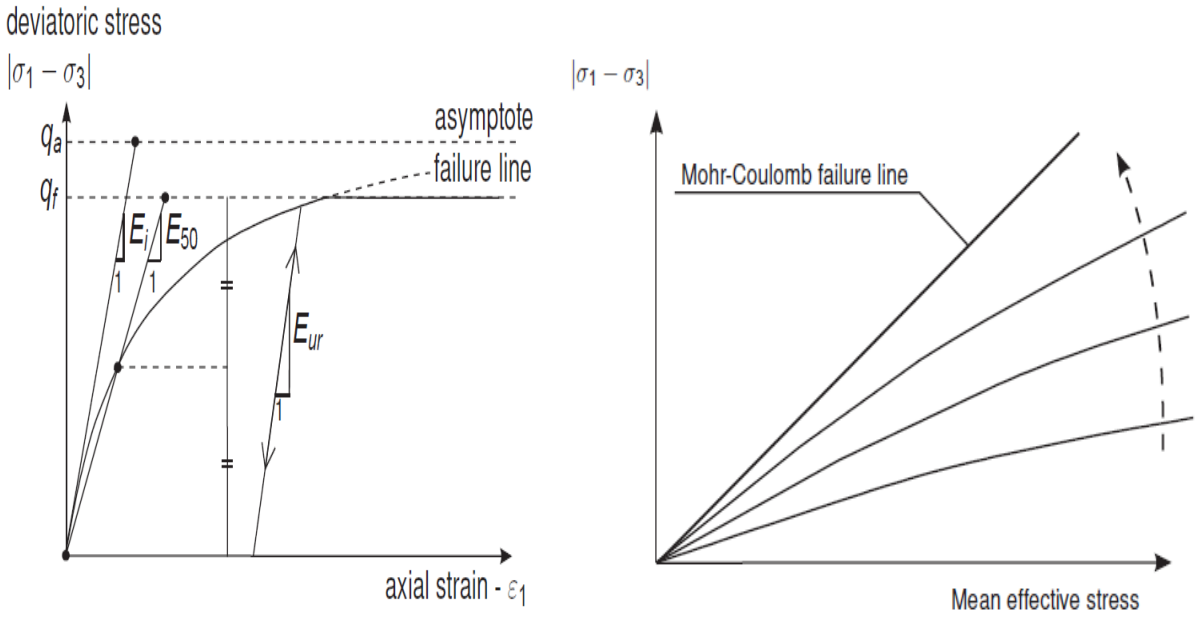

a) **b)**

Figure 2-8 a) hyperbolic stress-strain relationship in deviatoric loading (Plaxis model manual,2015), b) successive yeild loci due to shearing (Plaxis model manual, 2015).

The model parameters are listed below;

For hard soils (small volumetric strains);

$$\dot{\gamma}^p = -2\left(\varepsilon_1^p - \varepsilon_v^p\right) \approx -2\varepsilon_1^p \tag{2-33}$$

The flow rule of the model is expressed as;

$$\dot{\varepsilon}_v^p = sin\varphi_m \dot{\gamma}^p \tag{2-34}$$

Conditions:

For $sin\varphi_m < \frac{3}{4} sin\varphi$:

$$\varphi_m = 0 \tag{2-34a}$$

For $sin\varphi_m \geq \frac{3}{4} sin\varphi \; and \; \varphi > 0$;

$$sin\varphi_m = \max\left(\frac{sin\varphi_m - sin\varphi_{cv}}{1 - sin\varphi_m sin\varphi_{cv}}, 0\right) \tag{2-34b}$$

For $sin\varphi_m < \frac{3}{4} sin\varphi \; and \; \varphi \leq 0$:

$$\varphi_m = \varphi \tag{2-34c}$$

For $sin\varphi_m < \frac{3}{4} sin\varphi$:

$$\varphi_m = 0 \tag{2-34d}$$

If $\varphi = 0 \; \varphi_m = 0$

For volumetric cap; the equation defining the failure condition is written as

$$F_c = \frac{\tilde{q}^2}{M^2} + p'^2 - p'_p \tag{2-35}$$

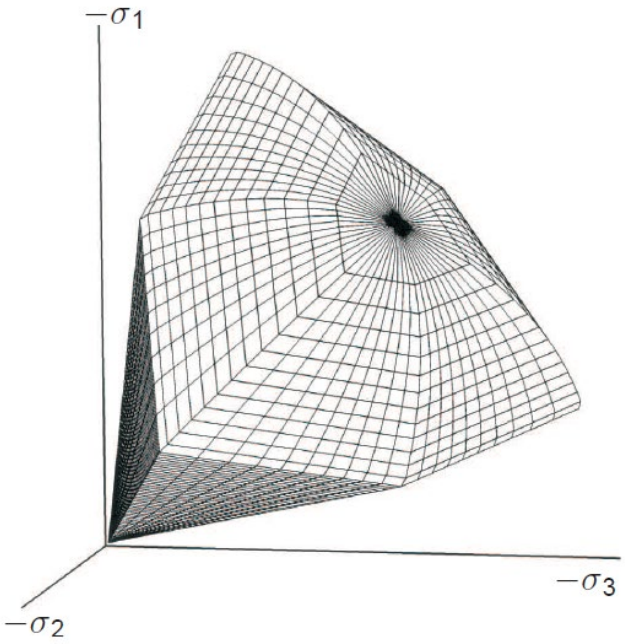

Figure 2-9 yield contours in principal stress space (Plaxis model manual, 2015)

The model stiffness parameters are stress and strain dependent enabling realistic modelling of soil stiffness versus depth. The stiffness parameters are used to describe shearing, volumetric and unloading/reloading strains in the soil and can be given as follows;

$$E_{oed} = E_{oed,ref}\left(\frac{c\cos\phi - \frac{\sigma_3'}{k_o^{NC}}\sin\phi}{c\cos\phi + p_{ref}'\sin\phi}\right)^m \quad (2\text{-}36)$$

$$E_{50} = E_{50,ref}\left(\frac{c\cos\phi - \sigma_3'\sin\phi}{c\cos\phi + p_{ref}'\sin\phi}\right)^m \quad (2\text{-}37)$$

$$E_{ue} = E_{ue,ref}\left(\frac{c\cos\phi - \sigma_3'\sin\phi}{c\cos\phi + p_{ref}'\sin\phi}\right)^m \quad (2\text{-}38)$$

$$G_o = G_{o,ref}\left(\frac{c\cos\phi - \sigma_3'\sin\phi}{c\cos\phi + p_{ref}'\sin\phi}\right)^m \quad (2\text{-}39)$$

2.6.2.2 Hs Parameters

Hs constitutive relationship has 17 parameters listed in following table 2-3.

Table 2-3 Hs parameters

Symbol	Description
Ψ	Dilation angle
Φ	Friction angle
C'	Cohesion
P_{op}', kPa	Previous overburden pressure
P_{ref}, kPa	Reference overburden pressure
$e_{initial}$	Initial void ratio
ɣ, kN/m^3	Unit weight
E_{oed}^{ref}, kPa	Oedometer stiffness at P_{ref},
E_{50}^{ref}, kPa	Stiffness at 50% of ultimate at P_{ref}
E_{ur}^{ref}, kPa	Reload stiffness at P_{ref},
v_{ur}	Unload-reload Poissons ratio
M	Exponent describing stiffness variation with overburden
PI	Plasticity Index
k_o,NC	At rest lateral earth pressure coefficient
R_f	Value descripting ratio of q_f/q

Hss differs than Hs in two parameters, G_o and $ɣ_{0.7}$ which were defined previously (Benz, 2006).

2.6.2.2.1 *Evaluation of Hs parameters*

Parameters of Hs model can be obtained by various methods, some direct and other are estimates based on correlations with other tests. Either field testing or lab testing can be used depending on the accuracy level and relevance. For the later, routine and more involved geotechnical lob tests are typically used to obtain Hs data. For example, Oedometer test can be

used to obtain E_{oed} and exponent m with $E_{oed,ur}$ while Triaxial testing can be employed to get E_{50} and E_{ur}. The following correlations can be used to obtain these parameters. Based on a study by Viggiani and Atkinson (1995), exponent m was reported to vary between 0.35-0.85 and was dependent of PI. Hitcher (1996) reported similar range and trend, however, with LL.

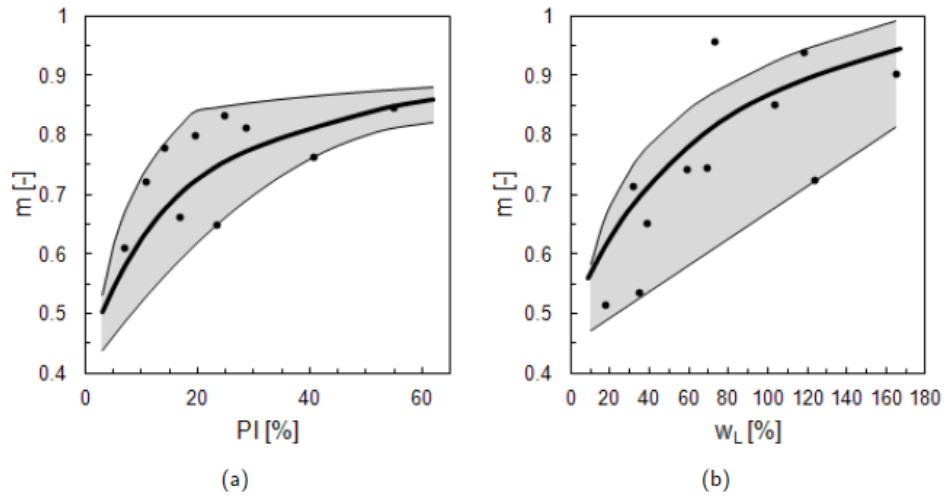

Figure 2-10 m exponent as a function of (a) PI from Viggiani and Atkinson (1995) and (b) LL from Hitcher (1996) (Obrzud and Truty, 2018)

For cohesive soils, k_o,NC was correlated to PI as follows (Alpan, 1967 ;Holtz & Kovacs, 1981);

$$k_o,NC = 0.19 + 0.233 \log PI \quad (2\text{-}40)$$

or

$$k_o,NC = 0.44 + 0.0042\ PI \quad (2\text{-}41a)$$

It should be noted that the at rest pressure is affected by OCR and this is typically taken into account by estimating k_o,NC and multiplying the value by a factor as follows;

$$k_o = k_o,NC * OCR^m \quad (2\text{-}41b)$$

with m being taken to be around 0.5.

Typical values for initial void ratios, correlations of Hs parameters are reported by Obrzud and Truty (2018) for a range of soils.

2.6.2.2.2 G_o

Defining G_o is important when modelling the cyclic behaviour of clay. In FEM studies of natural frequency, the clay is modelled using Hss constitutive model requiring definition of two additional parameters, in addition to those used in Hs model, to model soil hysteretic behaviour. These are the soil shear modulus, Go, and the threshold strain, $\gamma_{0.7}$. Vucetic (1994) and others have studied the influence of strain on the shear modulus, G. Vucetic and Dobry (1988) concluded that for clayey soils the decay of G/G_o was a function of PI. It can be noticed from Figure 2-11 that the threshold strain, which is the strain level after which significant drop in shear modulus happens-, typically taken as $\gamma_{0.7}$, varies according to PI. Other studies investigated the effects of mean effective stress level on this threshold strain and OCR. For clay only PI and OCR control this parameter.

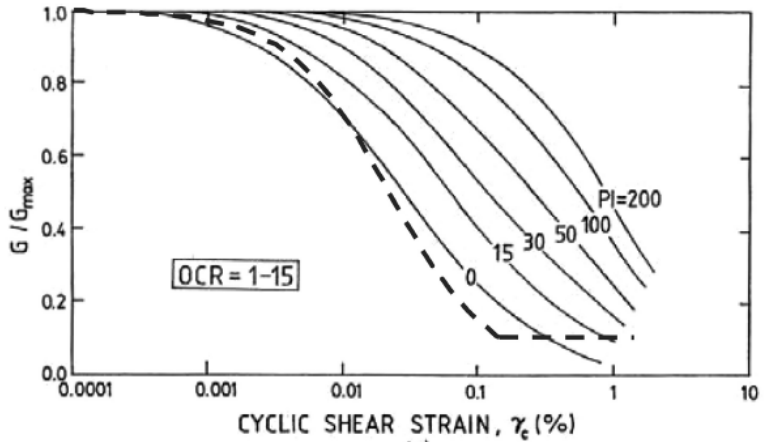

Figure 2-11 G_o Degradation curves for clay with different PI (Vucetic, 1984)

G_o (or G_{max}) can be obtained using correlations, in-situ measurements of shear wave velocity using cross hole, down/up-hole or seismic CPT testing or by laboratory tests on high quality

samples using Bender element test or Resonant column (Kramer, 1996). Typically G_o will show dependence on stress level, OCR, and void ratio and a general equation can be written (Obruzd and Truty,2018);

$$G_o = f(e,OCR,PI,sigma) \tag{2-30}$$

$$G_o = A*F(e)*OCR^k * (\frac{p}{p_{ref}})^m \tag{2-31}$$

Where k is around 0 in sand and 0.5 in high plasticity clay. A is between 13-74 and m is between 0.4-0.74. Table 2-4 and 2-5 list parameters of equation 2-31 for different clay materials.

Table 2-4 Parameters for estimation of Go (re-produced from Obrzud and Truty, 2018)

Soi tested	Ip(%)	A	F(e)	k	m	Reference
Quaternary Itailian Clay	-	60	$e^{-1.3}$	N/A	0.5	Jamiolkowski et al (1995)
Avezzano (Holocene-Pleistocene)	30-Oct	74	$e^{-1.27}$	N/A	0.46	Lo Presti and Jamiolkowski (1998)
Fucino (Holocene-Pleistocene)	45-75	64	$e^{-1.52}$	N/A	0.4	Lo Presti and Jamiolkowski (1998)
Garigliano (Holocene)	10-40	44	$e^{-1.11}$	N/A	0.58	Lo Presti and Jamiolkowski (1998)
Oanigaglia(Holocene)	44	44	$e^{-1.3}$	N/A	0.5	Lo Presti and Jamiolkowski (1998)
Montaldo di Castro clay (Pleistocene)	15-34	50	$e^{-1.33}$	N/A	0.4	Lo Presti and Jamiolkowski (1998)
Reconstituted Valericca clay (Pleistocene)	27	44	1	N/A	0.85	Rampello et al (1997)
Pisa clay (Pleistocene)	23-46	50	$e^{-1.43}$	N/A	0.44	Lo Presti and Jamiolkowski (1998)
London Clay (reconstituted)	41	13	1	0.25	0.76	Viggiani and Atkinson (1995)
Speswhite Kaolin clay (reconstiuted)	24	40	1	0.2	0.65	Viggiani and Atkinson (1995)
Kaolin clay	35	45	$\frac{(2.97-e)^2}{1+e}$	N/A	0.5	Marcusin and Wahls (1972)
Bentonite clay	60	4.5	$\frac{(4.4-e)^2}{1+e}$	N/A	0.5	Marcusin and Wahls (1972)

Table 2-5 exponent k (re-produced from Orzud and Truty, 2018)

I_p,%	Exponent k
0	0
20	0.18
40	0.3
60	0.41
80	0.48
>=100	0.5

2.6.2.2.3 ***Damping***

Cyclic loads affect structural response when the frequency of these loads is within 10% of the natural frequency of the structure. These loads can be magnified or attenuated based on the ratio of the frequency of the load to that of the structure as well as available damping. Damping is typically either a viscous damping which is dependent on the strain rate or hysteretic which depends on the material properties. For Offshore wind turbines, the sources of damping can include structural damping, soil damping, hydrodynamic damping and aerodynamic damping. Structural damping ranges between 0.15 and 1.5% and is affected by type of connections in the structure in addition to material damping. Soil damping results from soil-structure interaction (SSI) including hysteretic (material) damping of the soil, wave radiation damping (geometric dissipation) and, to a much lesser extent, pore fluid induced damping. Typically, it can be 0.444-1% of the total damping. Hydrodynamic damping from wave radiation and viscous damping due to hydrodynamic drag can give damping values in the range of 0.07-0.23%. Aerodynamic damping in the fore-aft direction for an operational turbine 1-6%, for a parking turbine or in the crosswind direction 0.06-0.23%. Aerodynamic damping is the result of the relative velocity between the wind turbine structure and the surrounding air. Aerodynamic damping depends on the particular wind turbine,

and is inherent in the popular Blade Element Momentum (BEM) theory for aeroelastic analysis of wind turbine rotors. The magnitude for a particular wind turbine also depends on the rotational speed of the turbine.

Typical soil shows hysteretic behaviour when loaded, unloaded and reloaded (figure). Unlike Rayleigh damping, which is frequency dependent, hysteric damping is dependent on the strain level. Similar effects of PI on G_{sec}/G_o are observed for damping. Damping can be defined as follows;

$$\zeta = 1*Ed/4\pi*Es \qquad 2\text{-}32$$

where;

Ed: Strain energy

Es: Space within one loop cycle

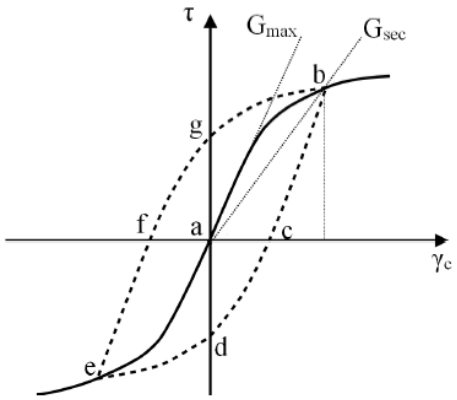

Figure 2-12 Backbone curve of load reversal on a soil sample (Lombardi, 2011)

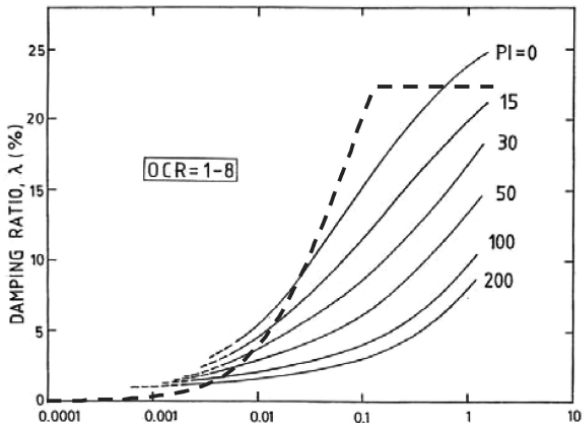

Figure 2-13 Typical calues of damping for different clay materials depending on PI

2.7 Previous studies

Several researchers conducted experimental studies to investigate the performance of monopiles and hybrid foundations in sand and in clay utilizing either full scale “prototype” or model scale (e.g., Wang et al. (2017), Abdelkader (2016), Cherchia (2014) and El-Marassi (2011)). Wang et al. (2017, 2016) investigated the effects of adding a plate to monopile in sand in a centrifuge study. Their results suggested that the plate increases the ultimate lateral stiffness and capacity of the hybrid foundation. Furthermore, the HF exhibited better lateral cyclic resistance than monopile.

Wang et al. (2018) reported that heavier plate increased the HF lateral stiffness and concluded that by increasing the vertical loads, the plate increases the confining pressure and consequently the skin friction at the monopile interface. In addition, it increases the lateral load resistance and rocking stiffness. Wang et al. (2018) proposed a logarithmic relationship based on their centrifuge models to evaluate the lateral deformation with cyclic loading i.e.;

$$\frac{y_N}{y_1} = 1 + b \ln (N) \tag{2-40}$$

where y_N and y_1 are deflection at N cycle and at first cycle, respectively. Parameter b depends on foundation type, load intensity, and soil type with values ranging from 0.36-1.6 (Wang et al., 2018).

However, their centrifuge models did not account for the boundary condition of centrifuge box and possible interference shear zone with side walls which can adversely indicate higher capacity of the system. Their results indicated that the cyclic loads increased the displacement but in a decreased rate with number of cycles and the effect of cyclic loading became negligible after 10 cycles.

Abdelkader (2016) studied the performance of HF in comparison with MP employing 1g model tests under monotonic and cyclic loading. The results demonstrated superior performance of the HF compared to the MP. El-Marassi (2011) investigated the performance of HF in sand and clay under static loading. He established normalized capacity curves, which indicated HF capacity is two to seven folds that of GBF.

The complex stress regime can increase the skin friction on the top portion of the pile, especially for long piles. Therefore, use of long piles with of length to cap width, L_p,/W > 1, provides best performance compared to shallow foundation, while using L_p/W ≤ 1 provides little improvement on axial capacity (El-Marassi, 2011). However, for all L_p/W ratios investigated, the lateral capacity

increased substantially. In the current study, L_p/W = 1 and 2 are investigated. Large L_p/W ratio ensures that the pile embedment below influence zone of shallow foundation minimizes degradation of lateral and rocking stiffness due to strain concentration below the pile tip (El-Marassi, 2011). Typical applied vertical load by maximum vertical capacity, V/V_u , is reported to be less than 0.3 (El-Marassi, 2011).

O'Neill et al. (1987) conducted monotonic and cyclic lateral load tests on single and pile groups installed in stiff clay onshore. The piles were 43 feet long steel pipe driven close-ended (L_p/d= 43). They reported that the lateral load carrying capacity decreased with increasing number of load cycles due to degradation of shear stiffness. They observed gaps formed at the pil-soil interface, which reduced the ultimate bearing capacity of the piles and contributed to accumulation of lateral deflections.

Lahane et al. (2010) conducted centrifuge modelling for OWT foundation systems in sand. They observed that piled foundation performed better than the shallow foundation in resisting moments and exhibited higher rotational stiffness.

Hong et al. (2017) studied the cyclic performance of piles embedded in soft clays. Their centrifuge modeling included two sets of tests, one on improved clay and the other on soft clay. They examined the effects of soil improvement on the performance of piles under cyclic loading. They reported that soil improvement reduced the lateral deflection and enhanced the resistance under low/ medium and high load levels. For low load level (15-35% of H_u), the deflection increased at decreased rate until 65 cycles and remained unchanged thereafter. For medium load level (15-45% H_u), both improved and unimproved piles exhibited increased deflection but at a diminishing rate. For high load level (65% H_u), the increase in deflection was linearly proportional

to number of cycles for pile in soft clay (ratcheting response), and shakedown response for improved soil case.

Klinkvort and Hededal (2014) conducted 10 centrifuge tests on rigid monopiles in very dense sand. They examined the effects of load eccentricity on the pile response. They concluded that load eccentricity affects the ultimate load resistance of piles. They observed that there is a limiting eccentricity beyond which changes in ultimate resistance is minimum. They found that using Rankine passive pressure as given by Broms (1964) underpredicts the ultimate resistance at large depths. Using the method proposed by Zhang (2005) gives a better approximation for the maximum pressure of soil-spring at certain depth, P_u.

Powrie and Daly (2007) studied embedded retaining wall with stabilising base in kaolin clay utilizing centrifuge modelling. There results indicated beneficial effects from stabilizing base to the system lateral performance characteristics.

Cherchia (2014) conducted centrifuge tests on two hybrid foundations (underfins and skirted GBF) systems and compared their behavior with that of the monopile. The foundation systems were tested in sand with relative density of 60%. Their tests were conducted at 50g within a steel tub. The MPs were drilled at 1g and placed before spinning the centrifuge. The lateral load was applied at e/D of 2 using a hydraulic jack with roller bearing to eliminate eccentricity. They reported that the MP exhibited highest stiffness under monotonic and cyclic loads and the lateral deformation at ultimate lateral load for the two HFs was almost twice that of the MP (almost 50mm). However, at operating load (i.e., serviceability limit of 6mm), the HS response was similar to that of the MP.

Lau (2015) investigated the performance of MPs in kaolin clay under monotonic and cyclic loading using centrifuge models. He conducted 9 tests lateral load tests on rigid piles and evaluate the ability of the API p-y approach to simulate their behaviour. He reported that the API approach underestimates the MP stiffness. His results indicate that locked-in stresses take place due to cyclic loading, which may cause residual bending moments.

Zhu et al. (2017) conducted field tests on large diameter open-ended driven piles in soft clay offshore China. Their tests involved driving 2 monopiles of 2.2 diameter in soft clay. They conducted both monotonic and low frequency cyclic lateral loading 50 days after pile installation. They evaluated the reliability of the API p-y approach in predicting the initial stiffness and ultimate capacity od the MPs. Consequently, they proposed new p-y curves (hyperbolic function) with a new factor (t) that varies with depth and load level to modify the p-y curves to account for the effect of cyclic loading. They reported that the API p-y approach for the soft clay underestimated both initial stiffness and ultimate capacity, possibly due to the soil reconsolidation after pile driving.

2.7.1 *Hybrid Foundation system for wind turbine*

The proposed hybrid system is composed of a monopile with a plate at the mudline. Figure 2-15 shows the proposed hybrid foundation system. The response of monopiles is improved by adding a plate at mudline due to 4 mechanisms:

A- Restoring moment resulting from the weight of the plate

B- Improving distribution of shear stresses between plate and monopile

C- Increasing passive pressure beneath plate thereby contributing to the resistance of lateral loads and finally

D- Restoring moment from pressure underneath plate to rotation.

This system was first proposed by Carder et al. (1993) and later investigated by many researchers as discussed previously. However, its behavior in clayey soil under cyclic loading was not investigated. Therefore, the objective of this study is to close this gap in the literature by providing comprehensive study of various effects pertaining to its utilization in soft (e.g., Gulf of Mexico) and stiff (e.g., North Sea) clayey bed (Byrne et al., 2015a).

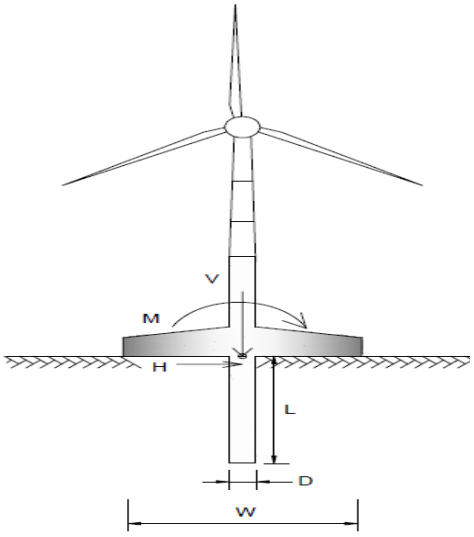

Figure 2-14 Proposed foundation system (El Marassi, 2011)

The proof-of-concept study investigated the monotonic and cyclic behavior of the proposed system in cohesive soil to establish its response characteristics. To achieve these objectives, the lateral ultimate capacity and stiffness characteristics of this system were investigated employing the finite element analysis. The performance of the hybrid foundation is compared to that of monopiles under serviceability and ultimate loading conditions considering clay with different shear strength values. In addition, a series of centrifuge model tests were conducted on the two

systems in over-consolidated saturated Kaolin clay. Two identical clay beds were prepared, tub1 and tub2. In the first tub, monotonic pushover tests were carried out on a monopile model. Similar tests were conducted on the hybrid foundation in a different tub with similar clay profile. The lateral loads were applied at eccentricity, e, to diameter ratio (e/d) of around 3.6.

2.8 References

Abdelkader, Ahmed Mohamed Reda, Investigation of Hybrid Foundation System for Offshore Wind Turbine (Scholarship@Western). 2016.

API, 1993. Recommended practice for planning, designing, and Constructing fixed offshore platforms. API, RPT2A-WSD. American Petroleum Institute (API), Washington, D.C.

Association EWE. The European Offshore Wind Industry‑Key Trends and Statistics 2016; January; 2017.

Bazeos N, Hatzigeorgiou GD, Hondros ID, Karamaneas H, Karabalis DL, Beskos DE. (2002), "Static, seismic and stability analyses of a prototype wind turbine steel tower", Engineering Structures, **24**, 1015-1025.

Beck, A., Springman, S. M., & Askarinejad, A. (2015). Scaling law of static liquefaction mechanism in geocentrifuge and corresponding hydromechanical characterization of an unsaturated silty sand having a viscous pore fluid. *Canadian Geotechnical Journal, 52*(6), 708-720. doi:10.1139/cgj-2014-0237

Bentley, K.J. and El Naggar, M.H., 2000. Numerical analysis of kinematic response of piles. Canadian Geotechnical Journal, Vol. 37, No. 6, pp. 1368-1382

Bowles, J. E. (1996). *Foundation analysis and design*. New York: McGraw-Hill.

Broms, B. B. (1964b). Lateral Resistance of Piles in Cohesive Soils. Journal of the Soil Mechanics and Foundations, **90**(2): 27-64.

Brown, D. A. (2007). Rapid lateral load testing of deep foundations. *DFI Journal - the Journal of the Deep Foundations Institute, 1*(1), 54-62. doi:10.1179/dfi.2007.005

Byrne, B.W. and Houlsby, G.T. (2003) "Foundations for Offshore Wind Turbines", Philosophical Transactions of the Royal Society of London, Series A, Vol. 361, December, pp 2909-2930.

Byrne B. W., McAdam R., Burd H. J., Houlsby G. T., Martin C. M., Zdravković L., Taborda D. M. G., Potts D. M., Jardine R. J., Sideri M., Schroeder F. C., Gavin K., Doherty P., Igoe D., Muir Wood A., Kellahave D. and Skov Gretlund J. 2015a. New design methods for large diameter piles under lateral loading for offshore wind applications. *Proceedings of Third International Symposium on Frontiers in Offshore Geotechics* 1, 705-710.

Byrne B. W., McAdam R., Burd H. J., Houlsby G. T., Martin C. M., Gavin K., Doherty P., Igoe D., Zdravković L., Taborda D. M. G., Potts D. M., Jardine R. J., Sideri M., Schroeder F. C., Muir Wood A., Kellahave D. and Skov Gretlund J. 2015b. Field testing of large diameter piles under lateral loading for offshore wind applications. *Proceedings of XVI European Conference on Soil Mechanics and Geotechnical Engineering*, Edinburgh, 1255-1260.

Byrne. Foundations for Offshore Wind Turbines (2013). Presentation. University of Oxford.

Cheah, C. B., & Ramli, M. (2011). The implementation of wood waste ash as a partial cement replacement material in the production of structural grade concrete and mortar: An overview.*Resources, Conservation & Recycling, 55*(7), 669-685. doi:10.1016/j.resconrec.2011.02.002

Cherchia, M. (2016). Centrifuge modeling of hybrid foundations for offshore wind turbines.

Das, B. M. (2006). *Principles of foundation engineering*. Boston: PWS Pub. Co.

El-Marassi M., Elnaggar, M.H, Newson, T. and Stone, K. Numerical modelling of the performance of a hybrid monopiled-footing foundation. GeoEdmonton, 2008.

El-Marassi M. Investigation of hybrid monopile-footing foundation systems subjected to combined loading: The University of Western Ontario; 2011.

Gerolymos, N., Giannakos, S., & Drosos, V. (2019). Generalised failure envelope for laterally loaded piles: Analytical formulation, numerical verification and experimental validation. *Géotechnique,* , 1-20. doi:10.1680/jgeot.18.P.051

Heidari, M., Jahanandish, M., Naggar, H. E., & Ghahramani, A. (2014). Nonlinear cyclic behavior of laterally loaded pile in cohesive soil. *Canadian Geotechnical Journal, 51*(2), 129-143. doi:10.1139/cgj-2013-0099

Heyer, Berry& Reese, L.C. Analysis of single piles under lateral loading. FHWA/TX-79/38+244-l. 1979

Jackson, F. A (2016). Assessment of earthquake site amplification and application of passive seismic methods for improved site classification in the greater vancouver region, british columbiaScholarship@Western.

Jonkman, J. M., Musial, W. D., & National Renewable Energy Laboratory (U.S.). (2010). *Offshore code comparison collaboration (OC3) for IEA task 23 offshore wind technology and deployment.* (No. 5000-48191.;5000-48191;). Golden, Colo: National Renewable Energy Laboratory.

Kramer, S. L. (1996). *Geotechnical earthquake engineering*. Upper Saddle River, N.J: Prentice Hall.

Lamb, Robert. "When will we run out of oil, and what happens then?" 21 April 2010. HowStuffWorks.com. <https://science.howstuffworks.com/environmental/energy/run-out-of-oil.htm> 15 May 2018

Lau, B. (2015). Cyclic behaviour of monopile foundations for offshore wind turbines in clay. ProQuest Dissertations Publishing.

Lehane B, Powrie W, Doherty J. Centrifuge model tests on piled footings in clay for offshore wind turbines. In: Proceedings of international conference in physical modelling in geotechnics, ICPMG2010 Rotterdam: Balkema; 2010.

Malhotra, S. "Design and Construction of Offshore Wind Turbine Foundations," Wind Turbines, pp. 231-264.

Mihaylov, D. G. (2011). *Seismic microzonation of great toronto area and influence of building resonances on measured soil responses*

Muir Wood, D. (2004). *Geotechnical modelling*. London;New York, NY;: Spon Press.

Novak, M. (1974). Dynamic Stiffness and Damping of Piles. *Canadian Geotechnical Journal*, *11*(4), 574–598. https://doi.org/10.1139/t74-059

Oh, K.-Y., Nam, W., Ryu, M. S., Kim, J.-Y., & Epureanu, B. I. (2018). A review of foundations of offshore wind energy convertors: Current status and future perspectives. *Renewable & Sustainable Energy Reviews*, *88*, 16–36. https://doi.org/10.1016/j.rser.2018.02.005

O'Neill, M. W., Reese, L. C., & Brown, D. A. (1987). Cyclic lateral loading of a large-scale pile group. *Journal of Geotechnical Engineering, 113*(11), 1326-1343. doi:10.1061/(ASCE)0733-9410(1987)113:11(1326)

Obrzud, F and Truty, A., 2018. THE HARDENING SOIL MODEL -A PRACTICAL GUIDEBOOK. Z Soil.PC 100701 reportrevised 21.10.2018

Powrie, W., and Daly, M. P. (2007). "Centrifuge modeling of embedded retaining walls with stabilizing bases." Geotechnique, 57(6), 485–497.

Poulos, H. G. (2016). Tall building foundations: Design methods and applications. *Innovative Infrastructure Solutions, 1*(1), 1-51. doi:10.1007/s41062-016-0010-2

Poulos, H. G. and Hull, T. (Role of analytical geomechanics in foundation engineering. Foundation engineering : current principles and practices. pp. 1578-1606 (1989). ILL item# 112694.

Rahman, M. (1984). Wave diffraction by large offshore structures: An exact second-order theory. *Applied Ocean Research, 6*(2), 90-100. doi:10.1016/0141-1187(84)90046-4.

Randolph, M. F., & Gourvenec, S. (2011). *Offshore geotechnical engineering*. New York: Spon Press.

Federal Highway Administration (FHWA). (2016). Design and Construction of Driven Pile Foundations – Volume I. U.S. Dept. of Transportation, Federal Highway Administration,

Toyosawa, Y., Itoh, K., Kikkawa, N., Yang, J. -., & Liu, F. (2013). Influence of model footing diameter and embedded depth on particle size effect in centrifugal bearing capacity tests.*Soils and Foundations, 53*(2), 349-356. doi:10.1016/j.sandf.2012.11.027

Vucetic M, Dobry R. Degradation of marine clays under cyclic loading. Journal of Geotechnical Engineering ASCE 1988;117(1):89–107.

Wang, X., Zeng, X., Yang, X., & Li, J. (2018). Feasibility study of offshore wind turbines with hybrid monopile foundation based on centrifuge modeling. *Applied Energy, 209*, 127-139. doi:10.1016/j.apenergy.2017.10.107

Hong, Y., He, B., Wang, L. ., Wang, Z., Ng, C. W. ., & Mašín, D. (2017). Cyclic lateral response and failure mechanisms of semi-rigid pile in soft clay: centrifuge tests and numerical modelling. *Canadian Geotechnical Journal*, *54*(6), 806–824. https://doi.org/10.1139/cgj-2016-0356

Zhang, G. (2017). A centrifuge study of the seismic response of pile–raft systems embedded in soft clay. *Géotechnique*, *67*(6), 479–490. https://doi.org/10.1680/jgeot.15.P.099

Zhu, B., Zhu, Z., Li, T., Liu, J., & Liu, Y. (2017). Field Tests of Offshore Driven Piles Subjected to Lateral Monotonic and Cyclic Loads in Soft Clay. *Journal of Waterway, Port, Coastal, and Ocean Engineering*, *143*(5), 5017003–. https://doi.org/10.1061/(ASCE)WW.1943-5460.0000399

Y. Hong, B. He, L.Z. Wang, Z. Wang, C.W.W. Ng, and D. Mašín. Cyclic lateral response and failure mechanisms of semi-rigid pile in soft clay: centrifuge tests and numerical modelling. Canadian Geotechnical Journal (2017)

Chapter 3: Lateral Loads Ultimate Capacity of Monopiles and Hybrid Foundations: Effects of Footing rigidity and L/D/(L_p/W) ratios

Lateral Loads Ultimate Capacity of Monopiles and Hybrid Foundations for Offshore Wind Turbines in Medium Depth Water: *Effects of Footing Rigidity and L/D/(L_p/W) Ratios and comparison at Serviceability Loading*

Abstract:

In this study, a hybrid foundation system (HF) comprising a plate with a diameter (W) fitted with a pile with a length (L_p) at the center is proposed as an alternative to monopiles. The HF system is investigated and compared with monopiles (MP) in different clayey beds. Specifically, the lateral ultimate capacity of both HF and MP is investigated considering laterally applied load with eccentricity e/D_t of 6.8 where e is the eccentricity and D_t is the tower diameter followed by a comparison study at serviceability loading. Three-dimensional nonlinear finite element models (FEM) were developed and validated to simulate the two foundation systems installed in six different cohesive soil. For each soil profile, HF with L_p/W ratios of 1 and 2 were investigated as well as 7 different MP length to diameter (L/D) ratios varying from 3.3 to 13.3. Results indicate MP normalized lateral capacity decreases as the soil elastic modulus increases and increases as L/D increases. For soft soils, MP behaves as a rigid pile and its normalized ultimate capacity increases linearly with L/D unlike stiffer soils in which normalized ultimate capacity plateaus at L/D = 5-8. Similarly, for HF systems, the normalized ultimate capacity increases with the pile length to plate width (L_p/W) ratio and decreases as the soil shear strength increases. The normalized capacity of HF was affected by plate width but is insensitive to monopile diameter for the considered pile diameters. Comparison under serviceability loading indicates the hybrid foundations of L_p/W of 2 and 1 can reduce the maximum bending moment by 45-30% compared to the case of a monopile with 30 m penetration and can lower tower tip displacement by 1-2.5%. These findings suggest the hybrid foundation can support newer generation of OWT installed in stiff clay mediums to benefit from shorter and smaller diameter piles used while at the same time provide similar performance to longer and heavier monopiles typically used to support OWT.

3.1 Introduction

Sustainable energy sources such as wind, hydro and solar are critical and under utilized. Global warming and increasing CO_2 emissions in the atmosphere and fear of increased frequency and severity of natural disasters such as extreme weather, flooding and tsunamis have driven government bodies, research institutes and industry to move at higher pace towards cultivating more energy from these sources in a bid to reduce dependency on fossil fuels. Specifically, exponential growth of wind energy has been achieved from Onshore and offshore wind farms (OWF) with offshore wind turbines (OWT) reaching a capacity of 14MW already available on the market. Figure 3-1 shows the energy output from Offshore Wind Farms in Europe between 2000-2016. This increase in capacity is realized by using heavier and taller turbines, often leading to very large foundation systems which can consume up to 40% of the total cost. In addition, wind turbines are installed in various ground conditions that can pose significant challenges for their foundation design. Different foundation systems are employed to support wind turbines such as fixed gravity base foundations (GBF), tripod structures, jackets, suction caissons, monopiles, buoyant fixed structures, rafts on s monopiles and pile groups (Abdelkader, 2016; El-Marassi, 2011; Byrne and Houlsby, 2003). Figure 3-2 presents some of the foundation systems used to support OWT.

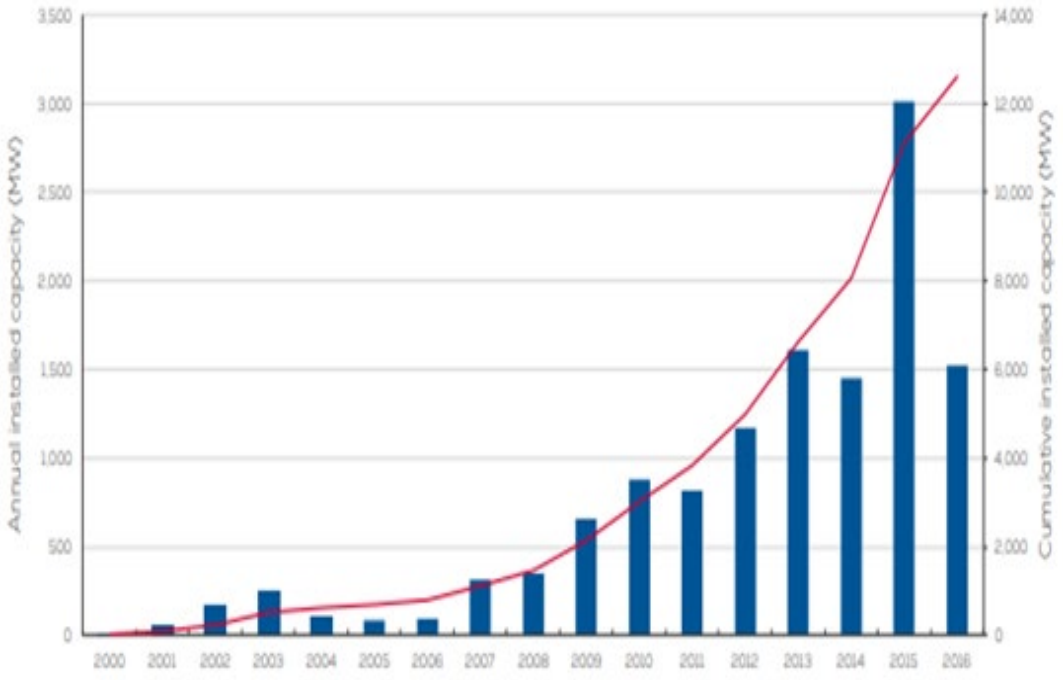

Figure 3-1 Capacity of wind farms installed in Europe (Wind Europe, 2016)

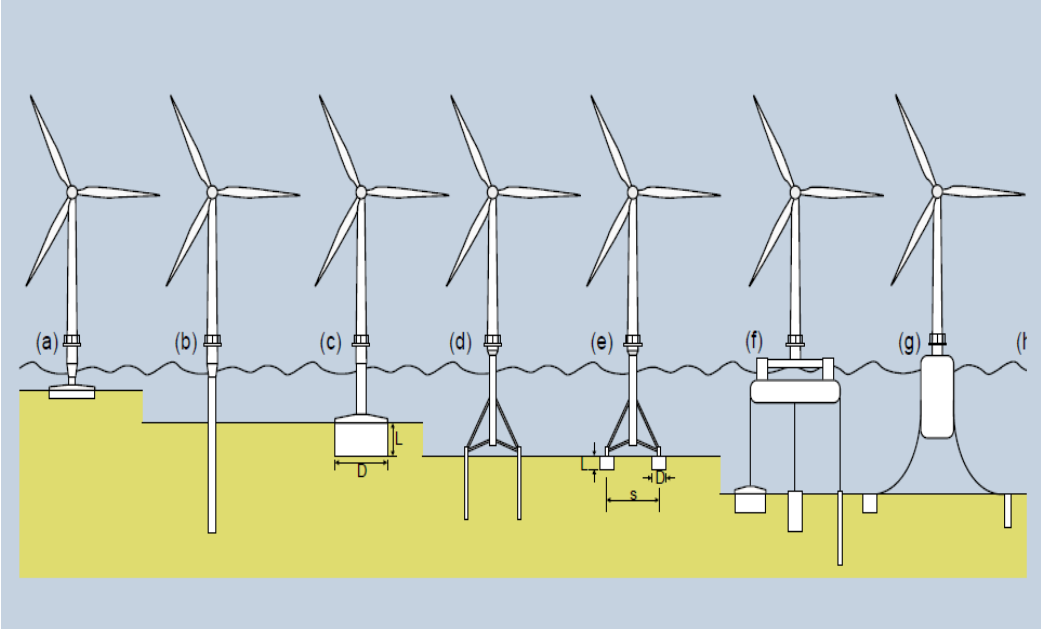

Figure 3-2 Available foundation options for offshore wind turbines (a) GBF (b) monopile (c) suction caisson (d) tripod/tetrapod piles (e) tripod/tetrapod suction caissons (f) multiple foundation options (h) guys with anchors (Byrne, 2013)

With development and installation of offshore wind turbines (OWT) in deeper water, OWT are subjected to ever higher lateral loads and bending moments resulting from wind and wave loading all of which must be accommodated within strict serviceability requirements (Byrne et al., 2015, Wang et al., 2017; Biosi and Halder, 2014). This typically leads to an increase in foundation geometry and, consequently, cost. Therefore, an alternative foundation for monopiles is considered by adding a plate on the mudline to a short monopile (i.e., pile cap) to increase the foundation stiffness and capacity. While monopiles lateral capacity has been investigated widely, few studies exist on lateral capacity of hybrid foundations (e.g., Brown (1978); O'Neill et al. (1987); Lahane et at. (2010); Klinkvort and Hededal (2014); Hong et al. (2017); Wang et al. (2018); Powrie and Daly (2007); El-Marassi (2011); Cherchia (2014); Abdelkader (2016)). Therefore, hybrid foundations (HF) and monopile foundations (MP) are studied in different clayey mediums with the aim to *characterise their lateral ultimate capacity under eccentric loading in a wide range of soil strengths and stiffnesses* and *to compare the two systems at serviceability loading*. The results obtained from this study can verify the results from Beam on Nonlinear Winkler Foundation (BNWF) analyses and benchmark new FEM results.

3.1.1 *Design considerations*

OWT foundations range from gravity base, monopiles, tripods, and jacket options. Of these MP accounts for around 80% of the installed foundations for OWTs. When it comes to the design of these foundations, two criteria must be met: ultimate limit state and serviceability limit states. Ultimate limit state deals with vertical, lateral, and moment capacity of the foundation while serviceability limit state ensures limiting displacement and rotation are not exceeded to ensure acceptable performance of the structural system and successful operation of the turbine. Usually, lateral loads due to wind and waves is the controlling factor when it comes to ultimate limit states.

With increased capacity and strict rotation requirements coupled with increased development in deep water, it is anticipated that the monopile diameter will continue to increase posing problems of drivability and cost for development of new OWT. Areas of improvement and innovations for OWT are increasing turbines output, reducing wake loses, improving farm layout, reducing tower and foundation costs (Chercia, 2014). Since the cost of foundations for OWT can consume up to 40% and since newer developments are expected to be installed further from shorelines and in deeper water, it is expected that the cost of such foundations will continue to increase. Hence, we build on previous research into innovative hybrid foundations with the goal to provide alternatives to monopiles. To reduce the diameter of monopiles, several researchers attempted to use a hybrid foundation system which is a plate fitted with a short monopile in its centerline. The idea of the plate emanates from pile cap analogy and hence is expected to reduce tilting and increase overall stiffness while providing extra support for the structure. This should come with reduced pile diameter and penetration. Therefore, this study builds on the previous research indicating potential benefits of the hybrid foundation to the overall performance under lateral loads. Since few studies exist on this system in clay beds, we attempt to close this gap in literature by studying this system in different clayey beds with the goal of providing closed form equations describing its lateral ultimate capacity under maximum applied eccentricity to pile's diameter ratio, e/D_p, of 6-8. The mechanics of this system is investigated and compared with monopiles. The lateral ultimate capacity of this innovative system in clayey bed is examined and its behavior is compared with monopile under serviceability loading using FEM. To do so, a case study containing lateral load testing on driven open ended monopiles is used to verify and calibrate the model parameters. Afterwards, prototype models are selected for the hybrid foundations and the monopiles for

parameter analyses and the performance of both systems is investigated under eccentric lateral loading.

Since monopiles are free headed, they can undergo significant tilting and mudline displacement when laterally loaded. Because of the strict regulations on the tolerable tilting and to preserve the integrity of the offshore wind turbine generator (OWG), the maximum allowable rotation is set at 0.5 degrees (Malhotra, 2009). To limit tilting of OWT, either the monopile thickness or its diameters are increased to increase the foundation overall stiffness. However, increasing monopile diameter can lead to increased wave loading especially in deep water as wave loading is proportional to embedded structure diameter. Alternatively, improving the soil or adding a plate can increase the lateral stiffness and reduce the mudline rotation. For instance, Powrie and Daly (2007) studied an embedded retaining wall with a stabilising base in kaolin clay utilizing centrifuge modelling. Their results indicated beneficial effects from the stabilizing base to the retaining wall system. Also, Hong et al. (2017) studied the cyclic performance of piles embedded in soft clays in a centrifuge study. They conducted two set of tests, one on soft clay and the other on improved clay and examined the effects of soil improvement on the performance of piles under cyclic loading. Their results indicated that the soil improvement reduced the lateral deflection and enhanced the lateral resistance under low, medium, and high load levels. Wang et al. (2018) conducted a centrifuge study to investigate different OWT foundation systems, including monopile, GBF, gravel and steel wheeled foundations installed in a sand deposit and subjected to lateral monotonic and cyclic loading. Based on the centrifuge test results, they proposed a logarithmic relationship for the accumulation of lateral deformation with the number of load cycles, i.e.

$$\frac{y_N}{y_1} = 1 + b \ln (N) \quad (3\text{-}1)$$

where y_1 and y_N are deflection at first and N cycles, respectively, and parameter b ranges from 0.36 to1.6 depending on foundation type, load intensity, and soil type (Wang et al., 2018).

They concluded that the hybrid foundation systems had higher stiffness compared to the monopile for both gravel and steel plate hybrid footings. Lehane et al. (2014) investigated the lateral and rocking responses of different hybrid foundations and suggested that the hybrid foundation plate improves the foundation performance through four mechanisms: it contributes to the restoring moment due to its weight, absorbs shear stresses between through contact with soil, increased passive pressure underneath the plate increases resistance of lateral loads from the pile, as well as adds restoring moment from soil contact pressure. Cherchia (2014) suggested that the hybrid foundation could have a considerable cost advantage because the diameter and length of the pile would be reduced, and the material weight could be significantly lower than that of the monopile. He conducted centrifuge tests at 50g on two hybrid foundations, underfins and skirted GBF, installed in a medium dense sand and compared their behavior with that of monopiles. The lateral load was applied at e/D_p, where e is eccentricity and D_p is pile's diameter, of 2 using a hydraulic jack. The experimental results demonstrated that under serviceability limits ( ), the response of the hybrid systems was similar to that of the considered monopile. However, the monopile exhibited higher stiffness under monotonic and cyclic loads at ultimate lateral load, and the response of the hybrid foundations was almost twice that of the monopile (almost 50mm).

Lateral ultimate capacity of monopiles is determined through beam on nonlinear Winkler foundation (BNWF), commonly referred to p-y approach, sophisticated FEM or Brom's approach. Commonly, p-y approach is used in the offshore industry where soil is replaced by independent springs each having a different load-displacement curve. Proposed earlier by McClelland and

Focht (1955) and validated by Matlock (1970) for the case of slender pile in soft soil and then by Reese (1975) who proposed p-y formulae for stiff soil. Nevertheless, the p-y approach suffered some limitations when it was applied to monopile foundation for offshore wind turbines. Firstly, the p-y approach was validated by Matlock (1970) testing slender piles in soft soil with diameter of 0.32m and length of 12.8m making L/D ratio of 39.5; however, current MP are rigid and have diameters of 3-7.8 and length of 20-80 m making the L/D ratios between 2.5-26. Numerous researchers pointed out that diameter effects were not included in the original method (Lai et al., 2020; Zhu et al., 2017, Byrne et al, 2015a; Byrne et al., 2015b; Lau, 2015). Secondly, the tested pile has only experienced 20 cycles of loading whereas expected cycles of loads the OWT experiences in its lifetime can be of the order of 10^7. Finally, the effect of cyclic loading is treated uniformly across pile depth with a reduction factor A of 0.9 irrespective of load level (Haigh, 2014). Improved p-y formulae have since been focused on closing these gaps in literature (Murph and Hamilton, 1993; Jeanjean, 2009, Byrne et ala, 2015; Byrne et al, 2015; Zhu et al., 2017). For instance, Lau (2015) conducted 9 centrifuge tests on monopiles installed in kaolin clay and subjected to monotonic and cyclic loading. The results were used to elucidate the behavior of rigid piles under lateral loading and compared the measured response with the predictions using the p-y approach. The results demonstrated that the API p-y curves of Matlock (1970) underestimate the stiffness properties of the monopiles and that the displacement and rotation under cyclic loading depend on number of load cycles and cyclic loads amplitude, which is not accounted for in the API p-y approach. Zhu et al. (2017) conducted field tests on large diameter open ended driven piles in soft clay offshore China. Their tests involved driving 2 monopiles of 2.2 diameter in soft clay and were subjected to both monotonic and low frequency cyclic lateral loading. The experimental results were used to examine the ability of the API p-y approach in predicting the

piles initial stiffness and ultimate capacity, and to proposed new p-y curves to simulate strength degradation with cyclic loading. Their results showed the API p-y curves underestimated both initial stiffness and ultimate capacity, possibly due to reconsolidation from pile driving, which is in line with results from Lau (2015). They proposed a hyperbolic function for p-y curves which provided excellent match to field tests. Additionally, their p-y curves included a degradation factor, t, as a function of depth and cyclic load level.

It is well known that pile capacity is affected by the loading eccentricity. For instance, Klinkvort and Hededal (2014) conducted 10 centrifuge tests on rigid monopiles in very dense sand to evaluate the effects of load eccentricity on the pile response. They reported that the load eccentricity affected the pile lateral ultimate load capacity which continued to decrease with increasing the eccentricity, but beyond 15D this change in the lateral ultimate capacity was less pronounced. This is in line with Brom's (1964a and 1964b) method which shows decreasing capacity as eccentricity increases. Hence, we have fixed the eccentricity to diameter ratio, e/D_t, to be 6.83 which is thought to be worst case scenario for an OWT in medium depth water (20-30m).

Since it can be difficult to produce p-y curves describing the effects of the plate on the overall performance and to differentiate the hybrid foundation from pile cap, a new normalization study is proposed to investigate whether the lateral capacity can be described by only the L/D ratio, a combination of L/D and normalized stiffness of monopile or by the plate width. Specifically, the normalization procedure considered normalizing the lateral ultimate capacity by the pile's/plate diameter and by the soil shear strength considering the effects of soil profile and pile/soil relative rigidity given by E_p^*/E_{50}, where E_p^* is the foundation normalized stiffness and E_{50} is the soil elastic modulus at 50% of ultimate deviatoric loading causing failure. Design charts are established to

develop the HF and MP lateral ultimate capacity considering L/D(Lp/W) and E_p^*/E_s ratios. Finally, the performances of MP and HF at the serviceability limit state were compared.

3.2 **Methodology**

Displacement controlled pushover analyses of both systems were done in various geometric and ground conditions and the lateral ultimate capacity was determined as either the maximum reached load or the load causing yield stresses in the structural elements. A new normalization method was utilized where the lateral capacity of both systems is divided by the shear strength and the diameter of pile's/plate to study monopile's lateral ultimate capacity and to explore whether hybrid foundations lateral ultimate capacity can be fit within the same framework. To eliminate the diameter effect on the results, a normalized foundation stiffness parameter is used. The effects of footing rigidity on the lateral ultimate capacity of monopiles and hybrid foundation is studied, and generic curves are established relating the ultimate lateral capacity of the foundation with respect to L/D or (Lp/W) and the foundation normalized stiffness E_p^* given by:

In particular, the effects of footing rigidity, termed E_p^*, with respect to soil stiffness, E_{50}, is investigated.

$$E_p^* = \frac{E_p I_p}{I_{scp}} \tag{3-2}$$

E_p^*: normalized stiffness of pile; E_p: Young's modulus of pile material; E_s: Elastic modulus of soil; I_p: Pile second moment of inertia; I_{scp}: moment of inertia of a solid cross-section pile of same diameter as the actual pile.

Three-dimensional (3D) finite element models (FEMs) were conducted to simulate the MP and HF foundations. Tetrahedron 10 node elements were used to discretize the soil while beam elements were used to discretize the tower and the pile. Solid zone equivalent to pile's diameter was used to take the pile geometry into consideration. To account for slippage and gap formation,

6 node interface elements were used to simulate contact between solids zone and soil. The strength of the interface elements was defined through a reduction factor, R_{int}, applied to the soil properties, which varied between 1 and 0.3 for soft and stiff soils, respectively.

The HF plate was discretized using plate elements with elastic nonporous material model with E, ɣ and thickness values of 27800 MPa, 23.6kN/m^3, and 2m, respectively. The tower was simulated as a beam element having unit weight, diameter, E and thickness of 77kN/m^3, 6m, 200GPa and 0.035m, respectively. It is rigidly connected to surrounding solid elements to ensure the load is transferred uniformly over the pile area. In all models, x and y boundaries were set at 7D from model center and restricted to move horizontally while allowed to move vertically. The bottom, z, boundary was fixed and placed at least 3D below pile tip to avoid any boundary effects and to model rotational stiffness correctly. The FEM had on average 25000 elements.

The soil behaviour was simulated employing the hardening soil (HS) model obeying Mohr-Coulomb (MC) failure criterion (Schanz 1998). The HS model can simulate the behaviour of both soft and stiff soils. It accounts for the stiffness stress dependency, allows plastic straining due to deviatoric and primary compression loading and can simulate the unloading stiffness being higher than loading stiffness, hence accounting for plastic straining before failure is reached. The clay behavior is accounted for by considering effects of two strain hardening; namely volumetric hardening (cap) and shear where contraction and densification cause the yield surface to expand. The soil stiffness parameters in the HS model can be determined as follows.

$$E_{oed} = E_{oed,ref}\left(\frac{c\cos\boldsymbol{\phi} - \frac{\sigma_3'}{k_o^{NC}}\sin\boldsymbol{\phi}}{c\cos\boldsymbol{\phi} + \boldsymbol{p_{ref}'}\sin\boldsymbol{\phi}}\right)^m \tag{3-3}$$

$$E_{50} = E_{50,ref}\left(\frac{c\cos\boldsymbol{\phi} - \sigma_3'\sin\boldsymbol{\phi}}{c\cos\boldsymbol{\phi} + \boldsymbol{p_{ref}'}\sin\boldsymbol{\phi}}\right)^m \tag{3-4}$$

$$E_{ur} = E_{ur,ref}\left(\frac{c\cos\phi - \sigma_3' \sin\phi}{c\cos\phi + p_{ref}' \sin\phi}\right)^m \quad (3\text{-}5)$$

The analysis involved four stages, including: Initial stage (initiation of geostatic stresses) in which equilibrium is established based on lateral earth pressure coefficient at rest, k_o; Construction stage in which all structures and interface elements are activated; Loading stages: where displacement-controlled loading is applied until failure is reached; and finally the Output stage at which the structural forces and soil deformation are examined to establish the failure load.

A convergence analysis was conducted to define models' boundaries. Boundaries were restricted horizontally and allowed to move vertically while the bottom boundary was distanced more than (3D) to ensure that rigid boundary will not affect stress/strain distribution and was assigned fixed in all directions x, y, and z. on average, around 25000 elements were used, and medium mesh size was considered after performing sensitivity analysis. Figure 3-3 and 3-4 show the meshing developed for one of the cases.

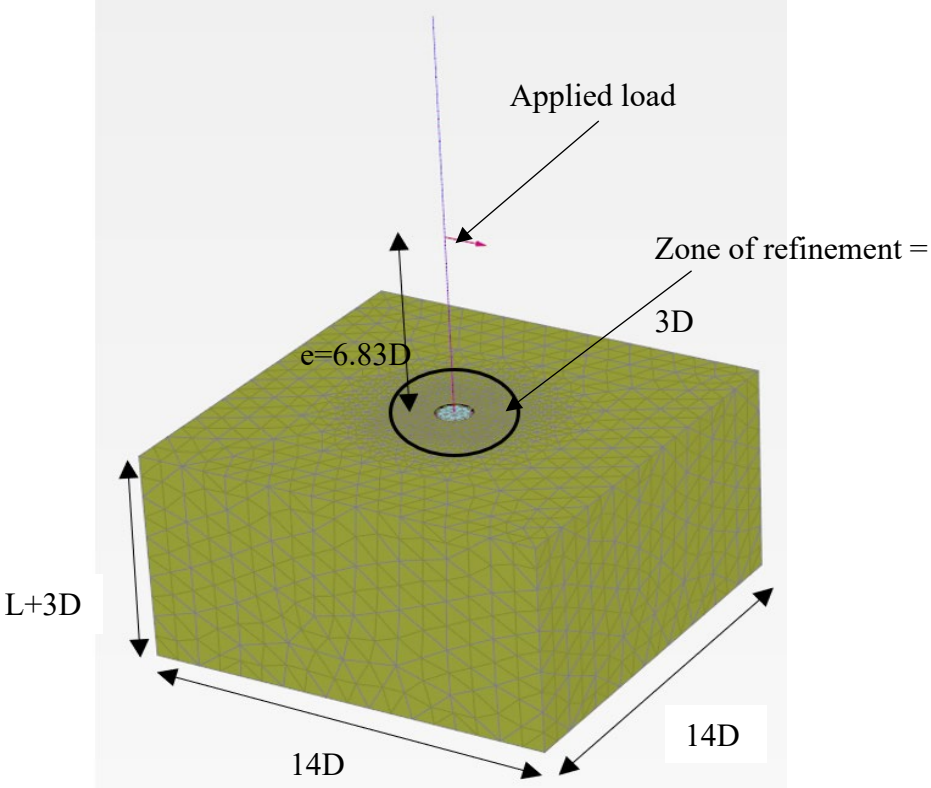

Figure 3-3 Developed mesh and location of lateral point load

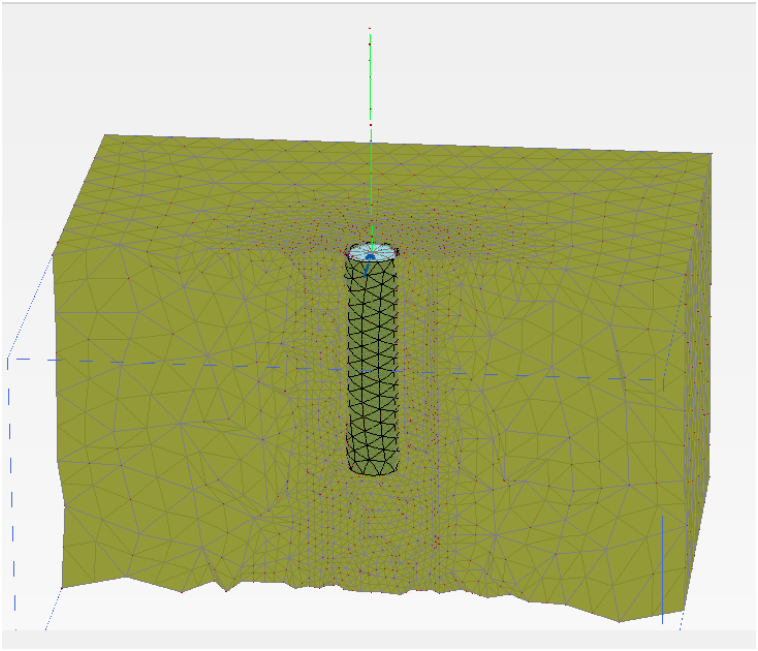

Figure 3-4 Cross section showing developed mesh

3.2.1.1 Verification

The FEM model was bench marked using a case study of field tests carried out on a 2.2 m diameter open ended pile driven offshore China (Zhu et al., 2017). The pile has a thickness of 0.03m and a depth of 57.4 m below seabed. Soil was characterised by mechanical cone penetrometer (CPT) equipped with soundings for shear wave velocity. Tip resistance was converted to S_u values using equation (3-6).

$$S_u = 0.07q_c+2 \tag{3-6}$$

S_u profile was checked with the equation by retrieving soil samples and doing CIUC tests and results plot well on the S_u profile validating the use of the equation 3-6. Figure 3-6 shows the S_u profile and OCR with depth while Figure 3-7 shows ko with depth.

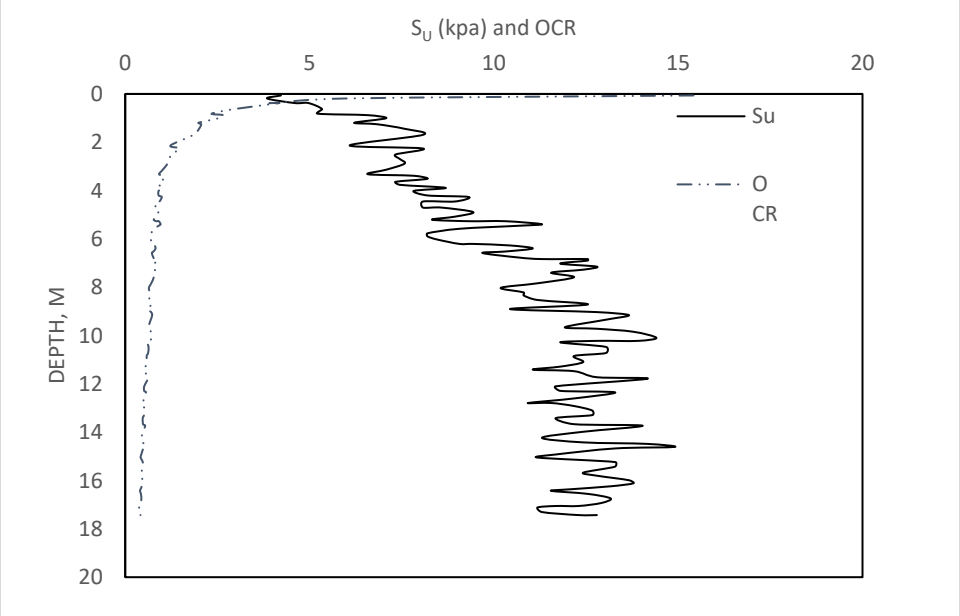

Figure 3-5 Su and OCR profile of case study (Zhu et al., 2017)

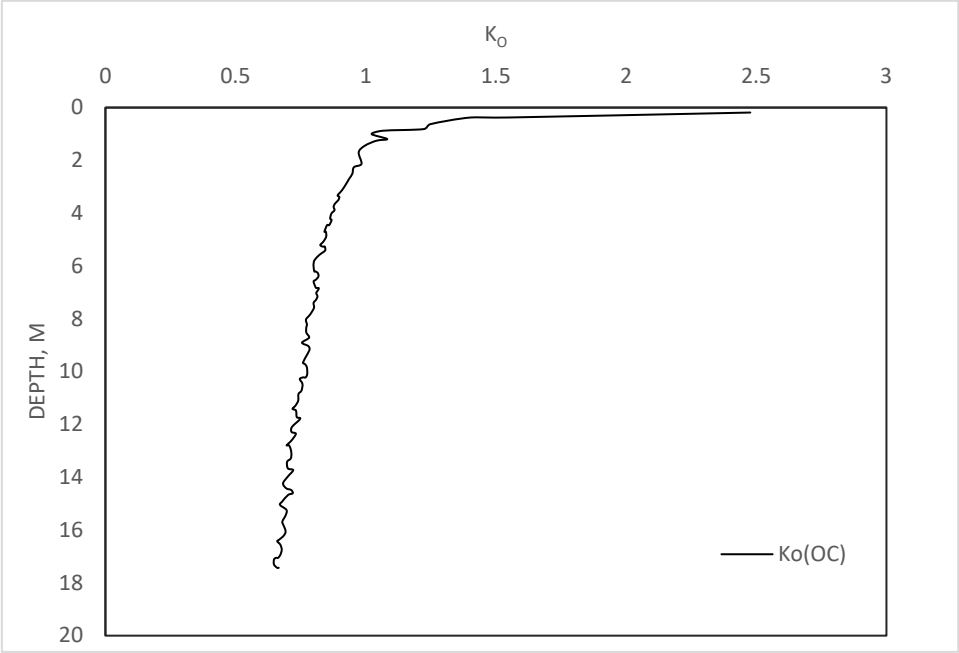

Figure 3-6 k_o of field test profile

3.2.1.1.1 ***Volume pile***

The model pile from the case study was modelled using volume pile. Due to lack of drained soil parameters from the case study, Hs constitutive relationship "undrained B" was adopted to model clay and underlaying sand and plate elements to model pile (elastic material) as a first order approximation. The soil data used in the analysis were calibrated using the load displacement curve for the field tests and were tuned until a best match was obtained. At first, the data from original paper contained scares information and rudimentary model using Hs undrained B with E_{50}, E_{oed} values of 2200 kPa and E_{ur} value of 6600 kPa. A Hydraulic Jack applied lateral load at 12.64 m above ground level. Figure 3-7 shows the developed mesh for this first order model, medium mesh with local refinement zone of 3D around pile, giving 45000 elements produced best fit. The clay can be considered to be N.C clay for the top 10 meters with thin crust of about a meter with OCR of about10. Below 10 meter the shear strength stays constant at about 13kPa, making it below

SHANSEP strength predictions (eqn.3-7) and hence the clay can be considered under consolidated. Figure 3-8 shows the load displacement curves of the field and FEM constructed using Plaxis 3D with Hs "undrained B" as a constitutive relationship. It can be seen that the developed mesh results in excellent match between load displacement curve at loading point and elastic deflection lines from inclinometer measurements. Figure 3-9 also shows the deflection of pile at different load levels giving excellent results compared to original data from Zhu et al. (2017). Results obtained in Figure 3-8 and 3-9 indicate the first order model gave good match between field test results and FEM.

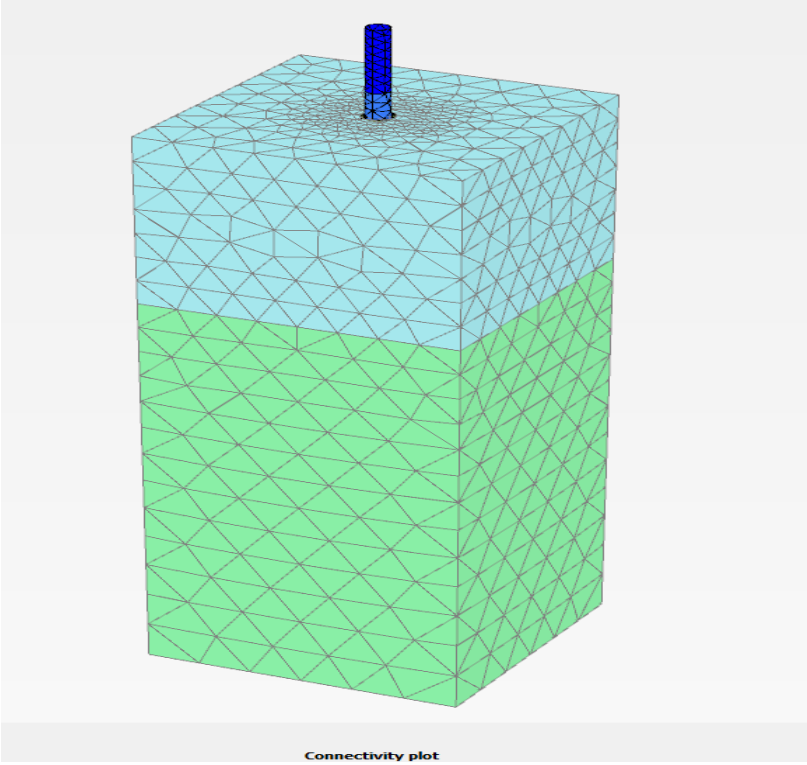

Figure 3-7 developed mesh

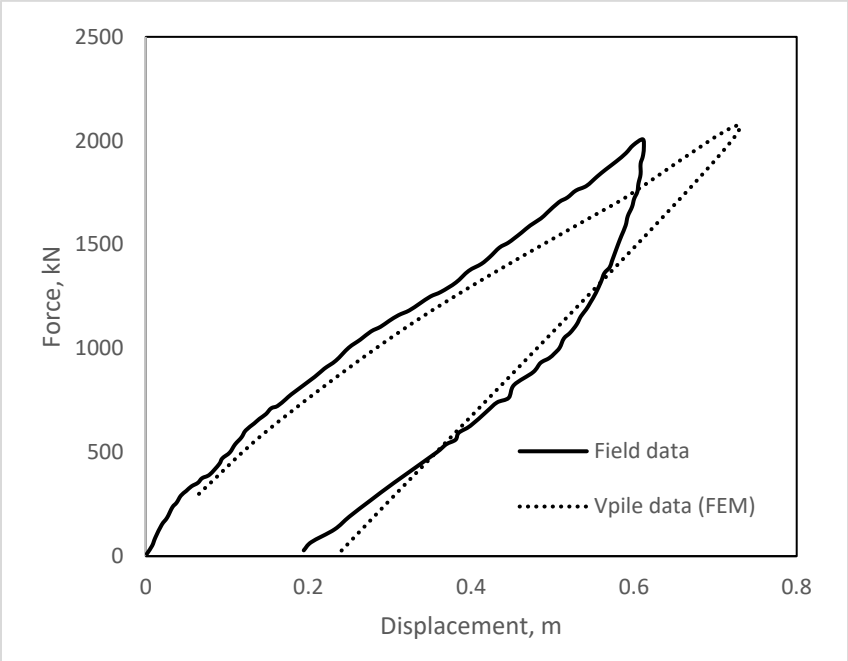

Figure 3-8 force displacement curve at loading point

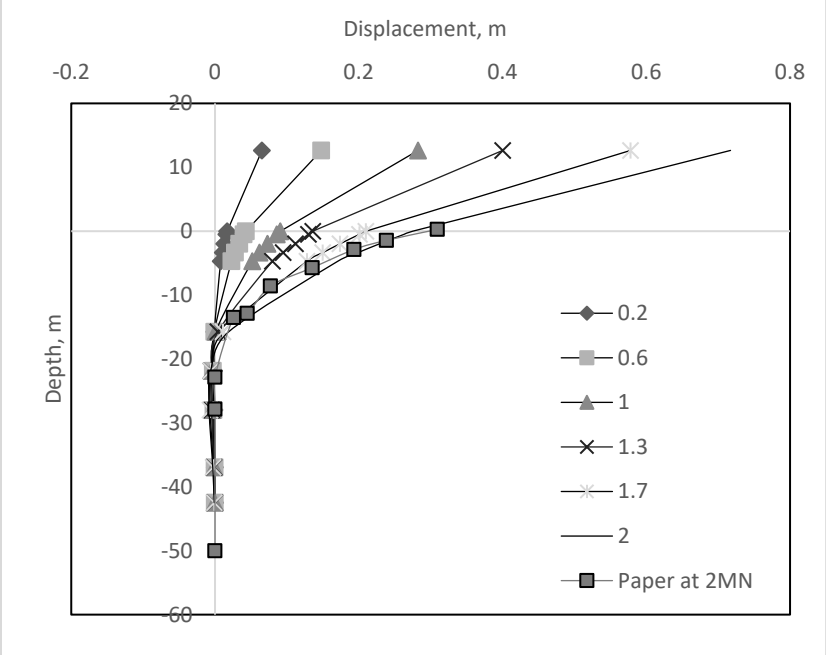

Figure 3-9 elastic line of structure at different loads (matching well with field data)

3.2.1.1.2 *Embedded beam pile within solid zone of 1D*

Because it was not possible to get the bending moment data from volume pile in Plaxis 3D and because this information is required to proceed with 3D FEM parametric studies, it was necessary to use a structural element from which the bending moment is obtained directly for efficient use of time. Hence, embedded pile elements surrounded by solid elastic material (nonporous circular pile) with EI value equivalent to EI value of real condition and same diameter were used. The embedded beam element had same I value of pile but was assigned E value 10^6 time less than that of the solid zone used to ensure the beam deflects with the solid zone. Rigid plate was applied at the mudline to ensure both the embedded beam and the solid zone are rigidly bonded. The output bending moment values are multiplied by 10^6 to obtain the actual B.M (Dao, 2011). The results indicated excellent displacement and B.M match with field data, although the field data are always higher than the embedded beam data, but shown trend is in excellent agreement. Hs constitutive relationship (undrained B as in volume pile) was used to model clay and underlaying sand and number of elements used is around 45000 elements (medium with refined zone of 3D around pile with 0.2 refinement factor). Figure 3-10 shows the load-displacement curve and displays the B.M profiles for various load steps against field data, excellent match is obtained as can be seen.

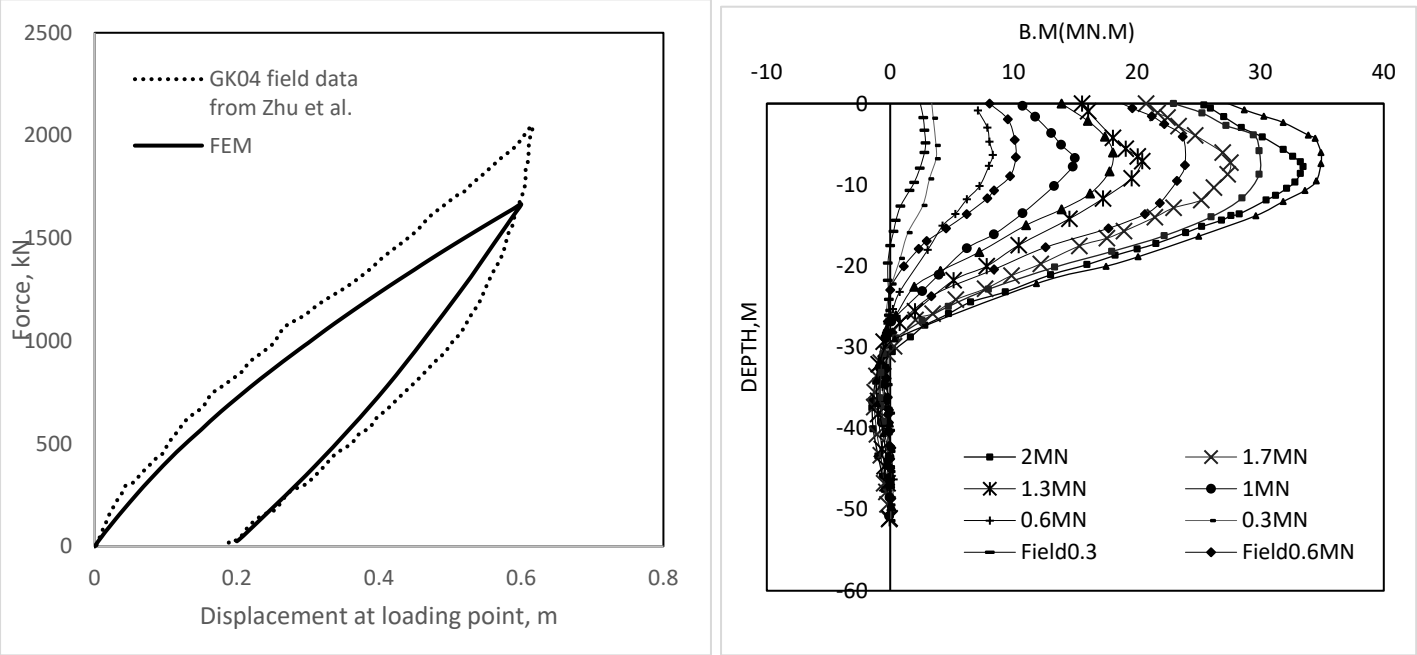

a) b)

Figure 3-10 a) load displacement curves of field and FE with embedded beam model b) Bending moment data versus field data at different loads

3.2.1.1.3 ***Further refinement and derivation of drained parameters (Undrained A)***

As can be seen in Figure 3-5, idealizing the soil profile using one layer will be a significant simplification. The Hs model, for instance, would have a parabolic relationship between E_{50}, E_{oed} and E_{ur} with depth, similar to the S_u profile. Nonetheless, the profile constructed within the program will depend on the correctness of the input K_o. To developed effective strength parameters to closely match the shear strength profile of the paper and yield best fit data, measured G_o data versus depth from field tests and S_u versus depth were used to calibrate the soil profile. The procedure involved changing the soil friction angle and the cohesion intercept until match is obtained with CPTu profile. Simultaneously, the m exponent is adjusted to match the G_o profile with that of field measurements. The E_{oed}^{ref} of the developed model was taken to be approximately $1.25E_{oed}^{ref}$, E_{ur}^{ref} was approximately $3E_{50}^{ref}$. Equations 3-7 until 3-11 along with equation 2-39 were

used to do so.. Table 3-1 shows the soil parameters used to model the case study, Hs"undrained A" is used to model clay behavior. Figure 3-11 displays the S_u, Go K_o and OCR profiles.

$$\tau \text{ (SHANSEP)} = C^* \sigma'^{A} \tag{3-7}$$

where C* and A are factors, C is between 0.19-0.29 and A is around 0.8

$$K_{0,NC} = 0.42+0.004PI \tag{3-8a}$$

$$\text{Alternatively } K_{o,\,NC} = 1 - \text{Sin}\phi' \tag{3-8b}$$

Where;

$$K_o = K_{0,NC} * OCR^{0.4} \tag{3-9}$$

The shear strength profile can be converted to an effective profile, it can be seen that when c' is chosen to be the S_u at ground surface then the friction can be derived from.

(Vertical effective stress);

$$\tau = c' + \sigma'_1 \tan\phi' \tag{3-10}$$

(Horizontal effective stress);

$$\tau = [(c'\cot(\phi') - \sigma'_3)*\frac{2\sin(\phi')}{1-\sin(\phi')}]/2 \tag{3-11}$$

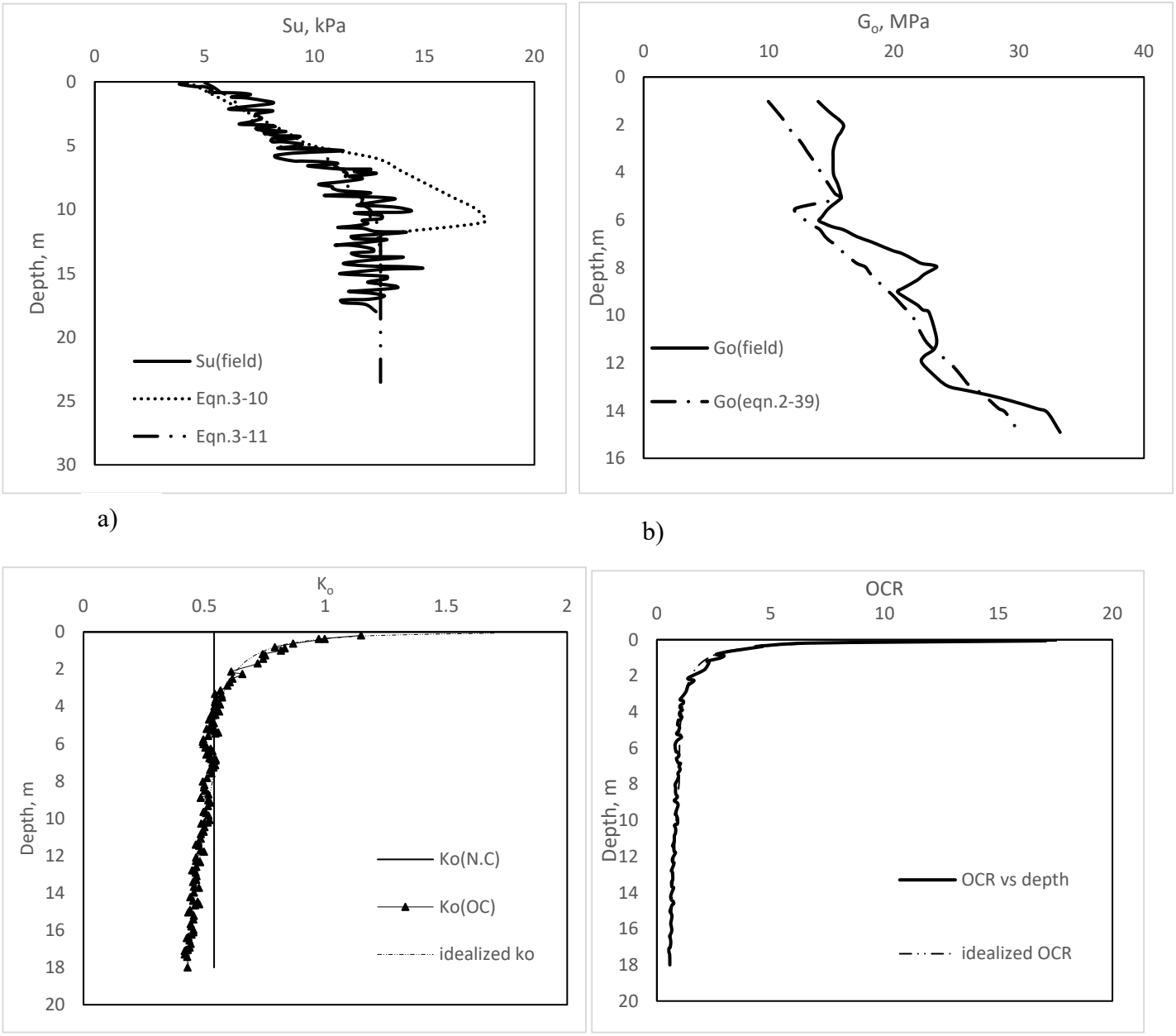

Figure 3-11 a) Su b) G_o profiles used to calibrate model drained parameter against field profile c) K_o profile and d) OCR profile

Table 3-1 Model parameters

Parameter	clay1	clay2	clay3
c'	4.23	6	13
Ψ	0	0	0
φ'	8	8	0
p'_{pop}, kPa	15	15	15
p'_{ref}, kPa	41	71	100
$e_{ini.}$	4.23	3.285	3.285
ɣ, kN/m^3	17.9	15	15
E^{ref}_{oed}, kPa	1406	2000	2000
E^{ref}_{50}, kPa	1758	2500	2500
E^{ref}_{ur}, kPa	5000	7500	7500
v_{ur}	0.2	0.2	0.2
M	0.6	0.8	1
PI, %	30	31	32
$K_{o, NC}$	0.86	0.86	0.87
R_f	0.9	0.9	0.9
Depth, m	0-5	5-10	10-24.5
Type of analysis	Undrained A	Undrained A	Undrained B

Using data from table 3-1, the load-displacement curve obtained is plotted in Figure 3-12 along with field data, excellent match was hence obtained.

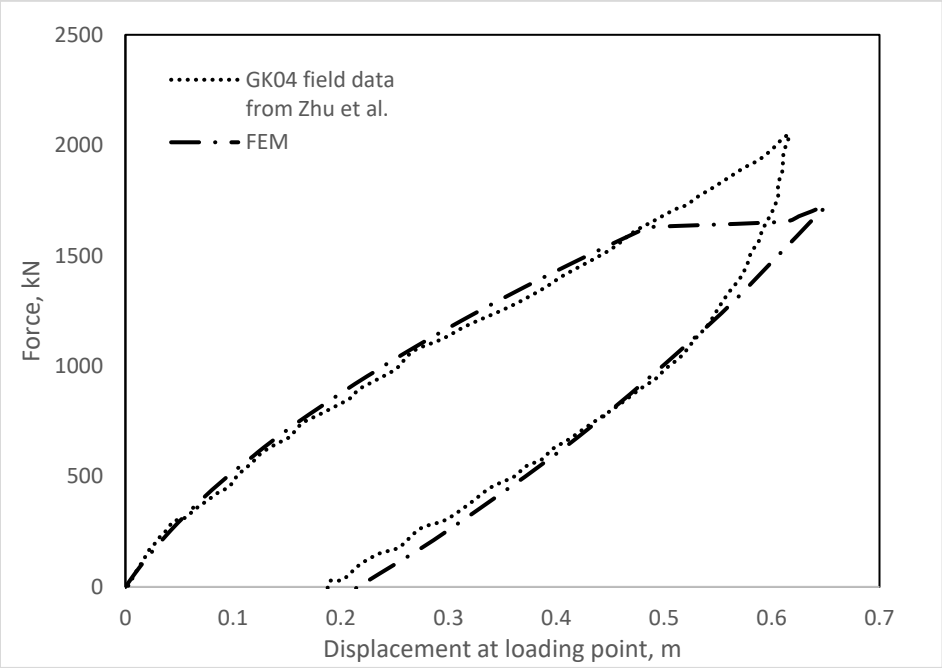

Figure 3-12 Load displacement curve using Hs undrained A parameters

3.2.1.1.4 ***Convergence study***

Once the final set of soil parameters were defined, the convergence analysis was carried out. The parameter variation study conducted contains varying geometry and for this reason convergence analyses were undertaken first to define the reference geometry and mesh size that will be followed in the parametric analysis. Figure 3-13 explains the dimensions studied herein.

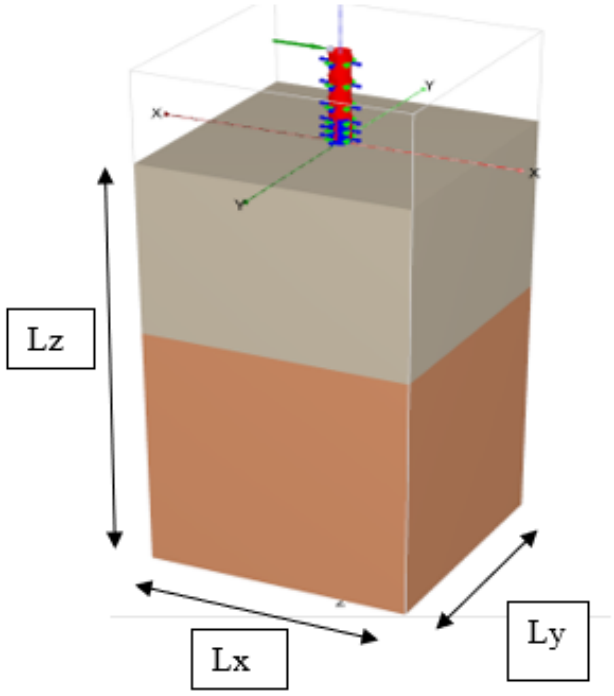

Figure 3-13 Boundary conditions varied in convergence analyses

In all analyses considered, global element size was chosen to be medium, a refinement zone of 3D, 5D, and 7D were conducted with changing coarseness factor, cf. Figures 3-18 until 3-22 show the results from convergence analyses.

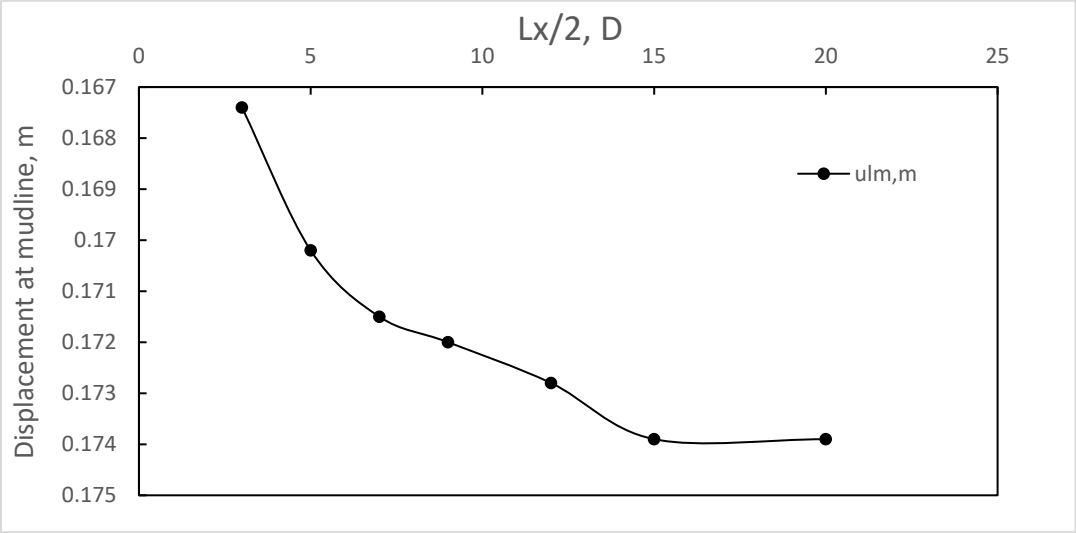

Figure 3-14 Effects of half length along load application direction on the displacement at mudline

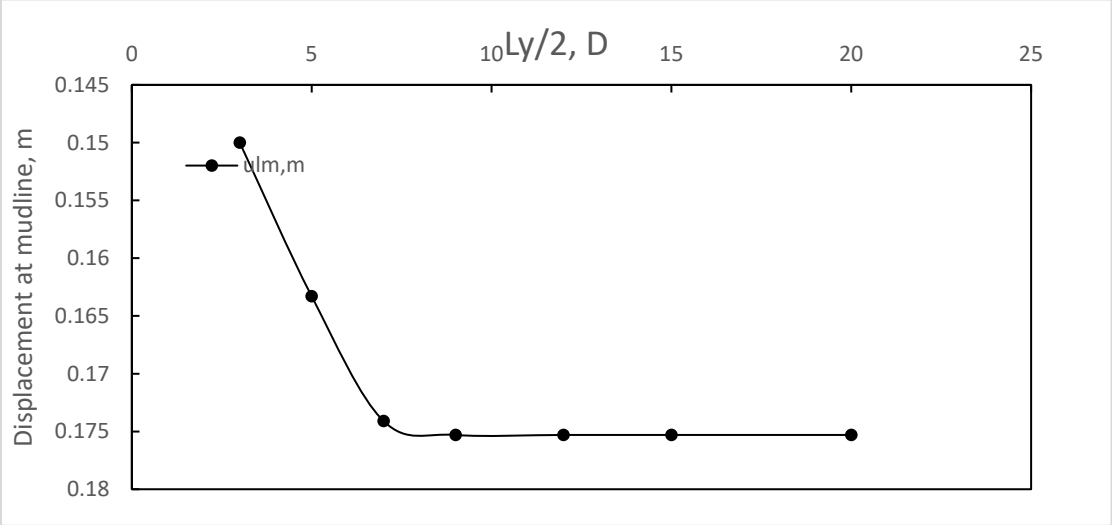

Figure 3-15 effects of $L_y/2$ on results accuracy

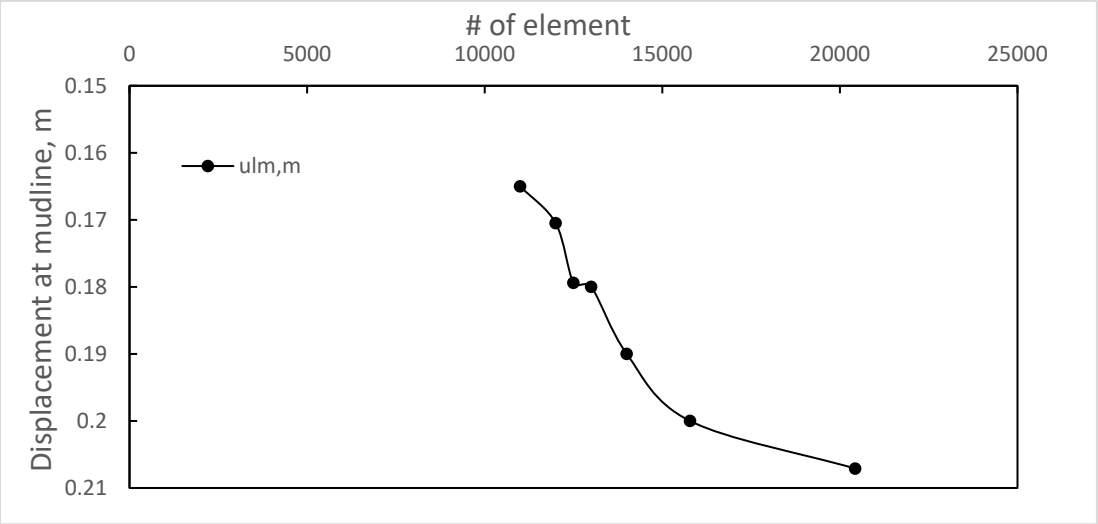

Figure 3-16 refinement zone of 3D around pile extending till model bottom boundary

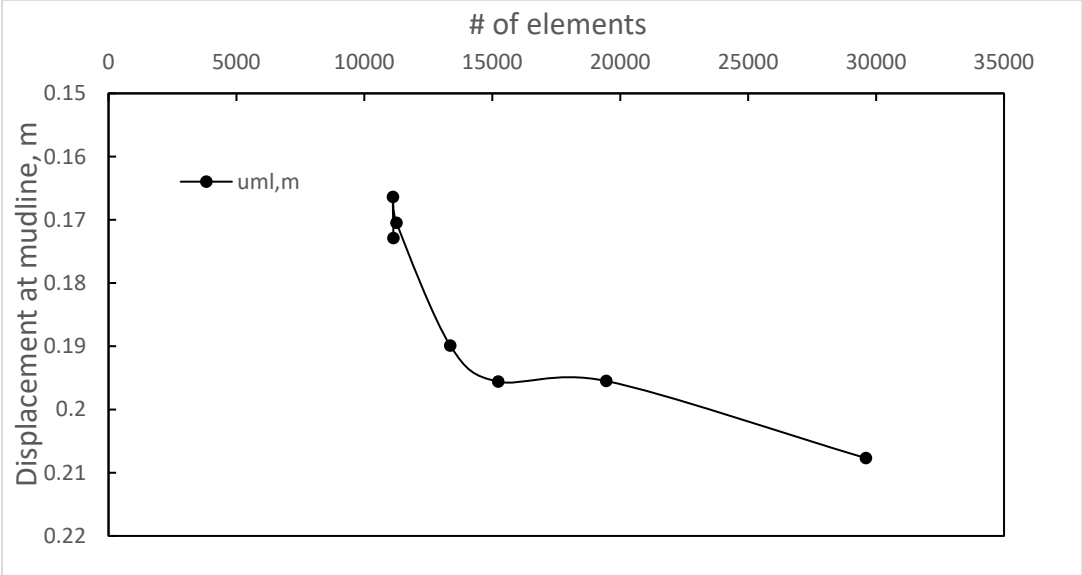

Figure 3-17 refinement zone of 5D around pile extending till model bottom boundary

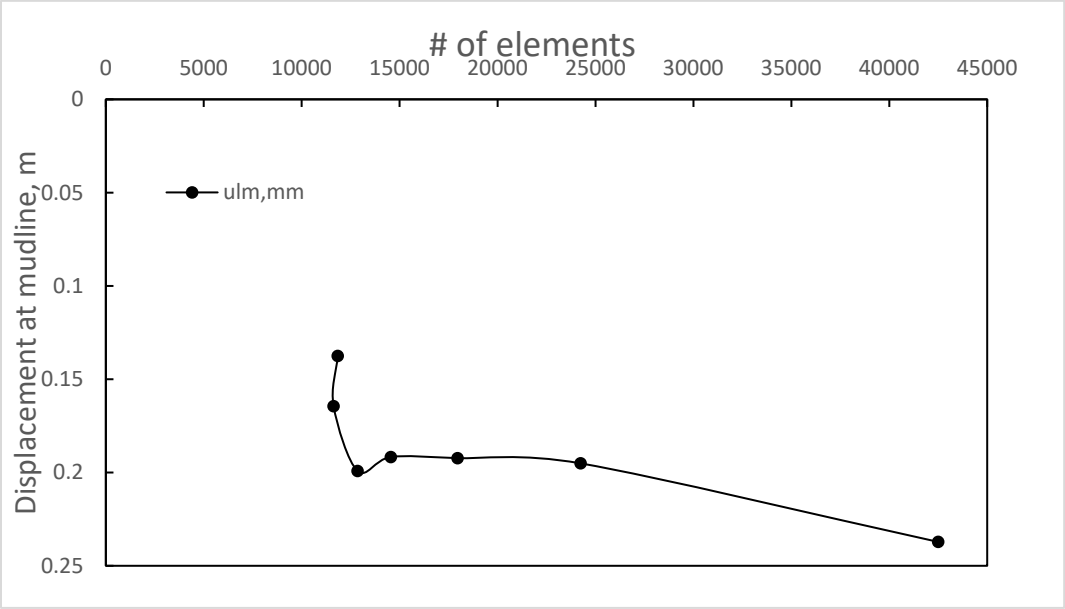

Figure 3-18 refinement zone of 7D around pile extending till model bottom boundary

Based on the convergence analyses, the selected boundary conditions are 7D in x,y from pile centerline in all directions with refinement zone of 3D and refinement factor of 0.2 yielding approximately 25000 elements. This range in good agreement with data reported by Lai et al. (2020).

3.3 Finite element modelling

A hybrid foundation system comprising a plate at mudline fitted with a pile in its center is studied as an alternative to monopile (MP) in different clayey bed. The (HF) system is compared with monopile (MP) for their ultimate capacity and their response under 2MN loads. All systems are studied under similar loading eccentricity and diameter of tower to thickness ratio, D_p/t, of 85. The vertical loads on the HF and MP comprised Rotor and Nacelle Assembly, RNA, mass and tower own weight. The tower thickness was 0.035m and its dimeter was considered constant at 6m throughout its 90 m height. The tower was rigidly connected to the plate and pile. The lateral load

was applied at eccentricity, e = 41m above mudline, (i.e. $e/D_t = 6.83$). MP diameter was selected to be 6 m while H.F plates as 14m in diameter with 4m pile embedded in its centerline. Monopile length was varied from 20-80 m while hybrid system pile was varied from 0 (S.F or GBF), 14 and 28m, L_p/W of 1 and 2, respectively. Figures 3-19 shows the two systems under consideration. Displacement controlled loading was applied until either geotechnical or structural failure has happened.

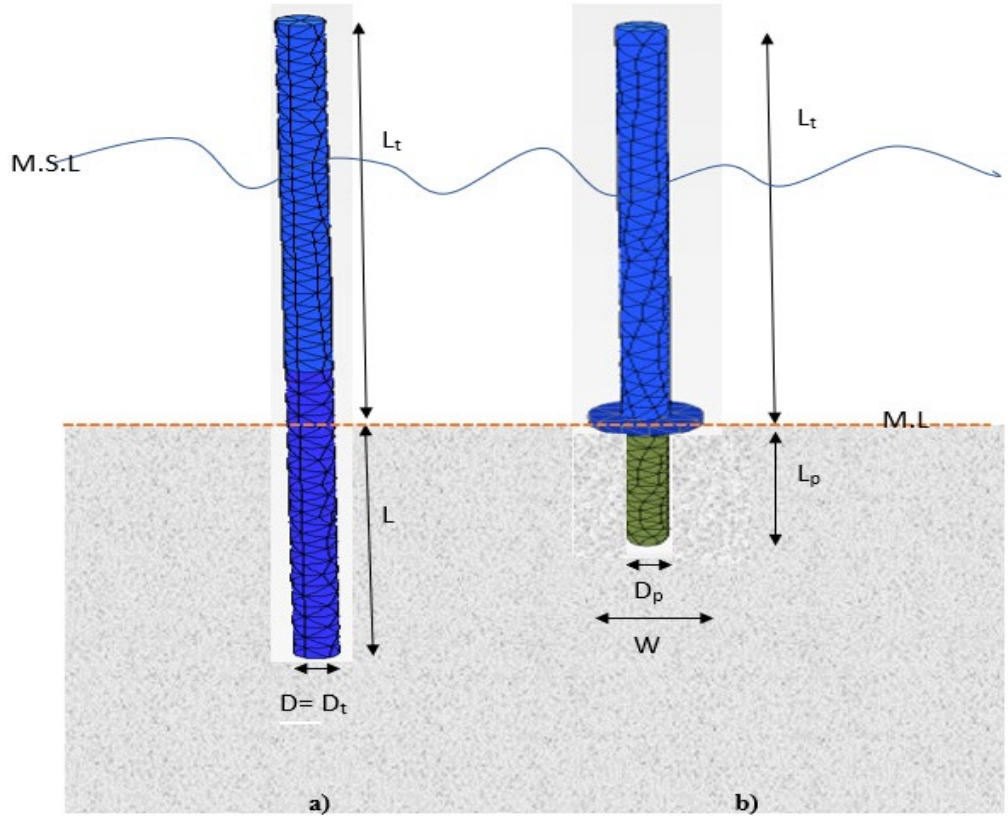

Figure 3-19 a) Monopile of D_p = 6m b) Hybrid foundation system with W=14m and D_p=4m. (Not to scale)

3.3.1 *Parameter analyses*

In total, 60 finite element models were carried out utilizing the commercial code PLAXIS 3D. Six types of soils were considered covering a wide range of soils encountered in practise as listed

in Table 3-2. Monopiles with diameter D = 6m and embedded length L = 20 m to 80 m were analyzed. In addition, HF with plate diameter, W = 14 m and center pile with embedded depth of 14 m and 28 m were analyzed. In all cases, the load is applied above the seabed elevation with eccentricity e = 6.8 D_t where D_t is the tower diameter. Table 3-2 shows the considered soil profiles while Table 3-3 shows the foundation geometry.

Table 3-2 Properties of clay profiles considered in the analysis

Parameter	clay1	Clay2	Clay3	Clay4	Clay5	Clay6
c'	4.23	24	44	87	170	354
Ψ	0	0	0	0	0	0
θ'	8	10	10	10	10	10
p'_{pop}, kPa	13	51	83	140	240	414
p'_{ref}, kPa	41	100	100	100	100	100
$e_{(ini).}$	4.209	4.209	4.209	4.209	4.209	4.209
ɣ, kN/m^3	17.9	17.9	17.9	17.9	17.9	17.9
E_{oed}^{ref}, kPa	1406	3461	14747	29040	56628	113134
E_{50}^{ref}, kPa	1758	4000	18439	36310	70805	141457
E_{ur}^{ref}, kPa	5000	10000	52444	103271	201380	402326
v_{ur}	0.2	0.2	0.2	0.2	0.2	0.2
M	0.6	0.6	0.6	0.6	0.6	0.6
PI	30	30	30	30	30	30
K_o, NC	0.54	0.54	0.54	0.54	0.54	0.54
Depth, m	0-25	0-26	0-27	0-28	0-29	0-30
R_f	0.9	0.9	0.9	0.9	0.9	0.9

In all FE models the procedure in 3.2.3.2 was followed with displacement-controlled loading until tower tip displacement reached a certain value. The failure was determined to be either

geotechnical or structural after examining output data and checking if applied load generates yielding conditions at mudline, if so, the lateral ultimate capacity is taken as the linear average between the two values on the other sides of the value causing structural capacity failure using linear interpolation theory.

Table 3-3 3D analyses conducted on the proposed foundation system

L, m	L/D/(L_p/W)	Foundation system	e/D_t	V, kN
20	3.33	Monopile	6.83	Own weight[1]
30	5		6.83	
40	6.67		6.83	
50	8.33		6.83	
60	10		6.83	
70	11.67		6.83	
80	13.33		6.83	
0	0	Hybrid	6.83	
14	1		6.83	
28	2		6.83	

L: Depth of embedment; D: Pile's diameter; e: eccentricity of applied loads(m); D_t: Tower's diameter; [1]: uniformly distributed

3.3.1.1 Monopile lateral ultimate capacity

Figure 3-20 shows the normalized ultimate capacity versus the normalized stiffness for the MP models. The normalized capacity varies linearly with increase in normalize stiffness and reaching a plateau at E_p^*/E_s of 984 for cases of L/D equal or less than 5. For cases involving L/D ratio more than 5, the normalized ultimate capacity varied in trilinear trend.

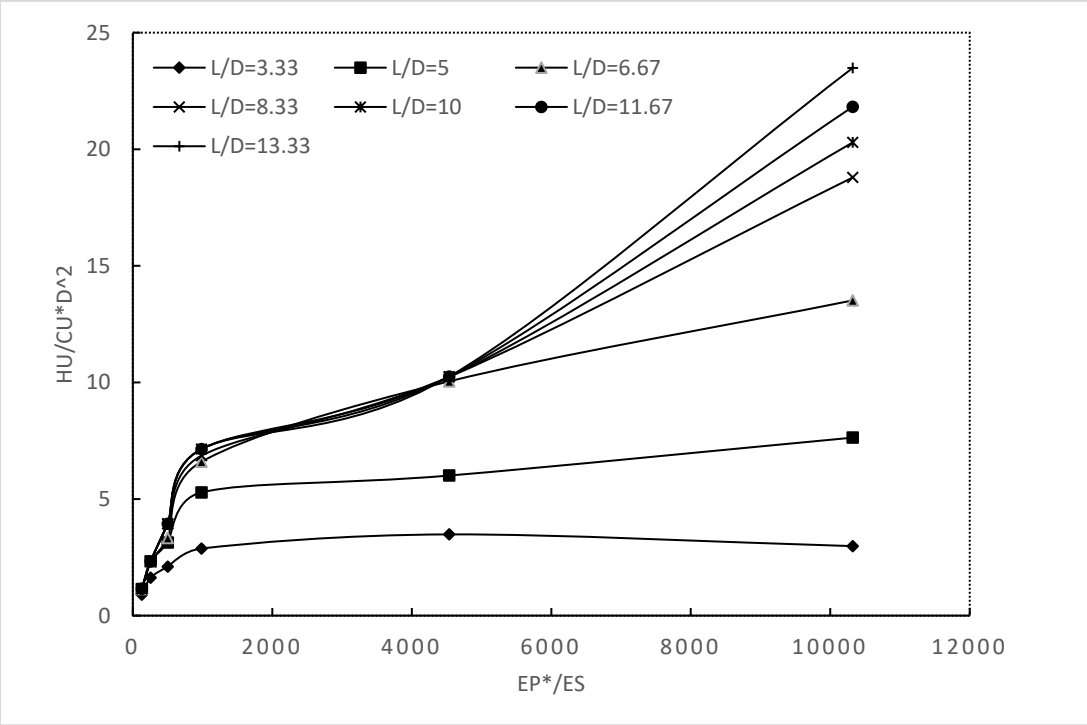

Figure 3-20 Effects of relative rigidity on normalized ultimate lateral load

For a given E_p^*/E_{50} ratio, the change of normalized ultimate capacity with different L/D ratio differs significantly between E_p^*/E_{50} of 10250 where 'rigid' response was observed for all L/D ratio and for E_p^*/E_{50} value of 127 where flexible pile response was observed. This can be explained by looking at the variation of normalized ultimate capacity versus L/D ratio for all soil profiles considered as shown in Figure 3-24. In Figure 3-21 it is shown that for a stiff clay site (E_p^*/E_{50} of less than 499), the pile lateral capacity reached a maximum at L/D ratio of between 5-8. For soft clay sites, the capacity increases for all L/D ratios.

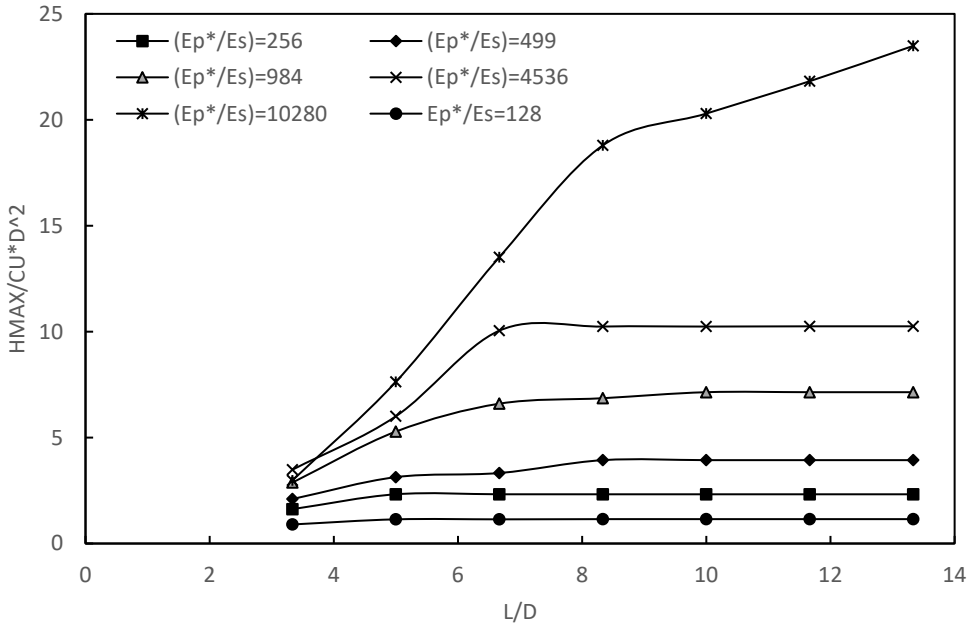

Figure 3-21 Normalized ultimate lateral capacity versus L/D for different soil profiles considered

3.3.1.1.1 ***Monopile bending moment at lateral ultimate capacity***

Examining the bending moment (B.M) profiles for MP at the lateral ultimate capacity can be helpful and supports the conclusions drawn from previous section. Figures 3-22 and 3-23 show the bending moment profiles for two soils, namely soil 1 and 6 considered in this study. In Figure 3-22, the B.M profile against normalized depth is plotted for different pile lengths in soft clay just before max reached loads (S_{uo} =4.2 kPa). As expected, the pile behaves rigidly in all cases with pile showing toe kick in behavior and zero B.M at pile tow. In contrast, the pile behaves rigidly for small L lengths up to 40 m and starts to show negative moment when the soil profile is stiff as shown in Figure 3-23 (S_{uo} = 354 kPa).

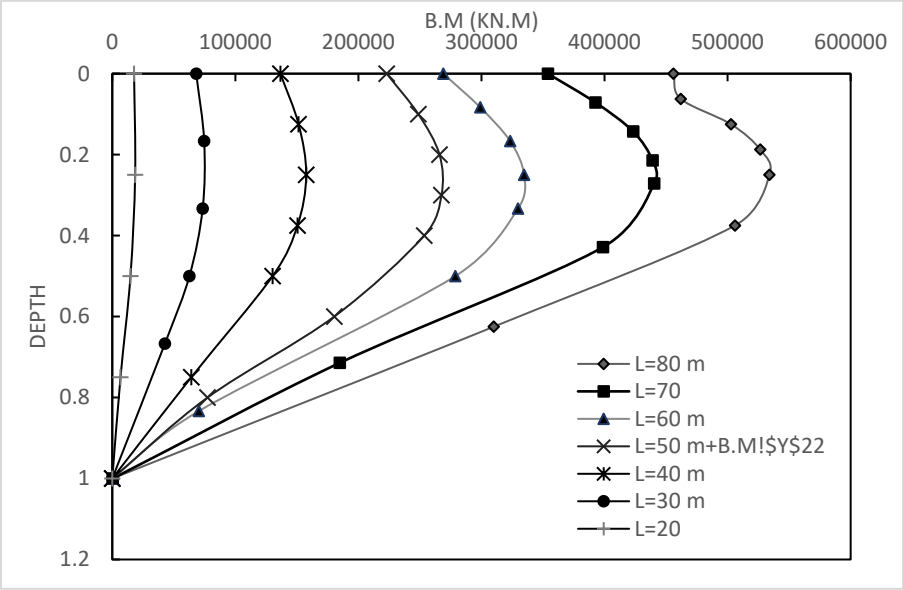

Figure 3-22 B.M versus normalized depth for soft soil (s_u=4.23 kPa) profile at or just before ultimate capacity was reached

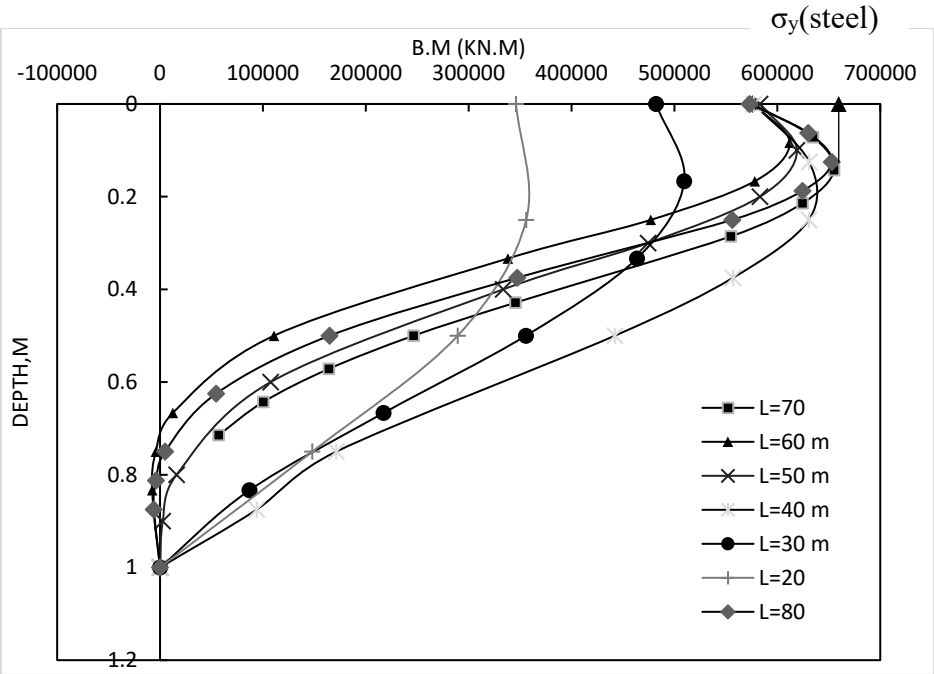

Figure 3-23 B.M versus normalized depth for stiff soil (clay6) profile at or just before ultimate capacity was reached

3.3.1.1.2 ***Fitting equations for determining lateral ultimate capacity for monopiles***

Using best fit curves for the data in Figure 3-21, one can obtain the following equations for determining lateral ultimate capacity of monopiles for various E_p^*/E_{50} ratios between 10280 and 128 and L/D ration between 3.33 and 13.33 for the case of e/d of 6.83 (medium water depth worst case scenario). Equations 3-12 till 3-17 describe ultimate capacity of MP in clayey medium. It can be seen that these equations produce excellent match with FE results in Figure 3-24 (regression values R between 0.9987 and 0.91).

For (E_p^*/E_{50} = 10280):

$$\frac{H_u}{C_u D^2} = -0.1897*(\frac{L}{D})^2 + 5.2326*(\frac{L}{D})-12.823 \qquad (R^2=0.9916)\ (3\text{-}12)$$

For (E_p^*/E_{50} = 4536):

$$\frac{H_u}{C_u D^2} = -0.1421*(\frac{L}{D})^2 + 2.9891*(\frac{L}{D})+4.8175 \qquad (R^2=0.949)\ (3\text{-}13)$$

For (E_p^*/E_{50} = 984):

$$\frac{H_u}{C_u D^2} = -0.0796*(\frac{L}{D})^2 + 1.6913*(\frac{L}{D}) - 1.5355 \qquad (R^2=0.9583)\ (3\text{-}14)$$

For (E_p^*/E_{50} = 499):

$$\frac{H_u}{C_u D^2} = -0.0315*(\frac{L}{D})^2 + 0.6905*(\frac{L}{D})+ 0.256 \qquad (R^2=0.9633)\ (3\text{-}15)$$

For (E_p^*/E_{50} = 256.3028):

$$\frac{H_u}{C_u D^2} = - 0.1203*(\frac{L}{D})^2 + 1.0909*(\frac{L}{D}) \qquad (R^2=0.9165)\ (3\text{-}16)$$

For (E_p^*/E_{50} = 128):

$$\frac{H_u}{C_u D^2} = -0.0014*(\frac{L}{D})^2 - 0.04*(\frac{L}{D}) + 0.3667 \qquad (R^2=0.9229)\ (3\text{-}17)$$

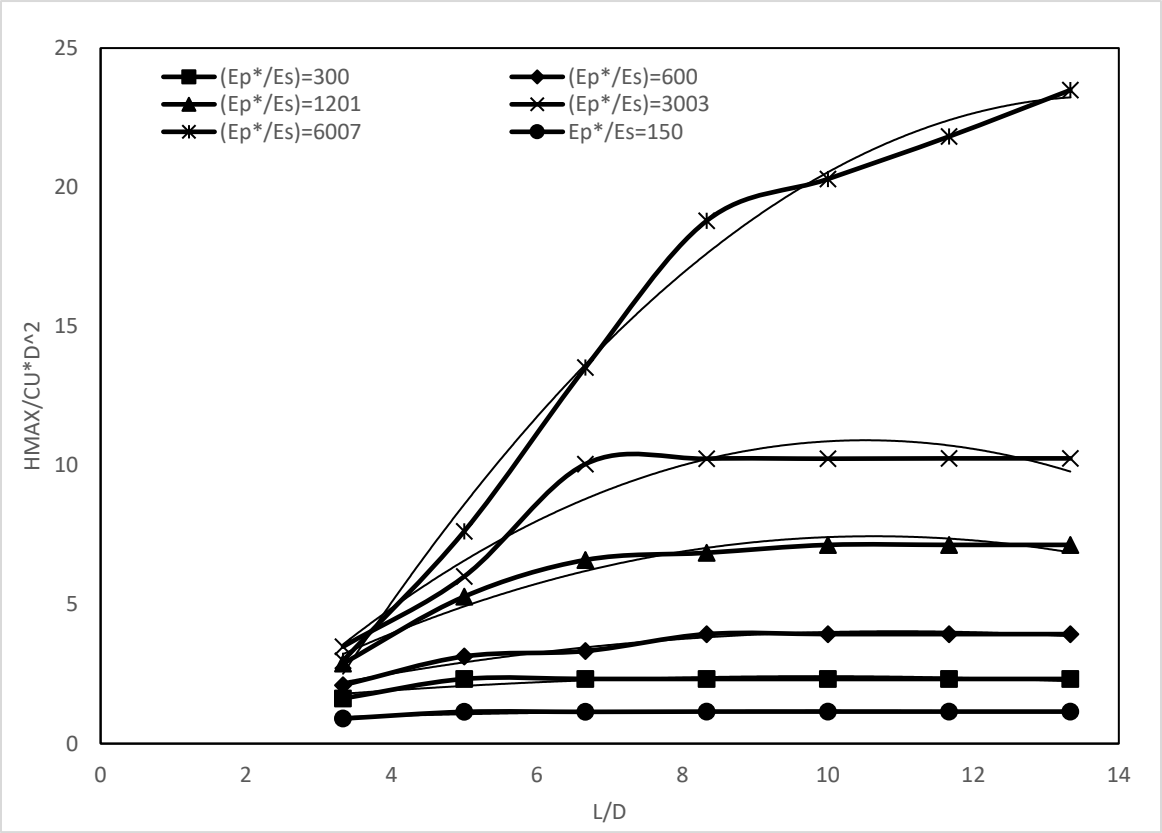

Figure 3-24 Fitting curves versus actual FEM results

3.3.1.2 Gravity base and hybrid Foundation lateral ultimate capacity

For GBF and H.F, the normalized ultimate capacity follows the same trend in MP foundations; however, the normalized capacity was not sensitive to pile dimeter but to the capacity of GBF. Hence, the lateral capacity of the hybrid foundations was compared to the base case ($L_p/W=0$; i.e., case of a GBF). Results showed the capacity of the system is substantially increased with addition of a pile with almost six-fold increase in lateral capacity for soft soil (S_{uo} = 4.2 kPa) while the trend of increase decrease with increase in shear strength of the soil profile. For the first two profiles, the lateral capacity increase for both L_p/W of 1 and 2 considered while for the other profiles the

increase was obtained for the first case only. This is because the yield moment capacity of the 4m diameter pile was reached for those cases.

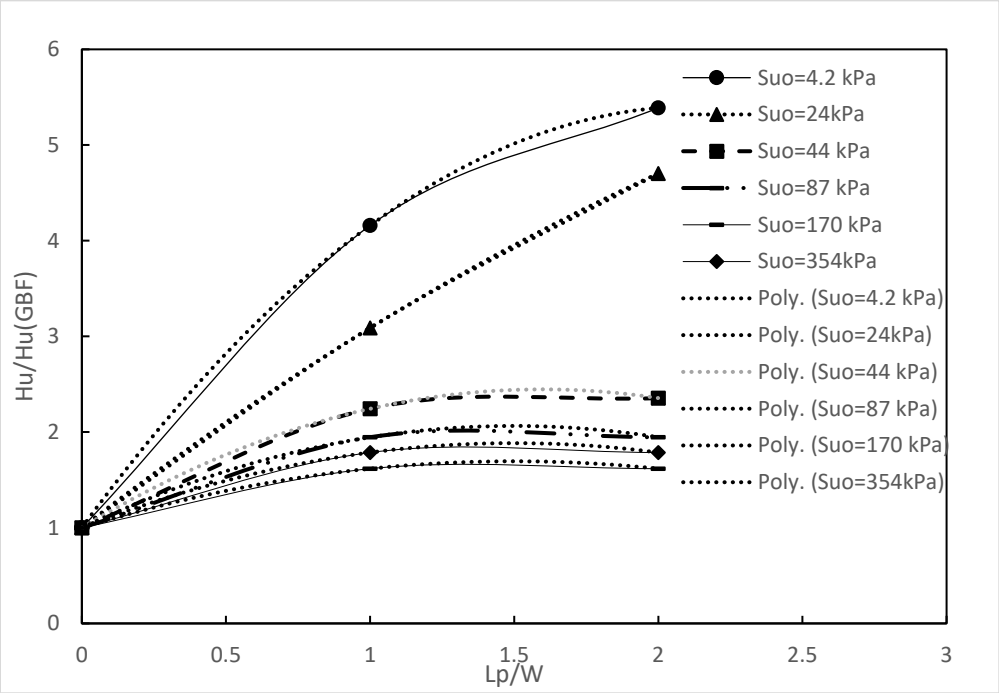

Figure 3-25 normalized ultimate capacity of H.F compared to GBF of 14m diameter.

3.3.1.2.1 ***Predictive equations for determining lateral ultimate capacity for H.F***

The lateral ultimate capacity of HF under eccentric loading value of e = 6.83D is considered here. This value of eccentricity is calculated for a 5MW offshore wind turbine installed in medium depth water. The results of ultimate lateral capacity of these structures under the considered eccentricity can be obtained by knowledge of limited soil parameters and HF geometry from the best fit equations provided herein. Equations 3-18 until 3-23 describe the hybrid foundation lateral ultimate capacity of these systems in different clay beds.

Clay1:

$$\frac{H_u}{H_{u,GBF}} = -0.3087\left(\frac{L_p}{W}\right)^2 + 0.9262\left(\frac{L_p}{W}\right) + 1 \quad (3\text{-}18)$$

Clay 2:

$$\frac{H_u}{H_{u,GBF}} = -0.3931\left(\frac{L_p}{W}\right)^2 + 1.1794\left(\frac{L_p}{W}\right) + 1 \quad (3\text{-}19)$$

Clay 3:

$$\frac{H_u}{H_{u,GBF}} = -0.4729\left(\frac{L_p}{W}\right)^2 + 1.4188\left(\frac{L_p}{W}\right) + 1 \quad (3\text{-}20)$$

Clay 4:

$$\frac{H_u}{H_{u,GBF}} = -0.5665\left(\frac{L_p}{W}\right)^2 + 1.8106\left(\frac{L_p}{W}\right) + 1 \quad (3\text{-}21)$$

Clay 5:

$$\frac{H_u}{H_{u,GBF}} = -0.2372\left(\frac{L_p}{W}\right)^2 + 2.3257\left(\frac{L_p}{W}\right) + 1 \quad (3\text{-}22)$$

Clay 6:

$$\frac{H_u}{H_{u,GBF}} = -0.2372\left(\frac{L_p}{W}\right)^2 + 2.3257\left(\frac{L_p}{W}\right) + 1 \quad (3\text{-}23)$$

The H_u/H_u (GBF) for the used eccentricity (e/D_t =6.83) can be estimated from Figure 3- 26 where H_u (GBF) can be obtained from equation 2-13.

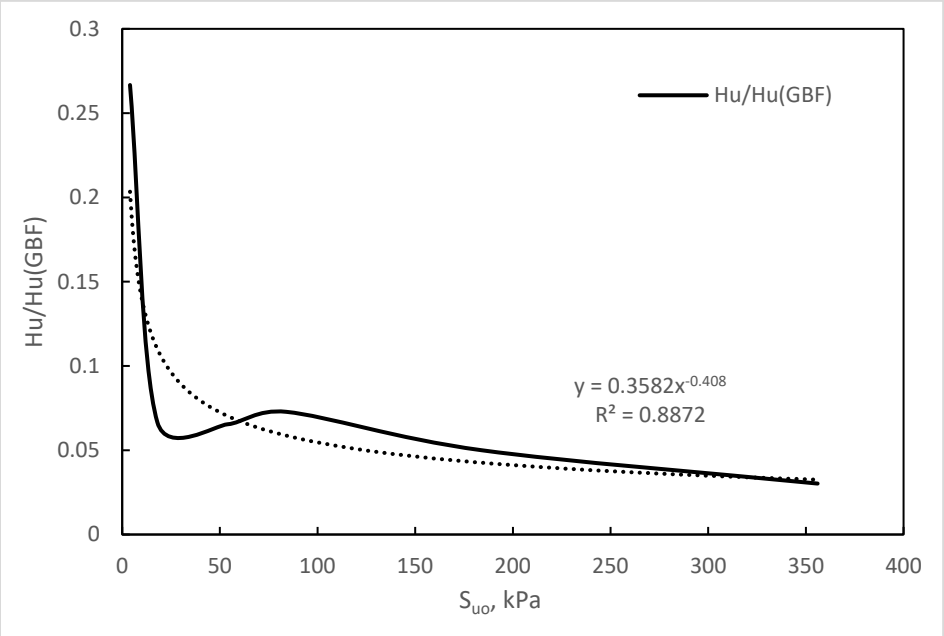

Figure 3-26 H_u/H_u(GBF) ratio

3.3.2 *Comparison at serviceability loading*

Parametric study is carried out to study the effects the soil bed has on the behavior of the system under serviceability lateral load of 2MN. The system maximum moment, shear force, maximum tip displacement (at tower tip) and mudline rotation are compared. To do so, a reference case of Monopile with diameter of 6m and depth of 30 meter is selected as a reference case at each soil profile for normalization purposes. This depth is chosen as it is around once and twice the depth of Hybrid Foundation pile at L_p/W of 1 and 2, respectively. Either Monopile (MP) or hybrid foundations (H.F) with length of pile to plate width (L_p/W) of 1 and 2 are used along with Gravity Base Foundation (G.B.F). Tables 3-2 and 3-3 show the considered soil and foundation properties while Figure 3-19 shows the foundation options. Same practice used to construct FEM for lateral ultimate capacity is followed except that instead of displacement-controlled loading in the previous part, point load was used and applied at e/D_t of 6.83 (41m above M.L).

3.3.2.1 Effects (L/D)/(Lp/W) ratio on the maximum moment

The bending behavior was also studied under the applied 2MN load and compared for all L/D ratio for MP, Figure 3-27. The difference in bending moment were lower than gain/loss of lateral ultimate capacity. This is because increasing pile's length results in changing location of pivot point, the point at which the pile rotates around its neutral axis typically lying at 0.7-0.75 of pile's depth (L). This in turns results in increased moment transferred to pile. The max difference happened for the case of clay1 having almost 6% more bending moment than the case of monopile with length of 30m (MP30). Reducing the pile's penetration reduced the attained BM for the same reason mentioned above. The difference in BM was defined as

$$\%\ \text{Difference in B.M} = \frac{\left(B.M\ of \frac{L}{D} of\ X - B.M\ of \frac{L}{D} of\ 5\right) * 100}{B.M\ of \frac{L}{D} of\ 5} \qquad (3\text{-}24)$$

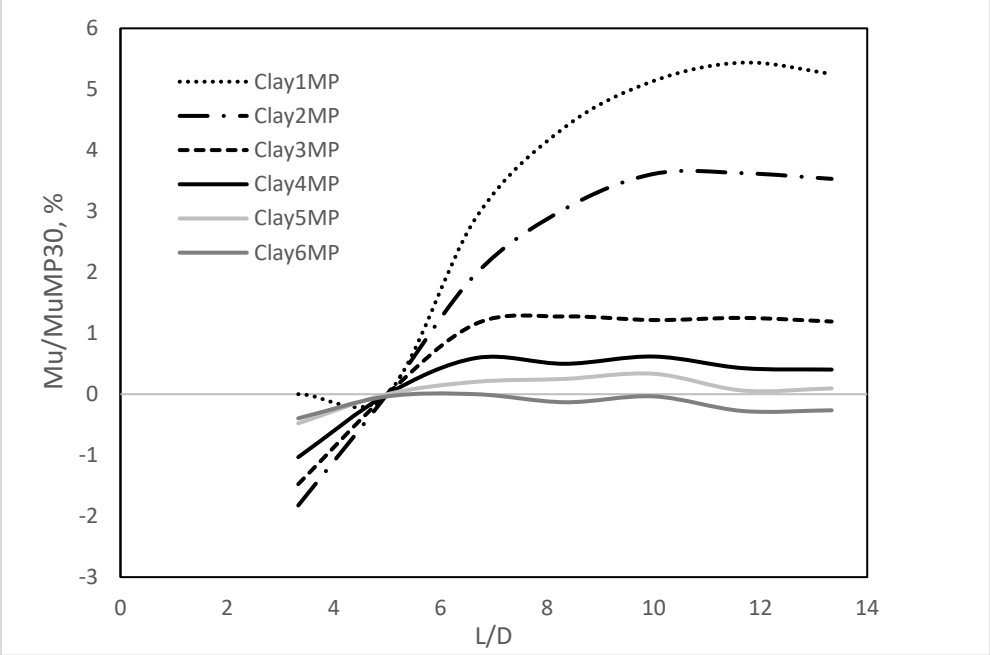

Figure 3-27 Effects of pile's L/D on the maximum moment value

The bending behavior was also studied under the applied 2MN load and compared for both L_p/W ratios for the H.F foundation system. Figure 3-28 shows substantial reduction in bending moment was obtained by introducing the plate into the foundation system even though the pile used was smaller in diameter, in this case 4 m compared to 6 m. The plate contribution is a result of shear stresses absorption at M.L and by moment resistance which reduced stresses transferred to MP and hence the use of smaller diameter pile. This enhanced system can increase the system stiffness and strength and be used as a retrofit option for already installed OWT. The difference in BM was defined as:

$$\% \text{ Difference in B.M} = \frac{\left(B.M\ of Lp/W of\ X - B.M\ of \frac{L}{D} of\ 5\right) * 100}{B.M\ of \frac{L}{D} of\ 5} \quad (3\text{-}25)$$

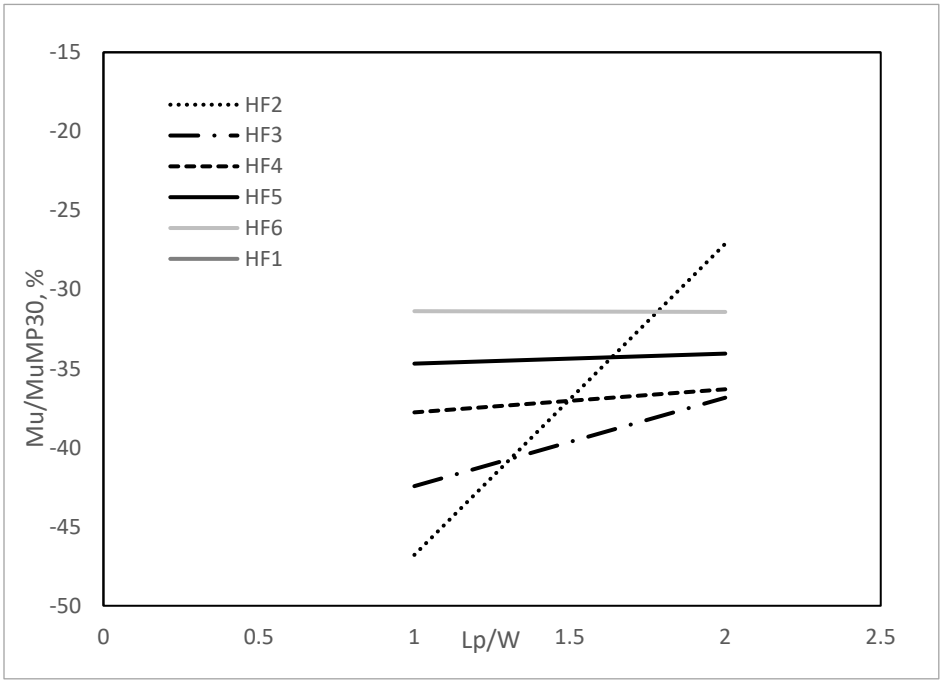

Figure 3-28 Effects of changing L_p/W on B.M of H.F

3.3.2.2 Effects (L/D)/(Lp/W) ratio on the S.F

Increasing L/D ratio meant increasing pivot point location, hence the B.M was increased. However, this meant more available pile length to take the shear stresses and hence lower S.F on deeper piles. Figure 3-29 shows that Clay1 had the highest difference amounting to reduction of almost 60% compared to MP30 in the same profile of soil. Lesser effect is obtained for clay 2-6 as the strength and stiffness do not increase substantially which means reaching limiting depth of pivot point and hence smaller reduction of shear stresses acting on the pile.

$$\% \text{ Difference in S.F} = \frac{\left(S.F of \frac{L}{D} X - S.F \ of \frac{L}{D} of\ 5\right) * 100}{S.F \ of \frac{L}{D} of\ 5} \tag{3-26}$$

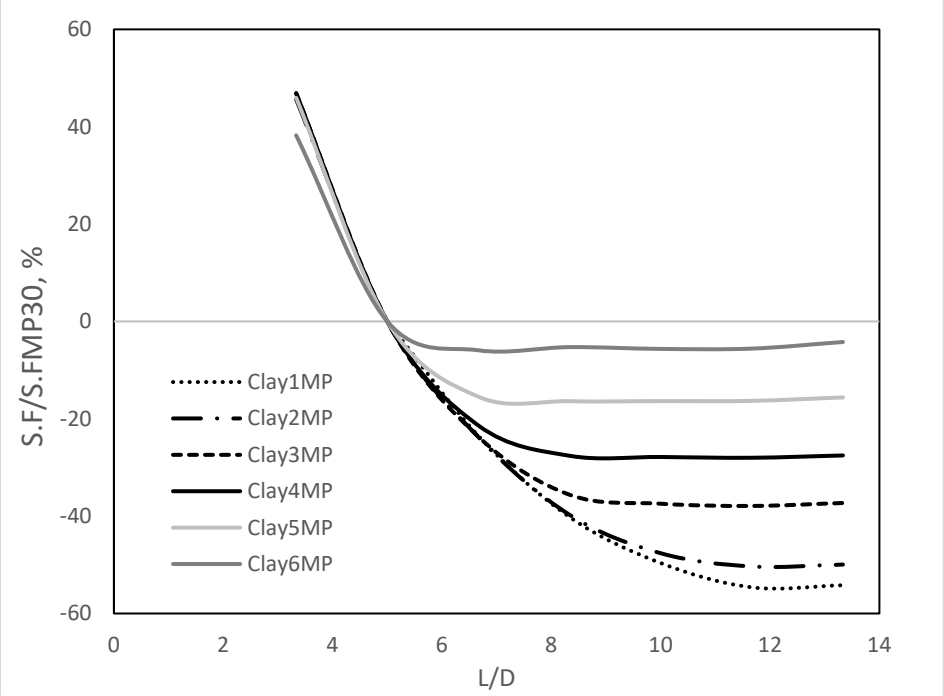

Figure 3-29 Effects of changing L/D ratio on max shear force on MP

The shear force was mostly increased in the case of H.F compared to MP30. For clay 1-3, a negative reduction was attained while for clay 4-6 an increase in S.F was realized. This is because

for clay 1-3 the mode of failure was overturning because of smaller capacity underneath plate and hence rigid rotation was observed. For clay 4-6 the increased strength and stiffness resulted in migration of pivot point downward resulting in fixation effects from pile and bending strength being realized. As this happened, larger contribution from pile to resisting lateral force was observed and hence higher shear forces being observed. Like MP, increasing the depth of the pile, L_p/W ratio, meant increasing the pivot point depth and hence the B.M while reducing the shear forces as seen in Figure 3-30.

$$\% \text{ Difference in S.F} = \frac{\left(S.F of \frac{Lp}{w} X - S.F\ of \frac{L}{D} of\ 5\right) * 100}{S.F\ of \frac{Lp}{w} of\ 5} \quad (3\text{-}27)$$

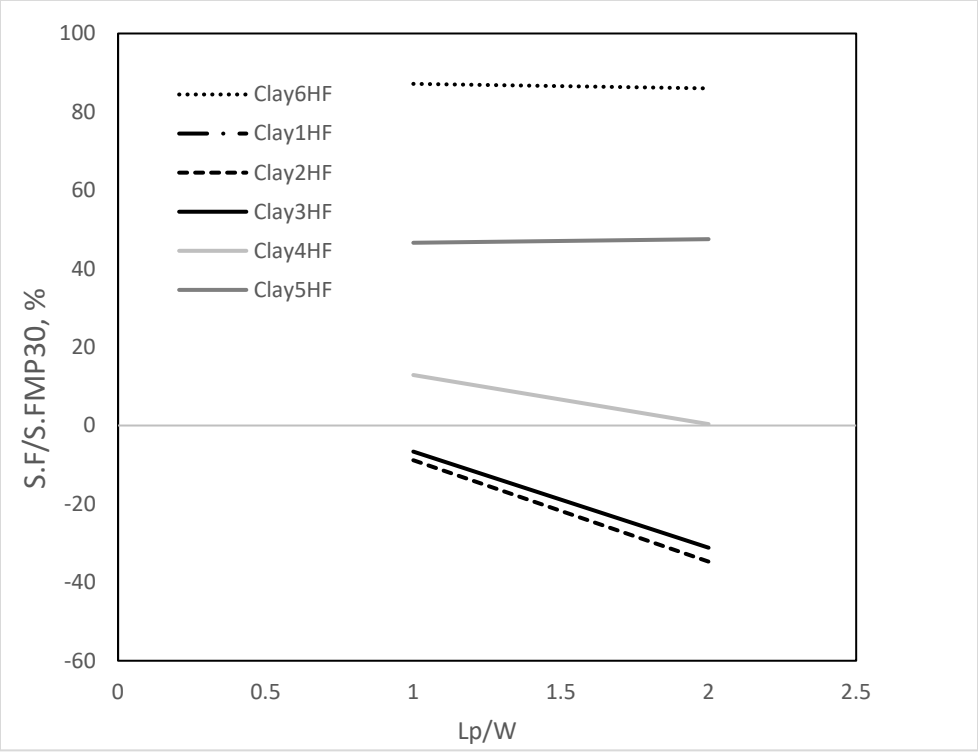

Figure 3-30 Effects of changing L_p/W in max shear force of H.F pile

3.3.2.3 Effects (L/D)/(L_p/W) ratio on the tower tip displacement (ttd)

Studying the effects of L/D ration on the tower tip displacement is indicative of system performance under serviceability conditions and can offer insight into overall behavior of the foundation while studying other effects such as B.M, S.F and the ultimate capacity. The effect of increasing the L/D was observed to increase the lateral ultimate capacity in section 3.2.5.5. Since soil stiffness is a function of strength it is expected that same behavior observed for ultimate is confirmed here as is the case. Figure 3-31 shows the effects of changing L/D ration on the difference in ttd (Eqn.3-28). Increasing the L/D ratio meant decreasing the ttd by 40-3% for the cases of clay1 and 6 respectively. This is because for the case of clay 1, the pile behavior was rigid and substantial gain in capacity was observed by changing L/D ratio. This means decreasing the fraction of applied load compared to H_u which reduces the mobilized shear strength of the soil. Accordingly, the change in ttd was maximum. For the case of stiffer soil, this effect decreases as the pile behavior migrates from purely rigid to semi-rigid to flexible (Clay6). As a result, the ratio of strength gain decreases for stiffer soil by change of L/D and smaller effects being realized.

$$\%\ \text{Difference in ttd} = \frac{\left(ttd\frac{L}{D}X - ttd\ \ of\frac{L}{D}of\ 5\right)*100}{ttd\ of\frac{L}{D}of\ 5} \tag{3-28}$$

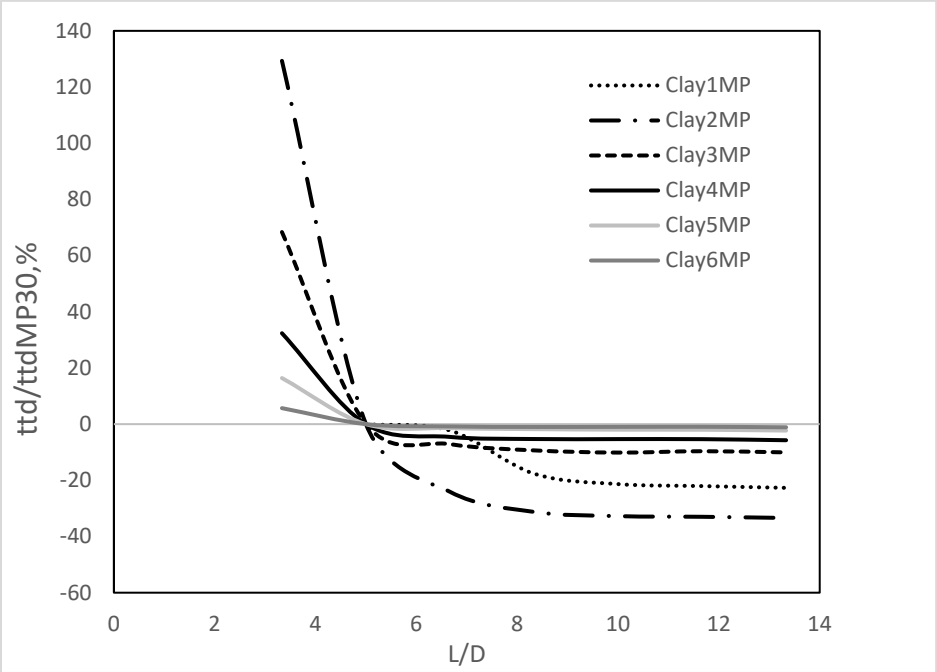

Figure 3-31 Effects of changing L/D ratio on ttd

Effects of changing L_p/w ratio on the tower tip displacement under serviceability conditions offers insight into overall behavior of the foundation while studying other effects such as B.M, S.F and the ultimate capacity. The effect of increasing the L_p/W was observed to increase the lateral ultimate capacity in section 3.2.5.5. Since soil stiffness is a function of strength it is expected that same behavior observed for ultimate is confirmed here as is the case. Figure 3-32 shows the effects of changing L_p/W ration on the difference in ttd (Eqn.3-29). Increasing the L_p/W ratio meant decreasing the ttd by 150-2% for the cases of Clay1 and 6, respectively. This is because for the case of Clay 1, the lateral ultimate capacity of the H.F was around 3MN meaning substantial portion of it being applied and hence higher mobilization of shear strength and stiffness of the soil. This meant higher rotation of the H.F for Clay 1. However, as the L_p/W was increased to 2, the capacity doubled and hence the H/H_u ratio decreased, and the stiffness increased with a reduction of the ttd displacement to that of MP30. This is because the behavior was rigid and substantial gain

in capacity was observed by changing L_p/W ratio. Accordingly, the change in ttd was maximum. For the case of stiffer soil, this effect decreases as the pile behavior migrates from purely rigid to semi-rigid to flexible (Clay6). As a result, the ratio of strength gain decreases for stiffer soil by change of L_p/W and smaller effects being realized.

$$\% \text{ Difference in ttd} = \frac{\left(ttd\frac{of Lp}{Wof}X - ttd\ of\frac{L}{D}of\ 5\right)*100}{ttd\ of\frac{L}{D}of\ 5} \tag{3-29}$$

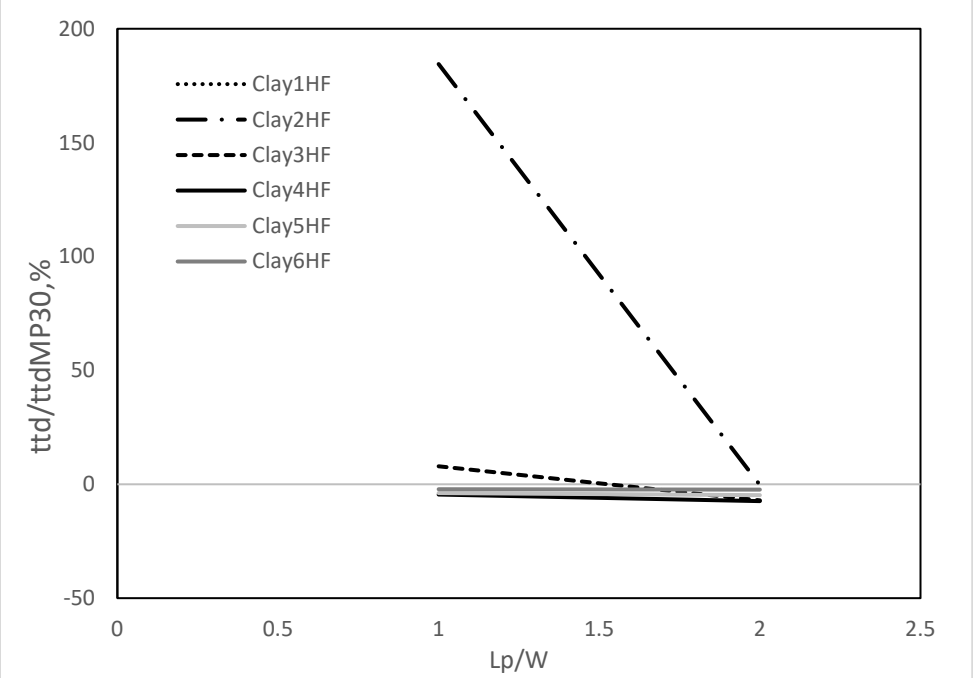

Figure 3-32 Effects of changing L_p/W on ttd

3.3.2.4 Effects (L/D)/(L_p/W) ratio on the mudline (M.L) rotation

Studying the effects of L/D ration on the tower mudline rotation is indicative of system performance under serviceability conditions and can offer insight into overall behavior of the foundation while studying other effects such as B.M, S.F and the ultimate capacity. The effect of increasing the L/D was observed to increase the lateral ultimate capacity in section 3.2.5.5. Since

soil stiffness is a function of strength it is expected that same behavior observed for ultimate is confirmed here as is the case. Figure 3-33 shows the effects of changing L/D ratio on the difference in M.L rotation (Eqn.3-30). Increasing the L/D ratio meant decreasing the M.L rotation by five folds for clay1, from 1.25 to less than 0,25 degrees, and by 20% of Clay 6 from 0.133 to 0.1, respectively. This is because for the case of clay 1, the pile behavior was rigid and substantial gain in capacity was observed by changing L/D ratio. This means decreasing the fraction of applied load H compared to H_u which reduces the mobilized shear strength of the soil. Accordingly, the change in M.L rotation was maximum. For the case of stiffer soil, this effect decreases as the pile behavior migrates from purely rigid to semi-rigid to flexible (clay6). As a result, the ratio of strength gain decreases for stiffer soil by change of L/D and smaller effects being realized. It can be deduced from Figure 3-33 that the serviceability condition, rotation of less than 0.25 degrees, is not met for the case of MP in Clay1. This will require increasing either the pile diameter, and not the thickness, to increase the strength of the system. This is because the pile B.M capacity was not reached and that a rigid behavior was observed across all L/D ratios. For the other soil profiles this criterion is met for clay 2 at L/D of 8.33 and clay 3 at L/D of 5 and clay 4 of around 4. For clay 5 and 6 this criterion is met for all L/D ratios.

$$\text{M.L rotation} = \frac{\left(ttd\,\frac{L}{D}\,of\,X - M.L\,displacement\,of\frac{L}{D}of\,x\right)}{L\,of\,tower} \tag{3-30}$$

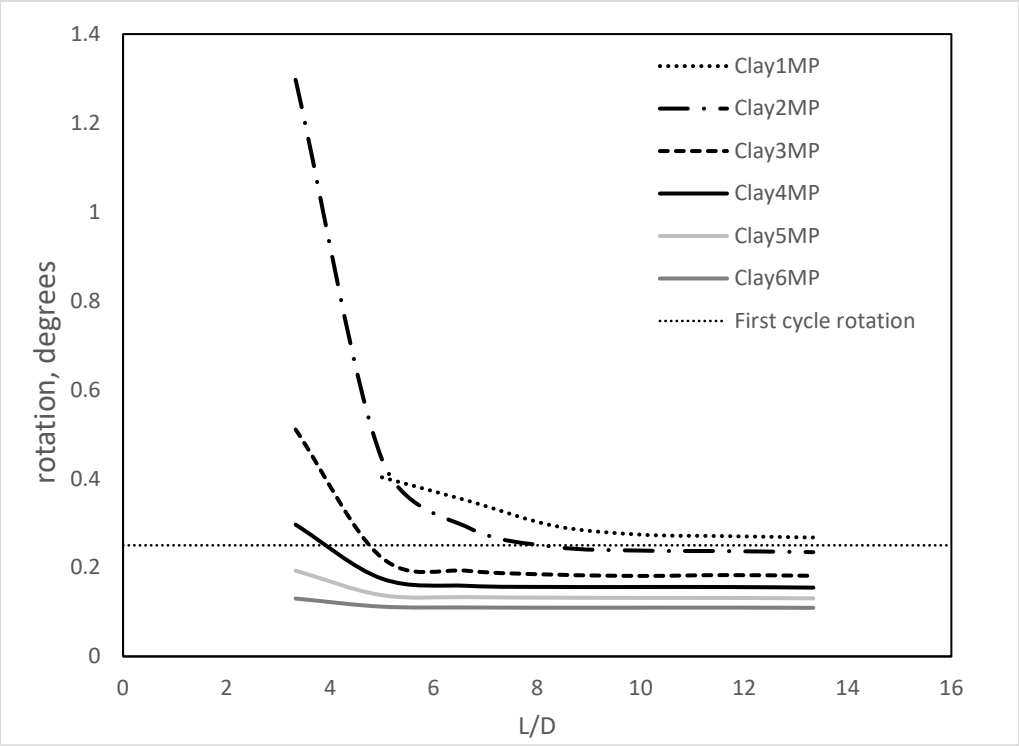

Figure 3-33 Effects of changing L/D on M.L rotation

The effect of L_p/W ratio on the mudline rotation is indicative of system performance under serviceability conditions and can offer insight into overall behavior of the foundation while studying other effects such as B.M, S.F and the ultimate capacity. The effect of increasing the L_p/W was observed to increase the lateral ultimate capacity in section 3.2.5.5. Since soil stiffness is a function of strength it is expected that same behavior observed for ultimate is confirmed here as is the case. Figure 3-34 shows the effects of changing L_p/W ratio on the difference in M.L rotation (Eqn.3-31). Increasing the L_p/W ratio meant decreasing the M.L rotation by more than 6 folds for Clay2, from 1.6 to less than 0.34 degrees, and by 50% for clay 6, from 0.2 to 0.1, respectively. This is because for the case of clay 2, the lateral ultimate capacity was very small and substantial gain in capacity was observed by changing L_p/W ratio. This means decreasing the fraction of applied load H compared to H_u which reduces the mobilized shear strength of the soil.

Accordingly, the change in M.L rotation was maximum. For the case of stiffer soil, this effect decreases as the pile behavior migrates from purely rigid to semi-rigid to flexible (clay6). As a result, the ratio of strength gain decreases for stiffer soil by change of L_p/W and smaller effects being realized. It can be deduced from Figure 3-34 that the serviceability condition, rotation of less than 0.25 degrees, is not met for the case of H.F in Clay 1 and Clay2. This will require increasing the plate diameter, and not the thickness and diameter of pile, to increase the strength of the system. This is because the pile B.M capacity was not reached and that a rigid behavior was observed across all L_p/W ratios. For the other soil profiles this criterion is met for clay 3 at L_p/W of 2 and clay 4 at L_p/W of 0.5, clay 5 and 6 at L_p/W of around 0.15.

$$\text{M.L rotation} = \frac{\left(ttd\,\frac{L}{D}\,of\ X - M.L\ displacement\ of \frac{L}{D} of\ x\right)}{L\ of\ tower} \tag{3-31}$$

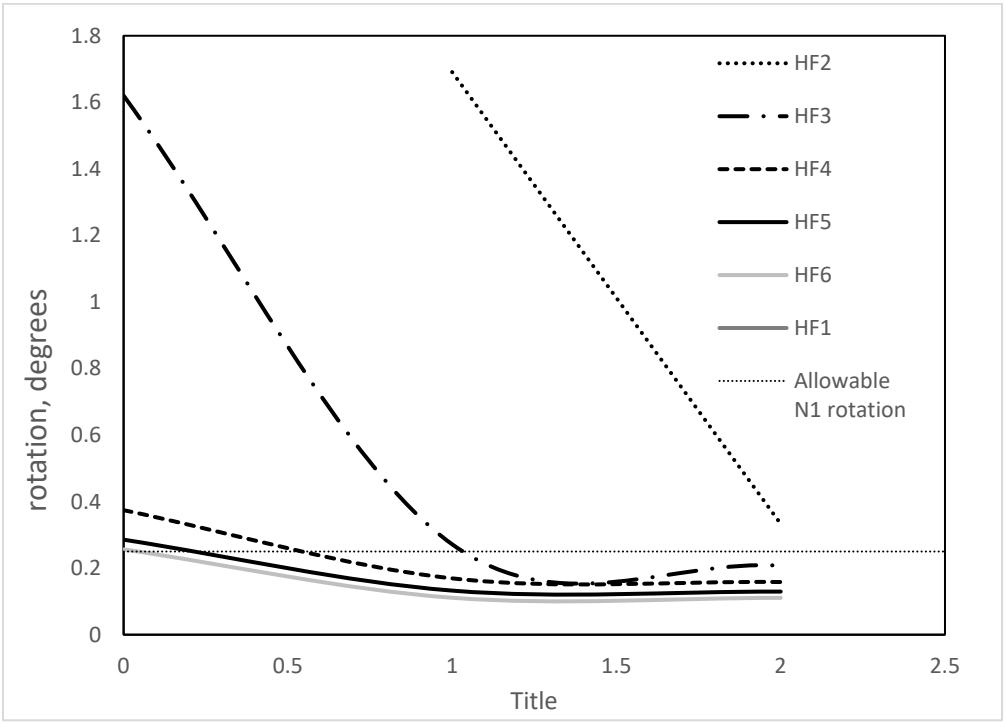

Figure 3-34 Effects of changing L_p/W on M.L rotation

3.4 Conclusion

Monopile foundations utilisation for OWT's plays important role for supporting development of green electricity alternative. Further development of OWT farms is expected to have bigger and heavier turbines to add more electricity in addition to being moved to deeper water locations. Therefore, behavior of monopiles and hybrid foundation system, which is composed of a pile supported by a circular plate at mudline, are investigated at ultimate capacity and compared to each other at expected service loading. Different soils conditions were considered, and a validated FE model was employed using Hs constitutive relationship with parameters calibrated and verified from field tests. Typical procedure involved K_o stage followed by installation stage which was then used to apply displacement-controlled loading, from which generic curves and best fit equations were established from which ultimate lateral capacity can be obtain for both systems. Several conclusions were drawn and are oriented in order to cover ultimate capacity of MP (notes 1-2) and H.F (notes 3-4) besides comparison between the two systems at 2MN lateral loading (notes 5-7).

1- The normalized ultimate capacity versus normalized stiffness of MP showed three distinct slopes, the normalized ultimate capacity was observed to increase significantly for E_p^*/E_{50} values less than 2000 for all L/D ratio. At normalized stiffness values of more than 2000, the effects of increasing the stiffness for a given L/D ratio was small for L/D ratios less than 6 and was considerable for higher L/D ratio

2- The normalized lateral ultimate capacity increase against L/D ratio was dependent on the normalized stiffness (E_p^*/E_{50}) values. At large E_p^*/E_{50} values, the piles behaved as rigid piles and cubic growth of normalized lateral ultimate capacity was observed for L/D ratios

considered herein. As normalized stiffness (E_p^*/E_{50}) values decrease below 1200, the effects of L/D ratio on lateral ultimate capacity diminish around L/D values of 5-8.

3- The normalized ultimate capacity of hybrid foundation was found to be independent on the pile diameter, hence it was normalized against GBF values for each soil.

4- Increase in L_p/W gave substantial increase in lateral capacity of H.F for all soils considered. However, it was noticed that for Clay profiles 3-6 increasing the L_p/W from 1 to 2 did not results in improvement on the lateral capacity because the structural capacity of the pile was reached.

5- Decreasing/increasing pile length compare to MP30 resulted in small decrease/increase of maximum bending moment of around 3%. However, the hybrid systems saw substantial reduction in maximum bending moments of around 35-40% compared to MP30. This added contribution of plate can therefore reduce steel used for foundation which is beneficial.

6- Maximum shear force was related to pile's length and varied from 20-30% when pile length was increased against MP30. Adding a plate and using smaller pile resulted in increase of maximum shear force. This is believed to be attributed to restoring forces acting below the plate adding additional pressures against the pile.

7- Increasing pile length in profile 1(rigid behavior) resulted in pronounced decrease in tower tip displacement for all depths considered. The amount of reduction of tower tip displacement was around 20% compared to MP30. For all other profiles, the increase in shear strength resulted in the critical depth of pile being reduced and therefore increase in stiffness beyond 40 m penetration was minimal. For Clay profiles 2,3,4,5 and 6 the

decrease of tower tip displacement was 12.2, 3.16, 1.2, 0.9, and 0.29% when increasing pile length from 40 to 80.

3.5 References

Abdelkader, Ahmed Mohamed Reda, Investigation of Hybrid Foundation System for Offshore Wind Turbine (Scholarship@Western). 2016.

API, 1993. Recommended practice for planning, designing, and Constructing fixed offshore platforms. API, RPT2A-WSD. American Petroleum Institute (API), Washington, D.C.

Association EWE. The European Offshore Wind Industry‑Key Trends and Statistics 2016; January; 2017.

Adamidis, O., & Madabhushi, S. P. G. (2014). On preparation of viscous pore fluids for dynamic centrifuge modelling. *International Journal of Physical Modelling in Geotechnics, 15* (3), 141-149. https://doi.org/10.1680/jphmg.14.00022

Bazeos N, Hatzigeorgiou GD, Hondros ID, Karamaneas H, Karabalis DL, Beskos DE. (2002), "Static, seismic and stability analyses of a prototype wind turbine steel tower", Engineering Structures, **24**, 1015-1025.

Beck, A., Springman, S. M., & Askarinejad, A. (2015). Scaling law of static liquefaction mechanism in geocentrifuge and corresponding hydromechanical characterization of an unsaturated silty sand having a viscous pore fluid. *Canadian Geotechnical Journal, 52*(6), 708-720. doi:10.1139/cgj-2014-0237

Bentley, K.J. and El Naggar, M.H., 2000. Numerical analysis of kinematic response of piles. Canadian Geotechnical Journal, Vol. 37, No. 6, pp. 1368-1382

Bisoi, & Haldar, S. (2019). 3D Modeling of Long-Term Dynamic Behavior of Monopile-Supported Offshore Wind Turbine in Clay. International Journal of Geomechanics, 19(7), 4019062–. https://doi.org/10.1061/(ASCE)GM.1943-5622.0001437

Bisoi, S., and S. Haldar. 2014. "Dynamic analysis of offshore wind turbine in clay considering soil-monopile-tower interaction." Soil Dyn. Earthquake Eng. 63: 19–35. https://doi.org/10.1016/j.soildyn.2014.03.006.

Black, J., Baker, N. & Ainsworth, A. 2014. Establishing a 50 g-ton geotechnical centrifuge at the University of Sheffield. Proceedings of the 8th International Conference on Physical Modelling in Geotechnics. Perth, Aus.,

Broms, B. B. (1964b). Lateral Resistance of Piles in Cohesive Soils. Journal of the Soil Mechanics and Foundations, **90**(2): 27-64.

Brown, D. A. (2007). Rapid lateral load testing of deep foundations. *DFI Journal - the Journal of the Deep Foundations Institute, 1*(1), 54-62. doi:10.1179/dfi.2007.005

Byrne, B.W. and Houlsby, G.T. (2003) "Foundations for Offshore Wind Turbines", Philosophical Transactions of the Royal Society of London, Series A, Vol. 361, December, pp 2909-2930.

Byrne B. W., McAdam R., Burd H. J., Houlsby G. T., Martin C. M., Zdravković L., Taborda D. M. G., Potts D. M., Jardine R. J., Sideri M., Schroeder F. C., Gavin K., Doherty P., Igoe D., Muir Wood A., Kellahave D. and Skov Gretlund J. 2015a. New design methods for large diameter piles under lateral loading for offshore wind applications. *Proceedings of Third International Symposium on Frontiers in Offshore Geotechics* 1, 705-710.

Byrne B. W., McAdam R., Burd H. J., Houlsby G. T., Martin C. M., Gavin K., Doherty P., Igoe D., Zdravković L., Taborda D. M. G., Potts D. M., Jardine R. J., Sideri M., Schroeder F. C., Muir Wood A., Kellahave D. and Skov Gretlund J. 2015b. Field testing of large diameter piles under lateral loading for offshore wind applications. *Proceedings of XVI European Conference on Soil Mechanics and Geotechnical Engineering*, Edinburgh, 1255-1260.

Cheah, C. B., & Ramli, M. (2011). The implementation of wood waste ash as a partial cement replacement material in the production of structural grade concrete and mortar: An overview.*Resources, Conservation & Recycling, 55*(7), 669-685. doi:10.1016/j.resconrec.2011.02.002

Cherchia, M. (2016). Centrifuge modeling of hybrid foundations for offshore wind turbines.

Das, B. M. (2006). *Principles of foundation engineering*. Boston: PWS Pub. Co.

El-Marassi M. Investigation of hybrid monopile-footing foundation systems subjected to combined loading: The University of Western Ontario; 2011.

Gerolymos, N., Giannakos, S., & Drosos, V. (2019). Generalised failure envelope for laterally loaded piles: Analytical formulation, numerical verification and experimental validation. *Géotechnique,* , 1-20. doi:10.1680/jgeot.18.P.051

Heidari, M., Jahanandish, M., Naggar, H. E., & Ghahramani, A. (2014). Nonlinear cyclic behavior of laterally loaded pile in cohesive soil. *Canadian Geotechnical Journal, 51*(2), 129-143. doi:10.1139/cgj-2013-0099

Jonkman, J. M., Musial, W. D., & National Renewable Energy Laboratory (U.S.). (2010). *Offshore code comparison collaboration (OC3) for IEA task 23 offshore wind technology and deployment.* (No. 5000-48191.;5000-48191;). Golden, Colo: National Renewable Energy Laboratory.

Lai, Y., Wang, L., Hong, Y., & He, B. (2020). Centrifuge modeling of the cyclic lateral behavior of large-diameter monopiles in soft clay: Effects of episodic cycling and reconsolidation. *Ocean Engineering*, *200*, 107048– https://doi.org/10.1016/j.oceaneng.2020.107048

Lehane B, Powrie W, Doherty J. Centrifuge model tests on piled footings in clay for offshore wind turbines. In: Proceedings of international conference in physical modelling in geotechnics, ICPMG2010 Rotterdam: Balkema; 2010.

Malhotra, S. "Design and Construction of Offshore Wind Turbine Foundations," Wind Turbines, pp. 231-264.

Muir Wood, D. (2004). *Geotechnical modelling*. London;New York, NY;: Spon Press.

O'Neill, M. W., Reese, L. C., & Brown, D. A. (1987). Cyclic lateral loading of a large-scale pile group. *Journal of Geotechnical Engineering, 113*(11), 1326-1343. doi:10.1061/(ASCE)0733-9410(1987)113:11(1326)

Powrie, W., and Daly, M. P. (2007). "Centrifuge modeling of embedded retaining walls with stabilizing bases." Geotechnique, 57(6), 485–497.

Rahman, M. (1984). Wave diffraction by large offshore structures: An exact second-order theory. *Applied Ocean Research, 6*(2), 90-100. doi:10.1016/0141-1187(84)90046-4.

Randolph, M. F., & Gourvenec, S. (2011). *Offshore geotechnical engineering*. New York: Spon Press.

Federal Highway Administration (FHWA). (2016). Design and Construction of Driven Pile Foundations – Volume I. U.S. Dept. of Transportation, Federal Highway Administration,

T.P.T. Dao. Validation of PLAXIS Embedded Piles for Lateral Loading. Delft University of Technology. 2011

Wang, X., Zeng, X., Yang, X., & Li, J. (2018). Feasibility study of offshore wind turbines with hybrid monopile foundation based on centrifuge modeling. *Applied Energy, 209*, 127-139. doi:10.1016/j.apenergy.2017.10.107

Wang, Z., Hong, Y., Ng, C. W. W., Wang, L. Z., Mašín, D., & He, B. (2017). Cyclic lateral response and failure mechanisms of semi-rigid pile in soft clay: Centrifuge tests and numerical modelling. *Canadian Geotechnical Journal, 54*(6), 806-824. doi:10.1139/cgj-2016-0356

Zhang, G. (2017). A centrifuge study of the seismic response of pile–raft systems embedded in soft clay. *Géotechnique*, *67*(6), 479–490. https://doi.org/10.1680/jgeot.15.P.099

Zhu, B., Zhu, Z., Li, T., Liu, J., & Liu, Y. (2017). Field Tests of Offshore Driven Piles Subjected to Lateral Monotonic and Cyclic Loads in Soft Clay. *Journal of Waterway, Port, Coastal, and Ocean Engineering*, *143*(5), 5017003–. https://doi.org/10.1061/(ASCE)WW.1943-5460.0000399

Chapter 4: Three Spring Stiffness Model for Monopile and Hybrid Foundation: Effects of Footing rigidity and L/D/(L_p/W) ratios

Three Springs Stiffness Model for Hybrid Foundations and Monopiles: Effects of Footing rigidity and L/D/(L_p/W) ratio

Abstract:

Offshore wind turbines (OWTs) are becoming increasingly installed across the globe as efficient means of electricity production. Moving into deep water to harness wind energy from OWTs creates specific challenges for their foundation design due high lateral loads and bending moments, all of which must be accommodated within strict rotation envelopes. Currently, monopiles account for 80% of the installed foundations with L/D ratio being less than 20 and diameters and depth of penetration reaching 7.8m and 80m, respectively. To limit monopiles geometry and cost, an improved monopile design was proposed in the previous chapter showing potential to replace monopiles in stiff clays. In this chapter, a 3 springs stiffness model at soil mudline is established by means of finite element modelling to model the mechanical behavior of the improved foundation system as well as that of monopiles at the soil mudline considering effects of soil profile and the pile rigidity. Closed form equations are provided by fitting the results to describe the foundation stiffness properties with few soil and foundation geometry data. The commercial F.E.M 3D program PLAXIS is used for this purpose. Six sets of soils profiles are considered that cover a wide range of soil profiles encountered in practice ranging from very soft (E_{50} = 2MPa) to very hard (E_{50} = 140MPa) clay. HF with L_p/W ratios of 1 and 2 were investigated as well as 7 different MP length to diameter (L/D) ratios varying from 3.3 to 13.3. For H.F systems, the normalized stiffness values were increasing with L_p/W ratio and decreasing for increase in shear strength. Results indicate the normalized stiffness of MP decreases as the E_{50} value of the soil increases and increases at varying rate with L/D ratio. For soft soils, foundations can be classified as rigid and showed exponential increase of normalized stiffness properties with increasing L/D ratio; however, stiff soil profiles showed that a plateau is reached at L/D ratio of about 5-8.

4.1 Introduction

Wind turbines are becoming increasingly installed across the globe as efficient means of electricity production. For instance, Westwood (2004) reported that the capacity of offshore wind turbines initiated in 2003 was more than the capacity of all previous years combined (Westwood, 2004). The offshore energy output grew exponentially over the last two decades (Wind Europe, 2016). A wind turbine comprises a generator with two or three blades placed on a mast that is mounted on a transition piece, which is supported by the foundation system. To harness more power, turbine sizes have increased significantly, with 14MW turbines already available in the market.

Different foundation systems are employed to support wind turbines. Onshore wind turbines can be supported by a shallow foundation, monopile, a raft on piles or pile groups. Offshore wind turbines are supported on gravity base foundations (GBF), tripod structures, jackets, suction caissons, monopiles (MP) and buoyant fixed structures (El-Marassi, 2011). Previous studies suggest that monopiles account for 80% of the installed foundations with diameter (D) and depth of penetration (L) reaching 7.8 m and 80 m, respectively. The selection of the foundation system depends on many factors including location and size of structure, subsurface conditions, magnitudes of loads and their distribution, local experience and availability of materials, durability and cost (Poulos, 2016). The foundation design must satisfy two criteria: the foundation, including the underlying soil, must be adequately safe against failure or the wind turbine could fail (ultimate limit state); and displacements (vertical, horizontal and rotation) must remain within tolerable limits so as not to affect the integrity and function of the wind turbine serviceability limit state).

The design of wind turbine foundations is generally governed by the serviceability limit states due the stringent rotation limits. This requires determining the foundation stiffness employing

rigorous method to ensure accurate prediction of displacements. Existing methods for determining the stiffness properties of wind turbine foundations (MP and GBF) and range from subgrade approach, nonlinear subgrade approach (p-y) and finite element method. With the development and installation of offshore wind turbines (OWTs) in deeper water, OWT's foundations are subjected to higher lateral loads and bending moments resulting from wind and wave loading all of which must be accommodated with strict serviceability requirements (Biosi and Halder, 2014, Byrne et al., 2015, Wang et al., 2017). This condition typically leads to increasing the foundation size and cost. Besides, OWTs are dynamically sensitive structures with strict regulations on their foundations' permissible rotation making the design of their support structures a cumbersome process. Furthermore, wind and waves loading are cyclic in nature, which may induce progressive and cumulative damage to the soil and hence the displacement and rotation may increase with time.

The increase in foundation size can increase its natural frequency, which may lead to interference with the loading frequency of rotor (1P) or blade passing loading frequency (3P) and subsequently may impact the foundation long-term performance. As the size of the wind turbines increases, it is expected that the size of the monopile will continue to increase to accommodate the extreme loading conditions OWTs encounter during their lifetime. Therefore, to limit the MP diameter and penetration, a hybrid foundation (HF) option is proposed, which comprises a plate with a diameter (W) fitted with a monopile with a length (L_p) and a diameter (D_p). The HF is expected to have higher lateral, rotational and coupling stiffness properties compared to MP. Therefore, this study investigates the stiffness characteristics of the MP and HF in order to ensure satisfying the serviceability limit state.

The stiffness constants of MP and HF installed in different clayey soils are established using calibrated and validated finite element models (FEMs). Consequently, three-spring stiffness models are established for MP and HF, which can be used to evaluate the first natural frequency of foundations. This conceptual model has been employed for MP (e.g., Bhattacharya et al., 2013; Arany et al., 2016) but has not been developed for hybrid foundations. Additionally, the FEMs used in the current study incorporate advanced constitutive models for the soil, which leads to more precise definition of soil stiffness and hence the foundation stiffness. The constitutive model used is Hs model and it incorporates a well defined soil material stiffness, E_{50}, unlike other models such as Mohr Coulomb. A case study that involved lateral load testing of driven open-ended monopiles is used to calibrate and validate the FEM parameters. Afterwards, prototype models of the MP and HF are considered in a comprehensive parametric study that investigated the performance of both systems.

4.2 Literature Review

Two criteria must be met for the foundation design: ultimate limit state and serviceability limit states. Ultimate limit state deals with vertical, lateral, and moment capacity of the foundation while serviceability limit state ensures limits of displacement and rotation are not exceeded to preserve the integrity of the structure (turbine, transition piece and mast) and foundation. Usually, lateral loads due to wind and waves are the controlling factor when it comes to ultimate limit states. With strict rotation requirements coupled with increased water depth, it is anticipated that monopiles with much larger diameter would be required, posing problems of noise, drivability, and cost for the development of new offshore wind farms (OWFs). Areas of improvement and innovations for OWF are increasing turbines output, reducing wake losses, improving farm layout, reducing tower and foundation costs (Chercia, 2014). The cost of foundations for OWTs can represent up to 40%

of the development principal, and since newer OWFs are expected to be installed farther from shorelines in deeper water, it is expected that the cost of their foundations will continue to increase. To reduce the diameter and possibly the length of penetration of monopiles, several researchers proposed using hybrid foundation system that comprises a plate fitted with a short monopile at its center. The plate is expected to reduce tilting and increase overall stiffness while providing extra support for the structure, and consequently the pile diameter and penetration may be reduced (Wang et al. 2018; Wang et al., 2017; Hong et al. 2017; Abdelkader 2016; Bhattacharya et al., 2015; Cherchia 2014; Klinkvort and Hededal 2014; Lahane et at. 2014; Lombardi et al., 2013: Bhattacharya et al., 2013; El-Marassi 2011; Powrie and Daly 2007).

To evaluate the stiffness properties of monopiles, different techniques can be used including closed form equations for fully flexible or fully rigid piles, beam on nonlinear Winkler foundation (BNWF) method, commonly referred to as p-y approach, or sophisticated numerical modeling techniques. For example, Novak (1974) investigated the vertical, lateral rotational and coupling stiffness characteristics for piles and provided simplified solutions for their evaluation, i.e.:

$$K_v = \frac{E_p I}{A} * f_v \tag{4-1}$$

$$K_L = \frac{E_p I}{R^3} * f_u \tag{4-2}$$

$$K_{RL} = \frac{E_p I}{R^2} * f_c \tag{4-3}$$

$$K_R = \frac{E_p I}{R} * f_y \tag{4-4}$$

Where: K_v, k_L, K_{LR}, K_R are vertical, horizontal, coupling, and rotational stiffness components; E_p, I and R are the pile Young's modulus, cross-section moment of inertia and radius; f_v, f_u, f_c and f_y are coefficients that depend on pile-soil relative rigidity, variation of soil stiffness along

the pile and at its base, pile slenderness ratio and its fixity conditions at head and toe, among other things.

Poulos and Davis (1980) established stiffness parameters for both, rigid and flexible piles in two types of soil profiles, one linearly increasing in stiffness with depth and one with constant stiffness with depth. Table 4-1 lists the formulation proposed by these studies to evaluate piles stiffness constants. Polous and Hull (1989) proposed a method to evaluate the pile rigidity, which classifies the pile as either flexible or rigid depending on its relative rigidity compared to the soil. This method defines upper and lower bound values of $E_pI_p/E_sL^4 = 0.0025$ and 0.208 for flexible and rigid piles, respectively (Hong et al., 2017). Meanwhile, Randolph (1991) investigated the stiffness characteristic of flexible piles and Carter and Kulhawy (1992) established stiffness properties for rigid piles. However, monopiles with typical dimensions fall in the middle range between flexible and rigid piles and there are no specific formulas to describe the stiffness in this range.

Table 4-1 Existing methods to determine subgrade stiffness values for different soil and pile conditions (After Arany, 2015)

Soil type and source	Flexible pile	Rigid pile
Constant k_h Polous and Davis, 1980	$\begin{bmatrix} F \\ M \end{bmatrix} = \begin{bmatrix} \frac{k_h D_p}{\beta} & -\frac{k_h D_p}{2\beta^2} \\ -\frac{k_h D_p}{2\beta^2} & \frac{k_h D_p}{2\beta^3} \end{bmatrix} \begin{bmatrix} \rho \\ \theta \end{bmatrix}$	$\begin{bmatrix} F \\ M \end{bmatrix} = \begin{bmatrix} k_h D_p L & -\frac{k_h D_p L^2}{2} \\ -\frac{k_h D_p L^2}{2} & \frac{k_h D_p L^3}{3} \end{bmatrix} \begin{bmatrix} \rho \\ \theta \end{bmatrix}$
Linear k_h Polous and Davis, 1980	$\begin{bmatrix} F \\ M \end{bmatrix} = \begin{bmatrix} 1.007\eta_h^{\frac{3}{5}}(E_p I_P)^{\frac{4}{5}} & -0.99\eta_h^{\frac{2}{5}}(E_p I_P)^{\frac{3}{5}} \\ -0.99\eta_h^{\frac{2}{5}}(E_p I_P)^{\frac{3}{5}} & 1.485\eta_h^{\frac{1}{5}}(E_p I_P)^{\frac{4}{5}} \end{bmatrix} \begin{bmatrix} \rho \\ \theta \end{bmatrix}$	$\begin{bmatrix} F \\ M \end{bmatrix} = \begin{bmatrix} \frac{1}{2}L^2\eta_h & -\frac{1}{3}L^3\eta_h \\ -\frac{1}{3}L^3\eta_h & \frac{1}{4}L^4\eta_h \end{bmatrix} \begin{bmatrix} \rho \\ \theta \end{bmatrix}$
Bedrock-shear modulus based (Randolph, 1991; Carter and Kulhawy, 1992	$\begin{bmatrix} F \\ M \end{bmatrix} = \begin{bmatrix} 3.15\, G^* D_p (\frac{E_e}{G^*})^{\frac{1}{7}} & -0.53\, G^* D_p^2 (\frac{E_e}{G^*})^{\frac{3}{7}} \\ -0.53\, G^* D_p^2 (\frac{E_e}{G^*})^{\frac{3}{7}} & 0.25\, G^* D_p^3 (\frac{E_e}{G^*})^{\frac{5}{7}} \end{bmatrix} \begin{bmatrix} \rho \\ \theta \end{bmatrix}$	$\begin{bmatrix} F \\ M \end{bmatrix} = \begin{bmatrix} \frac{3.15 G^* D_p^{\frac{2}{3}} L^{\frac{1}{3}}}{1-0.28(\frac{2L}{D_p})^{\frac{1}{4}}} & -\frac{2G^* D_p^{\frac{7}{8}} L^{\frac{9}{8}}}{1-0.28(\frac{2L}{D_p})^{\frac{1}{4}}} \\ -\frac{2G^* D_p^{\frac{7}{8}} L^{\frac{9}{8}}}{1-0.28(\frac{2L}{D_p})^{\frac{1}{4}}} & \frac{4G^* D_p^{\frac{4}{3}} L^{\frac{5}{3}}}{1-0.28(\frac{2L}{D_p})^{\frac{1}{4}}} \end{bmatrix} \begin{bmatrix} \rho \\ \theta \end{bmatrix}$

The connection of the monopile to the wind turbine is free to rotate (no fixation). Thus, the MP can undergo significant tilting and mudline displacement when subjected to large lateral load. To preserve the integrity of the offshore wind turbine generator, the maximum allowable rotation is set at 0.5 degrees (Malhotra, 2009). To limit tilting of OWT, either monopile diameter or wall thickness are increased to enhance its stiffness. On the other hand, as wave loading is proportional to the embedded structure diameter, increasing the MP diameter can lead to increased wave loading, especially in deep water. Alternatively, either adding a plate (i.e., hybrid foundation) or improving the soil employing soil improvement techniques can increase the lateral stiffness and reduce the mudline rotation. For instance, Powrie and Daly (2007) studied a retaining wall with an embedded stabilising base in kaolin clay utilizing centrifuge modelling. Their results indicated

beneficial effects from the stabilizing base to the retaining wall system. To examine the effects of soil improvement on the performance of piles under cyclic lateral loading, Hong et al. (2017) conducted a centrifuge study on piles embedded in either soft clay or improved clay. Their results indicated that the soil improvement reduced the lateral deflection and enhanced the lateral resistance under low, medium, and high load levels. Wang et al. (2018) conducted a centrifuge study to investigate the response of different OWT foundation systems, including MP, GBF, gravel and steel wheeled foundations installed in sand and subjected to lateral monotonic and cyclic loads. Based on the test results, they proposed a logarithmic relationship to evaluate the accumulated lateral deflection as a function of the number of load cycles, i.e.:

$$\frac{y_N}{y_1} = 1 + b \ln (N) \tag{4-5}$$

where y_1 and y_N are deflection at first and N cycles, respectively. The parameter b ranges from 0.36 to1.6 depending on foundation type, load intensity, and soil type (Wang et al., 2018). They concluded that wheeled foundation systems had higher stiffness and that both gravel wheel and steel wheel footings performed better than the monopile in resisting the lateral loads. Lehane et al. (2010) investigated the lateral and rocking responses of different hybrid foundations and suggested that the hybrid foundation plate improves the foundation performance through four mechanisms: it contributes to the restoring moment due to its weight; it absorbs shear stresses through contact with soil; it increases passive pressure underneath the plate thereby increasing resistance of lateral loads from the pile; and it adds restoring moment from soil contact pressure. Cherchia (2014) suggested that the hybrid foundation could have a considerable cost advantage because the diameter and length of the pile would be reduced, and the material weight could be significantly lower than that of the monopile. He conducted centrifuge tests at 50g on two hybrid foundations, underfins and skirted GBF, installed in a medium dense sand and compared their behavior with

that of monopiles. The lateral load was applied at e/D_p of 2 using a hydraulic jack. The experimental results demonstrated that under serviceability limits (6 mm), the response of the hybrid systems was similar to that of the considered monopile. However, the monopile exhibited higher stiffness under monotonic and cyclic lateral loads, and the response of the hybrid foundations was almost twice that of the monopile (almost 50mm).

Motivated by the previous research indicating potential benefits of the hybrid foundation to the overall performance under lateral loads, this study examined this system in different clay profiles with the goal of providing equations to describe its lateral and rocking stiffness properties. Prototype models of hybrid foundations with L_p = 14 m or 28 m and W = 14 m. The diameter of the hybrid foundation pile is 4 m and its diameter to thickness ratio, D_p/t = 85. The diameter of the monopile is 6 m with D_p/t = 85 and length varying from 20 m to 80 m.

4.2.1 *Natural frequency*

The structure natural frequency depend on the soil and tower stiffnesses. A first order estimate for the structure 1st natural frequency on rigid foundations ($F_{FB.}$) can be estimated from the following relationship:

$$F_{FB.} = \sqrt{\frac{k}{m_{eff.} + m_{RNA}}} \tag{4-6}$$

where k is the tower lateral stiffness and m_{eff} is the effective mass defined as $m_{eff} = \frac{33\,mT}{140}$ where m_T is the tower total mass, m_{RNA} is the turbine components mass and k is defined as $3EI_t/L^3$.

The soil flexibility adds some compliance to the tower base resulting in reduced value of 1st natural frequency (F_{n1}) compared to F_{FB}. Arany et al. (2016) developed a single degree of freedom (SDOF) representation of the OWT structure by modelling the soil as a three-spring stiffness at mudline. A set of differential equations describing the tower and foundation compliance were

proposed and the equations of motion for the SDOF model was solved to obtain the eigen frequency accounting for the tower properties and foundation stiffness, i.e.,

$$F_{n1} = F_{FB} * C_R * C_{LR} \quad (4\text{-}7)$$

Where,

$$C_{LR} = 1 - \left(\frac{1}{1 + b\left(\eta_L - \frac{\eta_{LR}^2}{\eta_R}\right)}\right) \quad (4\text{-}8)$$

$$C_R = 1 - \left(\frac{1}{1 + a\left(\eta_R - \frac{\eta_{LR}^2}{\eta_L}\right)}\right) \quad (4\text{-}9)$$

Their results indicated that F_{n1} can be as low as 50% of F_{FB}. In Equations 4-7 to 4-9, a and b are empirical constants and can be taken as a = 0.6 and b = 0.5. The applicability of these equations is limited to $6\ \eta_R > 1.2\frac{\eta_{LR}^2}{\eta_R}$ and $\eta_L > 1.2\frac{\eta_{LR}^2}{\eta_R}$ (Arany et al., 2016).

The natural frequency of the foundation system can be estimated employing different approaches as shown schematically in Figure 4-1. The foundation can be assumed fixed at the mudline (Figure 4-1a), which simplifies the analysis but could seriously overestimate the natural frequency. The apparent fixity method assumes the monopile is fixed at a certain depth below mudline (Figure 4-1b). Alternatively, the foundation stiffness can be calculated using the p-y approach, which discretizes the soil into layers simulated as independent springs (Figure 4-1c). This approach may give good results but requires certain soil input and a suitable p-y curves model. Sophisticated FE models can also be used to rigorously simulate the foundation-soil system and determine its stiffness. However, it requires using a FE program and more detailed soil parameters, which can be costly. In addition, FE analysis requires good knowledge of suitable soil constitutive models and boundary conditions, and the computational effort could be time and resources

consuming. Finally, the foundation stiffness can be evaluated from sway-rocking models, in which the foundation mechanical behavior is represented by either two or three springs.

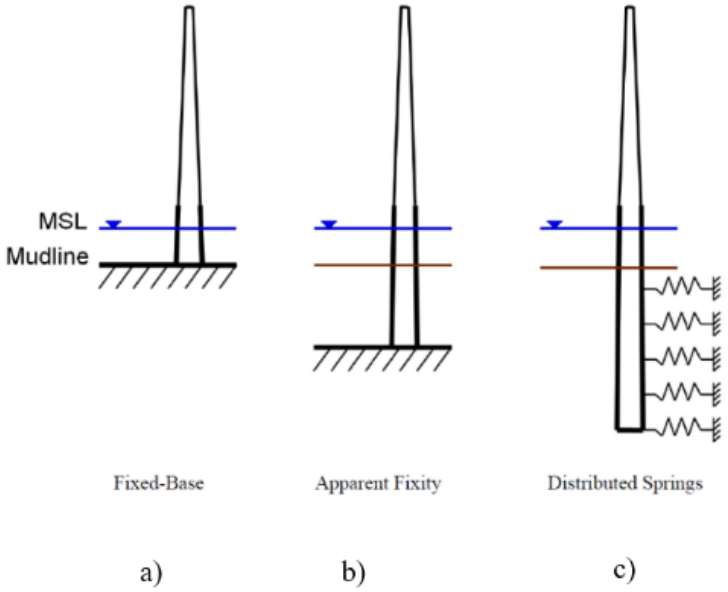

Figure 4-1 Various approximation used to model structure response to cyclic loading (Bush and Manuel, 2009)

OWTs are dynamically sensitive (Wang et al., 2017, Bhattacharya et al., 2015; Lombardi et al., 2013, Bhattacharya et al., 2013; Malhotra 2009) and their design must satisfy two criteria: rotation at mudline cannot exceed certain limit (typically 0.004 radians); and the lowest natural frequency should be ± 10% from the forcing frequency. Accordingly, the typical design of OWT is either:

1- **Soft-soft:** where first natural frequency lies below 1P frequency, rotor frequency, and the foundation stiffness is very small. Ideally this system is too soft to resist ultimate limit states loads and technically cannot be applied to OWT. However, it was reported in one case that it was used for a 3MW wind turbine (Lau,2015).

2- **Soft-stiff:** where the first natural frequency exists between 1P and 3P, blade passing, frequencies. This is what most measured/estimated values of OWT foundations first natural frequency reported in the literature as shown in Figure 4-2.

3- **Stiff-stiff:** when the first natural frequency is above 3P. This typically leads to very stiff and expensive foundation option, which is not economically feasible in many cases.

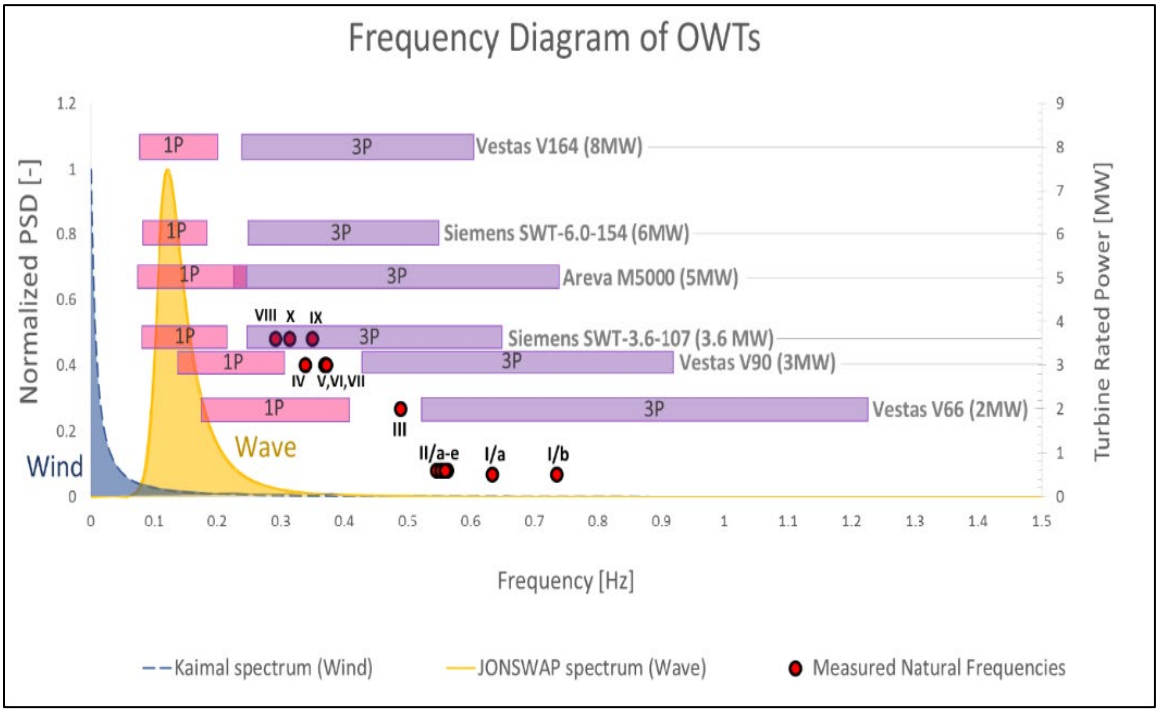

Figure 4-2 Wind, wave, 1P and 3P spectra with frequency range of OWT (Arany et al., 2016)

4.3 Methodology

The stiffness properties of hybrid and monopile foundations are investigated considering different cohesive soil profiles. A 3-spring method is used to idealize the foundation elements at mudline. Figure 4-3 presents the idealized 3 spring stiffness model.

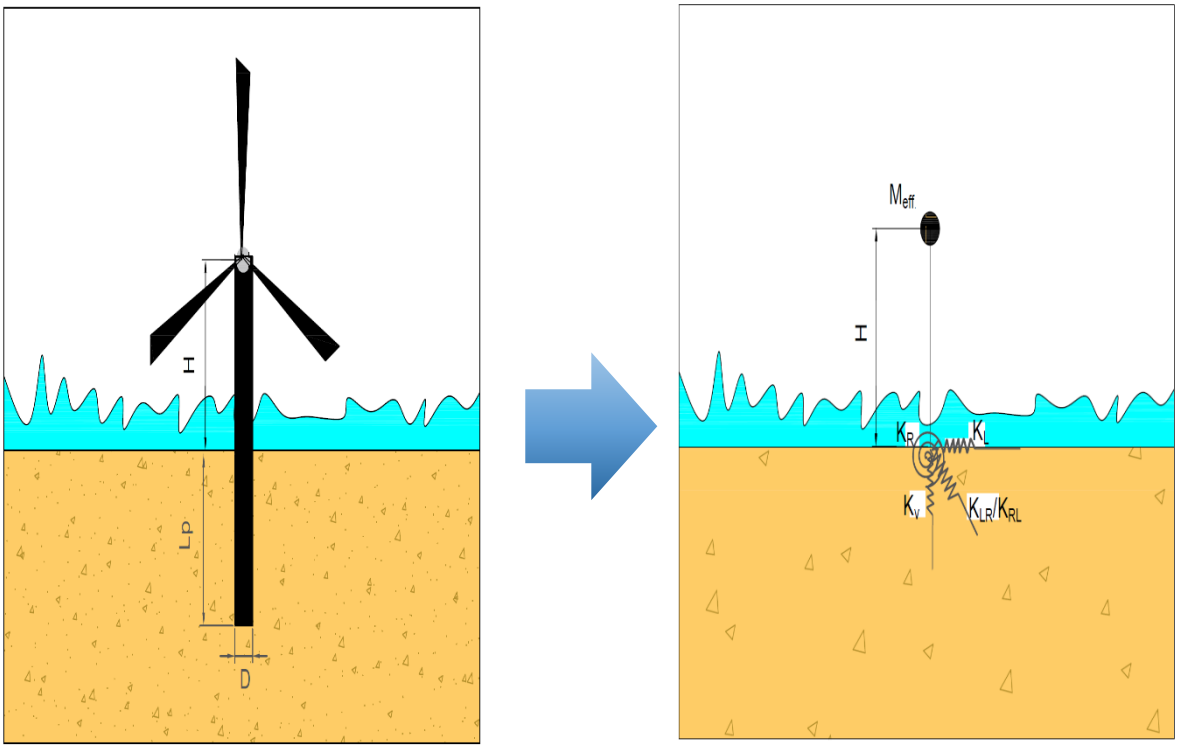

Figure 4-3 a: actual foundation, b: idealized mathematical model of 3-springs stiffnesses

4.3.1 *Analysis approach*

The aim of this study is to define η_L, $\eta_{LR/RL}$, and η_R for HF and MP foundations covering a range of cohesive soil profiles. The developed equations account for the effects of footing relative rigidity, termed E_p^*, with respect to soil stiffness, E_{50}, given by:

$$E_p^* = \frac{E_p I_p}{I_{scp}} \tag{4-10}$$

E_p^*: normalized pile stiffness; E_p: Young's modulus of pile material; E_s: Soil elastic modulus; I_p: Pile cross-section second moment of inertia; I_{scp}: moment of inertia of a solid cross-section of same diameter as actual pile.

In total, 120 finite element models (FEMs) were established utilizing the commercial code PLAXIS 3D and were utilized to obtain the stiffness properties. Six types of soils were considered

covering a range of soil profiles that were selected to bound soil profiles encountered in practise. For each case, horizontal loading was applied at M.L and the foundation rotation and displacement were recorded and used to obtain K_L and $K_{LR/RL}$. Additionally, a moment loading was applied in a separate case and displacement and rotations were recorded and used to calculate K_R and $K_{RL/LR}$. This process was repeated for all models. Figure 4-4 shows the procedure followed for all models.

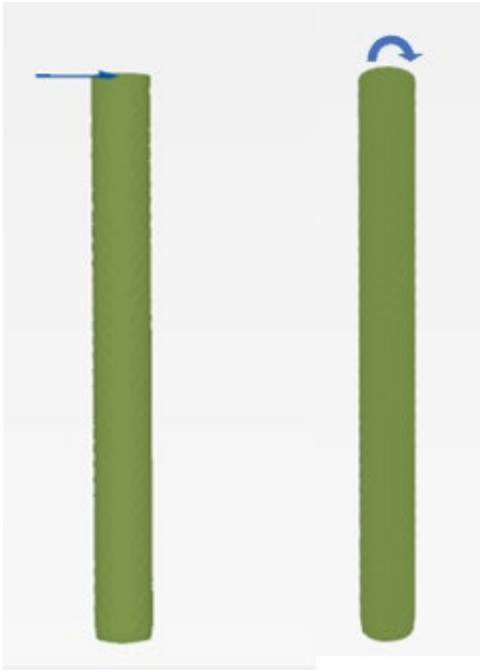

(a) (b)

Figure 4-4 Procedure for stiffnesses determination for a monopile with 80m depth (a) for determining K_L and K_{LR} (b) for determining K_{LR} and K_R

It was necessary to normalize the stiffness parameters so that generalized equations can be applied to any foundation geometry. For GBF and HF, the normalized stiffness properties are normalized by the plate width. Table 4-2 shows the normalization equations for MP and HF. The three spring stiffness values are given by:

$$K_L = \frac{Lateral\ load\ applied\ at\ M.L}{Lateral\ displacement\ at\ M.L} \quad (4\text{-}11)$$

$$K_{LR/RL} = \frac{Lateral\ load\ applied\ at\ M.L}{Lateral\ rotation\ at\ M.L} = \frac{Lateral\ moment\ applied\ at\ M.L}{Lateral\ displacement\ at\ M.L} \quad (4\text{-}12)$$

$$K_R = \frac{Lateral\ moment\ applied\ at\ M.L}{Lateral\ rotation\ at\ M.L} \quad (4\text{-}13)$$

Table 4-2 Normalization procedure for MP and HF

Parameter	Units	MP	HF
K_L	Force/length	$\eta_L = \frac{K_L D^3}{E_{50}}$	$\eta_L = \frac{K_L W^3}{E_{50}}$
$K_{LR/RL}$	Force	$\eta_{LR/RL} = \frac{K_{LR} D^2}{E_{50}}$	$\eta_{LR/RL} = \frac{K_L W^2}{E_{50}}$
K_R	Force*length/rotation	$\eta_R = \frac{K_R D}{E_{50}}$	$\eta_R = \frac{K_L W}{E_{50}}$

4.3.2 *Finite element model*

Monopiles' lateral, coupling, and rotational spring stiffness values are controlled by soil and pile properties. Hence it is important to simulate their correct behavior. Piles can be modelled using plate elements in Plaxis 3D or embedded beam elements. Both, however, are assumed to behave elastically. While volume elements do not provide information on structural forces, embedded beam elements do provide structural forces and can be used to check if structural failure is reached. It is for this reason that use of such elements is utilized to capture the effects of structural forces on pile's ultimate capacity and stiffness properties. With incorporation of a solid zone around the pile, Dao (2011) indicated that the embedded beam elements behaved similarly to volume piles. All HF models and MP systems are studied under own weight and D_p/t=85. The tower diameter was 6 m along its 90 m height, and its thickness was taken as 0.035 m. The MP diameter was taken as 6 m while HF plate was 14 m with 4 m pile inserted in the soil at its centre.

The MP length was varied from 20-80 m while The HF pile was considered either 0 (i.e. GBF), 14 m or 28 m (i.e., $L_p/W = 0$, 1 and 2), respectively. Table 4-3 shows the range of structure geometry considered herein and the information regarding applied loads and their corresponding locations. Table 4-4 shows the used soil profiles. 3D FE models were conducted to construct the OWT foundations. Figures 4-5 shows the foundation systems being studied. Tetrahedron 10-node elements were used to discretize the soil domain while beam elements were used to discretize the tower. Embedded beam elements with solid element confinement were used to simulate the pile while plate elements were used to simulate the foundation plate. The constitutive relationship utilized to simulate the soil behaviour was Hardening Soil (Hs) obeying Mohr-Coulomb failure criterion. The Hs model can simulate the behaviour of both soft and stiff soils. It was first proposed by Schanz (1998) as a second order model, which differs from first order models such as MC in that the stress dependency of stiffness can be modeled, plastic straining due to deviatoric and primary compression loading can be obtained, and that unloading stiffness is higher than loading stiffness giving plastic straining before reaching failure. The shear strength in Hs model, the clay the behavior accounted for effects of two strain hardening; namely volumetric hardening (cap) and shear where contraction and densification cause the yield surface to expand. The stiffness parameters are given by:

$$E_{oed} = E_{oed,ref}\left(\frac{c\cos\phi - \frac{\sigma'_3}{k_0^{NC}}\sin\phi}{c\cos\phi + p'_{ref}\sin\phi}\right)^m \quad (4\text{-}14)$$

$$E_{50} = E_{50,ref}\left(\frac{c\cos\phi - \sigma'_3\sin\phi}{c\cos\phi + p'_{ref}\sin\phi}\right)^m \quad (4\text{-}15)$$

$$E_{ur} = E_{ur,ref}\left(\frac{c\cos\phi - \sigma'_3\sin\phi}{c\cos\phi + p'_{ref}\sin\phi}\right)^m \quad (4\text{-}16)$$

To account for slippage and gap formation between the solids (pile and foundation plate) and soil, interface elements were used to simulate the contact between solids zone and soil. The interface elements were 6-noded elements having strength and stiffness properties as a percentage of the soil properties, defined through a reduction factor, R_{int}, varying between 1 for soft soils and 0.3 for stiff soils. The hybrid foundation plate was 2 m thick and was modelled with plate elements using elastic nonporous material model described with elastic modulus E = 27800 MPa and unit weight, $\gamma = 23.6 kN/m^3$. The tower was modelled as a beam element having unit weight, diameter, E and thickness of $77 kN/m^3$, 6 m, 200GPa and 0.035 m, respectively. The tower was connected to the embedded beam elements and surrounding solid elements through a rigid body to ensure the load is transferred uniformly over the pile area and to account for the diameter effect.

A convergence analysis was conducted to define models' boundaries. Vertical boundaries were restricted horizontally and allowed to move vertically while the bottom boundary was distanced more than 7D to ensure that rigid boundary will not affect stress/strain distribution and was assigned fixed in all directions x, y, and z. on average, around 25000 elements were used, and medium mesh size was considered after performing sensitivity analysis. Figure 4-6 and Figure 4-7 show the meshing developed for one of the cases. The z boundary was placed at least 3D below pile tip to avoid any stiffening effects and to model rotational stiffness correctly.

The analysis involved four stages, including: Initial stage (initiation of geostatic stresses) in which equilibrium is established based on lateral earth pressure coefficient at rest, k_o; Construction stage in which all structures and interface elements are activated; Loading stages: where either load or moment were applied; and finally the Output stage at which the foundation's deformations are examined to establish the mudline displacement and rotation to calculate the three spring stiffness parameters.

Table 4-3 3D analyses conducted on the proposed foundation system

L, m	L/D/(L_p/W)	Foundation system	e/D_t	V, kN
20	3.33	Monopile	6.83	Own weight[1]
30	5		6.83	
40	6.67		6.83	
50	8.33		6.83	
60	10		6.83	
70	11.67		6.83	
80	13.33		6.83	
0	0	Hybrid	6.83	
14	1		6.83	
28	2		6.83	

L: Depth of embedment; D: Pile's diameter; e: eccentricity of applied loads(m); D_t: Tower's diameter; 1: uniformly distributed, (Lp/W): length of pile/plate width

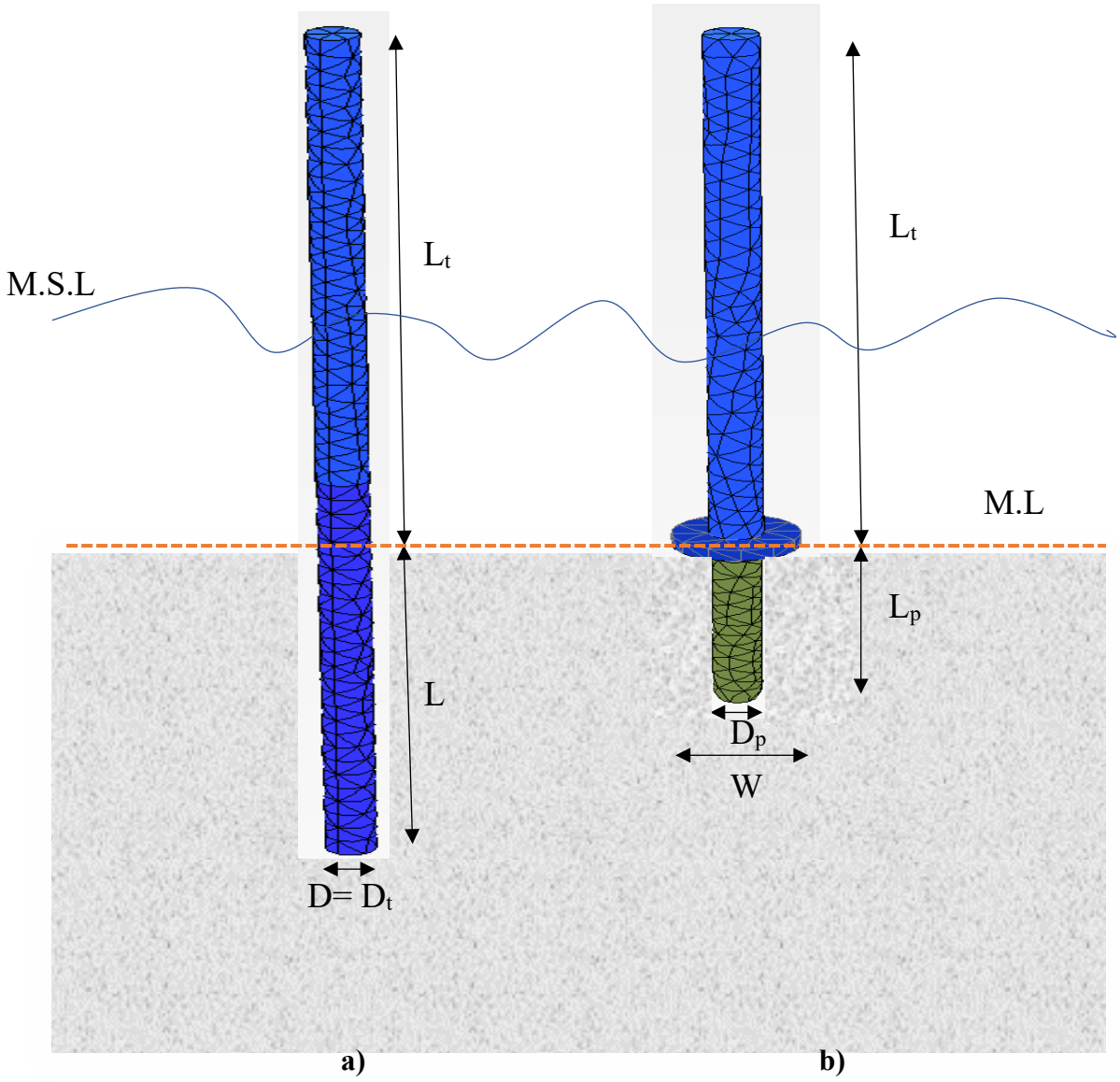

Figure 4-5 a) Monopile of D_p = 6m b) Hybrid foundation system with W=14m and D_p=4m. (Not to scale)

Table 4-4 Hs model properties for considered soils

Parameter	Clay1	Clay2	Clay3	Clay4	Clay5	Clay6
c'	4.23	24	44	87	170	354
Ψ	0	0	0	0	0	0
θ'	8	10	10	10	10	10
p'_{pop}, kPa	13	51	83	140	240	414
p'_{ref}, kPa	41	100	100	100	100	100
$e_{(ini).}$	4.209	4.209	4.209	4.209	4.209	4.209
ɣ, kN/m^3	17.9	17.9	17.9	17.9	17.9	17.9
E_{oed}^{ref}, kPa	1406	3461	14747	29040	56628	113134
E_{50}^{ref}, kPa	1758	4000	18439	36310	70805	141457
E_{ur}^{ref}, kPa	5000	10000	52444	103271	201380	402326
v_{ur}	0.2	0.2	0.2	0.2	0.2	0.2
M	0.6	0.6	0.6	0.6	0.6	0.6
PI	30	30	30	30	30	30
$K_{o,}$ **NC**	0.54	0.54	0.54	0.54	0.54	0.54
Depth, m	0-25	0-26	0-27	0-28	0-29	0-30
R_f	0.9	0.9	0.9	0.9	0.9	0.9

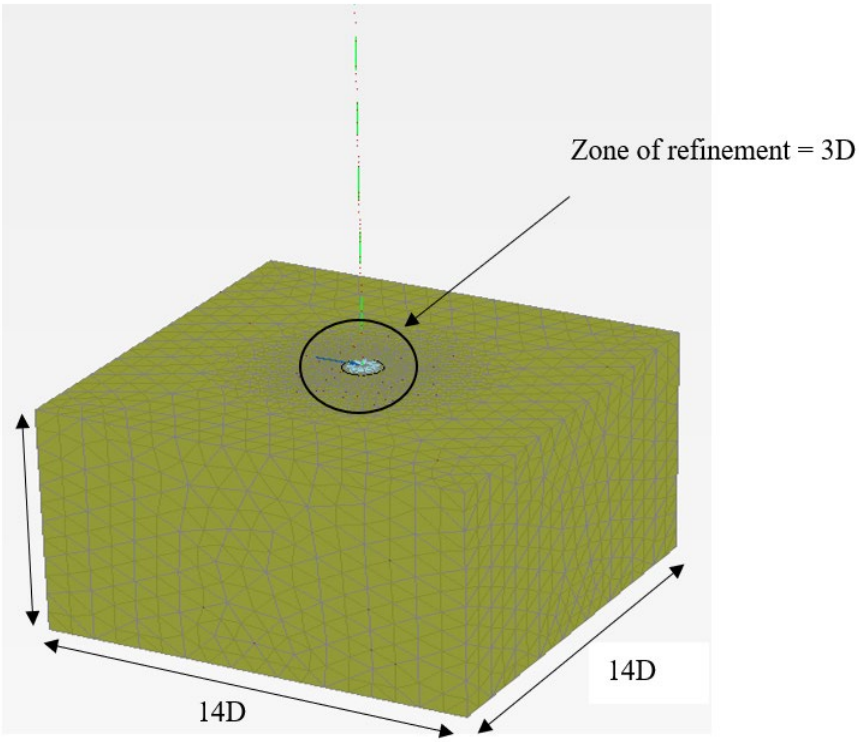

Figure 4-6 Typical model configuration

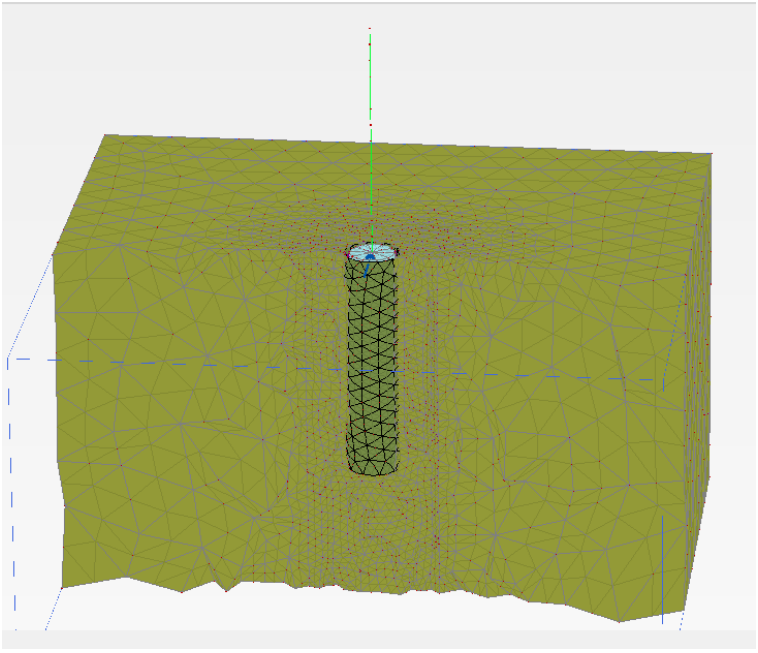

Figure 4-7 Cross section of developed mesh

4.3.3 *Finite Element Model Validation*

A case study reported by Zhu et al. (2017) was used to calibrate and validate the model. The validation results are reported in section 3.2.3.1 with convergence analysis.

4.4 Parameter study

4.4.1 *Monopile normalized stiffness*

Figures 4-8 through 4-10 show the normalized stiffness parameters versus the relative pile/soil stiffness, E_p^*/E_{50}, for the MP in different clayey soil profiles. The normalized stiffness η_L increases almost linearly with the increase in E_p^*/E_{50} for all cases of L/D. Inspecting these results reveals that the change follows the trend observed in normalized ultimate capacity curves although a plateau was not reached for the case of L/D=13.33. Small increase in normalized stiffness values was observed for stiff soils indicating a flexible pile behavior, i.e., for E_p^*/E_{50} less than 499 the piles length has little impact on the normalized stiffness. However, at E_p^*/E_{50} value of 984 a discernible difference is observed as the penetration depth increases. The same behavior was observed for the rotational and coupling stiffness values as shown in Figure 4-9 and Figure 4-10, respectively.

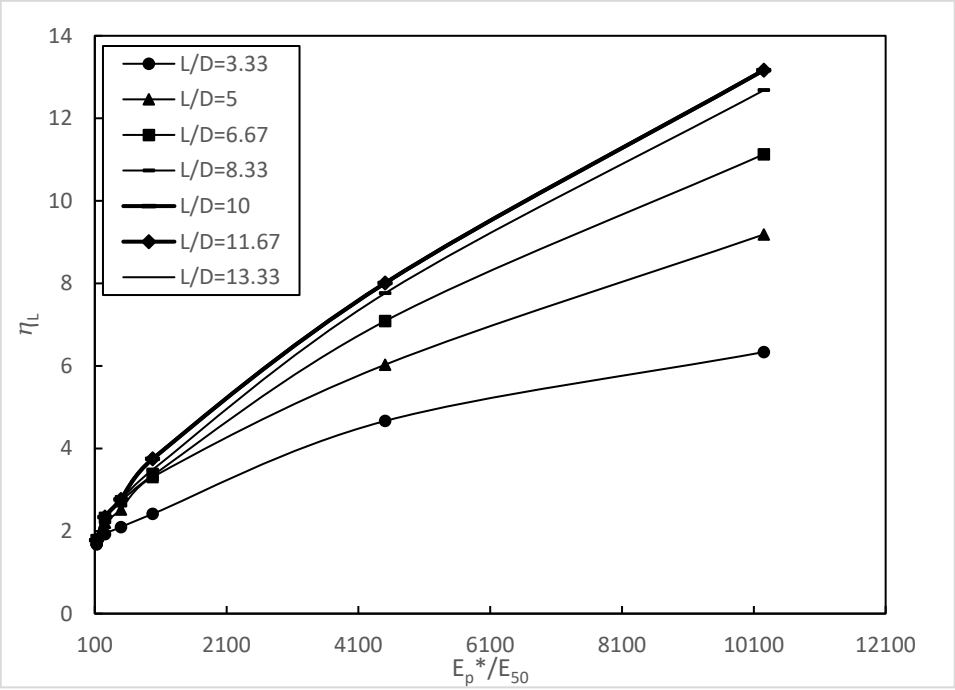

Figure 4-8 Effects of relative rigidity on normalized horizontal stiffness

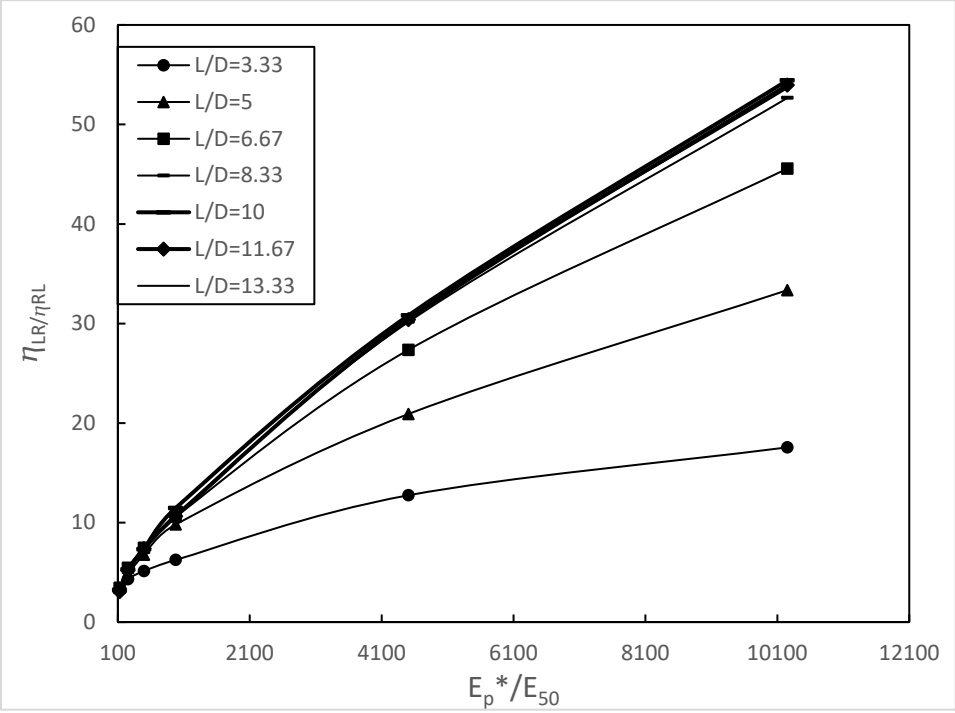

Figure 4-9 Effects of relative rigidity on normalized coupling stiffness

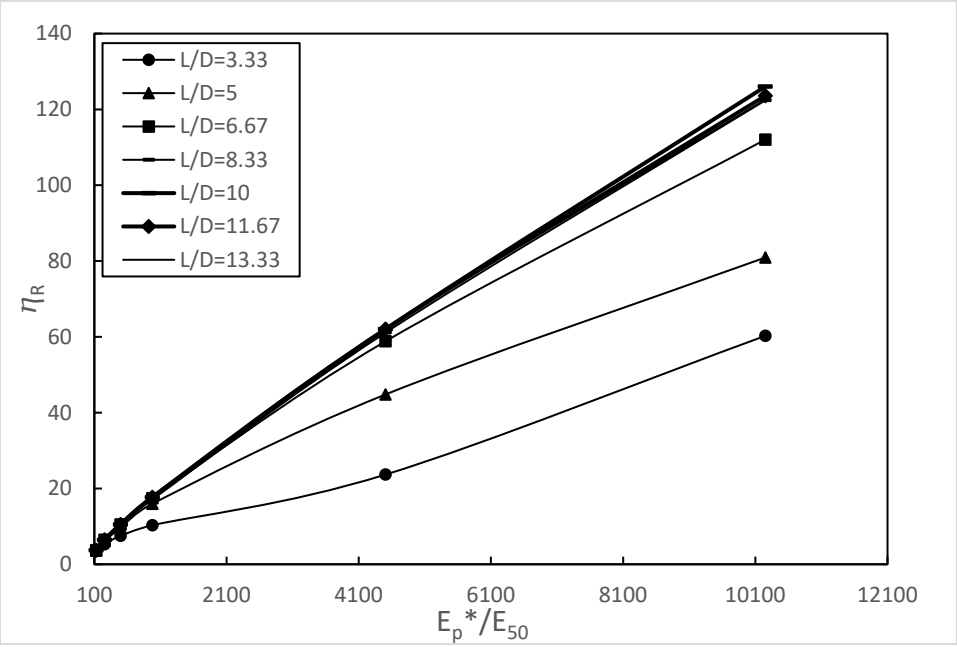

Figure 4-10 Effects of relative rigidity on normalized rocking stiffness

For a given E_p^*/E_{50} ratio, the change of normalized stiffness values with different L/D ratio differs significantly between E_p^*/E_{50} of 10208 where 'rigid' pile response was observed for all L/D values and for E_p^*/E_{50} value of 128 where flexible pile response was observed as reported in the previous chapter. This observation can be explained by looking at the variation of normalized stiffness values versus L/D ratio for all soil profiles considered as shown in Figures 4-8 until 4-10. In Figure 4-8, it is shown that for a stiff clay site (E_p^*/E_{50} of less than 984), the pile lateral stiffness reached a maximum at L/D ratio of between 5-8. For soft clay sites, the stiffness increases for all L/D ratios. These observations can be linked to variations of B.M in Figures 3-28 and 3-29 where it could be seen that the pile response was rigid for the case of clay1 with no flexing and toe kick-in while for clay 6 the pile experienced flexing with rotation around a pivot point located at around 0.7L beneath M.L. From Figures 4-8 until 4-10, curves have been fitted with polynomial functions to link the variation of normalized stiffness parameters with pile's geometry and soil properties, a

series of fitting equations to estimate these parameters are produced accordingly as shown in Figures 4-11 until 4-13.

4.4.1.1 Predictive equations for MP η_L

This section provides best fit equations for the horizontal normalized stiffness component at mudline for MP across different clayey soils. Figure 4-11 compares the equations prediction for η_L values for MP along with the FE data, and an excellent agreement is observed.

L/D =3.33

$$\eta_L = -3.699E0\text{-}8*(\frac{E_p^*}{E_{50}})^2 + 0.000836*(\frac{E_p^*}{E_{50}}) + 1.654 \qquad (R^2 = 0.999) \quad (4\text{-}17)$$

L/D =5

$$\eta_L = 1.915E0\text{-}11*(\frac{E_p^*}{E_{50}})^3 - 3.25E\text{-}7*(\frac{E_p^*}{E_{50}})^2 + 0.002059*(\frac{E_p^*}{E_{50}}) + 1.5999 \qquad (R^2 = 0.999) \quad (4\text{-}18)$$

L/D = 6.67

$$\eta_L = 1.244E0\text{-}11*(\frac{E_p^*}{E_{50}})^3 - 2.317E\text{-}7*(\frac{E_p^*}{E_{50}})^2 + 0.001988*(\frac{E_p^*}{E_{50}}) + 1.693 \qquad (R^2 = 0.998) \quad (4\text{-}19)$$

L/D =8.33

$$\eta_L = 1.259E0\text{-}11*(\frac{E_p^*}{E_{50}})^3 - 2.341E\text{-}7*(\frac{E_p^*}{E_{50}})^2 + 0.002152*(\frac{E_p^*}{E_{50}}) + 1.668 \qquad (R^2 = 0.9985) \quad (4\text{-}20)$$

L/D =10

$$\eta_L = 1.969E0\text{-}11*(\frac{E_p^*}{E_{50}})^3 - 3.242E\text{-}7*(\frac{E_p^*}{E_{50}})^2 + 0.002572*(\frac{E_p^*}{E_{50}}) + 1.571 \qquad (R^2 = 0.999) \quad (4\text{-}21)$$

L/D =>11.67

$$\eta_L = 1.969E0\text{-}11*(\frac{E_p^*}{E_{50}})^3 - 3.242E\text{-}7*(\frac{E_p^*}{E_{50}})^2 + 0.002572*(\frac{E_p^*}{E_{50}}) + 1.571 \quad (R^2 = 0.999) \quad (4\text{-}22)$$

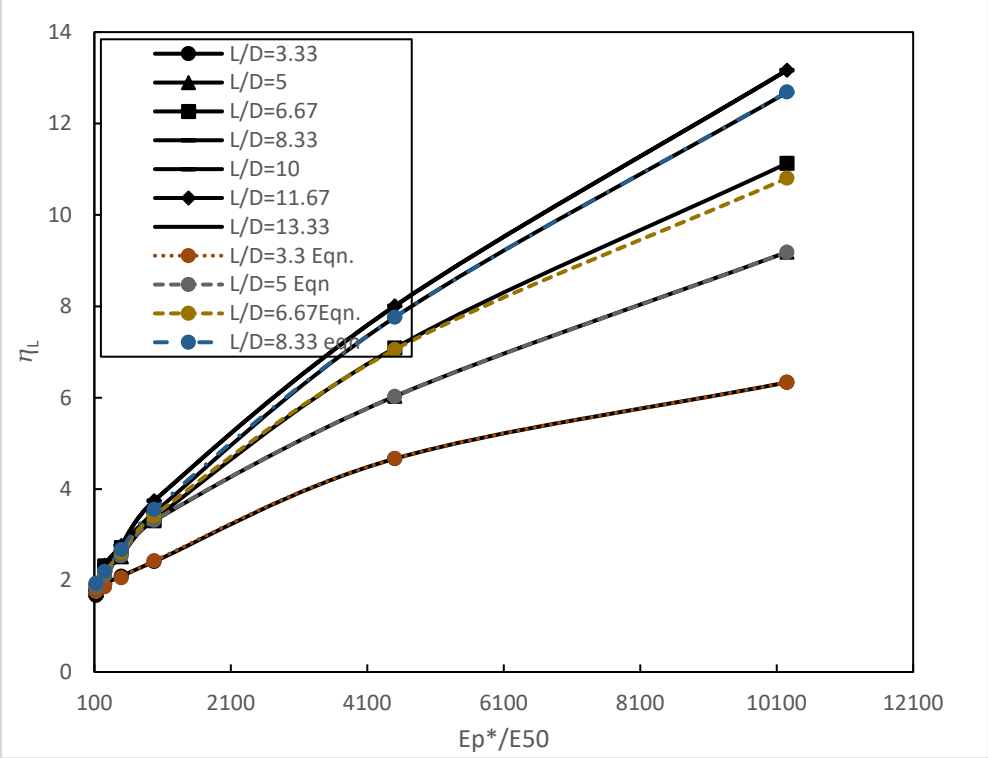

Figure 4-11 fitting equations describing η_L

4.4.1.2 Predictive equations for MP $\eta_{LR/RL}$

This section provides best fit equations for the coupling spring normalized stiffness component, $\eta_{LR/RL}$, at mudline for MP across different clayey soils. The equations were plotted with the FE data and showed excellent match, Figure 4-12.

L/D=3.33

$$\eta_{LR/RL} = 2.554E0\text{-}11*(\frac{E_p^*}{E_{50}})^3 - 5.041E\text{-}7*(\frac{E_p^*}{E_{50}})^2 + 0.003896*(\frac{E_p^*}{E_{50}}) + 3.079 \quad (R^2 = 0.996) \quad (4\text{-}23)$$

L/D=5

$$\eta_{LR/RL} = 8.653E0\text{-}11*\left(\frac{E_p^*}{E_{50}}\right)^3 - 1.464E\text{-}6*\left(\frac{E_p^*}{E_{50}}\right)^2 + 0.008917*\left(\frac{E_p^*}{E_{50}}\right) + 2.524 \qquad (R^2 = 0.9996) \quad (4\text{-}24)$$

L/D=6.67

$$\eta_{LR/RL} = 6.203E0\text{-}11*\left(\frac{E_p^*}{E_{50}}\right)^3 - 1.138E\text{-}6*\left(\frac{E_p^*}{E_{50}}\right)^2 + 0.009323*\left(\frac{E_p^*}{E_{50}}\right) + 2.762 \qquad (R^2 = 0.999) \quad (4\text{-}25)$$

L/D=8.33

$$\eta_{LR/RL} = 5.362E0\text{-}11*\left(\frac{E_p^*}{E_{50}}\right)^3 - 1.005E\text{-}6*\left(\frac{E_p^*}{E_{50}}\right)^2 + 0.009546*\left(\frac{E_p^*}{E_{50}}\right) + 2.623 \qquad (R^2 = 0.999) \quad (4\text{-}26)$$

L/D=>10

$$\eta_{LR/RL} = 7.433E0\text{-}11*\left(\frac{E_p^*}{E_{50}}\right)^3 - 1.314E\text{-}6*\left(\frac{E_p^*}{E_{50}}\right)^2 + 0.01075*\left(\frac{E_p^*}{E_{50}}\right) + 2.249 \qquad (R^2 = 0.9997) \quad (4\text{-}27)$$

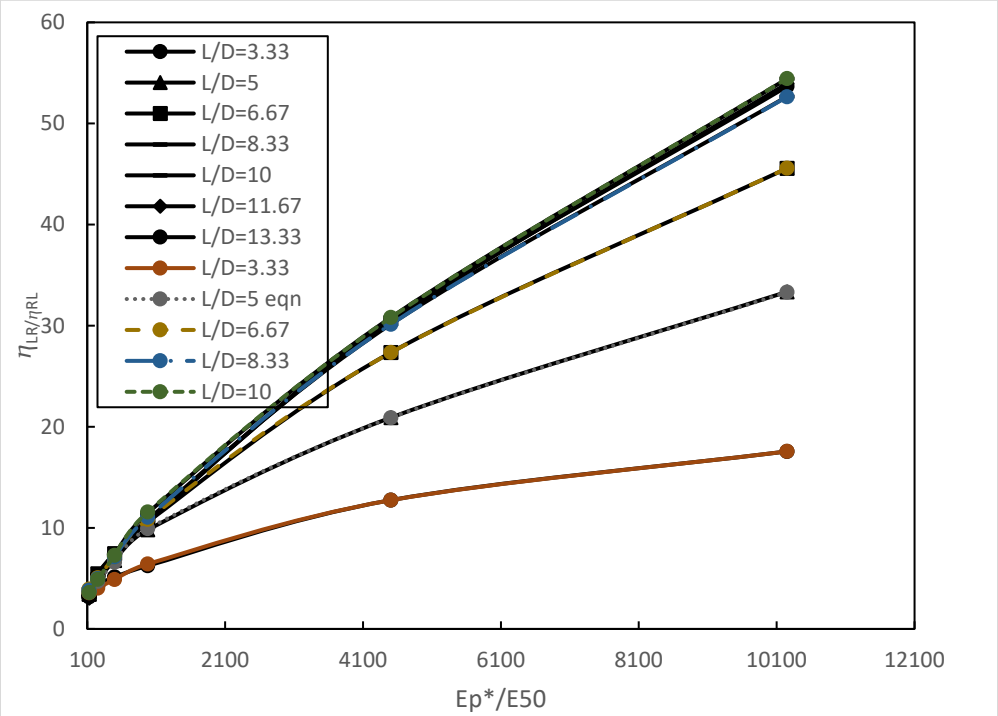

Figure 4-12 Fitting equations describing ηLR

4.4.1.3 Predictive equations for MP ηR

This section provides best fit equations for the rocking spring normalized stiffness component, η_R, at mudline for MP across different clayey soils. The equations were plotted with the FE data and showed excellent match, Figure 4-13.

L/D=3.33

$$\eta_R = 1.214E\text{-}10*\left(\frac{E_p^*}{E_{50}}\right)^3 - 1.623E\text{-}6*\left(\frac{E_p^*}{E_{50}}\right)^2 + 0.009496*\left(\frac{E_p^*}{E_{50}}\right) + 2.725 \qquad (R^2 = 0.9995) \quad (4\text{-}28)$$

L/D=5

$$\eta_R = 1.216E\text{-}10*\left(\frac{E_p^*}{E_{50}}\right)^3 - 2.113E\text{-}6*\left(\frac{E_p^*}{E_{50}}\right)^2 + 0.0166*\left(\frac{E_p^*}{E_{50}}\right) + 1.774 \qquad (R^2 = 0.9999) \quad (4\text{-}29)$$

L/D=6.67

$$\eta_R = 7.12E\text{-}11*\left(\frac{E_p^*}{E_{50}}\right)^3 - 1.38E\text{-}6*\left(\frac{E_p^*}{E_{50}}\right)^2 + 0.01741*\left(\frac{E_p^*}{E_{50}}\right) + 1.876 \qquad (R^2 = 0.9999) \quad (4\text{-}30)$$

L/D=>8.33

$$\eta_R = 5.33E\text{-}11*\left(\frac{E_p^*}{E_{50}}\right)^3 - 1.025E\text{-}6*\left(\frac{E_p^*}{E_{50}}\right)^2 + 0.01664*\left(\frac{E_p^*}{E_{50}}\right) + 2.041 \qquad (R^2 = 0.9999) \quad (4\text{-}31)$$

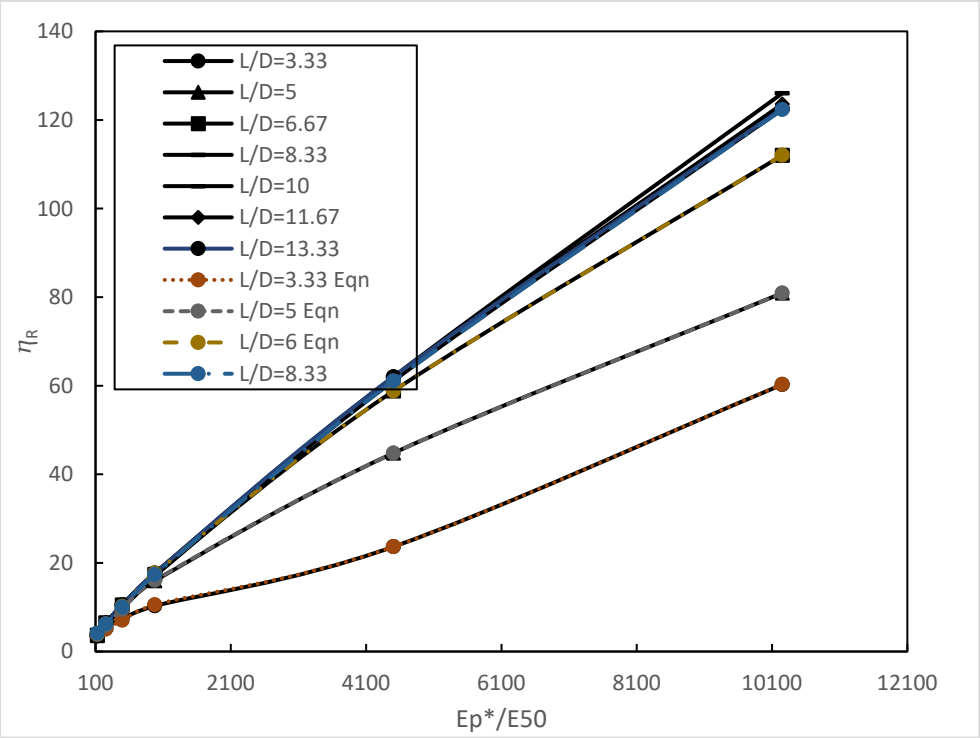

Figure 4-13 Fitting equations describing ηR

4.4.2 *Hybrid foundation normalized stiffness*

Figures 4-14 through 4-16 show the normalized stiffness parameters versus the Lp/W ratio the HF for different clay profiles. The normalized stiffness η_L vary almost linearly with the increase in normalized stiffness for all cases of L_p/W. However, a close look reveals that the change follows the trend observed in normalized ultimate capacity curves although a plateau was not reached for the case of Lp/W=2. Small increase in normalized stiffens values was observed for stiff soils indicating a flexible behavior was reached however at higher E_p^*/E_{50} a discernible difference is observed when increasing penetration depth. This behavior was consistently observed with the coupling stiffness values and the rotational stiffness as well, as seen in Figure 4-15 and Figure 4-16, respectively.

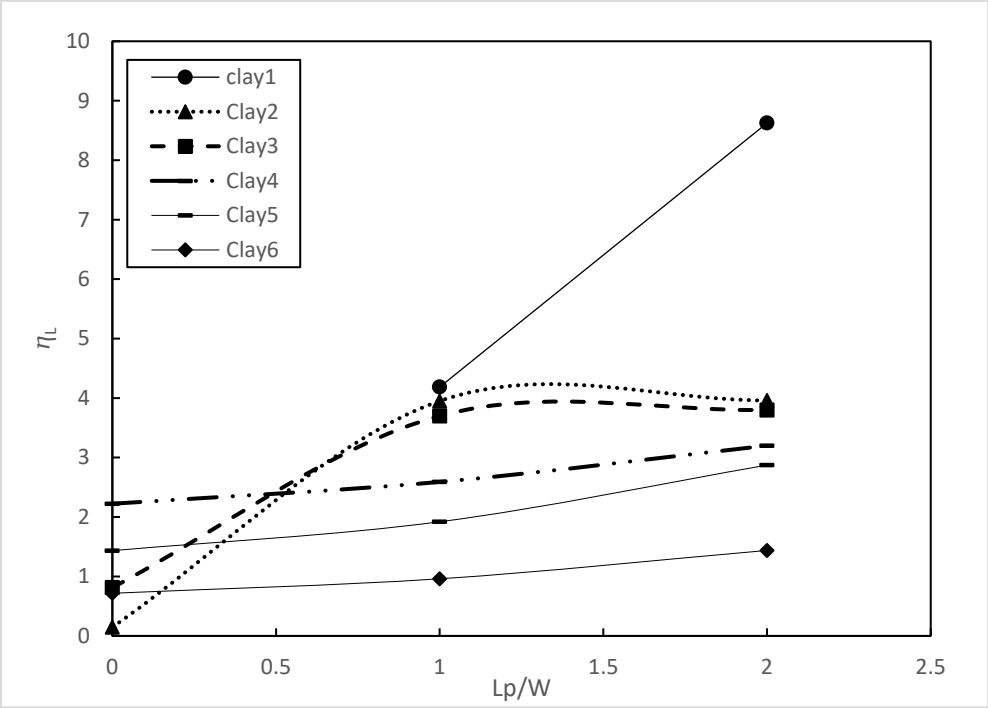

Figure 4-14 ηL for GBF/H.F across various soils

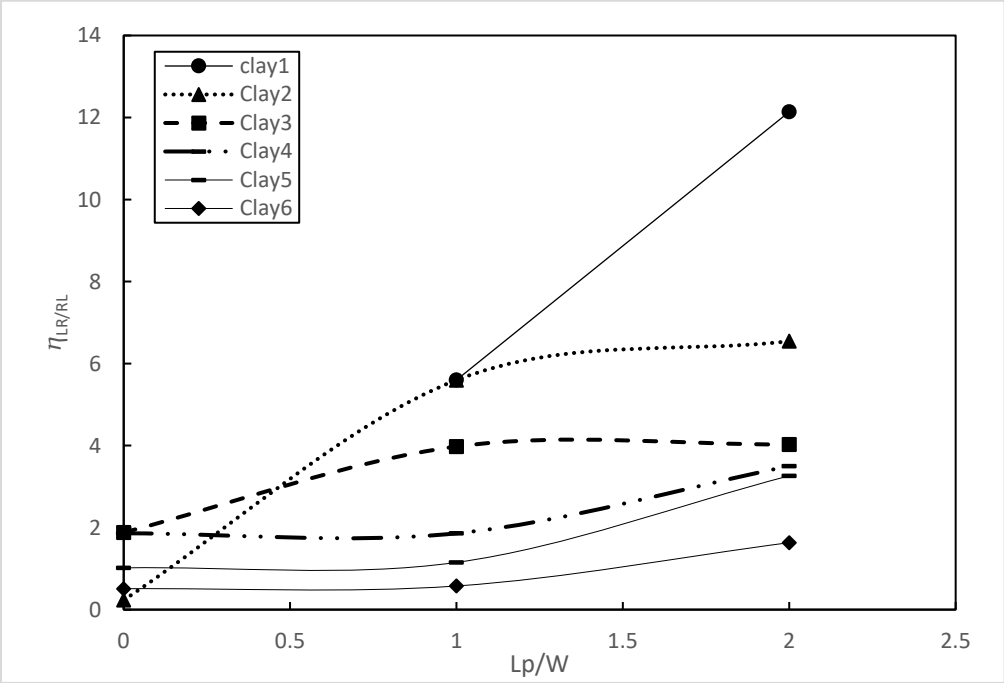

Figure 4-15 ηLR/RL values for GBF/H.F across various clay profiles

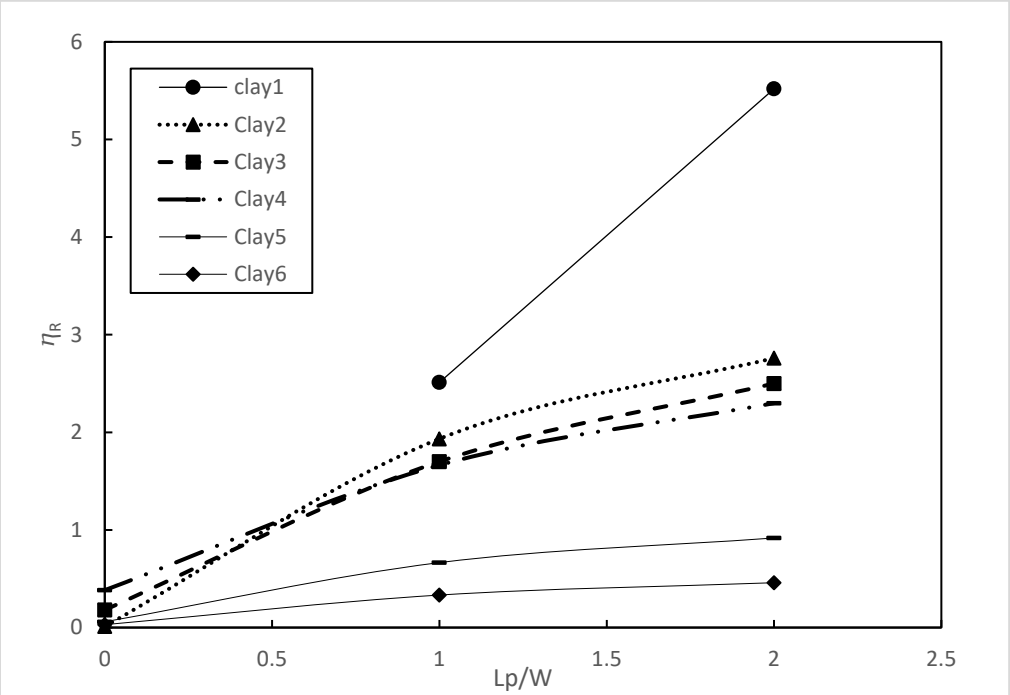

Figure 4-16 ηR values for GBF/H.F across various clay profiles

Similar conclusions are drawn from previous figures as the values of the normalized stiffness follow the same trend observed in MP foundations. Results showed the stiffness of the system is substantially increased with addition of a pile with six-fold increase in lateral stiffness for soft soil (S_{u0}=4.2 kPa) while the trend of increase in stiffness values decreases with the increase of soil's shear strength. For the first two profiles, the horizontal stiffness increase for both L_p/W of 1 and 2 considered while for the other profiles the increase beyond L_p/W of 1 was negligible.

4.4.2.1 Predictive equations for HF ηL

This section provides best fit equations for the horizontal normalized stiffness component at mudline for HF across different clayey soils. Figure 4-17 compares the equations prediction for η_L values for HF along with the FE data, and an excellent agreement is observed.

Clay1:

$$\eta_L = 0.177*(\frac{L_p}{W})^2 + 3.9082*(\frac{L_p}{W}) + 0.1 \qquad (R^2=1) \quad (4\text{-}32)$$

Clay2:

$$\eta_L = -1.8966*(\frac{L_p}{W})^2 + 5.6995 * (\frac{L_p}{W}) + 0.1478 \qquad (R^2=1) \quad (4\text{-}33)$$

Clay3:

$$\eta_L = -1.3931*(\frac{L_p}{W})^2 + 4.2792 * (\frac{L_p}{W}) + 0.8139 \qquad (R^2=1) \quad (4\text{-}34)$$

Clay4:

$$\eta_L = 0.4886*(\frac{L_p}{W}) + 2.1822 \qquad (R^2=0.98) \quad (4\text{-}35)$$

Clay5:

$$\eta_L = 0.7193*(\frac{L_p}{W}) + 1.3561 \qquad (R^2=0.9662) \quad (4\text{-}36)$$

Clay6:

$$\eta_L = 0.3601*(\frac{L_p}{W}) + 0.6788 \qquad (R^2=0.9662) \quad (4\text{-}37)$$

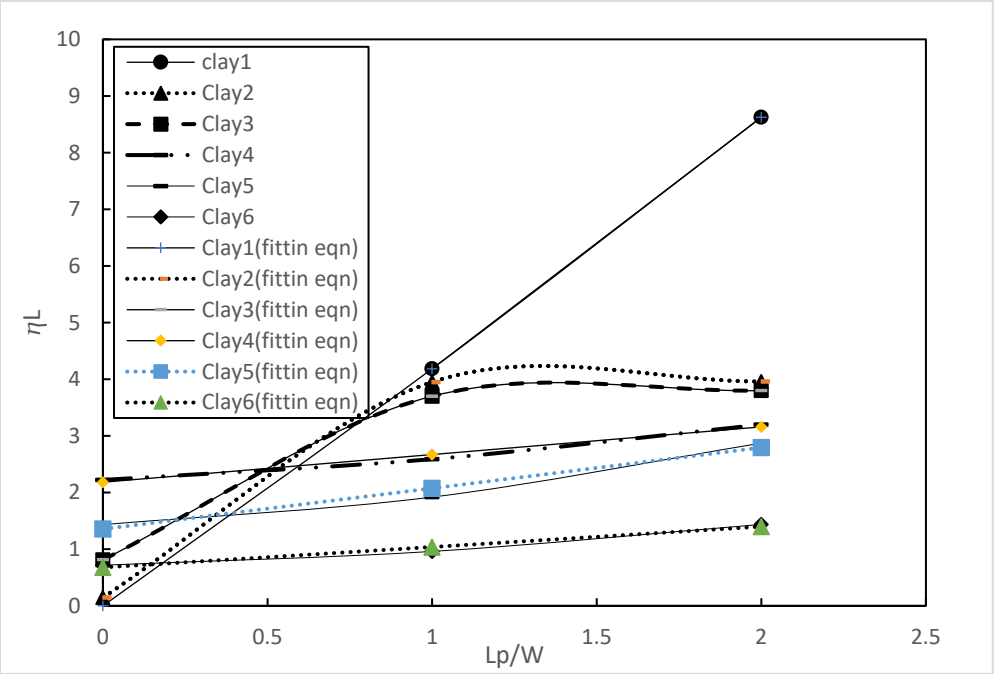

Figure 4-17 η_L for GBF/H.F across various soils with fitting equations

4.4.2.2 Predictive equations for HF $\eta_{LR/RL}$

This section provides best fit equations for the coupling spring normalized stiffness component, $\eta_{LR/RL}$, at mudline for HF across different clayey soils. The equations were plotted with the FE data and showed excellent match, Figure 4-18.

Clay1:

$$\eta_{LR/RL} = 0.5697*(\frac{Lp}{W})^2+4.8303*(\frac{Lp}{W}) + 0.2 \qquad (R^2=1)\ (4\text{-}38)$$

Clay2:

$$\eta_{LR/RL} = -2.2077*(\frac{Lp}{W})^2 + 7.5717 * (\frac{Lp}{W}) + 0.2335 \qquad (R^2=1)\ (4\text{-}39)$$

Clay3:

$$\eta_{LR/RL} = -1.0221*(\frac{L_p}{W})^2 + 3.1177 * (\frac{L_p}{W}) + 1.8811 \qquad (R^2=1)\ (4\text{-}40)$$

Clay4:

$$\eta_{LR/RL} = 0.8195*(\frac{L_p}{W})^2 - 0.8195* (\frac{L_p}{W}) + 1.8611 \qquad (R^2=1)\ (4\text{-}41)$$

Clay5:

$$\eta_{LR/RL} = 0.989*(\frac{L_p}{W})^2 - 0.8556* (\frac{L_p}{W}) + 1.018 \qquad (R^2=1)\ (4\text{-}42)$$

Clay6:

$$\eta_{LR/RL} = 0.495*(\frac{L_p}{W})^2 - 0.4283* (\frac{L_p}{W}) + 0.5096 \qquad (R^2=1)\ (4\text{-}43)$$

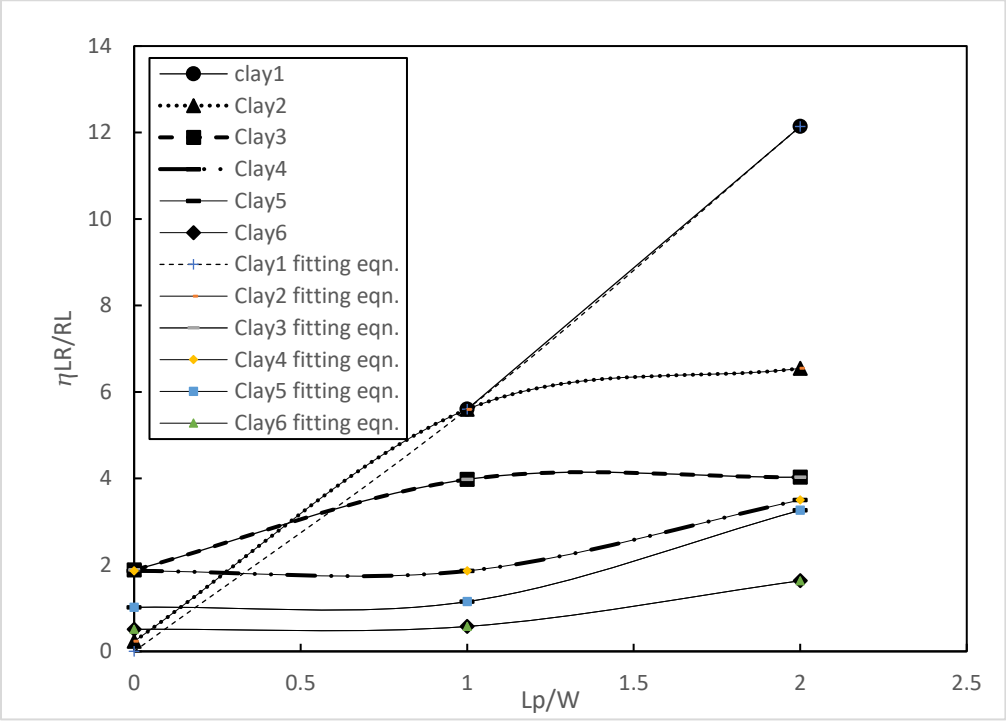

Figure 4-18ηLR/RL values of HF and those from fitting equations

4.4.2.3 Predictive equations for HF ηR

This section provides best fit equations for the rocking spring normalized stiffness component, η_R, at mudline for HF across different clayey soils. The equations were plotted with the FE data and showed excellent match, Figure 4-19.

Clay1:

$$\eta_R = 0.2532*(\frac{L_p}{W})^2 + 2.248*(\frac{L_p}{W}) + 0.01 \qquad (R^2=1)\ (4\text{-}44)$$

Clay2:

$$\eta_R = -0.5474*(\frac{L_p}{W})^2 + 2.4689*(\frac{L_p}{W}) + 0.012 \qquad (R^2=1)\ (4\text{-}45)$$

Clay3:

$$\eta_R = -0.3597*(\frac{L_p}{W})^2 + 1.879*(\frac{L_p}{W}) + 0.1807 \qquad (R^2=1)\ (4\text{-}46)$$

Clay4:

$$\eta_R = -0.3225*(\frac{L_p}{W})^2 + 1.6028*(\frac{L_p}{W}) + 0.3833 \qquad (R^2=1)\ (4\text{-}47)$$

Clay5:

$$\eta_R = -0.1767*(\frac{L_p}{W})^2 + 0.7827*(\frac{L_p}{W}) + 0.0593 \qquad (R^2=1)\ (4\text{-}48)$$

Clay6:

$$\eta_R = -0.0884*(\frac{L_p}{W})^2 + 0.3918*(\frac{L_p}{W}) + 0.0297 \qquad (R^2=1)\ (4\text{-}49)$$

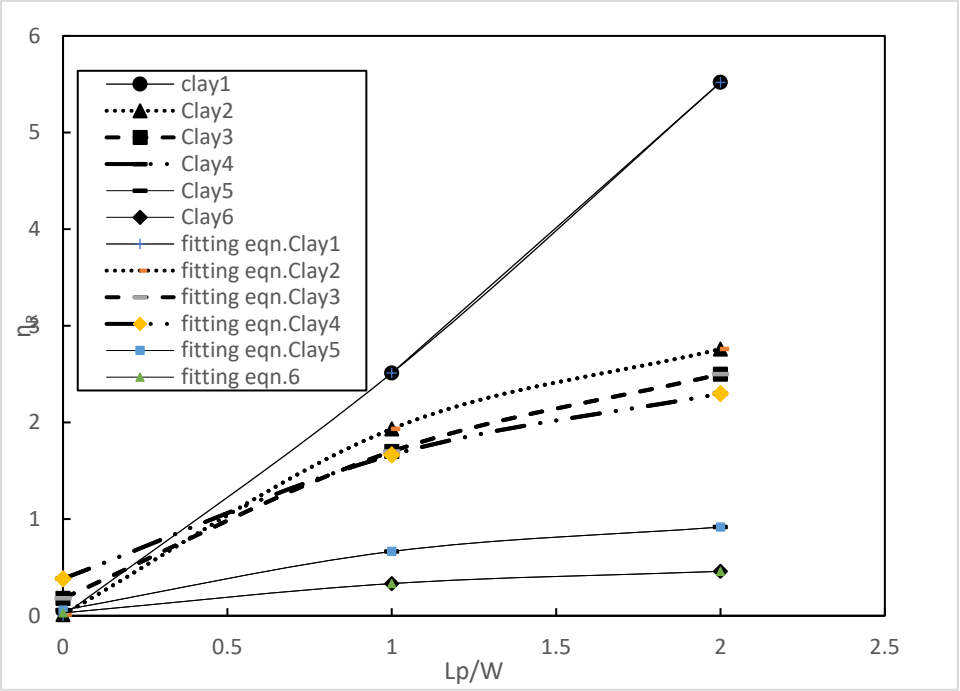

Figure 4-19 η_R values for HF foundations from fitting equations and FE

4.5 Conclusion

Monopile foundations utilisation for OWT's plays an important role for supporting the development of green electricity alternatives. Future developments of OWF are expected to be challenging for designers and require massive weight of foundations. A hybrid foundation is proposed and is studied, along with monopile, for their stiffness properties. A three-spring stiffness model is adopted to characterise the mechanical behavior of these foundations at soil mudline. Adding a plate around monopiles can change the behavior and a new normalization procedure is applied to obtain the stiffness properties of hybrid foundation as well. Different soils conditions were considered, and generic curves were established from which stiffness properties can be obtained. For HF, the selected range of pile's length to plate diameter, Lp/W, were 1 and 2, respectively while for MP, the L/D ratios vary from 3.33 to 13.33. Several conclusions were drawn:

- The normalized stiffness parameters versus normalized foundation stiffness showed almost linear increase in normalized stiffness values for all L/D ratio, unlike the normalized lateral ultimate capacities which showed a plateau for normalized stiffness values less than 2000. This is because the difference in applied lateral loads which, in the case of lateral ultimate capacity, caused structural failure in piles thereby reducing normalized capacity
- For the normalized horizontal stiffness for MP, η_L, the normalized stiffness values ceased to increase after L/D ratio of 11.67
- For the normalized coupling stiffness for MP, $\eta_{LR/RL}$, the normalized stiffness value ceased to increase after L/D ratio of 10
- For normalized coupling stiffness for MP, η_R, the normalized stiffness values ceased to increase after L/D ratio of 8
- The normalized lateral stiffness properties of hybrid foundations increase against Lp/W ratios and the increase rate was dependent on the clay shear strength. At small shear strength values, considerable increase in relative stiffness was obtained because of the addition of hybrid foundation pile. This is in line with normalized lateral ultimate capacity findings which showed the capacity, and hence the stiffness of this foundation option is dependent on the foundation plate diameter and is insensitive to the pile' length
- The normalized horizontal stiffness for HF, η_L, the normalized stiffness values increased with increasing L_p/W ratio, however, at different rates. They showed highest increase for clay 1 and least increase for clay6. For clays from 2 to 6, the increase in the normalized stiffness between Lp/W 1 and 2 was smaller than the increase in clay 1. These findings are in line with lateral ultimate capacity findings where the normalized lateral ultimate capacity

of this system showed little to no improvement when increasing the Lp/W ratio mainly because the structural capacity of the hybrid foundation pile hindered any further gain in lateral load resistance.

- The normalized coupling stiffness for HF, $\eta_{LR/RL}$, showed similar trends as in η_L
- For normalized coupling stiffness for HF, η_R, the normalized stiffness values increased for all Lp/W; however, the increase was observed to be at a decaying rate as the soil shear strength increased. Similar findings of increase in stiffness, although small, beyond Lp/W of 1 were observed, unlike normalized lateral ultimate capacity which is attributed to range of applied forces being within structural capacity of hybrid system pile and therefore no plateau was reached.

4.6 References

Abdelkader, Ahmed Mohamed Reda, Investigation of Hybrid Foundation System for Offshore Wind Turbine (Scholarship@Western). 2016.

Achmus, M., Kuo, Y.-S., & Abdel-Rahman, K. (2009). Behavior of monopile foundations under cyclic lateral load. *Computers and Geotechnics*, *36*(5), 725–735. https://doi.org/10.1016/j.compgeo.2008.12.003

API, 1993. Recommended practice for planning, designing, and Constructing fixed offshore platforms. API, RPT2A-WSD. American Petroleum Institute (API), Washington, D.C.

Arany, L., Bhattacharya, S., Macdonald, J. H. ., & Hogan, S. J. (2016). Closed form solution of Eigen frequency of monopile supported offshore wind turbines in deeper waters incorporating stiffness of substructure and SSI. *Soil Dynamics and Earthquake Engineering (1984)*, *83*, 18–32. https://doi.org/10.1016/j.soildyn.2015.12.011

Association EWE. The European Offshore Wind Industry‑Key Trends and Statistics 2016; January; 2017.

Bentley, K.J. and El Naggar, M.H., 2000. Numerical analysis of kinematic response of piles. Canadian Geotechnical Journal, Vol. 37, No. 6, pp. 1368-1382

Bisoi, & Haldar, S. (2019). 3D Modeling of Long-Term Dynamic Behavior of Monopile-Supported Offshore Wind Turbine in Clay. International Journal of Geomechanics, 19(7), 4019062–. https://doi.org/10.1061/(ASCE)GM.1943-5622.0001437

Bisoi, S., and S. Haldar. 2014. “Dynamic analysis of offshore wind turbine in clay considering soil-monopile-tower interaction.” Soil Dyn. Earthquake Eng. 63: 19–35. https://doi.org/10.1016/j.soildyn.2014.03.006.

Bush, E.; Manuel, L. Foundation Models for Offshore Wind Turbines. 47th AIAA Aerospace Sciences Meeting Including The New Horizons Forum and Aerospace Exposition5 - 8 January 2009, Orlando, Florida

Broms, B. B. (1964b). Lateral Resistance of Piles in Cohesive Soils. Journal of the Soil Mechanics and Foundations, **90**(2): 27-64.

Bhattacharya, S, Nikitas,;N, Garnsey; N.A. Alexander; J.Cox; D. Muir Wood and D. F.T.Nash (2013) Observed dynamic soil–structure interaction in scale testing of offshore wind turbine foundations. Soil Dynamics and Earthquake Engineering, 54. 47 - 60. ISSN 0267-7261

Byrne, B.W. and Houlsby, G.T. (2003) “Foundations for Offshore Wind Turbines”, Philosophical Transactions of the Royal Society of London, Series A, Vol. 361, December, pp 2909-2930.

Byrne B. W., McAdam R., Burd H. J., Houlsby G. T., Martin C. M., Zdravković L., Taborda D. M. G., Potts D. M., Jardine R. J., Sideri M., Schroeder F. C., Gavin K., Doherty P., Igoe D., Muir Wood A., Kellahave D. and Skov Gretlund J. 2015a. New design methods for large diameter piles under lateral loading for offshore wind applications. *Proceedings of Third International Symposium on Frontiers in Offshore Geotechics* 1, 705-710.

Byrne B. W., McAdam R., Burd H. J., Houlsby G. T., Martin C. M., Gavin K., Doherty P., Igoe D., Zdravković L., Taborda D. M. G., Potts D. M., Jardine R. J., Sideri M., Schroeder F. C., Muir Wood A., Kellahave D. and Skov Gretlund J. 2015b. Field testing of large diameter piles under lateral loading for offshore wind applications. *Proceedings of XVI European Conference on Soil Mechanics and Geotechnical Engineering*, Edinburgh, 1255-1260.

Byrne. Foundations for Offshore Wind Turbines (2013). Presentation. University of Oxford.

El-Marassi M., Elnaggar, M.H, Newson, T. and Stone, K. Numerical modelling of the performance of a hybrid monopiled-footing foundation. GeoEdmonton, 2008.

El-Marassi M. Investigation of hybrid monopile-footing foundation systems subjected to combined loading: The University of Western Ontario; 2011.

Jackson, F. A (2016). Assessment of earthquake site amplification and application of passive seismic methods for improved site classification in the greater vancouver region, british columbiaScholarship@Western.

Jonkman, J. M., Musial, W. D., & National Renewable Energy Laboratory (U.S.). (2010). *Offshore code comparison collaboration (OC3) for IEA task 23 offshore wind technology and deployment.* (No. 5000-48191.;5000-48191;). Golden, Colo: National Renewable Energy Laboratory.

Lamb, Robert. "When will we run out of oil, and what happens then?" 21 April 2010. HowStuffWorks.com. <https://science.howstuffworks.com/environmental/energy/run-out-of-oil.htm> 15 May 2018

Lombardi, D., Bhattacharya, S., & Muir Wood, D. (2013). Dynamic soil–structure interaction of monopile supported wind turbines in cohesive soil. Soil Dynamics and Earthquake Engineering (1984), 49, 165–180. https://doi.org/10.1016/j.soildyn.2013.01.015

Malhotra, S. "Design and Construction of Offshore Wind Turbine Foundations," Wind Turbines, pp. 231-264.

Novak, M. (1974). Dynamic Stiffness and Damping of Piles. *Canadian Geotechnical Journal*, *11*(4), 574–598. https://doi.org/10.1139/t74-059

Poulos, H. G. (2016). Tall building foundations: Design methods and applications. *Innovative Infrastructure Solutions, 1*(1), 1-51. doi:10.1007/s41062-016-0010-2

Poulos, H. G. and Hull, T. (1989) Role of analytical geomechanics in foundation engineering. Foundation engineering: current principles and practices. pp. 1578-1606 (1989). ILL item# 112694.

Powrie, W., and Daly, M. P. (2007). "Centrifuge modeling of embedded retaining walls with stabilizing bases." Geotechnique, 57(6), 485–497.

T.P.T. Dao. Validation of PLAXIS Embedded Piles For Lateral Loading. Delft University of Technology. 2011

Rahman, M. (1984). Wave diffraction by large offshore structures: An exact second-order theory. *Applied Ocean Research, 6*(2), 90-100. doi:10.1016/0141-1187(84)90046-4.

Wang, X., Zeng, X., Yang, X., & Li, J. (2018). Feasibility study of offshore wind turbines with hybrid monopile foundation based on centrifuge modeling. *Applied Energy, 209*, 127-139. doi:10.1016/j.apenergy.2017.10.107

Wang, Z., Hong, Y., Ng, C. W. W., Wang, L. Z., Mašín, D., & He, B. (2017). Cyclic lateral response and failure mechanisms of semi-rigid pile in soft clay: Centrifuge tests and numerical modelling. *Canadian Geotechnical Journal, 54*(6), 806-824. doi:10.1139/cgj-2016-035

Westwood, A. Offshore wind statistics. barriers to wind. refocus, 2004, 5, (5), 20. (2005). Fuel and Energy Abstracts, 46(4), 248-248. doi:10.1016/S0140-6701(05)81686-8

Y. Hong, B. He, L.Z. Wang, Z. Wang, C.W.W. Ng, and D. Mašín. Cyclic lateral response and failure mechanisms of semi-rigid pile in soft clay: centrifuge tests and numerical modelling. Canadian Geotechnical Journal (2017).

Zhu, B., Zhu, Z., Li, T., Liu, J., & Liu, Y. (2017). Field Tests of Offshore Driven Piles Subjected to Lateral Monotonic and Cyclic Loads in Soft Clay. *Journal of Waterway, Port, Coastal, and Ocean Engineering*, *143*(5), 5017003–. https://doi.org/10.1061/(ASCE)WW.1943-5460.0000399

Chapter 5: Dynamic Characteristics of Wind Turbine Foundations

Chapter5

Abstract:

Offshore Wind Farms play an essential role for supporting development of green electricity alternatives. Large capacity turbines of 3MW-6MW are usually supported on cylindrical superstructures that are slender, and whose natural frequency may coincide with the forcing frequency of the wind, waves, and currents. Hence, it is vital that the natural frequency of the system is evaluated correctly to enable its design to avoid resonance conditions with forcing frequencies of rotor frequency,1P, and blade passing frequency, 3P, and those of the wind and the waves. DNV code requires that the frequency of the system be +-10% away from those frequencies to avoid resonance. The aim of this study is to investigate the effects of soil compliance on the first natural frequency for hybrid foundations (HF) and monopiles (MP) in different clayey beds. The commercial finite element program PLAXIS 3D is used to develop three-dimensional models of the foundation-soil system considering six different soil profiles to cover a range of soil profiles encountered in practice ranging from very soft (E_{50} = 2 MPa) to very hard (E_{50} = 140 MPa) clay. HF with L_p/W ratios of 1 and 2 were investigated as well as 7 different MP length to diameter (L/D) ratios varying from 3.3 to 13.3. For HF systems, the normalized 1st natural frequency values were increasing with L_p/W ratio and shear strength of soil. Results indicate the normalized first natural frequency of MP also increases as L/D ratio and shear strength increase. For soft soils, foundations can be classified as rigid and highest increase of normalized ultimate capacity with increasing L/D ratio; however, stiff soil profiles showed that a plateau is reached at L/D ratio of about 5-8. Closed form equations are provided and fitted to the results to describe the first natural frequency properties of the tower with a few soil and foundation geometry data.

5.1 Introduction

The size of wind turbines has grown tremendously to enable higher electricity output, which in turn resulted in an increase in the required area for their installation as well as their weight weight and exposure to lateral loads from wind. Therefore, offshore wind turbines (OWTs) are increasingly installed across the globe as efficient means of electricity production as they can benefit from better wind fields for energy production and alleviate the demand on required space. However, they exacerbate issues pertaining to increased weight of and lateral loading on the foundations. In addition, moving into deep water to harness more wind energy creates specific challenges for their foundation design due to the higher lateral loads and bending moments due to wind, waves and current, all of which must be accommodated for within strict rotation envelopes. Large diameter turbines of 3MW-6MW are usually supported on a cylindrical superstructure that is slender, and whose natural frequency may coincide with the forcing frequency of the wind, waves, and currents. Hence, it is vital that the natural frequency of the system is evaluated carefully, and the substructure be designed in such a way as to avoid forcing frequencies of rotor frequency, 1P, and blade passing frequency, 3P, and those of the wind and the waves. DNV code requires that the frequency of the system be ± 10% away from those frequencies to avoid resonance. Meanwhile, there is a lack of tools for practicing engineers to obtain the fundamental natural frequency of the foundation systems considered herein. Hence, the aim of this part of the research is to:

1. Establish a finite element model (FEM) and calibrate it and verify it employing the results of a known case study involving free vibration.

2. Use the validated model to carry out a parametric study to investigate the effect of HF length of pile to plate width (L_p/W) ratio and MP length to diameter (L/D) ratio on their 1st (fundamental) natural frequency considering clay profiles with varying stiffness.
3. Develop analytical solutions for the rocking, coupling and lateral stiffness (K_R, K_{LR}, K_L) of the considered foundation systems (MP and HF) by curve fitting the results obtained from the parametric study.

5.2 Literature Review

OWTs are being installed in various ground conditions and their foundation systems vary accordingly. Their foundations are subjected to dead loads and environmental loads (periodic) and can be subjected to transient loads from impact by ships beside 1P and 3P loading. The dead load component emanates from the turbine's own weight, blades, generator etc., plus tower (submerged and above mean sea level). Environmental loads are caused by wind, waves, current and earthquakes. These are random in nature and typically govern the design (Elmarassi, 2011, Abdelkader, 2016). The increase in power production is realized by using heavier and larger turbine components, often leading to very large foundation systems. Cost of such foundation systems for OWT's constitute a large portion of the total cost, being around 25-40% compared to onshore wind turbine foundations (Byrne and Houlsby, 2003). OWT foundations range between gravity base, monopiles, tripods, and jacket options. The complex loading on OWT foundations due to the combined wind, wave and self-weight loading effects, must be accommodated within very small displacement envelopes and natural frequency bands to allow the turbines to operate effectively. Currently, monopiles account for 80% of the installed foundations with L/D ratio being less than 20 and diameters and depth of penetration reaching 7.8m and 80m, respectively. Two criteria must be met for the design of these foundations: ultimate limit state and serviceability

limit states. The ultimate limit state deals with vertical, lateral, and moment capacity of the foundation to preserve the integrity of the structure while serviceability limit states ensure limiting displacement and rotation are not exceeded to maintain the operation of the structure (turbine, transition piece and mast) and foundation. Usually, lateral loads from wind and waves control ultimate limit states. With increased wind turbine capacity and strict rotation requirements coupled with increased development in deep water, it is anticipated that the monopile diameter will continue to increase, posing problems of drivability and cost for development of new OWF. Areas of improvement and innovations for OWF include increasing turbines output, reducing wake losses, improving farm layout, and reducing tower and foundation costs (Chercia, 2014). Since the cost of foundations for OWT can consume up to 40% of the total cost and since newer improvements are expected to be installed further from shorelines and in deeper water, it is expected that the cost of such foundations will continue to increase. To limit monopiles' geometry and cost, an improved monopile design, a hybrid foundation (HF) comprising a plate fitted with a short monopile at its center was proposed in chapter 3, which can be used as an effective OWT foundation in stiff clays. The idea of the plate emanates from pile cap analogy and hence is expected to reduce tilting and increase overall stiffness while providing extra support for the structure. This should come with reduced pile diameter and penetration (Wang et al. 2018; Wang et al., 2017; Hong et al. 2017; Abdelkader 2016; Bhattacharya et al., 2015; Cherchia 2014; Klinkvort and Hededal 2014; Lahane et at. 2014; Lombardi et al., 2013; Bhattacharya et al., 2013; El-Marassi 2011; Powrie and Daly 2007; O'Neill et al. 1987; Novak 1974). In this chapter, effects of soil compliance on the 1st natural frequency of a typical 5MW OWT is established for HF and MP by means of finite element modelling. A case study involving free vibration testing on a monopile is utilized calibrate the model parameters and validate its predictions. The validated FEM

is then utilized to analyze the dynamic characteristics of hybrid foundations and monopiles and to evaluate the effect of soil compliance as well as pile rigidity on the 1st natural frequency of the studied systems. Generic curves are established relating natural frequency of the foundation with respect to L/D ratio and the E_p^*/E_s where E_p^* is the foundation normalized stiffness and E_{50} is the soil's stiffness at 50% of maximum deviatoric loading from triaxial testing. The commercial program PLAXIS 3D is used for this purpose. Six soil profiles are considered in the analysis, which cover a wide range of soil profiles encountered in practice ranging from very soft (E_{50} = 3MPa) to very hard (E_{50} = 120MPa) clay. HF with L_p/W ratios of 1 and 2 as well as MP (L/D) ratios varying from 3.3 to 13.3.

5.2.1 *Wind Turbine Natural frequency*

The structure's natural frequency is dependent on the soil stiffness and tower stiffness. A first order estimate for the structure's first natural frequency ($F_{FB.}$) on rigid foundations is given by:

$$F_{FB.} = \sqrt{\frac{k}{m_{eff.}+m_{RNA}}} \tag{5-1}$$

Where k defined as $3EI_t/H^3$ is the tower lateral stiffness and m_{eff} is the effective mass defined as $m_{eff} = \frac{33\,mT}{140}$ where m_T is the total mass of tower, m_{RNA} is the turbine components mass, E is Young's modulus, I is second moment of inertia of tower, and H is tower height.

Nevertheless, the soil flexibility adds some compliance to the tower base resulting in reduced value of natural frequency, F_{n1}, compared to F_{FB}. Arany et al. (2011) studied the free vibration response of monopiles in different soils employing a mathematical model of a 2-spring stiffness model representing the monopile's mechanical behavior at mudline. Bhattacharya et al. (2013) improved the earlier model of Arany et al. (2011) to include the coupling stiffness into the transcendental equations. Arany et al. (2016) developed a single degree of freedom (SDOF) model describing the tower and foundation compliance and solved a set of differential equations of

motion for a 3-spring stiffness model taking tower properties and foundation stiffness into account. Their results indicated that the first natural frequency at first cycle of loading, F_{n1}, can be as low as 50% of F_{FB} according to the following equation:

$$F_{n1} = F_{FB} * C_R * C_{LR} \tag{5-2a}$$

where

$$C_{LR} = 1 - \frac{1}{1 + b\left(\eta_L - \frac{\eta_{LR}^2}{\eta_R}\right)} \tag{5-2b}$$

$$C_R = 1 - \frac{1}{1 + a\left(\eta_R - \frac{\eta_{LR}^2}{\eta_L}\right)} \tag{5-2c}$$

In the preceding equations, a and b are empirical constants and can be taken as a = 0.6 and b = 0.5. The applicability of Eq. 2 is limited to $6\ \eta_R > 1.2\frac{\eta_{LR}^2}{\eta_R}$ and $\eta_L > 1.2\frac{\eta_{LR}^2}{\eta_R}$ (Arany et al., 2016).

As shown in Fig. 5-1, methods used to estimate the natural frequency of the MP system include:

A. **Fixed at mudline models**; the benefit of this is that it is easy to use but at cost of accuracy as it overestimates the natural frequency

B. **Extended a certain depth models** Using p-y approach, easy to use but requires soil input and a Numerical program such as LPile which discretizes soil layer as independent springs and can give good results.

C. **Sophisticated FE models,** which require detailed soil parameters that can be costly. In addition, FE analysis requires significant computational effort.

D. **Sway-rocking** models in which the foundation mechanical behavior is represented by either two or three springs to account for foundation flexibility.

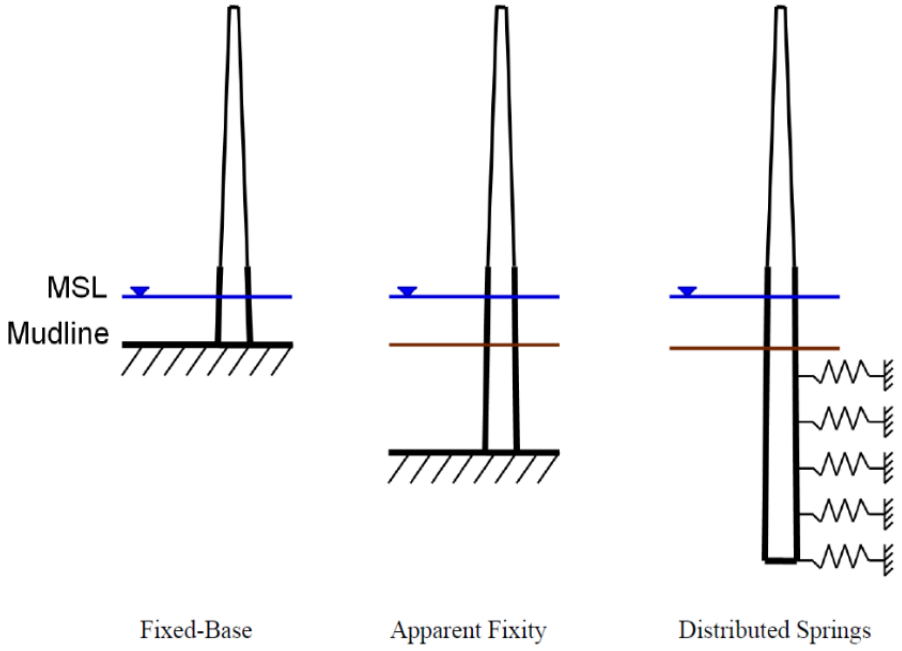

Figure 5-1 Various approximation used to model SSI on fundemntal frequency
(After Bush and Manuel, 2009)

OWTs are dynamically sensitive structures (Wang et al., 2017, Bhattacharya et al., 2015; Lombardi et al., 2013, Bhattacharya et al., 2013 ; Malhotra 2009). Their design criteria are dictated by two factors:

A- Rotation at mudline cannot exceed certain limits (typically 0.004 radians)

B- Their lowest natural frequency should be separated by ±10% from the forcing frequency

Typical design of dynamic behavior of OWT depends on the soil stiffness as follows.

4- **Soft-soft:** where first natural frequency lies below 1P frequency and the foundation stiffness is very small. Ideally this system is too soft to resist ultimate capacity and technically cannot be applied to OWT. However, it was reported in one case that it was used for a 3MW wind turbine (Lau, 2015).

5- **Soft-stiff:** where the first natural frequency exists between 1P and 3P frequencies. This is where most reported data of OWT foundations was measured/estimated in literature as shown in Figure 5-2.

6- **Stiff-stiff:** when the first natural frequency is above 3P. This will lead to a very heavy and expensive foundation option that is not feasible.

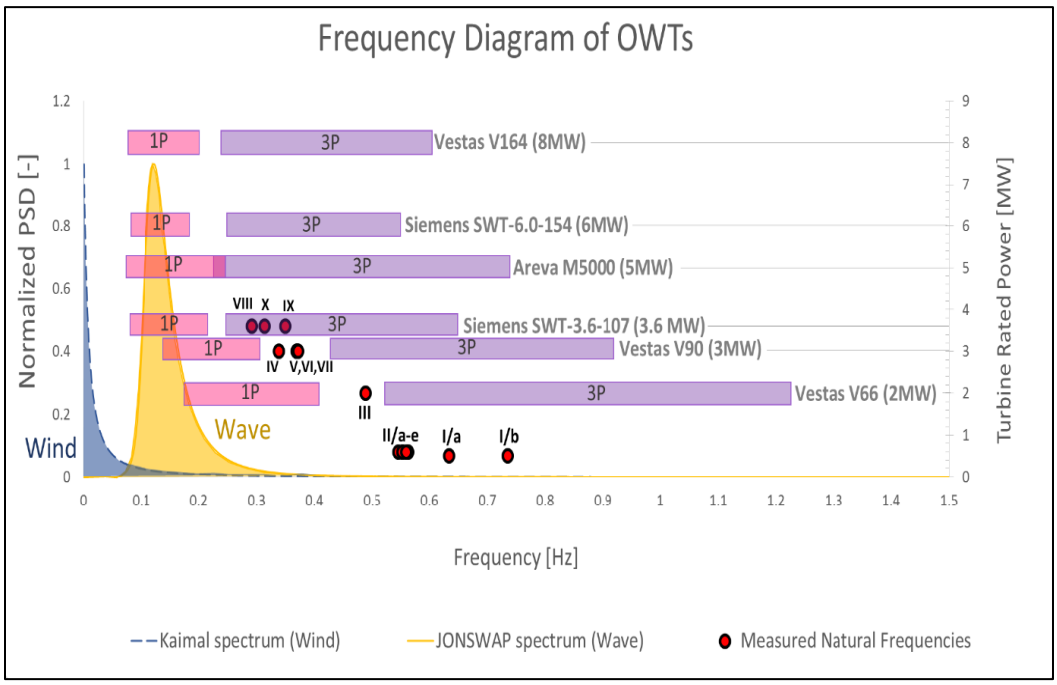

Figure 5-2 Wind, Wave, 1P and 3P spectra with frequency range of OWT (Arany et al., 2016)

5.2.2 *Governing equations*

The general equation of motion of the structure is given by:

$$M\ddot{U} + C\dot{U} + KU = F \tag{5-3}$$

where:

K: Stiffness Matrix

$\ddot{U}$, $\dot{U}$, and U: Acceleration, velocity and displacement, respectively

C: Viscosity Coefficient

M: Mass matrix

F: External applied force

The solution for equation 5-3 is obtained either through explicit or implicit (iterative) methods and will depend on the general nature of the modelled problem.

5.3 Problem Definition

The effect of soil compliance on the first natural frequency properties of a typical 5MW wind turbine supported by either hybrid foundation or monopile is investigated considering different soil conditions. The tower of the wind turbine was considered to be 90 m high, 6 m in diameter and its wall thickness was taken as 0.035 m. MP diameter was selected to be 6m while HF plate was 14 m with a 4 m diameter pile at its center. The length of MP was varied from 20 m to 80 m while length of HF pile was varied from 0 (S.F or GBF) to 14m and 28 m (i.e. $L_p/W = 1$ and 2). Figure 5-3 shows the considered foundation systems while Figure 5-4 shows the mechanical representation of the OWT and foundation used in this study.

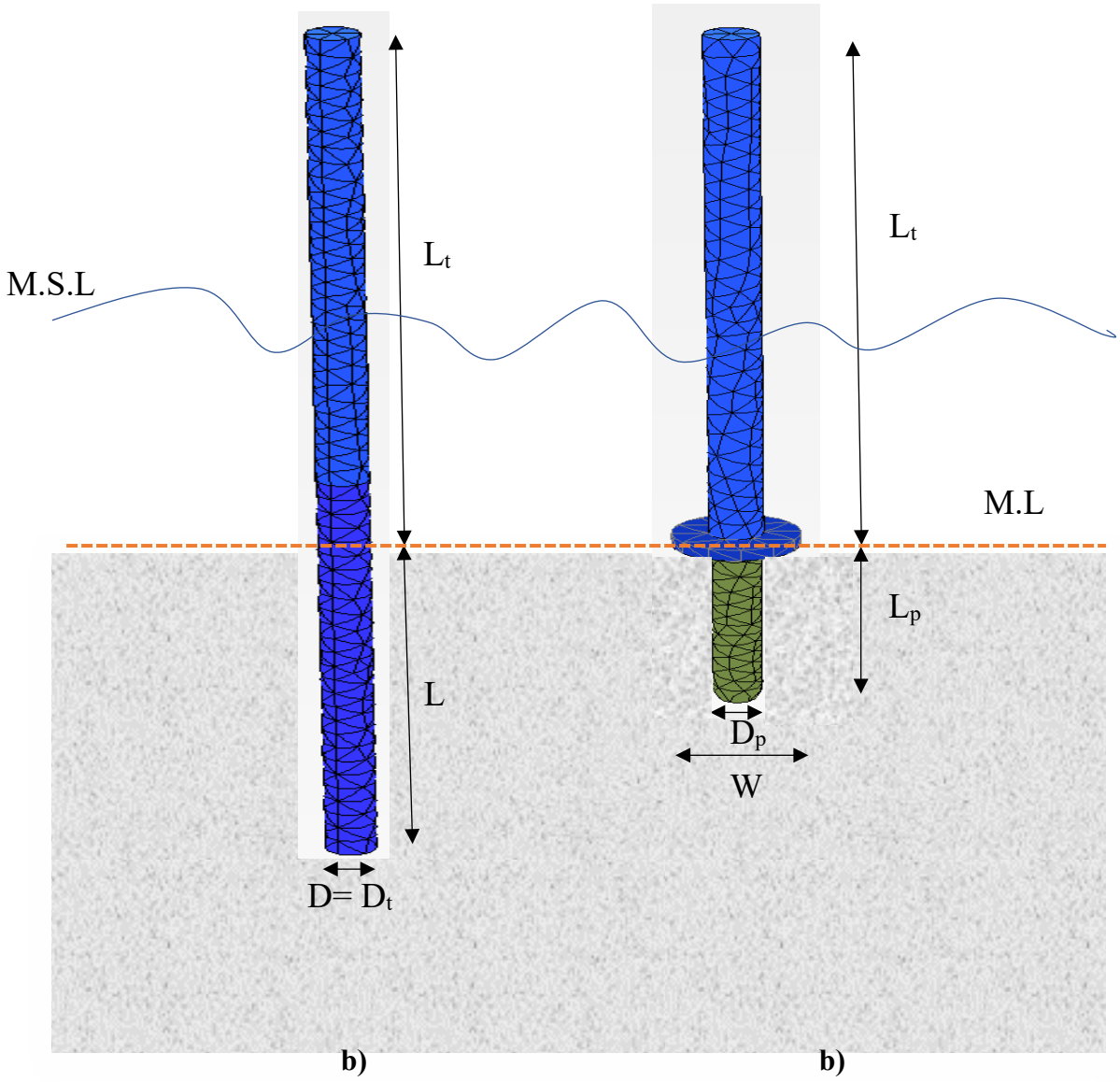

Figure 5-3a) Monopile of D_p = 6m b) Hybrid foundation system with W=14m and D_p=4m. (Not to scale)

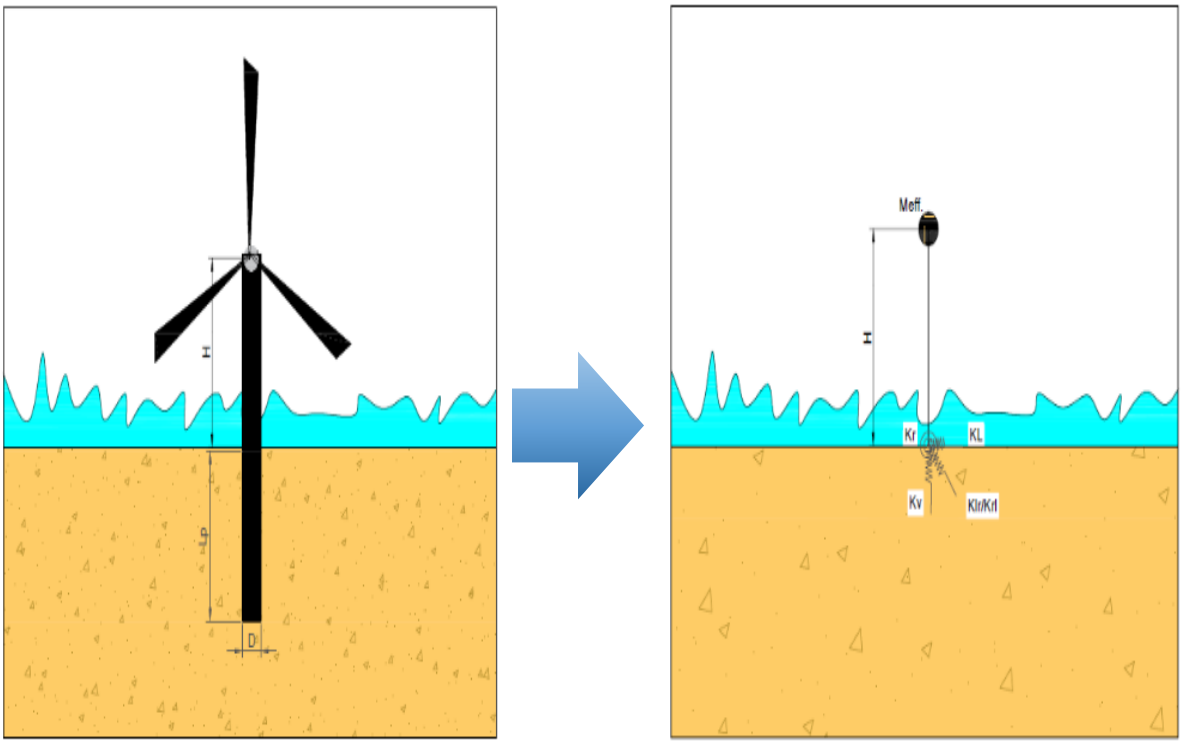

Figure 5-4 a: actual foundation, b: idealized mathematical model of 3 springs stiffnesses

5.3.1 *Methodology*

The aim of this study is to characterise the first natural frequency of a 5MW wind turbine in a wide range of strength and stiffness properties. Effects of soil compliance on the first natural frequency has been studied extensively. A series of damped free vibration were conducted on finite element models of a typical 5MW OWT founded on either HF or MP foundations in different cohesive soil profiles with the aim to correlate the calculated natural frequency from the FEM to the three spring stiffness properties defined in chapter 4 in order to provide easy to use closed form equations to evaluate the first natural frequency of OWTs. A load was applied and released, and the resulting tower motion was recorded. The recorded time history was converted to frequency domain using Fast Fourier function in MATLAB and the frequency corresponding to first peak of measured response was recorded as the first natural frequency. The procedure is repeated for all

systems considered in different soil profiles, for a total of 60 FE calculations. In particular, the effects of footing rigidity, termed E_p^*, with respect to soil stiffness, E_s, is investigated.

$$E_p^* = \frac{E_p I_p}{I_{scp}} \tag{5-4}$$

E_p^*: normalized stiffness of pile; E_p: Young's modulus of pile material; E_s: Elastic modulus of soil; I_p: Pile second moment of inertia; I_{scp}: moment of inertia of a solid cross-section pile of same diameter as the actual pile.

Table 5-1 shows the range of foundations' geometry considered herein and the information regarding applied loads and their corresponding locations. Tables 5-2 shows the considered soil profiles. Three-dimensional (3D) FEMs were established to simulate the OWT foundations. Tetrahedron 10 node elements were used to discretize the soil domain while beam elements were used to discretize the tower. Plate elements were used to simulate the pile and hybrid foundation plate. The soil behaviour was simulated using the small strain hardening (Hss) soil constitutive model obeying Mohr-Coulomb failure criterion. The Hss model is advanced model which can simulate the behaviour of both soft and stiff soils. It was first developed by Benz (2006) as a second order model. The Hss model differs from Hs model in that it simulates small strain behavior by including G_o, small strain modulus, and the threshold strain value, $\gamma_{0.7}$. Hss model accounts for the stress dependency of stiffness and can provide plastic straining due to deviatoric and primary compression loading. It also allows unloading at higher stiffness than loading stiffness, hence can give plastic straining before reaching failure. The shearing behaviour odf the clay accounts for effects of two strain hardening; namely volumetric hardening (cap) and shear where contraction and densification cause the yield surface to expand. The stiffness parameters in Hss can be determined as follows.

$$E_{oed} = E_{oed,ref}\left(\frac{c\cos\phi - \frac{\sigma'_3}{k_o^{NC}}\sin\phi}{c\cos\phi + p'_{ref}\sin\phi}\right)^m \quad (5\text{-}5)$$

$$E_{50} = E_{50,ref}\left(\frac{c\cos\phi - \sigma'_3\sin\phi}{c\cos\phi + p'_{ref}\sin\phi}\right)^m \quad (5\text{-}6)$$

$$E_{ur} = E_{ur,ref}\left(\frac{c\cos\phi - \sigma'_3\sin\phi}{c\cos\phi + p'_{ref}\sin\phi}\right)^m \quad (5\text{-}7)$$

To account for slippage and gap formation, interface elements were used to model contact between solids zone and soil and were modelled with 6 node elements having strength and stiffness properties as percentage of the soil defined through a reduction factor, R_{int}, varying between 1 for soft soils and 0.3 for stiff soils. The hybrid foundation plate was modelled with 2 m thick plate elements using elastic nonporous model with E and γ values of 27800 MPa and 23.6 kN/m^3, respectively. The tower was modelled using plate elements having unit weight, diameter, E and thickness of 77 kN/m^3, 6 m, 200 GPa and 0.035 m, respectively. The piles were also constructed using plate elements and were surrounded by interface elements. In all models, x and y boundaries were set at a distance equal to 7D from model center and restricted to move horizontally while allowed to move vertically; z boundary was fixed and placed at least 3D below pile tip to avoid any stiffening effects and to model rotational stiffness correctly. On average, around 5000 elements were used, and coarse mesh size was considered after performing sensitivity analysis. Figure 5-5 shows the meshing developed for one of the cases. Newmark ß value of one-fourth is selected so as to secure the calculation stability and at least five structural vibration waves are investigated after releasing a horizontal loading at the tower head.

Stages of analysis included the following.

Initial stage: k_o calculation to establish stress profile

Construction stage: Activating all structures and interface elements

Loading stages: Applying load

***Dynamic stage*:** Applying viscous boundaries and releasing load

Output stage: Checking structural forces and soil deformation to establish failure load

Table 5-1 3D analyses conducted on the proposed foundation system

L, m	L/D/(L_p/W)	Foundation system	e/D_t	V, kN
20	3.33	Monopile	6.83	Own weight[1]
30	5		6.83	
40	6.67		6.83	
50	8.33		6.83	
60	10		6.83	
70	11.67		6.83	
80	13.33		6.83	
0	0	Hybrid	6.83	
14	1		6.83	
28	2		6.83	

L: Depth of embedment; D: Pile's diameter; e: eccentricity of applied loads(m); D_t: Tower's diameter; 1: uniformly distributed, (L_p/W): length of pile/plate width

Table 5-2 Hss model properties for considered soils

Parameter	clay1	Clay2	Clay3	Clay4	Clay5	Clay6
c'	4.23	24	44	87	170	354
Ψ	0	0	0	0	0	0
θ'	8	10	10	10	10	10
p'_{pop}, kPa	13	51	83	140	240	414
p'_{ref}, kPa	41	100	100	100	100	100
$e_{(ini).}$	4.209	4.209	4.209	4.209	4.209	4.209
ɣ, kN/m^3	17.9	17.9	17.9	17.9	17.9	17.9
E^{ref}_{oed}, kPa	1406	3461	14747	29040	56628	113134
E^{ref}_{50}, kPa	1758	4000	18439	36310	70805	141457
E^{ref}_{ur}, kPa	5000	10000	52444	103271	201380	402326
v_{ur}	0.2	0.2	0.2	0.2	0.2	0.2
m	0.6	0.6	0.6	0.6	0.6	0.6
PI	30	30	30	30	30	30
$K_{o,}$ NC	0.54	0.54	0.54	0.54	0.54	0.54
Depth, m	0-25	0-26	0-27	0-28	0-29	0-30
R_f	0.9	0.9	0.9	0.9	0.9	0.9

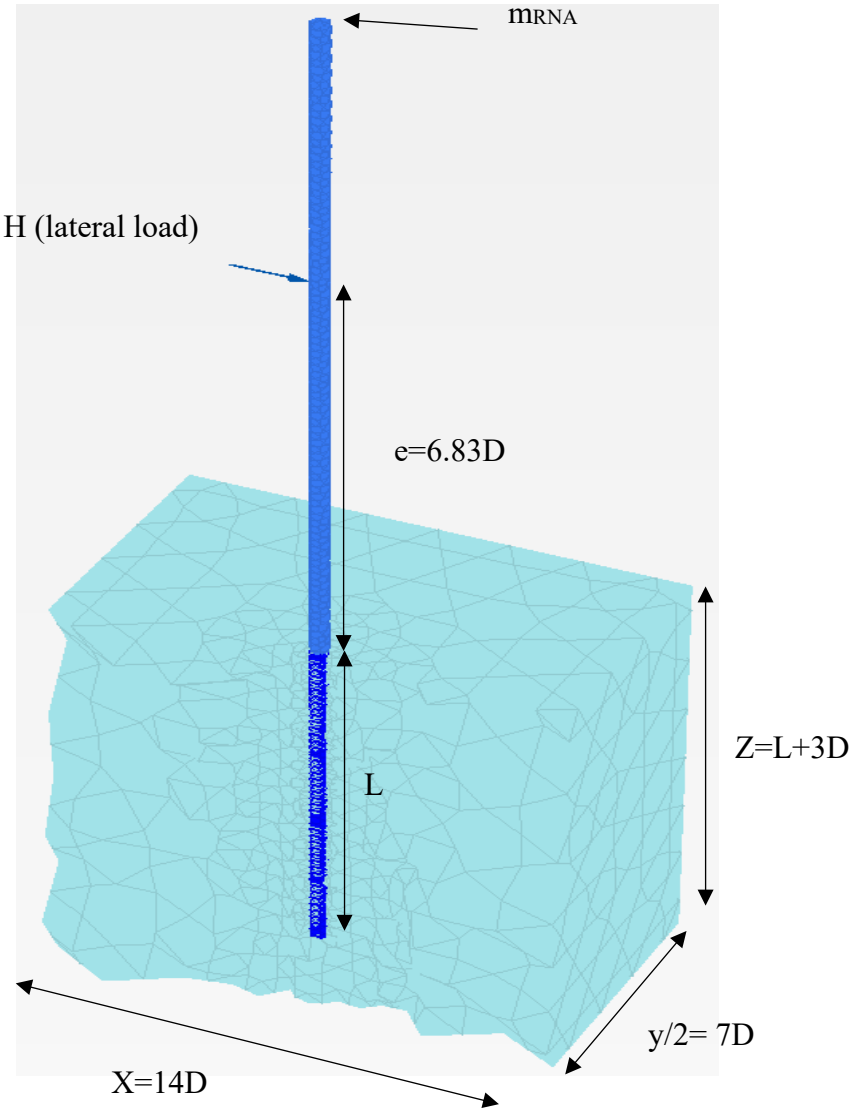

Figure 5-5 Developed mesh and location of lateral point load

5.3.2 *Validation*

The model was calibrated using the results of laboratory tests conducted by Lombardi et al. (2013). The experiments involved modelling free vibration of a monopile in lightly over consolidated bed in a strong box at 1g. Commercial program Plaxis 3D was used to model the

experimental results. Tetrahedron 10 node elements were used to model the soil elements while plate elements were used to model the tower and the pile to calibrate the FEM model yielding satisfactory results. The pile was embedded 0.5m into the soil and supported a 1m turbine mast carrying a small turbine at (1:100) scale. The pile had an outer diameter of 2.2cm and a wall thickness of 1.3mm with EI of 3.18E8 N/mm^2 while the tower had slightly thicker wall of 1.6mm and EI of 2.125E9 N/mm^2.

Applying a force and measuring the decay of acceleration enabled measuring the natural frequency of the scaled OWT, which was recorded at 3.3Hz (Lombardi, 2011).

The steps for free vibration calculation involved in the numerical model:

1- **K_o calculation:** in which the initial stress regime is established
2- **Activation of structural elements calculation:** where structural elements are activated
3- **Plastic calculation:** where a static load is applied to the tower to establish the initial condition
4- **Dynamic calculation:** where the load is removed, and the structure is allowed to oscillate for a period of time (typically allowing five full cycles based on expected frequency range)

Table 5-3 Model parameters

Parameter	OC clay
c'	10
Ψ	0
φ'	0
p'_{pop}, kPa	15
p'_{ref}, kPa	41
$e_{ini.}$	4.23
ɣ, kN/m^3	17.9
E^{ref}_{oed}, kPa	1406
E^{ref}_{50}, kPa	1758
E^{ref}_{ur}, kPa	5000
ν_{ur}	0.2
M	1
PI, %	30
$K_{o,NC}$	0.86
R_f	0.9
Depth, m	0.6
G_o, kPa	6000
$\gamma_{0.7}$	1.2E-4
Type of analysis	Undrained B

An in-depth convergence analysis of case study was conducted in order to understand the mechanics of the model and importance of input parameter. Figure 5-5 shows developed model. The average size of the elements was 0.02m and the number of elements was 6000. In all models, the smallest element size, ℓ, was checked to be less than critical element length necessary to ensure that the generated wavelength is well captured, and that element dimension is not too big compared to wavelength as given in Equations 5-8 and 5-9 (Khalil et al., 2019; Lian et al., 2019; Lombardi, 2011).

$$G_o = \ln (S_u) - 4.73 \quad (5\text{-}8)$$

$$\ell_{critical} = 1/5 - 1/8 \; vs/f \quad (5\text{-}9)$$

Viscous boundaries were not applied in the case of calibration because of existence of strong box but were applied in all parametric study calculations. It is necessary to apply these boundary conditions to ensure generated waves due to cyclic motion of the foundations are not reflected into model creating errors in calculations when modelling infinite soil boundaries, as is the case for all parameter studies. After the recorded natural frequency (3.14Hz) was deemed acceptable and close to measured values, the modeling scheme was considered to be validated (Figures 5-6 and 5-7).

5.4 Parametric analyses

In total, 60 free vibration simulations were conducted to calculate the first natural frequency of the considered systems (both MP and HF). The sequence of modelling involved the following:

1- **Ko Loading:** In which in-situ stresses are established.
2- **Plastic analysis:** Where all structural elements and interface elements around them are activated
3- **Loading analysis:** A plastic analysis in which a lateral load was applied at the tower tip to produce elastic deformation
4- **Dynamic analysis:** Where the load was deactivated and interface elements on the vertical boundaries were activated and assigned viscous elements to absorb incoming waves and avoid wave reflection (box effects)

Two types of solvers exist in Plaxis 3D, Picos and Pardiso, which implement implicit and explicit time integrations of the governing equations, respectively. The implicit analysis provides a stable solution always while the stability of the explicit solution is dependent on the input time step. To avoid calculation error and solution instability, the size of time step care selected such that the max step and sub steps produce time step that does not exceed max allowed time step based on the minimum size of the element, i.e.,

$$t_{critical} = \frac{l_{critical}}{v_s} \quad (5\text{-}10)$$

After setting up the FE model and inspecting the input parameters, a point is selected for view for post processing of the results. The time history of the tower tip displacement is converted to frequency domain by applying Fast Fourier Transform. A typical time history of the displacement vs. time and amplitude vs. frequency is shown in Figures 5-6 and 5-7.

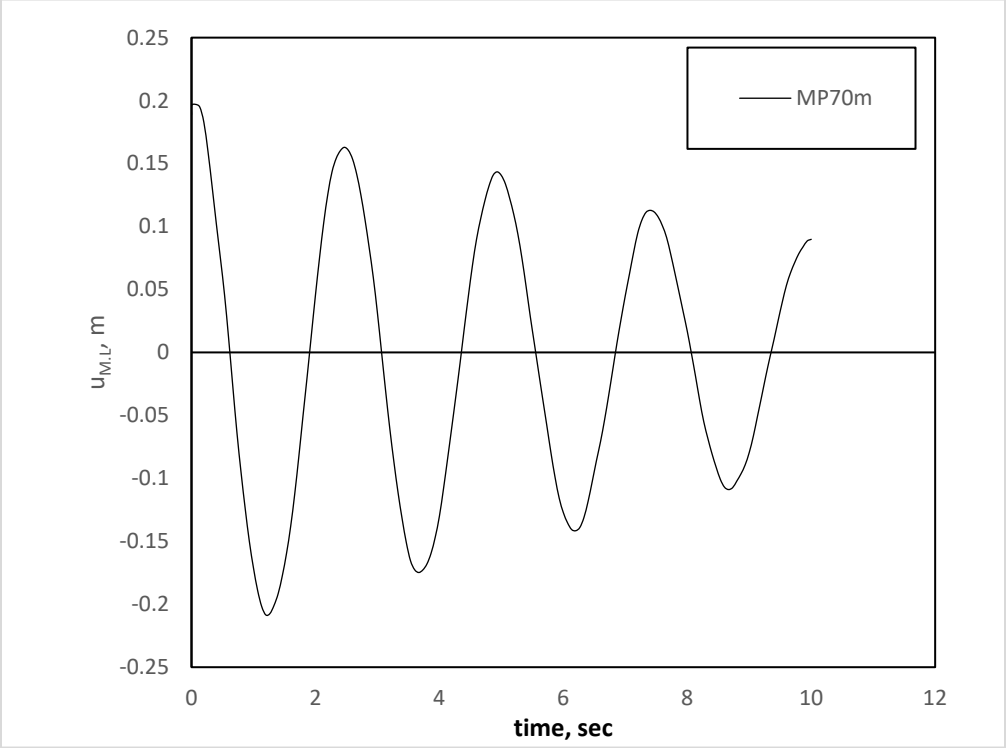

Figure 5-6 Free vibration result of a 5MW turbine founded on a 70m monopile

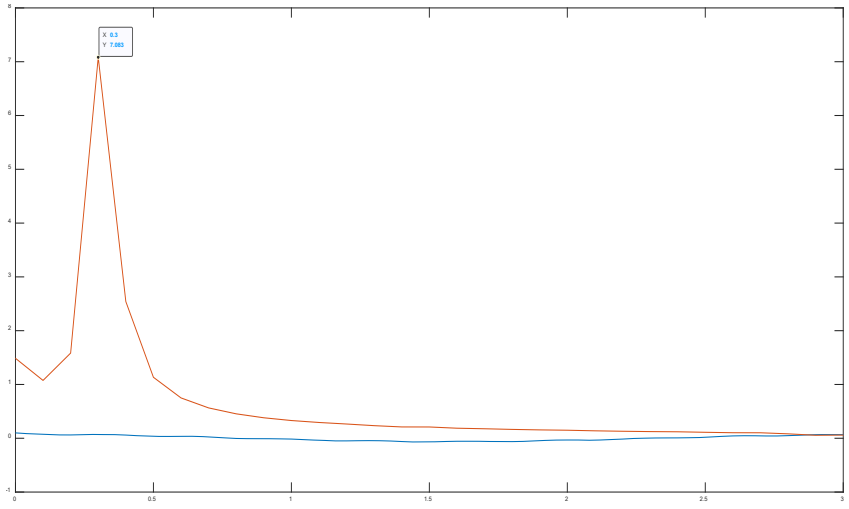

Figure 5-7 FFT of a typical free vibration results

5.4.1 *Monopile first natural frequency*

For each FE analysis, the lowest frequency of peak amplitude was selected as the 1st natural frequency of the respective analysis. The results were then normalized against the1st natural frequency of fixed-base tower (assuming rigid foundation). The normalized natural frequency values were plotted against L/D for all clay profiles considered as shown in Figure 5-8. It is observed from Figure 5-8 that the soil compliance of the soft soil (Clay 1 with S_{uo} =4.2kPa) resulted in considerable reduction of the system 1st natural frequency. However, this reduction in the 1st natural frequency tended to diminish as the pile length increased and plateaued at L/D =10. The maximum reduction of 1st natural frequency was for the MP with L/D = 3.33 in clay 1 which amounted to 52% reduction compared to the fixed base. Clay 2 and 3 had similar effects on the system 1st natural frequency but to a lesser extent. For these profiles, the reduction in 1st natural frequency amounted to 34% for L/D = 3.33 and 20% for L/D = 6.67. The effects of pile penetration depth on the 1st natural frequency for these profiles was negligible beyond L/D = 6.67. For clay 4,

5 and 6, the effects of pile penetration depth on the normalized 1st natural frequency was negligible as they represented stiff clay profiles.

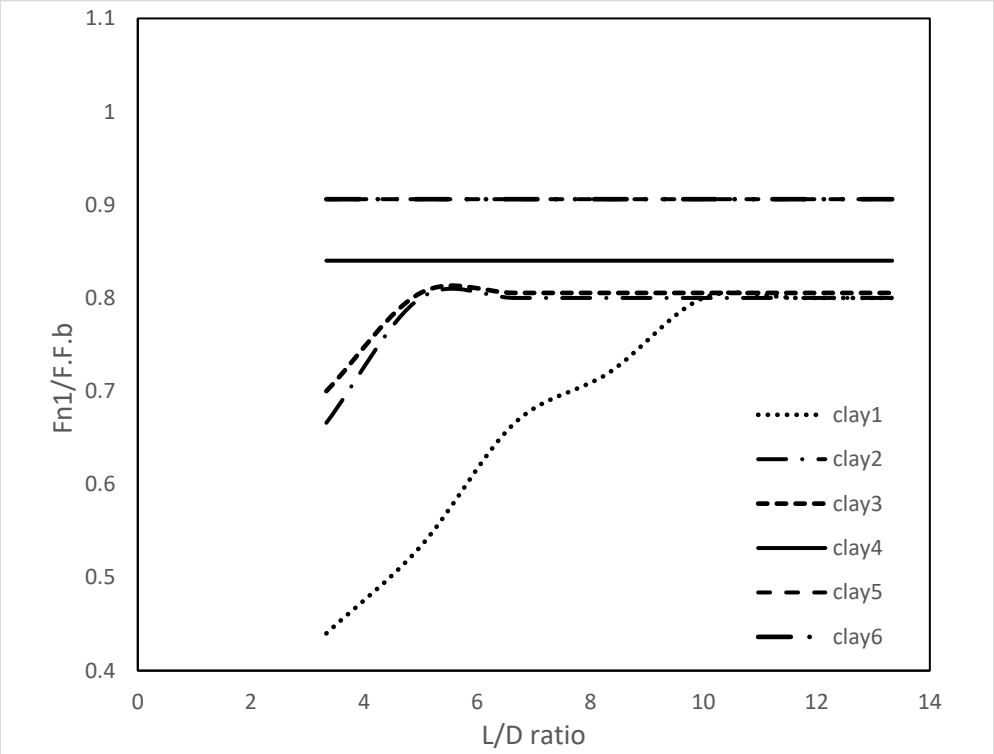

Figure 5-8 1st natural frequncy variations for MP in different L/D ratios and clayey beds

5.4.1.1 Predictive equations

The results of the 1st natural frequency were fitted to Equation 5-11 and then are plotted in Figure 5-9. Equation 5-11 accounts for the foundation compliance through the factors C_R and C_{LR} defined below. The errors of the predictions of Equation 11 are within 4% and therefore, the equation is considered suitable for predicting the 1st natural frequency of the system.

$$F_{n1} = F_{FB} * C_R * C_{LR} * C_1 \quad (5\text{-}11a)$$

Where;

$$C_{LR} = 1 - \frac{1}{1 + b(\eta_L - \frac{\eta_{LR}}{\eta_R})}) \quad (5\text{-}11b)$$

$$C_R = 1 - \frac{1}{1 + a(\eta_R - \frac{\eta_{LR}}{\eta_L})}) \quad (5\text{-}116)$$

Table 5-4 fitting parameters describing 1st natural frequency

Clay	A	B	C_1	Errors, %
1	4675275	889167	0.25*(L/D)^0.479	-5.8 to 8.12
2	270082176.6	0.0798	0	-6 to 2.8
3	270082176	0.2936	0	-1.5 to 1.04
4	270082178.2	0.744	0	-5.5 to 1.66
5	270082173.2	2.474	0	-0.3 to 2.3
6	270082173.2	2.474	0	-0.3 to 2.3

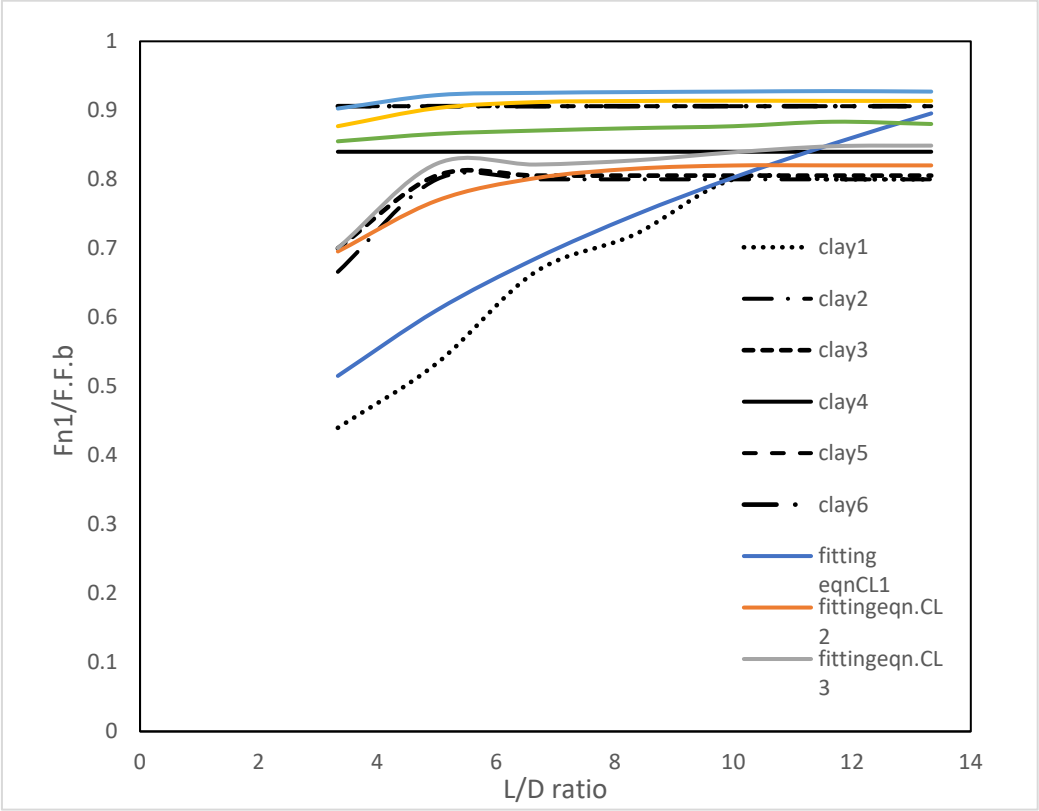

Figure 5-9 Fitting equations from Table 5-4 against FE data

5.4.2 *Hybrid first natural frequency*

The displacement time histories of the tower top were processed and converted to frequency domain using fast Fourier transform (FFT) in MATLAB. For all models, the lowest frequency of peak amplitude was selected as the 1st natural frequency of the respective analysis. The results were then normalized against the 1st natural frequency of the fixed-base tower. The normalized 1st natural frequency was plotted against Lp/W for all clay profiles considered as shown in Figure 5-10. It is observed from Figure 5-10 that the soil compliance had considerable effect on the system 1st natural frequency in clay 1 and 2 (S_{uo} =4.2kPa and 18kPa). This strong effect tended to diminish for Lp/W = 2. The maximum reduction of 1st natural frequency was for the GBF and HF with

Lp/W = 1 in clay 1 and 2, which amounted to 40% reduction compared to the fixed base. Clay 3 and 4 had similar effects on the system 1st natural frequency but to a lesser extent, with reduction of 20% regardless of use of hybrid foundation pile. For clay 5 and 5 profiles, 1st natural frequency was equivalent to fixed based counterpart indicating stiff clay profiles, regardless of use of hybrid foundation pile.

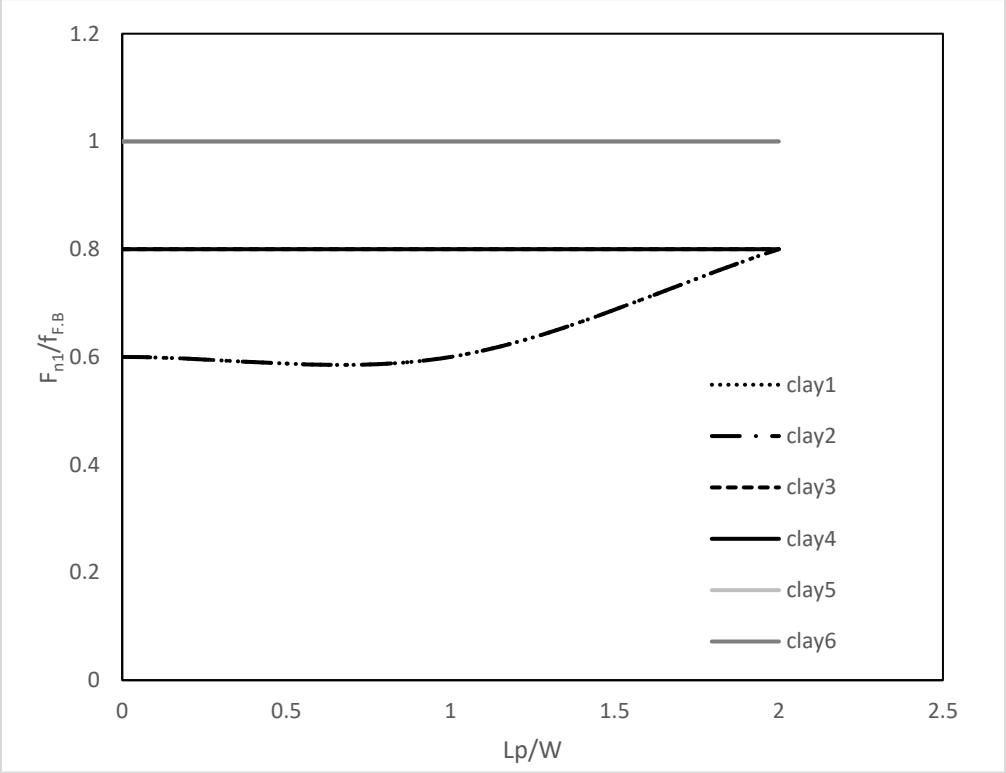

Figure 5-10 Effects of clay type and foundation geometry of HF on 1st natural frequency

5.4.2.1 Predictive Equations

The results of the 1st natural frequency were fitted to Equation 5-12 and then are plotted in next figure. The equation used takes foundation compliance into consideration through C_R and C_{LR} factors defined below. The errors of Equation 5-12 predictions are within 9% and therefore it is

deemed suitable to calculate the 1st natural frequency of the 5MW wind turbine supported by the hybrid foundation system.

$$F_{n1} = F_{FB}*A*(1-e^{-k*C\hat{}n)} \quad (5\text{-}12a)$$

where

$$C\ (\eta_L R, \eta_{LR}, \eta_R) = \eta_L - \frac{\eta_{LR}}{\eta_R} \quad (5\text{-}12b)$$

Table 5-5 Fitting parameters describing 1st natural frequency

Clay#	A	K	N	Errors
Clay1	72.9	0.0090	0.041	-2.96 to 9.96
Clay2	73.1	0.0091	0.042	0.1 to 16
Clay3	77.7	0.0103	0	-7.00E-08
Clay4	77.7	0.0103	0	-7.00E-08
Clay5	87	0.0115	3.45382E-06	-0.00012 to 8.98E-5
Clay6	87	0.0115	0	-2.67E-5

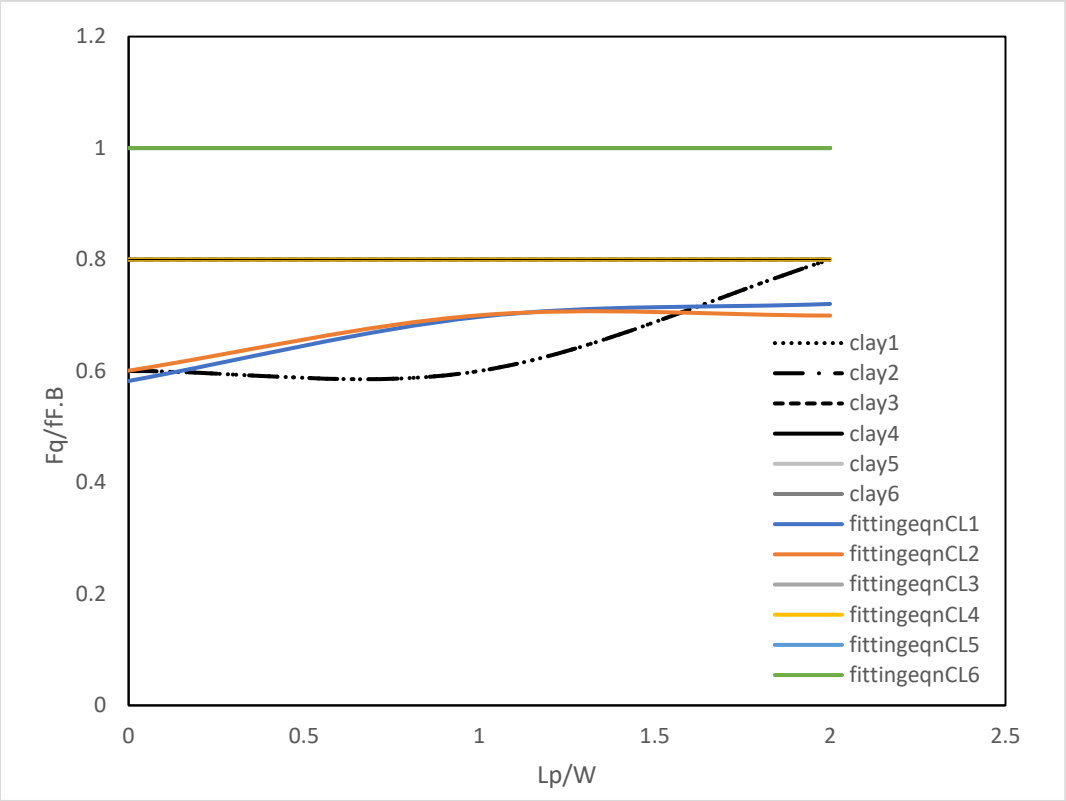

Figure 5-11 Predictive curves from equation 5-12 and FE data

5.5 Conclusion

The 1st natural frequency of wind turbines can be affected by soil compliance and there is a lack of tools for practicing engineers to assess its value for wind turbines supported by hybrid foundations. Hence, this study evaluated the effects of the configuration and soil conditions on the value of 1st natural frequency employing a validated 3D FE models. Free vibration FE were conducted for a typical 5MW wind turbine founded on HF and MP with different geometry in different clayey deposits. The resulting time history of displacement was converted to frequency domain and the 1st natural frequency was determined. Several conclusions may be drawn.

1- The dynamic response of OWTs is dependent on the foundation's flexibility. For soft soils, the foundation geometry had a significant effect on the 1st natural frequency of the system. For stiff soils, the response was dependent on the soil properties.

2- The natural frequency was impacted by L/D ratio for soft to stiff clays. For very stiff to hard clay, the MP penetration depth had no effect on the system 1st natural frequency.

3- The 1st natural frequency of wind turbine supported by MP can be less than half of that obtained assuming rigid foundation. The maximum difference was obtained for the case of L/D = 3.33 in soft clay where the 1st natural frequency was only 48% of the $F_{F.B}$.

4- For clay for firm to stiff clay, a plateau was reached where the 1st natural frequency did not change beyond. This L/D ratio was found to be between 5 and 6.67

5- The effect of foundation compliance on the 1st natural frequency was of lesser extent for the cases of HF.

6- The maximum reduction of 1st natural frequency compared to fixed base for HF/GBF happened for GBF and HF with Lp/W = 1 in soft to firm clay. In those cases there was a 40% reduction from foundation flexibility

7- The change of Lp/W resulted in increase in Fn1 for the cases of clay 1 and 2 only, for other soil profiles the effect of Lp/W on the 1st natural frequency is negligible

8- The change in clay type resulted in increase of the ratio of $f_{n1}/f_{F.B}$, the lowest ratio was 0.6 for clay 1 and 2. For clay 3 and 4, this ratio was 0.8. For clay 5 and 6, the soil compliance has no effects on the fixed base 1st natural frequency and the foundation can be represented as a rigid foundation.

5.6 References

Abdelkader, Ahmed Mohamed Reda, Investigation of Hybrid Foundation System for Offshore Wind Turbine (Scholarship@Western). 2016.

API, 1993. Recommended practice for planning, designing, and Constructing fixed offshore platforms. API, RPT2A-WSD. American Petroleum Institute (API), Washington, D.C.

Achmus, M., Kuo, Y.-S., & Abdel-Rahman, K. (2009). Behavior of monopile foundations under cyclic lateral load. *Computers and Geotechnics*, *36*(5), 725–735. https://doi.org/10.1016/j.compgeo.2008.12.003

Adamidis, O., & Madabhushi, S. P. G. (2014). On preparation of viscous pore fluids for dynamic centrifuge modelling. *International Journal of Physical Modelling in Geotechnics, 15* (3), 141-149. https://doi.org/10.1680/jphmg.14.00022

Association EWE. The European Offshore Wind Industry‑Key Trends and Statistics 2016; January; 2017.

Arany, L., Bhattacharya, S., Macdonald, J. H. ., & Hogan, S. J. (2016). Closed form solution of Eigen frequency of monopile supported offshore wind turbines in deeper waters incorporating stiffness of substructure and SSI. *Soil Dynamics and Earthquake Engineering (1984)*, *83*, 18–32. https://doi.org/10.1016/j.soildyn.2015.12.011

Bentley, K.J. and El Naggar, M.H., 2000. Numerical analysis of kinematic response of piles. Canadian Geotechnical Journal, Vol. 37, No. 6, pp. 1368-1382

Bowles, J. E. (1996). *Foundation analysis and design*. New York: McGraw-Hill.

Broms, B. B. (1964b). Lateral Resistance of Piles in Cohesive Soils. Journal of the Soil Mechanics and Foundations, **90**(2): 27-64.

Bhattacharya, S, Nikitas,;N, Garnsey; N.A. Alexander; J.Cox; D. Muir Wood and D. F.T.Nash (2013) Observed dynamic soil–structure interaction in scale testing of offshore wind turbine foundations. Soil Dynamics and Earthquake Engineering, 54. 47 - 60. ISSN 0267-7261

Byrne, B.W. and Houlsby, G.T. (2003) "Foundations for Offshore Wind Turbines", Philosophical Transactions of the Royal Society of London, Series A, Vol. 361, December, pp 2909-2930.

Byrne B. W., McAdam R., Burd H. J., Houlsby G. T., Martin C. M., Zdravković L., Taborda D. M. G., Potts D. M., Jardine R. J., Sideri M., Schroeder F. C., Gavin K., Doherty P., Igoe D., Muir Wood A., Kellahave D. and Skov Gretlund J. 2015a. New design methods for large diameter piles under lateral loading for offshore wind applications. *Proceedings of Third International Symposium on Frontiers in Offshore Geotechics* 1, 705-710.

Byrne B. W., McAdam R., Burd H. J., Houlsby G. T., Martin C. M., Gavin K., Doherty P., Igoe D., Zdravković L., Taborda D. M. G., Potts D. M., Jardine R. J., Sideri M., Schroeder F. C., Muir Wood A., Kellahave D. and Skov Gretlund J. 2015b. Field testing of large diameter piles under lateral loading for offshore wind applications. *Proceedings of XVI European Conference on Soil Mechanics and Geotechnical Engineering*, Edinburgh, 1255-1260.

Byrne. Foundations for Offshore Wind Turbines (2013). Presentation. University of Oxford.

El-Marassi M., Elnaggar, M.H, Newson, T. and Stone, K. Numerical modelling of the performance of a hybrid monopiled-footing foundation. GeoEdmonton, 2008.

El-Marassi M. Investigation of hybrid monopile-footing foundation systems subjected to combined loading: The University of Western Ontario; 2011.

Jackson, F. A (2016). Assessment of earthquake site amplification and application of passive seismic methods for improved site classification in the greater vancouver region, british columbiaScholarship@Western.

Jonkman, J. M., Musial, W. D., & National Renewable Energy Laboratory (U.S.). (2010). *Offshore code comparison collaboration (OC3) for IEA task 23 offshore wind technology and deployment.* (No. 5000-48191.;5000-48191;). Golden, Colo: National Renewable Energy Laboratory.

Kramer, S. L. (1996). *Geotechnical earthquake engineering*. Upper Saddle River, N.J: Prentice Hall.

Lamb, Robert. "When will we run out of oil, and what happens then?" 21 April 2010. HowStuffWorks.com. <https://science.howstuffworks.com/environmental/energy/run-out-of-oil.htm> 15 May 2018

Lombardi, D., Bhattacharya, S., & Muir Wood, D. (2013). Dynamic soil–structure interaction of monopile supported wind turbines in cohesive soil. Soil Dynamics and Earthquake Engineering (1984), 49, 165–180. https://doi.org/10.1016/j.soildyn.2013.01.015

Malhotra, S. “Design and Construction of Offshore Wind Turbine Foundations,” Wind Turbines, pp. 231-264.

Poulos, H. G. (2016). Tall building foundations: Design methods and applications. *Innovative Infrastructure Solutions, 1*(1), 1-51. doi:10.1007/s41062-016-0010-2

Poulos, H. G. and Hull, T. (Role of analytical geomechanics in foundation engineering. Foundation engineering: current principles and practices. pp. 1578-1606 (1989). ILL item# 112694.

T.P.T. Dao. Validation of PLAXIS Embedded Piles for Lateral Loading. Delft University of Technology. 2011

Rahman, M. (1984). Wave diffraction by large offshore structures: An exact second-order theory. *Applied Ocean Research, 6*(2), 90-100. doi:10.1016/0141-1187(84)90046-4.

Wang, X., Zeng, X., Yang, X., & Li, J. (2018). Feasibility study of offshore wind turbines with hybrid monopile foundation based on centrifuge modeling. *Applied Energy, 209*, 127-139. doi:10.1016/j.apenergy.2017.10.107

Wang, Z., Hong, Y., Ng, C. W. W., Wang, L. Z., Mašín, D., & He, B. (2017). Cyclic lateral response and failure mechanisms of semi-rigid pile in soft clay: Centrifuge tests and numerical modelling. *Canadian Geotechnical Journal, 54*(6), 806-824. doi:10.1139/cgj-2016-035

Westwood, A. Offshore wind statistics. barriers to wind. refocus, 2004, 5, (5), 20. (2005). Fuel and Energy Abstracts, 46(4), 248-248. doi:10.1016/S0140-6701(05)81686-8

Y. Hong, B. He, L.Z. Wang, Z. Wang, C.W.W. Ng, and D. Mašín. Cyclic lateral response and failure mechanisms of semi-rigid pile in soft clay: centrifuge tests and numerical modelling. Canadian Geotechnical Journal (2017)

Chapter 6: Research Programme

6.1 Introduction

The centrifuge technology offers a powerful means for investigating complex geotechnical problems. Centrifuge testing has been used to investigate a wide range of civil engineering problems such as soil liquefaction, soil structure Interaction (SSI), slope stability and behaviour of foundation structures (Lai et al., 2020; Wang et al., 2018; Wang et al, 2017; Hu et al., 2017; Alnuaim, 2015; Abuhajar, 2013; El-Marassi, 2011). Centrifuge testing has been used in the current study to comparatively evaluate the performance of monopile and hybrid foundation systems installed in clay.

6.2 Overview

Model tests of geotechnical problems offer several advantages in terms relatively small cost, short model construction time and ability change parameters of significance, such as width, depth of foundation. In addition, it facilitates measurement of important response quantities such as response of test models as well as stresses and deformations of soil and pore pressure. Additionally, use of scaled models can expediate long term process such as consolidation and low frequency loads and can therefore be of significant help to gain insight in long term behavior of offshore soil sediments under waves, winds, and currents loading which are characterised by low frequency range (0.07-1 Hz) as elaborated in section 6.3.2. Nonetheless, there exist some limitations that centrifuge/model testing has such as particle size, boundary conditions and installation methods. Further, some spatial and soil properties cannot fully replicate soil condition due to time effects and damage to structures of soil used in centrifuge which might affect the accuracy of results. Table 6-1 presents the scaling laws used for centrifuge modeling.

Table 6-1 Centrifuge Scaling Laws (Madabushi, 2017).

Property	Model	Prototype
Length	1/N	1
Moment of inertia	$1/N^4$	1
Stress	1	1
Strain	1	1
Displacement	1/N	1
Area	$1/N^2$	1
Volume	$1/N^3$	1
Mass	$1/N^3$	1
Density	1	1
Force	$1/N^2$	1
Time (dynamic)	1/N	1
Time (diffusion)	$1/N^2$	1
Time (Viscose flow)	1	1
Acceleration	N	1
Velocity	N	1
Frequency	N	1
Energy	$1/N^3$	1
Elastic modulus	1	1
Flexural stiffness	$1/N^2$	1
Strain rate (dynamic)	N	1
Strain rate (Diffusion)	N^2	1

First applications of centrifuge testing for civil engineering problems involved modeling mine roof integrity in the USA and embankment and slope stability problems in the Soviet Union (Ng, 2014). The centrifuge test results can provide excellent data for calibrating and validating the

results of numerical models. Centrifuge modeling has been used widely to investigate different problems related to ocean engineering, especially foundations for offshore structures. For example, a few centrifuge studies were performed to evaluate the performance of hybrid foundation systems under different types of loading as discussed in Chapter 2. Nevertheless, to the author's knowledge, the behaviour of hybrid foundation installed in clay has not been investigated experimentally. Therefore, the aim of this study is to cover this gap in literature by testing scaled models to evaluate the performance of hybrid foundation compared to monopile foundation.

This objective of the centrifuge testing reported herein is to simulate the response of different OWT foundations under vertical-horizontal- moment (VHM) loading conditions of a typical 5MW wind turbine installed in shallow -medium depth water in over-consolidated (OC) clay. This chapter describes the centrifuge test facility, the preparation of the physical models, the instrumentation, the design and preparation of soil profile, the design and setup of the test headwork, and the testing plan.

6.3 Centrifuge Modelling

Successful centrifuge models requires properly simulating different prototype phenomena such the as relative size and stiffness of test model and soil bed, dynamic and diffusion conditions, density of materials and boundary conditions. The following sections discuss some of these issues relevant to testing of OWT foundations.

6.3.1 *Particle size*

When scaling down the prototype structure to model size structure, the ratio of foundation dimeter to the particle size changes significantly. This can be reduced by using smaller particle size. However, this can lead to different soil behavior. Toyosawa et al. (2013) noted that the

bearing capacity is not affected by the particle size if the ratio of foundation diameter to mean particle size (D_{50}) is more than 33. This problem, given the clay particle size, will not have effects on the capacity of foundations tested in centrifuge modelling.

6.3.2 *Viscosity*

Adamidis and Madabhushi (2014) discussed the consideration of viscosity in dynamic and diffusion scaling arising from use of centrifuge models. Use of pore fluid not satisfying the diffusion laws can present untrustworthy results. Water would dissipate N times higher than the prototype scale, which means the recorded excess pore pressure and the associated settlement/deflections can be significantly under and overestimated. To satisfy the scaling factor, dynamic time in model, t_m, should be n times lower than the prototype dynamic time i.e.,

$$t_m = \sqrt{\frac{L_m}{a_m}} = \sqrt{\frac{\frac{L_p}{n}}{a_p * n}} = \frac{t_p}{n} \tag{6-1}$$

where:

a: acceleration; n: scaling factor ; t_p&t_m: prototype and model dynamic time.

Nonetheless, considering diffusion phenomena, compatibility should be ensured between model and prototype diffusion times. The dimensionless time factor, T_v, for consolidation settlement is;

$$T_v = C_v \frac{t}{d^2} \tag{6-2}$$

Where C_v is the coefficient of consolidation. Therefore

$$C_{v,m} \frac{t_m}{d_m^2} = C_{v,p} \frac{t_p}{d_p^2} \tag{6-3}$$

If the same soil is used in the model, i.e., $C_{v,m}$=$C_{v,p}$, and given d_m=d_p/n, Hence,

$$t_m = \frac{t_p}{n^2} \quad (6\text{-}4)$$

It is noted that the dynamic time scaling and diffusion time scaling produced n more permeable soil, which is handled in centrifuge testing through using more viscous pore fluid or by taking into consideration this effect of time difference. Hydroxypropyl methylcellulose (HCMP) aquatic solution can be used instead of water to replicate the excess pore pressure more precisely.

6.3.3 *Gravity Switch-On*

When spinning the centrifuge, the model undergoes stress variation in short time which can lead to lock in stresses. To overcome this problem, it is generally recommended to accelerate the centrifuge in steps from 0 to required g level. At each step, a halt is recommended for 2-5 minutes to ensure stabilized response of the soil layers and eliminate stresses lock in.

6.3.4 *Effective radius*

The test model would have geometry that extends away from the center of gravity, C.G, and this creates differences in the acceleration field across the model. It is recommended that the g level to be calculated at an effective radius of R= R+2l/3 where L is the model embedded depth and R is the distance from the center of rotation to strong box.

6.4 CEIG facility

The Broadbent beam centrifuge housed at the Centre for Energy and Infrastructure Ground (CEIG) is located at the Department of Civil and Structural Engineering at The University of Sheffield, UK. The Broadbent beam centrifuge has effective radius of 2 m and has a maximum payload of 1 ton at 50g and a maximum centrifugal acceleration of 150g (Black et al., 2014). The centrifuge facility is equipped with National Instrument data acquisition with 32 channels to aid

installation of different geotechnical systems within the centrifuge box and obtaining abundant information on parameters such as earth pressure, settlement/deformation, strain, PIV/cameras and pore water pressure. Also, geotechnical shear strength profiles can be established by using specially designed probing T-bar or CPT to establish the shear strength profile. Figure 6-1 shows Broadbent beam centrifuge at GIEG center.

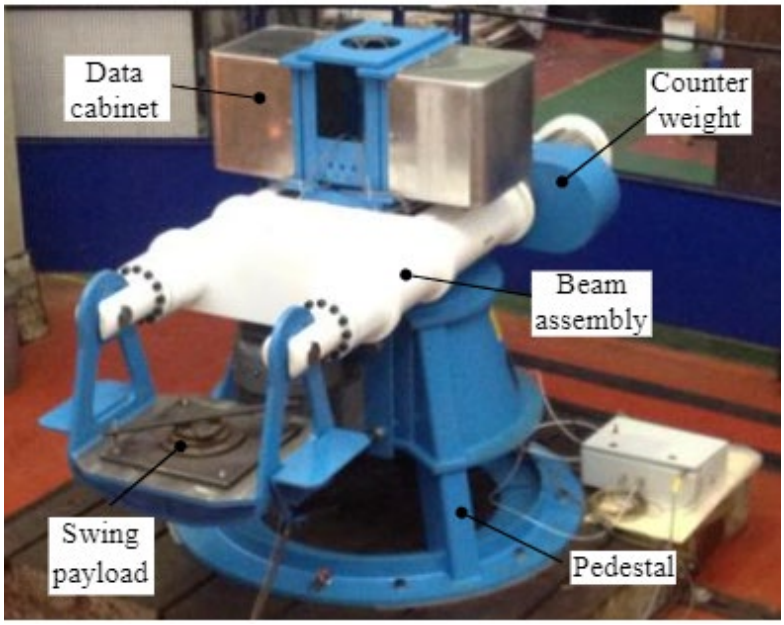

Figure 6-1 University of Sheffiled CEIG Broadbent beam centrifuge (Black et al., 2014)

6.5 Testing program

This proof-of-concept study aims at delineating the behaviour of scaled down foundations representing offshore wind turbine foundations and to compare two foundations options. Monopile (MP) and hybrid foundation (HF) models were manufactured and tested to investigate their lateral loading capacity and stiffness properties. Also, the results from these model tests will be used to calibrate and validate finite element models to further investigate the performance characteristics

of these foundations. The models were installed in an OC Kaolin clay made by Imerys, UK. The objectives of this study are to:

1- Investigate the lateral stiffness properties of MP and HF systems.

2- Investigate the lateral ultimate capacity of the considered systems.

3- Provide insights into comparative static performance of test models.

4- Bridge gap in literature by providing high quality data on these systems in a soft clay bed.

6.5.1 *Methodology*

Prototype foundations of the MP and H.F were chosen according to previous research by Abdelkader (2016) and limited FE models, which suggested they have similar capacity under lateral loading. They were scaled down by $1/6^{th}$ (virtual model). These virtual models were then scaled by centrifuge laws (N = 50) to produce models that can be fit-in within the centrifuge tub without violating boundary conditions of the tub. This exercise of scaling could shed some light on normalization and keeping some foundation parameters ratio ratios in perspective such as (L/D, L_p/W, EI_t/EI_p, D_t/D_p, $D_{p,MP}/D_{p,HF}$) and observations of which can be summarized as follows:

1- Soil shear strength cannot be scaled, this leads to change in EI_p/E_s between prototype and models if only N scaling is followed. This is because rigidity of structural elements is scaled by N^4 while shear strength variation cannot be factored as much. Typical range of gravity used in centrifuge testing ranges between 20-100g meaning difference between structural elements stiffness in prototype and model can be between 160,000 and 100,000,000 while shear strength cannot be scaled more than 500 times given range of shear strength of soil materials is between 2kPa and 1000 kPa typically. This results in different behavior of piles tested laterally. Therefore, caution must be exercised when mapping centrifuge results to

prototype results. This can be achieved through the normalization of Monopiles and Hybrid foundation ultimate capacity following the improved normalization procedure presented in Chapter 3 (Eq. 3-1).

2- Obeying linear and centrifuge laws and meeting the two can be extremely difficult to accomplish, especially with limited materials E values to choose from. This resulted in some differences in L/D ratio for MP and W/D_p for HF. Also, D_t/D_p ratio had to be kept in mind which resulted in difference between MP tower diameter (but not lateral stiffness) and HF tower diameter.

3- The HF incorporates a smaller diameter pile; thus, an HF system with 4m pile in prototype scale was chosen to compare against an MP with 6m diameter, keeping this ratio between the two was important, which resulted in some of the differences mentioned above.

Figure 3-2 presents the three test models (not to scale) while Tables 6-2 and 6-3 present the scaling applied to produce models from prototype.

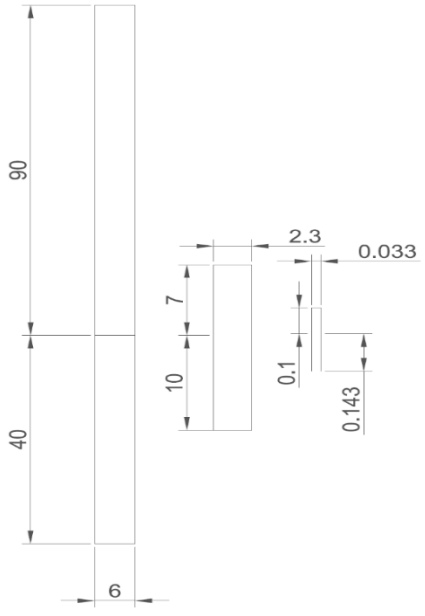

Figure 6-2 (a) prototype, (b) Scaled proptotype model (c) model (Not to scale, dimesions in meters)

6.5.2 *Scaling*

Table 6-2 Scaling laws between Prototype, virtual model and model for MP

	Properties	Prototype	Virtual model	Model
Tower	L,m	90	7	0.1
	D_t, m	6	2.31	0.033
	t_t,m	0.035	0.0024	0.003
	EI, kN.m^2	583450775	2316238	0.102
	EA, kN	260815022	838192628	848
	Material	Steel	Steel	Acrylic
Monopile	L_p, m	40	10	0.143
	D_p,m	6	2.31	0.033
	t_p,m	0.07	0.0047	0.013
	EI, kN.m^2	1146601521	4522430	0.185
	EA, kN	260815022	6807774	2613
	Material	Steel	Steel	Acrylic
	N	1	4	70

Table 6-3 Scaling between prototype, virtual model and model

Element	Properties	Prototype	Virtual model	Model
Tower	L, m	90	5	0.1
	D_t, m	6	1.4	0.028
	t_t, m	0.035	0.0028	0.000
	EI, kN.m^2	583450775	565722	0.103
	EA, kN	131177201	2475605	848
	Material	Steel	Steel	Acrylic
Monopile	L_p, m	28	5	0.1
	D_p, m	4	0.93	0.022
	t_p, m	0.047	0.0037	0
	EI, kN.m^2	228049735	235230	0.037
	EA, kN	116735928	2161192	1216
	Material	Steel	Steel	Acrylic
	N	1	5.57	50
	M_t/M_{plate}	0.81	0.822	0.92
Plate	W, m	14	2.50	0.05
	t, m	2	0.8	0.0145
	EI, kN.m^2	255603860.2	263651	0.0406
	EA, kN	4215766849	134431340	6283
	Material	RC	RC	Acrylic

Subscript t= tower, Subscript p = pile, t = thickness, RC= reinforced concrete, L = length, D = diameter of tower

Figures 6-3 presents a plan view showing the test locations in tub2, similar configuration is followed for tub1. The elevation views of the models showing instrumentations used are shown in Figures 6-4 and 6-5. The tests locations are distanced more than 7D center to center while loading direction was to the tub centerline.

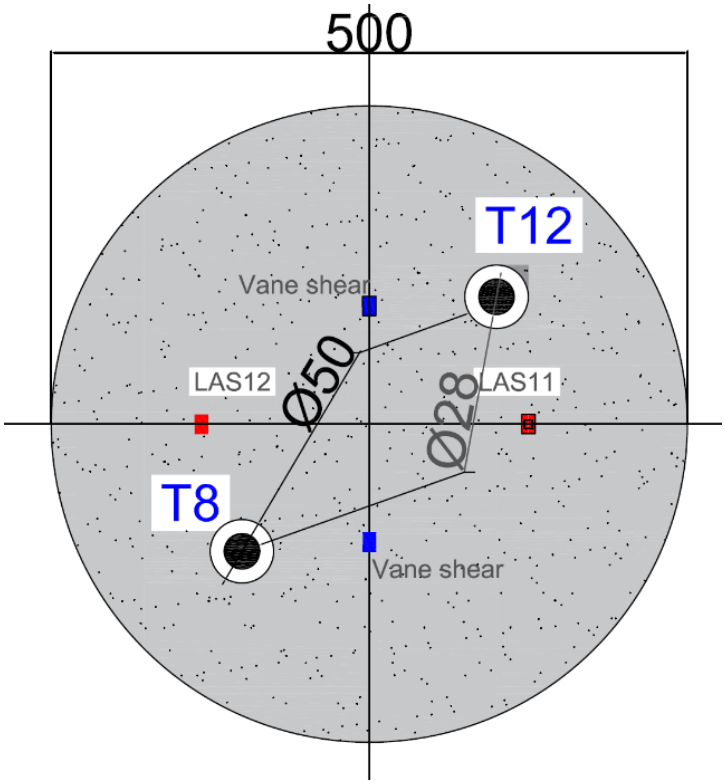

Figure 6-3 Top view and tests locations

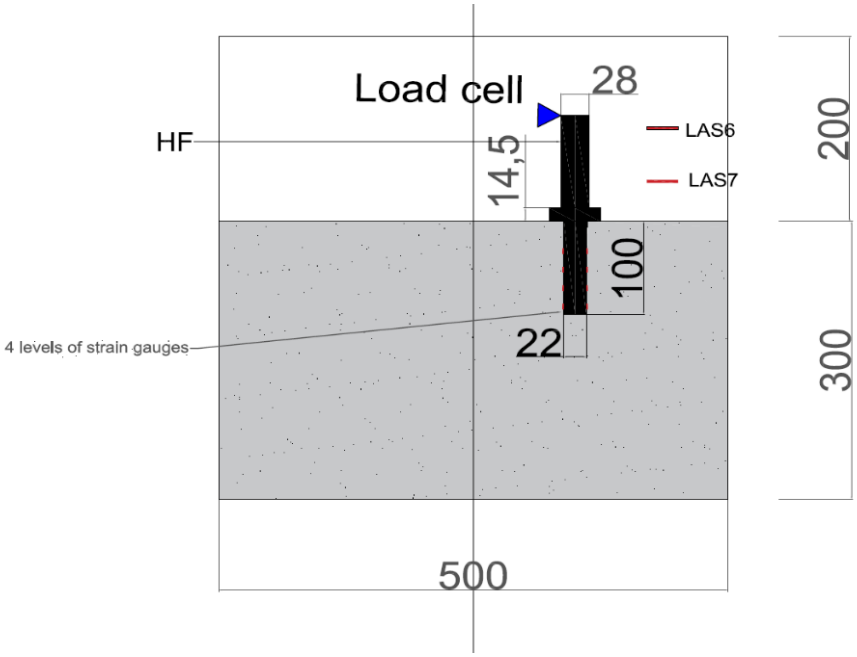

Figure 6-4 Cross section of H.F showing instrumentations

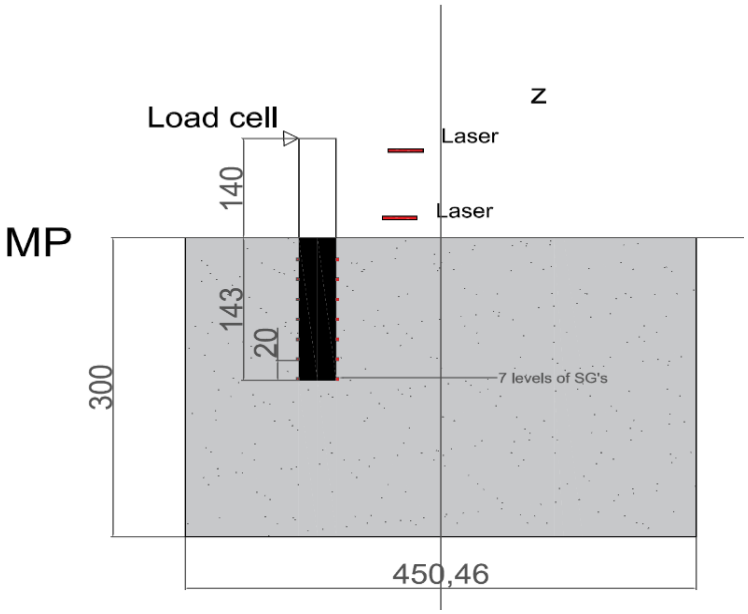

Figure 6-5 Cross section of MP showing instrumentations

6.5.3 *Bed design*

The kaolin was mixed at 1(kaolin):1.2 (water) ratio employing a Winkworth UT150 horizontal shaft mixer which has a capacity of 150 L. The mixed slurry was poured layer by layer into a cylindrical rigid box with a plaster scoop to minimize air entrainment and avoid segregation. It was placed over a 5cm sand and a filter paper for drainage and was left to settle under its own weight. The tub had a diameter of 500 mm and height of 500 mm. After placing all soil materials in the tub, it was moved to the centrifuge swing and was spun in stages till 70g. Figure 6-6 shows the tub with headwork mounted on the centrifuge before inflight consolidation. A sand layer 10 cm thick was added on top of the clay layer to enhance over consolidation ratio and to increase shear strength near surface. The intended depth of the clay layer after consolidation was 30 cm; therefore, the clay depth before spinning was set around 49 cm. Two tubs were made, one for each model to maintain quality of tests while increasing efficiency by testing at three different locations within each tub. The test models were placed more than 7D apart within the tub and were situated at least three times the monopile diameter (D) or HF plate width (W) from the tup rigid boundary, which was deemed to be sufficient to avoid boundary condition (Zhang et al., 2017). The first test tub involved lateral loading of the MP to establish its stiffness properties and ultimate lateral capacity. The second tub was made to conduct similar lateral load tests on the HF. These model tests would serve as baseline for comparison of lateral stiffness and capacity of the two foundations . Since Wind Turbines are subject to VHM loading, it is necessary to apply vertical loading to the model foundations during the lateral load tests. Thus, weights were added representing about 20% of the vertical capacity of the foundation system, which was established using finite element models prior to the centrifuge tests.

Table 6-4 Test matrix

Test ID	Foundation	Description	e, mm
T4	Monopile	Mono. Lateral load	120
T5	Monopile	Mono. Lateral load	120
T8	Hybrid foundation	Mono. Lateral load	115
T12	Hybrid foundation	Mono. Lateral load	115

Table 6-4 presents the different tests conducted as part of this study to evaluate the response of MP and HF systems subject to different VHM loading conditions. Table 6-5 presents the procedure of inflight consolidation followed to prepare the soil bed. Figure 6-6 shows the clay slurry before consolidation on the beam platform. Figures 6-7 and 6-8 present a plan view and side view of test setup from a mock up test. Figure 6-9 shows a predicted settlement profile used for the purpose of estimating initial and final clay height.

Table 6-5: Loading/unloading increments

Condition	g level		Duration (minutes)
	From	To	
Loading	1	10	2
Loading	10	20	2
Loading	20	30	2
Loading	30	40	1440
Loading	40	70	2880
Unloading	70	1	1440

Figure 6-6 Solid tub used to prepare clay samples showing newly casted clay before spinning

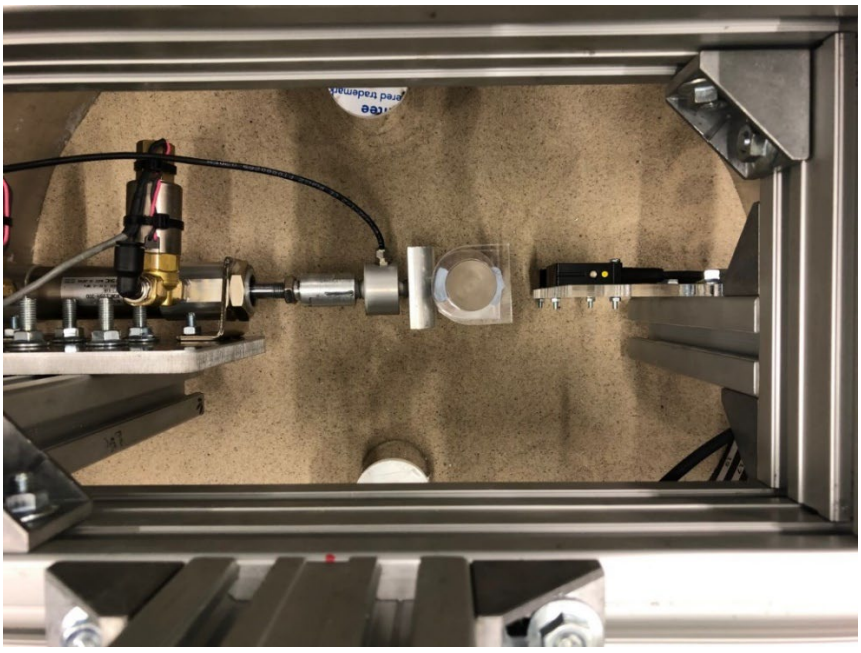

Figure 6-7 Top view of headworks and test setup in mock-up test

Figure 6-8 Side view of HF1 showing laser sensors used and load cell and actuator

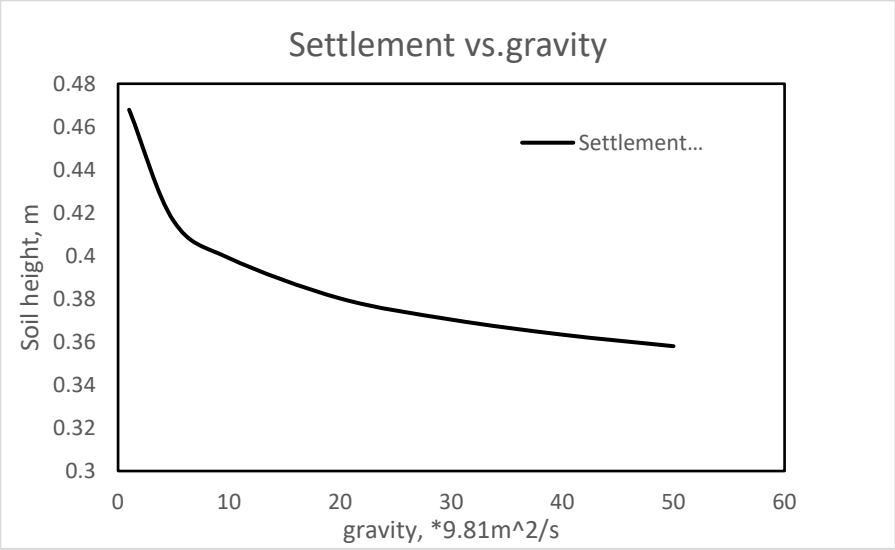

Figure 6-9 Predicted settlement versus g level

6.5.4 *Settlement at 70g*

Figure 6-10 displays the recorded settlement profile of the clay bed after the gravity filed reached 70g. The Cv value was estimated from the recorded settlement data according to Taylor's method, i.e.

$$t_{90} = (56.5\text{-}51.2)^2 = 591 \text{ min.} = 35475 \text{ sec.}$$

$$\text{Average sample height, } d = 29.05 + \frac{7.8-4.5}{2} = 30.7 \text{ cm}$$

$$C_v = 0.848 * \frac{(\frac{0.37}{2})^2}{35475} = 8.2\text{E-}7\text{m}^2/\text{s}$$

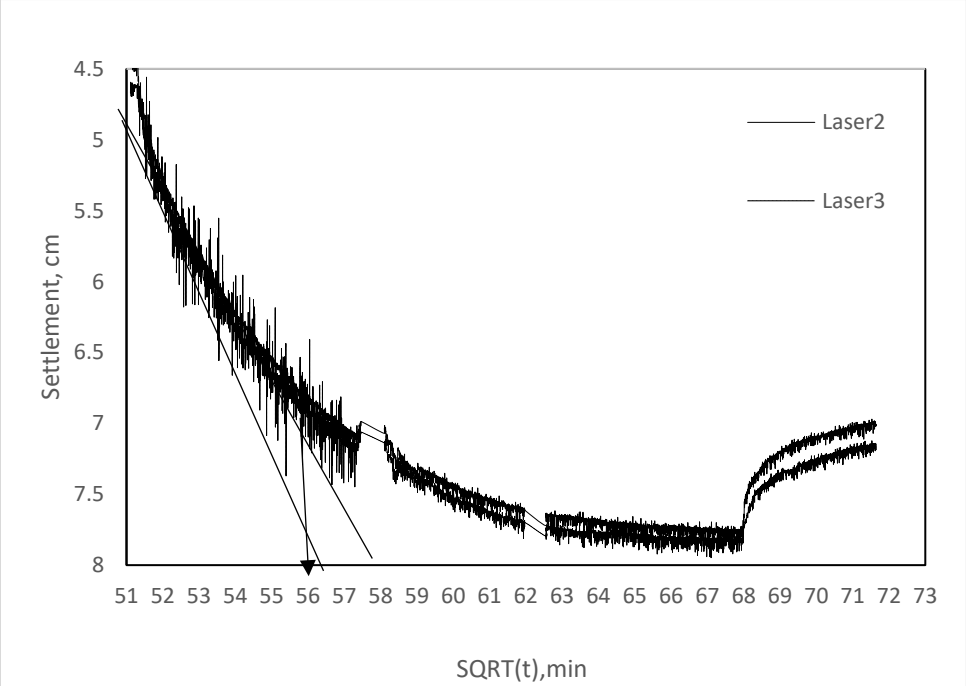

Figure 6-10 Consolidation settlement versus time using Talyor's method

Figure 6-11 presents the same data following the logarithmic time method. The general trend indicates that the consolidation was complete, i.e., has reached t_{100} by the end of consolidation record before spin down.

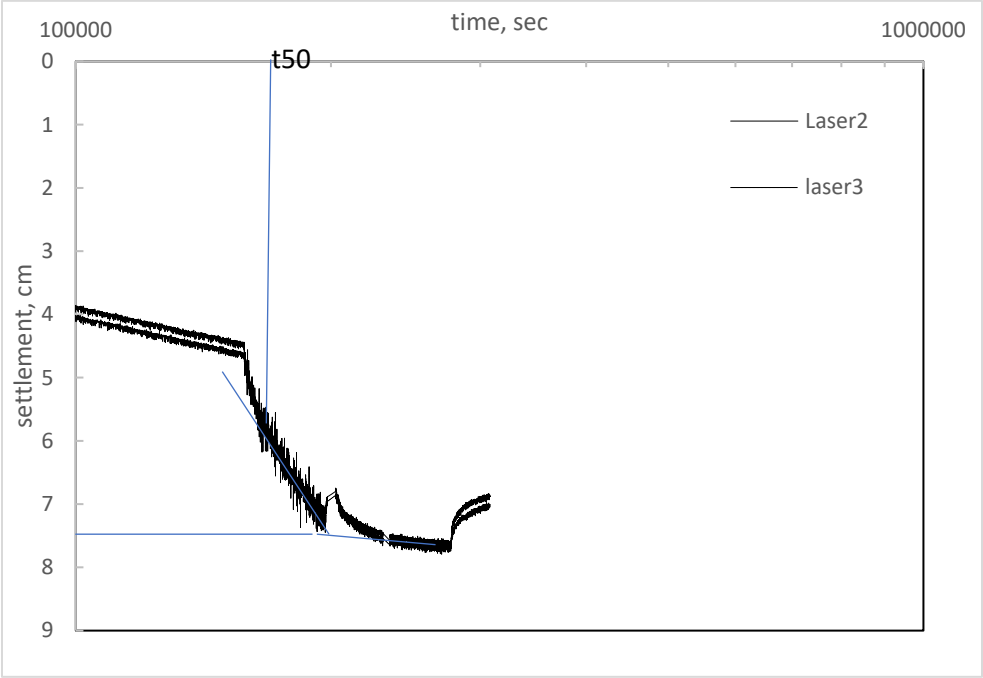

Figure 6-11 Casagrande representation of consolidation settlement to ensure 100% primary consolidation is reached before spin down.

6.5.5 *Vane shear strength and SHANSEP prediction at 70g*

Six vane shear tests were conducted after spin down in 1g environment in two separate locations to establish the shear strength profile. As shown in Figure 6-12, a uniform soil shear strength profile was established by the consolidation process, which indicated consistent shear strength data. A parabolic variation of S_u is accomplished which is typical for overconsolidated clays (Hong et al., 2017; Lau, 2015; Zhang et al., 2011).

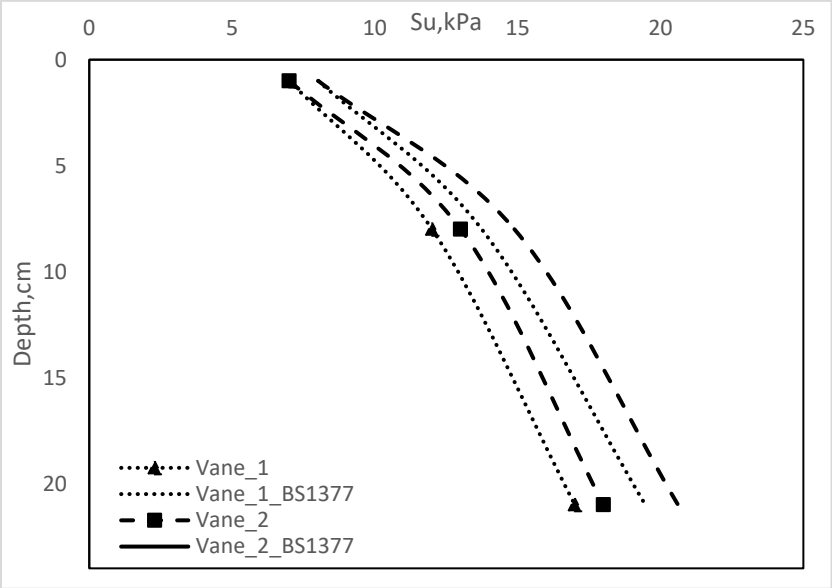

Figure 6-12 Vane shear strength

Figure 6-13 shows normalized shear strength data of average vane shear tests conducted after spin down (at 1g). In order to map the shear strenght data to get the Su profile at the g level used for testing,the Su at 1g was best fit according to the SHANSEP procedure, equation 6-5. Having accomplish this, the Su profile can be predicted for any g level knowing the soil effective stress and OCR values. From best fit equation (equation 6-5), the C_1 and C_3 were determined. C_1 and C_3 based on the fitting equation were 0.325 and 0.8, respectively. Hence, the shear strength profile at 70g can be established. Figure 6-13 shows the normalization procedure followed to establish C1 and C3 from equation 6-5. Figure 6-14 present the predicted OCR values for the soil profile at 70g. Figure 6-15 shows the predicted shear strength profile at 70g employing equation 6-5 and using fitting parameter from Figure 6-13.

$$S_u \text{ (SHANSEP)} = C_1 * \sigma' * OCR^{C_3} \quad (6\text{-}5)$$

where: C_1 and C_3 are fitting parameters and range between (0.18-0.35) and (0.51-0.9).

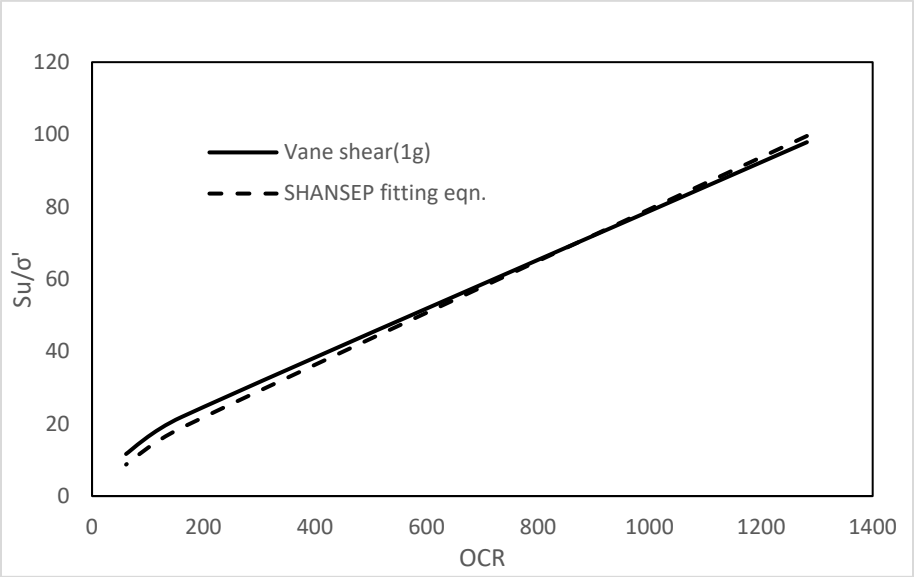

Figure 6-13 Ladd's chart of 1g vane shear tests

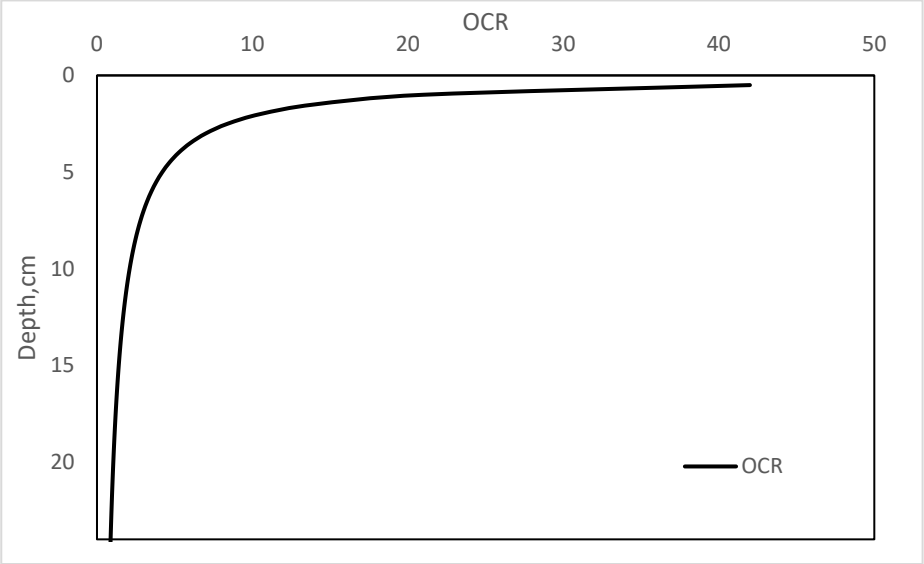

Figure 6-14 OCR profile of Tub-1

It can be seen from Figures 6-13 and Figure 6-15 that the shear strength profile obtained is close to reality with shear strength increasing at a rate of 1kPa/m with S_{uo} of around 15 kPa and OCR of around 42. The average shear strength at the zone of influence is around 22kPa. These values agree well with data from Alnuaim (2015).

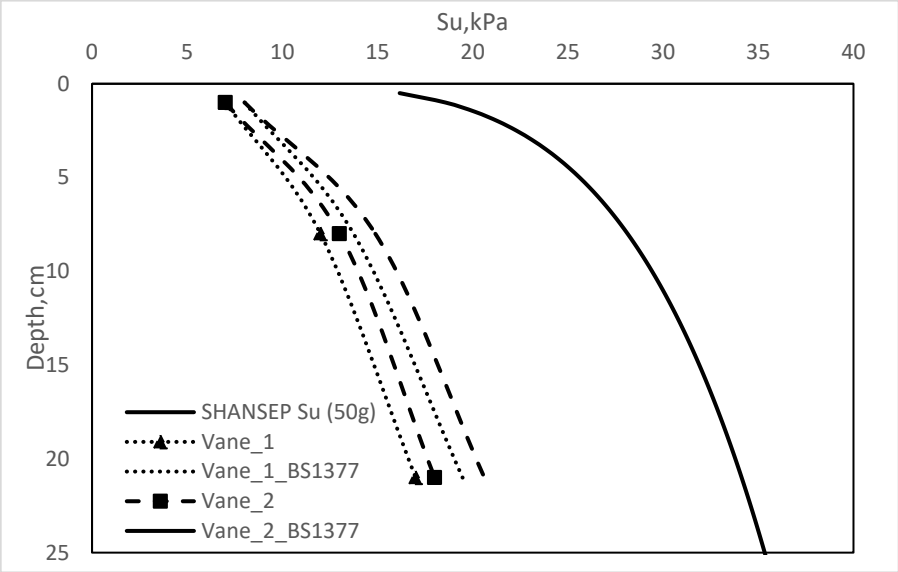

Figure 6-15 Mapped Shear strength profile at 70g based on 1g data

6.6 Instrumentation

Strain gauges, laser beams and pore pressure transducers were used to record bending strains along the monopile shaft, settlement, and pore water pressure. All instrumentations were calibrated to ensure their functionality and to verify their measurements. Table 6-6 and Table 6-7 present instrumentation details used for the conducted tests.

Table 6-6 Instrumentation plan for MP

Type	Description	PPT	Laser sensors	Strain gauges
MP	**Purpose**	**Record consolidation**	**Record displacement and rotations**	**Record bending moment**
	Numbers	3	2	7
	Location	Centerline	Opposite to load application	at different depths
	Depths, m	0.1, 0.2, and 0.3	@0.1m vertical distance	each 0.02m from pile toe

Table 6-7 Instrumentation plan for hybrid systems

Type	Description	PPT	Laser sensors	Strain gauges
H.F	**Purpose**	**Record consolidation**	**Record displacement and rotations**	**Record bending moment**
	Number	3	2	4
	Location	Centerline	Opposite to load application	at different depths
	Depths, m	0.1, 0.2 and 0.3	@0.1m vertical distance	each 0.02m from pile toe

6.7 Calibration

6.7.1 *Laser Transducers*

The laser transducers used in this experimental program were Baumer OADM 12U6460/S35A with reading limit of 104 mm and resolution of 2µm-120µm and voltage output between 1-10v. The lasers were calibrated by a special device in which the laser is fixed and attached to a data acquisition system connected to a PC. Changing the distance of the reflecting surface is measured

by the running voltage measurements. Figures 6-16, 6-17, 6-18 show the voltage signal recorded by the system corresponding to the measured displacement for different lasers.

6.7.1.1 (Short range to monitor displacement)

Short range Baumer OADM 12U6460/S35A laser sensors were used to measure lateral deflection and monitor reconsolidation data. Figures 6-16 till 6-18 show the results of calibrating the three laser sensors used.

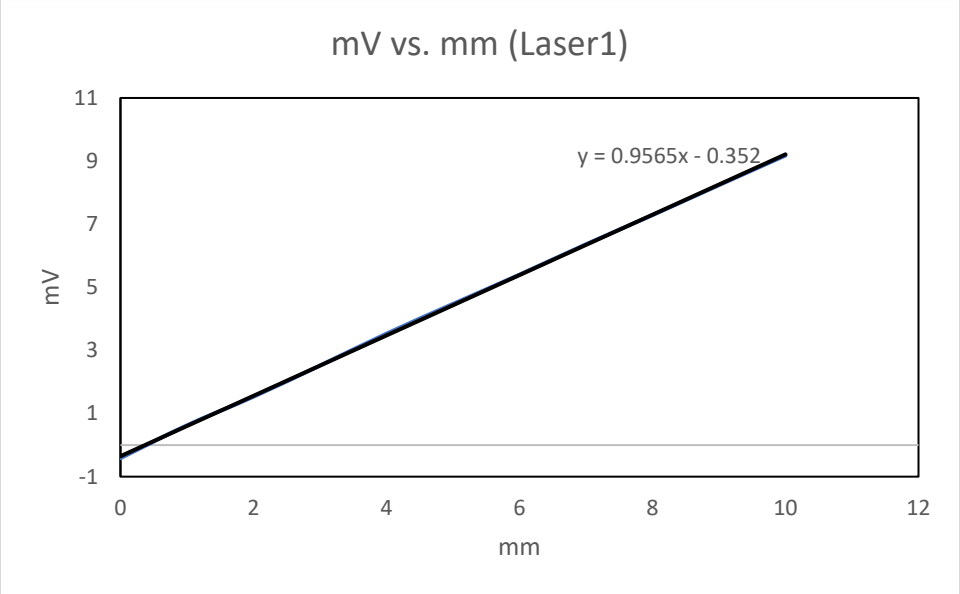

Figure 6-16 calibration data for laser 1

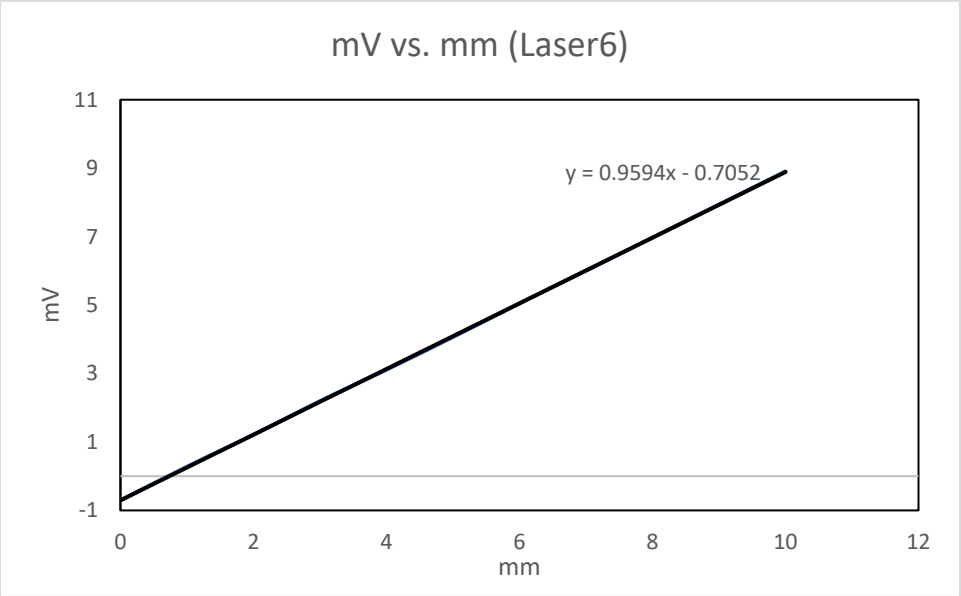

Figure 6-17 Calibration data for laser 6

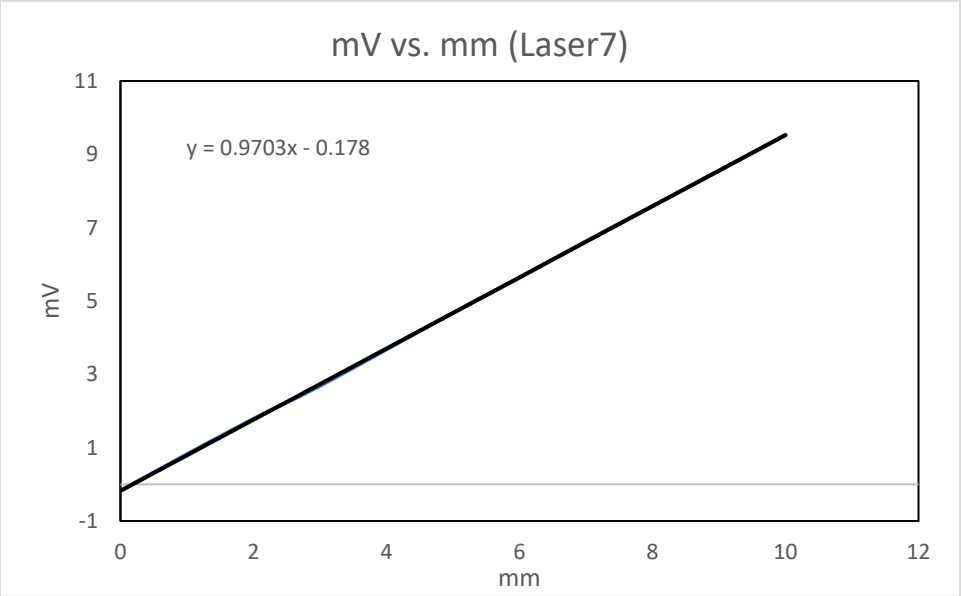

Figure 6-18 calinbration data for laser 7

6.7.1.2 (Long range to monitor consolidation)

Long range Baumer OADM 12U6460/S35A laser sensors were used to measure consolidation settlement. Figure 6-20 shows the results of calibrating the two laser sensors used to record settlement.

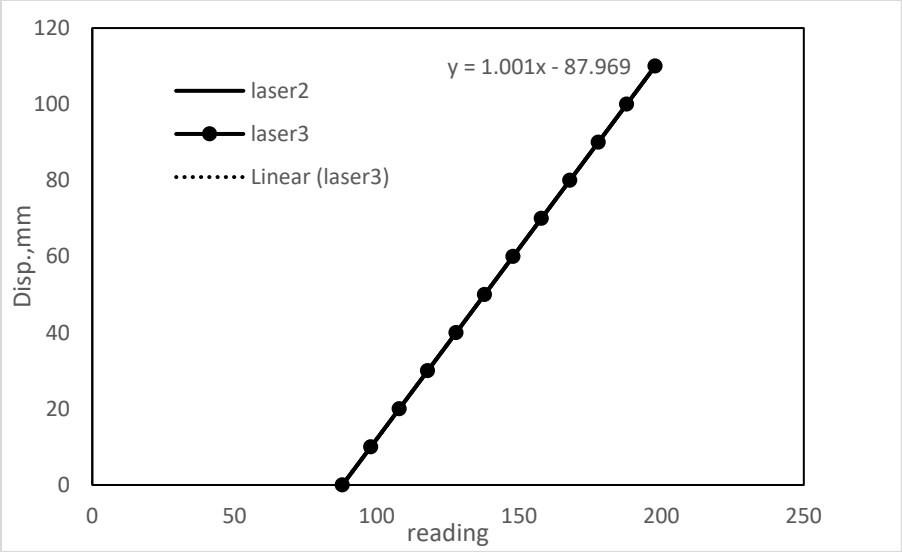

Figure 6-19 Calibration data of long range laser sensors

As seen in Figure 6-3, two laser sensors were used to trace settlement at 125mm from tub center. Shallow surface of sand and a plastic dark disks were mounted on the surface of the clay to allow precise reading of the location of mudline. Figure 6-21 shows Laser 2 against black disk used to trace mudline surface from a GoPro Camera during inflight consolidation. Figure 6-22 compares the predicted (using 1-D Terzaghi's Theory) and average measured height changed at end of consolidation at 70g.

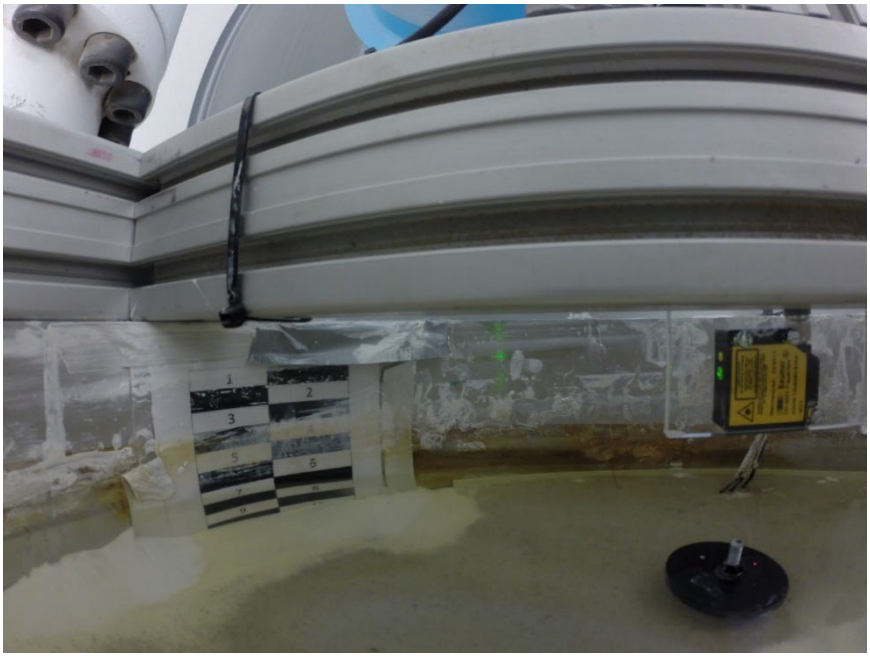

Figure 6-20 Laser 2 measurements during inflight consolidation

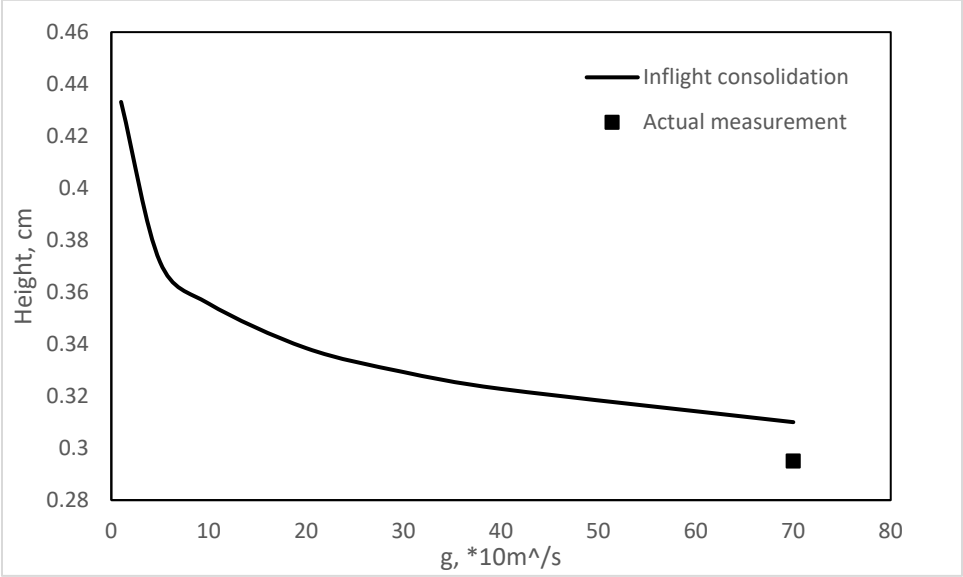

Figure 6-21 Predicted and measured (average) height change at end of consolidation

6.7.2 *Strain gauges*

The strain gauges used to measure strains in the test models were from Tokyo Measuring Instruments model GFLA-3-350 with operational temperature of -20-150C and resistance of 350

ohm. The strain gauges were oriented in half bridge form to double the output and offer temperature compensation. They were glued to MP and HF by using speciality adhesive and insulated with coating. They were then calibrated by attaching each model to a strong table and laying the models horizontal while applying increased vertical loads from 0-100N. Knowing the applied load, the strain gauge recorded voltage was correlated with theoretical moment. Figure 6-23 shows the process of calibrating the strain gauges used for HF while Figure 6-24 shows the theoretical bending moment diagram from the setup configuration. The voltage signal recorded by the system corresponding to the estimated bending moment is then best fit to a polynomial equation for direct estimates of pile's bending moment from test data (Figure 6-25). Figures 6-26 and 6-27 show the same procedure applied for MP.

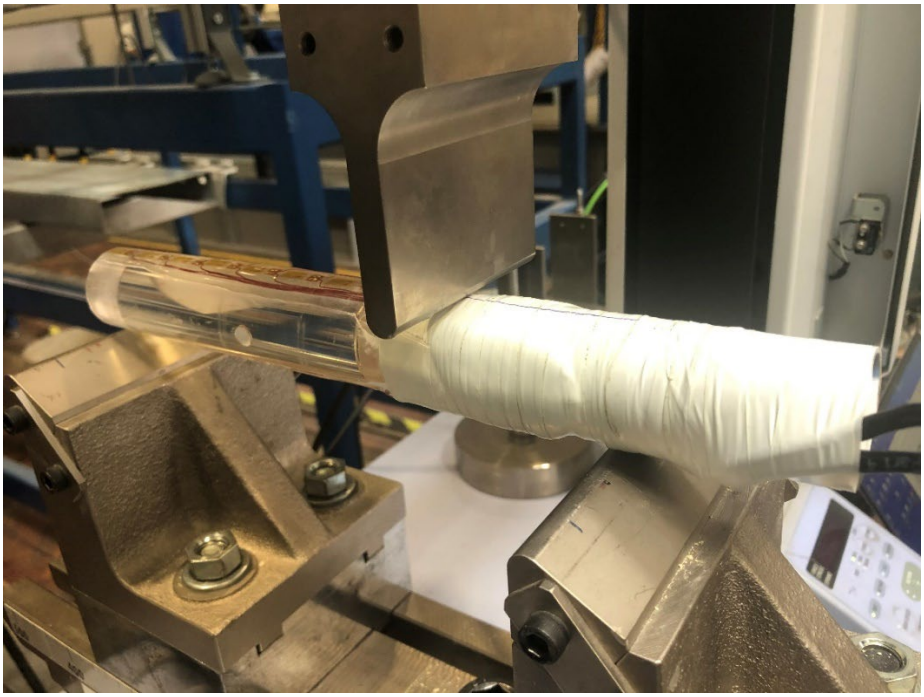

Figure 6-22 MP strain gauge calibration process

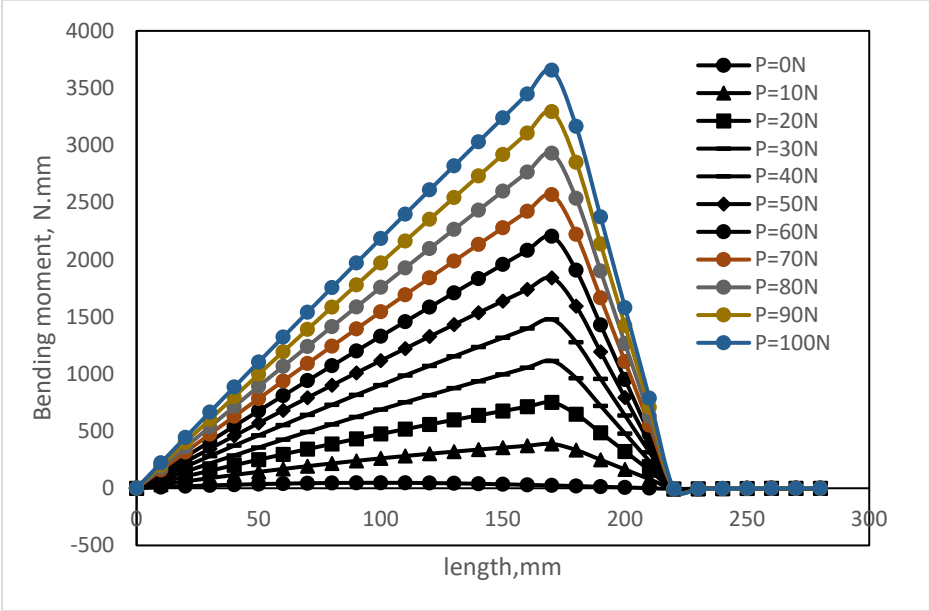

Figure 6-23 Theoritical moment at different load levels for MP

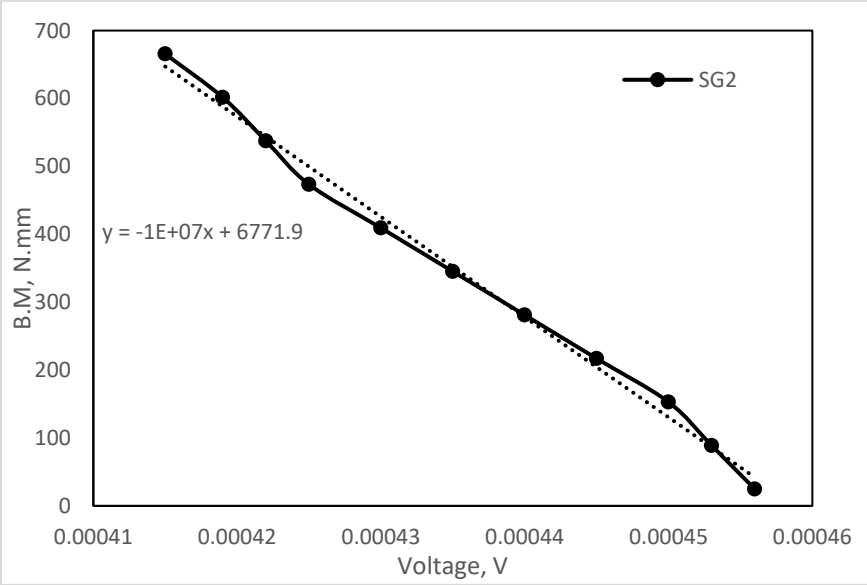

Figure 6-24 correlated moment at one of the SG locations

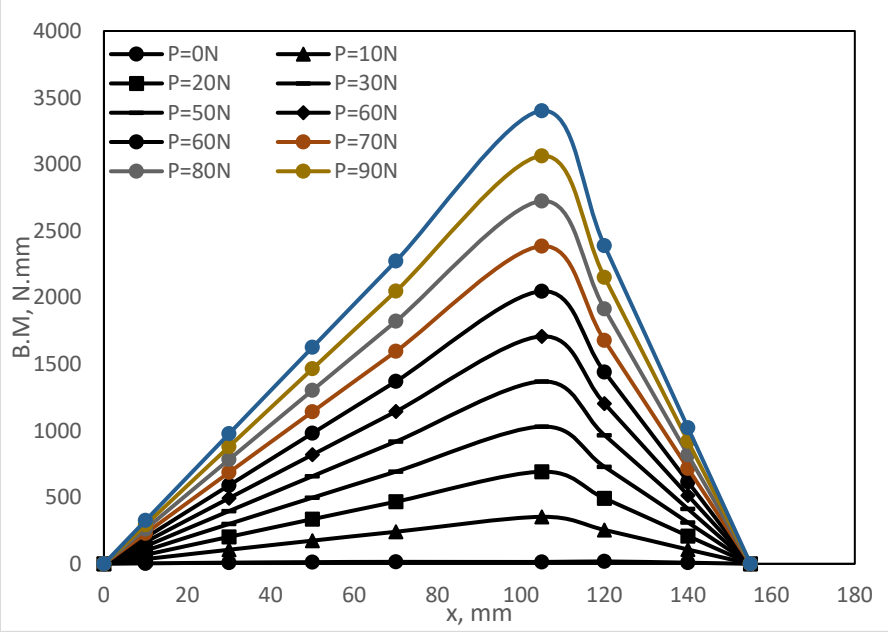

Figure 6-25 Theoritcal moment at different load levels for HF

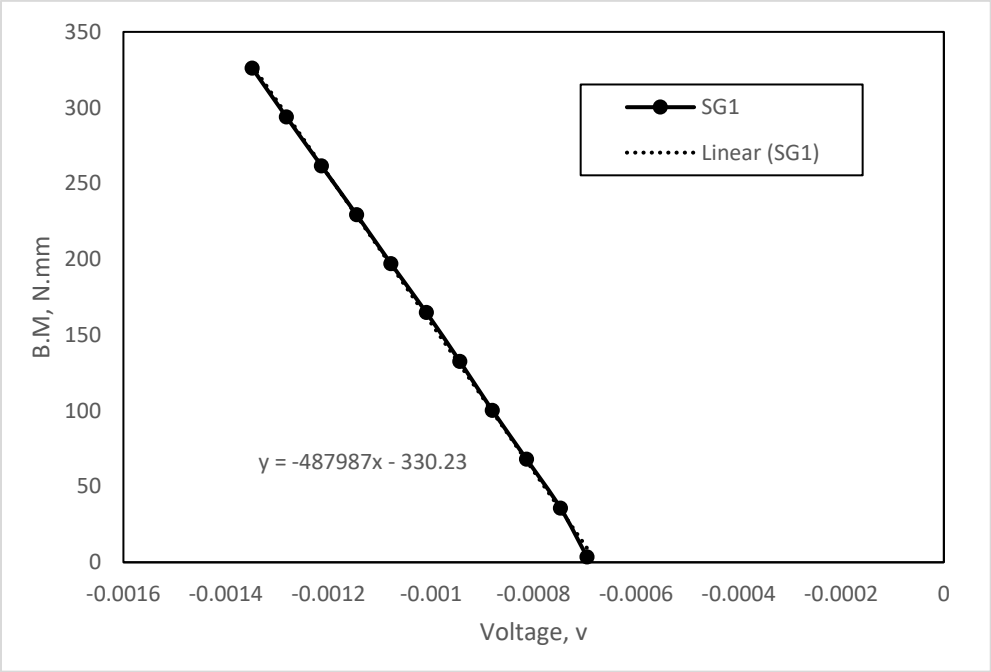

Figure 6-26 Recorded volatege for SG1 correlated with BM from previous figure

6.7.3 *Pore Pressure Transducers (PPT)*

The used PPTs were Kiowa model with maximum pressure value of 900kPa. The PPTs were calibrated by a speciality device in which the PPT was first submerged for a day to ensure saturation. Next, the PPT was placed in a chamber filled with water connected to a pressure line. A certain pressure was applied and the measured value of pressure by PPT was within 5% of the applied pressure. Three PPT were used for recording consolidation data and monitoring excess pore pressure decay. Figure 6-28 presents the calibration data for the PPTs.

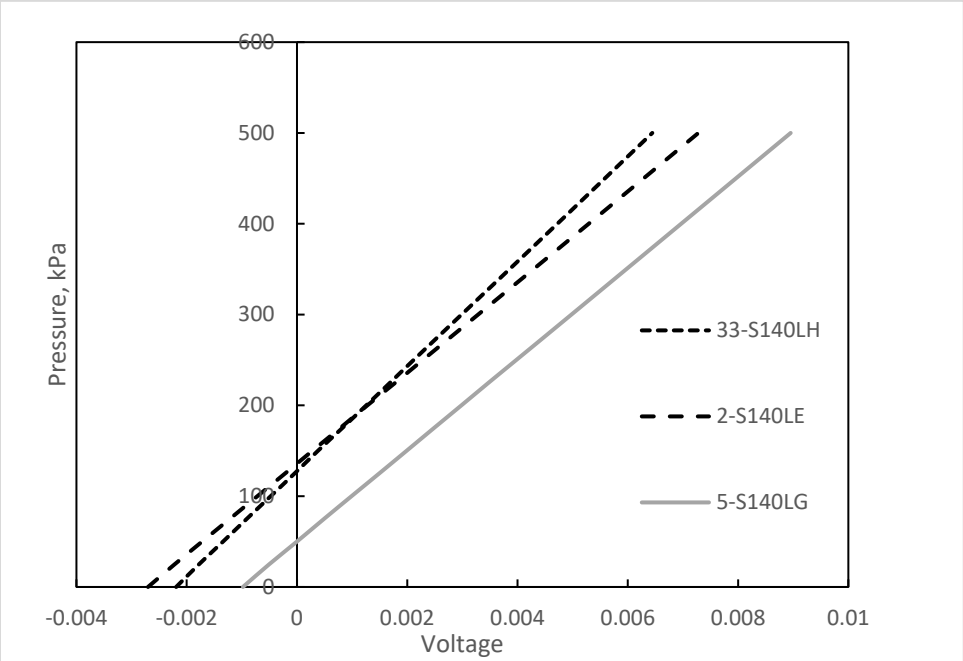

Figure 6-27 Calibration data for PPT

6.7.4 *Load cell*

The pneumatic load actuator used was a SMC type with load range up to 7bars giving net 375N (Bayton et al., 2018). It was connected with a 200 series in-line load cell calibrated for the expected range of applied load. The process of calibration involved connecting the load cell to a DAS and placing it under varying loads. The loads were then measured by the piezoelectric load cell and logged into the LABVIEW program in volts with a sampling rate of 5000 samples per seconds. Averaging these reading enabled plotting the load versus voltage and fitting the line with a first order polynomial, Figure 6-29 shows the calibration device used to calibrate the load cell while Figure 6-30 shows the voltage force relationship.

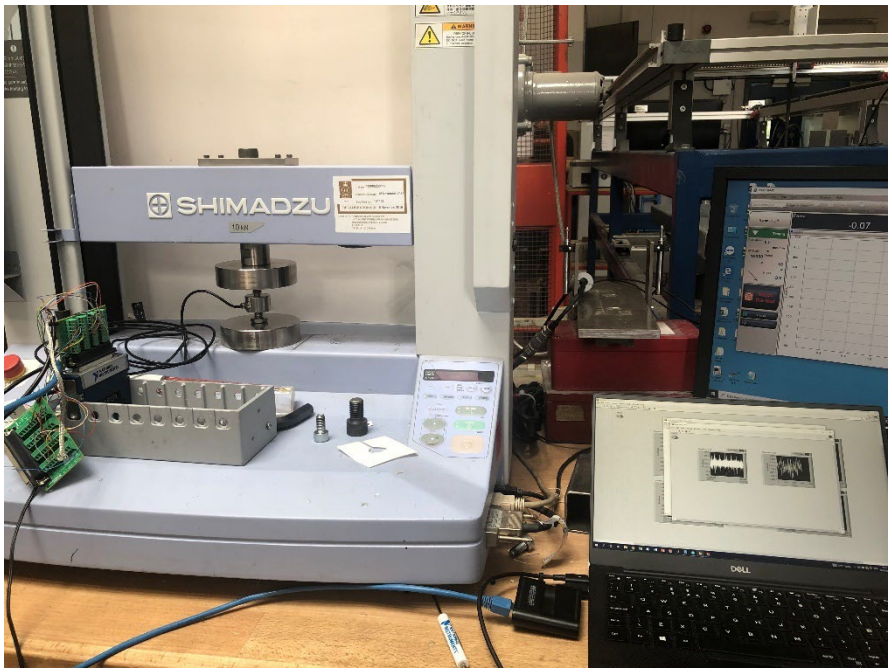

Figure 6-28 Load cell calibration

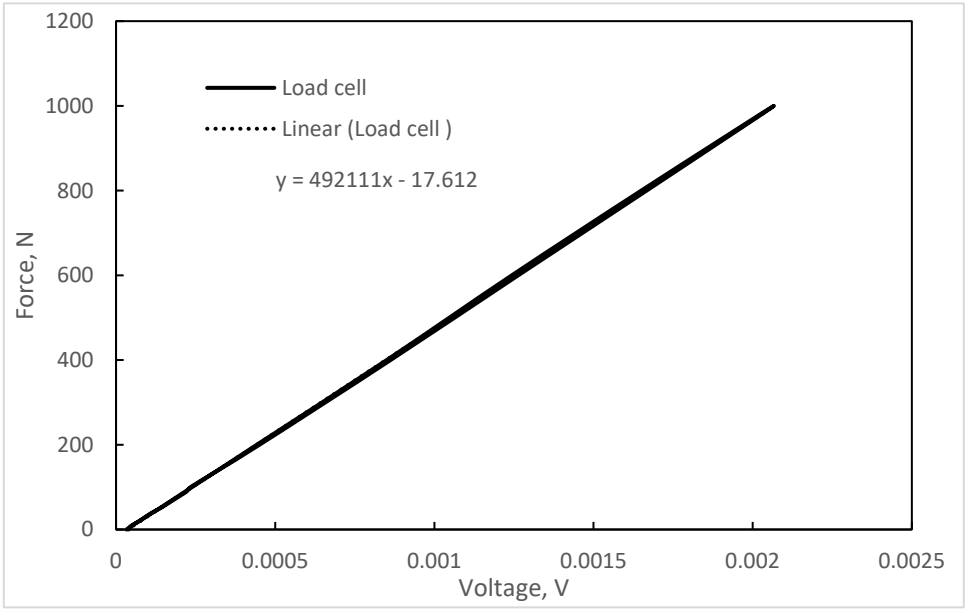

Figure 6-29 Force voltage relationship of load cell

6.8 Summary

Centrifuge models were manufactured following the centrifuge scaling laws stated in table 6-1 to simulate 2 prototype foundation types used for NREL 5MW turbine: namely, a monopile (MP) and a hybrid Foundation (HF). Due to centrifuge schedule, it was anticipated that the consolidation of the clay bed will take around one month and to shorten the experiments time it was decided that inflight consolidation should be used to shorten bed preparation time. Additionally, fitting one tub with more than one test locations enables efficient use of centrifuge setup in timely manner to maximize gain in results without compromising accuracy. Therefore, a scaled down version of the prototype was established. The prototype dimensions necessitated using a virtual model in order to test at a convenient g level. The scaled down version was around one fourth the size of the original wind turbine structure and the centrifuge laws were used to get this dimension preserving important rations such as EI_{tower}/EI_{Plate}, EI_{tower}/EI_{pile}, e/D_t, L_p/W, L/D and W/D_p. Using centrifuge laws alone meant prototype dimensions needed to be scaled at almost 280g in order to produce model that will fit in centrifuge tub without violating boundary conditions of tub. This exercise can be helpful when trying to map model data to prototype dimensions, few lessons were learnt.

1- Soil shear strength cannot be scaled, this leads to change in EI_p/E_s between prototype and models if only N scaling is followed. This is because rigidity of structural elements is scaled by N^4 while shear strength variation cannot be as much. Typical range of gravity used in centrifuge testing ranges between 20-100g meaning difference between structural elements stiffness in prototype and model can be between 160000 and 100000000 while shear strength cannot be scaled more than 500 times given range of shear strength of soil materials is between 2kPa and 1000 kPa typically. This results in different behavior of piles tested laterally. Therefore, caution must be exercised when mapping centrifuge results to

prototype results. This can be achieved by understanding work done in section 5.2.4 where a light is shed on Monopiles and Hybrid foundation ultimate capacity by a normalization procedure

2- Obeying linear and centrifuge laws and meeting the two can be extremely difficult to accomplish, especially with limited materials E values to choose from, this resulted in some differences in L/D ratio for MP and W/D_p for HF. Also, D_t/D_p ratio had to be kept in mind which resulted in difference between MP tower diameter (but not lateral stiffness) and HF tower diameter.

3- One of the aims of HF is to have smaller diameter piles, a HF with 4m pile in prototype scale is chosen to compare against a 6m MP, keeping this ratio between the two was important which resulted in some of the differences mentioned above

4- Scaling centrifuge results to prototype directly can be achieved only if EI_p^*/E_S ratio is similar, if not then change in pile behavior can happen resulting in overestimation/underestimation of results.

6.9 Co-Authorship Statement

Scaling of work was done by the candidate himself under supervision of Prof. Hesham El-Naggar and Prof. Timothy Newson and Dr. Jonathan A. All data calibration was done by candidate with under supervision of Dr. Jonathan Black. Dr. Jonathan carried out much of the rest of work because of Covid-19 impact on labs which meant candidate could not stay in UK to finish rest of the work. Work included writing of data graphic user interface program, preparation of headwork, carrying out element tests and providing final data candidate is thankful for Dr. Jonathan for his help.

6.10 References

Adamidis, O., & Madabhushi, S. P. G. (2014). On preparation of viscous pore fluids for dynamic centrifuge modelling. *International Journal of Physical Modelling in Geotechnics, 15* (3), 141-149. https://doi.org/10.1680/jphmg.14.00022

Alnuaim, A. M. (2014). Performance of micropiled raft in sand and clay-centrifuge and numerical studies.(School of Graduate and Postdoctoral Studies, University of Western Ontario, 2014).

Abdelkader, Ahmed Mohamed Reda, Investigation of Hybrid Foundation System for Offshore Wind Turbine (Scholarship@Western). 2016.

API, 1993. Recommended practice for planning, designing, and Constructing fixed offshore platforms. API, RPT2A-WSD. American Petroleum Institute (API), Washington, D.C.

Association EWE. The European Offshore Wind Industry‐Key Trends and Statistics 2016; January; 2017.

Black, J., Baker, N. & Ainsworth, A. 2014. Establishing a 50 g-ton geotechnical centrifuge at the University of Sheffield. Proceedings of the 8th International Conference on Physical Modelling in Geotechnics. Perth, Aus.,.

Byrne, B.W. and Houlsby, G.T. (2003) “Foundations for Offshore Wind Turbines”, Philosophical Transactions of the Royal Society of London, Series A, Vol. 361, December, pp 2909-2930.

Byrne B. W., McAdam R., Burd H. J., Houlsby G. T., Martin C. M., Zdravković L., Taborda D. M. G., Potts D. M., Jardine R. J., Sideri M., Schroeder F. C., Gavin K., Doherty P., Igoe

D., Muir Wood A., Kellahave D. and Skov Gretlund J. 2015a. New design methods for large diameter piles under lateral loading for offshore wind applications. *Proceedings of Third International Symposium on Frontiers in Offshore Geotechics* 1, 705-710.

Byrne B. W., McAdam R., Burd H. J., Houlsby G. T., Martin C. M., Gavin K., Doherty P., Igoe D., Zdravković L., Taborda D. M. G., Potts D. M., Jardine R. J., Sideri M., Schroeder F. C., Muir Wood A., Kellahave D. and Skov Gretlund J. 2015b. Field testing of large diameter piles under lateral loading for offshore wind applications. *Proceedings of XVI European Conference on Soil Mechanics and Geotechnical Engineering*, Edinburgh, 1255-1260.

Byrne. Foundations for Offshore Wind Turbines (2013). Presentation. University of Oxford.

El-Marassi M., Elnaggar, M.H, Newson, T. and Stone, K. Numerical modelling of the performance of a hybrid monopiled-footing foundation. GeoEdmonton, 2008.

El-Marassi M. Investigation of hybrid monopile-footing foundation systems subjected to combined loading: The University of Western Ontario; 2011.

Jackson, F. A (2016). Assessment of earthquake site amplification and application of passive seismic methods for improved site classification in the greater vancouver region, british columbiaScholarship@Western.

Jonkman, J. M., Musial, W. D., & National Renewable Energy Laboratory (U.S.). (2010). *Offshore code comparison collaboration (OC3) for IEA task 23 offshore wind technology and deployment.* (No. 5000-48191.;5000-48191;). Golden, Colo: National Renewable Energy Laboratory.

Kong, Zhu, J., Long, Y., Zhu, B., Yang, Q., Gao, Y., & Chen, Y. (2021). Centrifuge modelling on monotonic and cyclic lateral behaviour of monopiles in kaolin clay. Géotechnique, 1–14. https://doi.org/10.1680/jgeot.19.P.402

Lai, Y., Wang, L., Hong, Y., & He, B. (2020). Centrifuge modeling of the cyclic lateral behavior of large-diameter monopiles in soft clay: Effects of episodic cycling and reconsolidation. *Ocean Engineering*, *200*, 107048 https://doi.org/10.1016/j.oceaneng.2020.107048

Lau, B. (2015). Cyclic behaviour of monopile foundations for offshore wind turbines in clay. ProQuest Dissertations Publishing.

Madabhushi, G. (2017). *Centrifuge modelling for civil engineers* (First edition.). Boca Raton, FL: CRC Press, an imprint of Taylor and Francis. https://doi.org/10.1201/b17250

Malhotra, S. "Design and Construction of Offshore Wind Turbine Foundations," Wind Turbines, pp. 231-264.

Ng, C. W. W. (2014). The state-of-the-art centrifuge modelling of geotechnical problems at HKUST. *Journal of Zhejiang University. A. Science*, *15*(1), 1–21. https://doi.org/10.1631/jzus.A1300217

Poulos, H. G. (2016). Tall building foundations: Design methods and applications. *Innovative Infrastructure Solutions, 1*(1), 1-51. doi:10.1007/s41062-016-0010-2

Poulos, H. G. and Hull, T. (Role of analytical geomechanics in foundation engineering. Foundation engineering : current principles and practices. pp. 1578-1606 (1989). ILL item# 112694.

TOYOSAWA, Y., ITOH, K., KIKKAWA, N., YANG, J.-J., & LIU, F. (2013). Influence of model footing diameter and embedded depth on particle size effect in centrifugal bearing capacity tests. *Soils and Foundations*, *53*(2), 349–356. https://doi.org/10.1016/j.sandf.2012.11.027

Rahman, M. (1984). Wave diffraction by large offshore structures: An exact second-order theory. *Applied Ocean Research, 6*(2), 90-100. doi:10.1016/0141-1187(84)90046-4.

Wang, X., Zeng, X., Yang, X., & Li, J. (2018). Feasibility study of offshore wind turbines with hybrid monopile foundation based on centrifuge modeling. *Applied Energy, 209*, 127-139. doi:10.1016/j.apenergy.2017.10.107

Wang, Z., Hong, Y., Ng, C. W. W., Wang, L. Z., Mašín, D., & He, B. (2017). Cyclic lateral response and failure mechanisms of semi-rigid pile in soft clay: Centrifuge tests and numerical modelling. *Canadian Geotechnical Journal, 54*(6), 806-824. doi:10.1139/cgj-2016-035

Zhang, White, D., & Randolph, M. (2011). Centrifuge Modeling of the Cyclic Lateral Response of a Rigid Pile in Soft Clay. Journal of Geotechnical and Geoenvironmental Engineering, 137(7), 717–729. https://doi.org/10.1061/(ASCE)GT.1943-5606.0000482

Zhu, B., Zhu, Z., Li, T., Liu, J., & Liu, Y. (2017). Field Tests of Offshore Driven Piles Subjected to Lateral Monotonic and Cyclic Loads in Soft Clay. *Journal of Waterway, Port, Coastal, and Ocean Engineering*, *143*(5), 5017003–. https://doi.org/10.1061/(ASCE)WW.1943-5460.0000399

Westwood, A. Offshore wind statistics. barriers to wind. refocus, 2004, 5, (5), 20. (2005). Fuel and Energy Abstracts, 46(4), 248-248. doi:10.1016/S0140-6701(05)81686-8

Yang, Gao, Y., Kong, D., & Zhu, B. (2019). Centrifuge modelling of lateral loading behaviour of a “semi-rigid” Mono-pile in soft clay. Marine Georesources & Geotechnology, 37(10), 1205–1216. https://doi.org/10.1080/1064119X.2018.1545004

Y. Hong, B. He, L.Z. Wang, Z. Wang, C.W.W. Ng, and D. Mašín. Cyclic lateral response and failure mechanisms of semi-rigid pile in soft clay: centrifuge tests and numerical modelling. Canadian Geotechnical Journal (2017).

Chapter 7: Results of Lateral Monotonic Loading on Monopile (MP) and Hybrid Foundation (HF)

Monopole and Hybrid Foundation systems Comparison Under Monotonic Lateral Loading

Abstract:

Offshore foundation systems are constantly evolving to meet the needs of new developments in energy sector. Moving into ever deeper water for hydrocarbon recovery or creating foundation systems for renewable energy sources, such as offshore wind Turbines (OWT) farms, creates specific challenges. Large fixed vertical turbine tower structures are typically used to support OWT inducing complex loading on foundations as a result of combined wind, wave and self-weight loading effects, all of which must be accommodated within very small rotation envelopes and natural frequency band to allow the turbines to operate effectively. A series of centrifuge tests were conducted to investigate the benefits of adding a circular plate at the mudline to monopiles to form a "hybrid foundation system". This type of foundation system can benefit OWT since the turbine are subjected to high overturning moments. The scaled physical modelling has been used to investigate the lateral capacity and stiffness under monotonic loading. Two models were tested: a monopile (MP) and two hybrid foundations (H.F) with the same plate and monopile diameter, W and D_p, respectively, but with different pile penetration depths (L). Lateral loads were applied at eccentricity, e, for both models to replicate prototype (field) conditions. to increase the shear strength in the zone of influence of the model foundations, models were tested at 70g in over consolidated kaolin clay bed prepared by inflight consolidation and a sand surcharge. S_u and OCR varied from 12-22 to 27-0.3 at the surface to the base of the tub, respectively. Results indicated adding a plate improves the relative lateral ultimate capacity, whilst enabling a reduction of monopile penetration depth and diameter for similar capacities. Specifically, comparable lateral ultimate capacity for monotonic loading was reached for an L/W of 2.

7.1 Introduction

Wind generated electricity production are on the rise, with UK and Germany leading in Europe with output generating more than 20% of their electricity needs. Other countries are resorting to this green energy source including Canada, US, China and few other countries. First onshore wind turbine was constructed in early 90s in Denmark with subsequent increased demand and limited space/aesthetic and public demands leading to first offshore wind turbine being developed. Offshore wind turbines have larger areas and undeterred wind which means higher production (Lombardi et al., 2013). However, this comes with higher grid cost, difficulty in maintenance and, from civil engineering perspective, complicated loading leading to expensive foundation options.

Typically, OWTs support structures are predominately of fixed nature with floating still in research. Majority of fixed structures, about 80%, are monopiles. Other types of fixed supports including gravity base foundations (GBF), jackets steel structure and suction caissons. Cyclic loading imparted on OWT's lead to variety of issues including excessive displacement and rotation, scouring, resonance and fatigue to the supporting foundation. The turbine is typically carried on a tapered tower (superstructure) which is 3-6 m in diameter supported on a transition piece which mounts on the foundation system (substructure).

Besides ultimate limit states, however, two issues become clearly important when designing a substructure for OWT, being:

1- Natural frequency and its variation with repeated loading during the service period (typically 2—30 years)

2- Permissible rotation of foundation, which is typically less than 0.5 degrees

With increased capacity and strict rotation requirements coupled with increased development in deep water to harness more wind power, it is anticipated that the monopile diameter will continue to increase posing problems of drivability and cost for development of new OWT. Hence, a hybrid foundation system is investigated and compared to a monopile system using centrifuge testing to establish the following.

1. Compare MP and HF behavior under lateral loading by using scaled models and testing them using centrifuge considering VHM loading representative of OWT's loading characteristics and geometry (e/D_p, V/V_u, H/H_u, L/D, EI_p/E_{50} and T_v)
2. Compare MP and HF stiffness and ultimate capacity under lateral loading
3. Provide high quality data of the considered systems for the geotechnical community
4. Use results from 1 and 2 to calibrate/validate further FEM models

7.2 Literature Review

Since monopiles are free headed, they may undergo significant tilting and mudline displacement when laterally loaded. Because of strict regulations on tolerable tilting and to preserve the integrity of the offshore wind turbine generator, the maximum allowable rotation is set at 0.5 degrees (Malhotra, 2009). To limit tilting of OWT, either monopile thickness or diameters are increased to increase the foundation overall stiffness. However, increasing monopile diameter can lead to increased wave loading, especially in deep water, because it is proportional to embedded structure diameter. Alternatively, improving the soil or adding a plate can increase the lateral stiffness and reduce the mudline rotation. To reduce the diameter of monopiles, several researchers attempted to use a hybrid foundation system, which comprises a plate fitted with a short monopile in its centerline (Wang et al., 2018; Wang et al., 2017; Abdelkader, 2016; Cherchia,

2014, Lehane et al., 2014; Elmarassi, 2011; Stone et al., 2007). Mechanisms by which improvement to response of monopiles with plate added at mudline can be categorised into 4 causes: it contributes to the restoring moment due to its weight; absorbs shear stresses through contact with soil; increases passive pressure underneath the plate thereby increasing resistance of lateral loads from the pile; and adds restoring moment from soil contact pressure (Lehane, 2014). Several researchers evaluated the contribution of these mechanisms to the HF resistance. For instance, Powrie and Daly (2007) studied embedded retaining wall with stabilising base in kaolin clay utilizing centrifuge modelling. Their results indicated beneficial effects from stabilizing base to the system. Also, Hong et al. (2017) studied the cyclic performance of piles embedded in soft clays in a centrifuge study. They conducted two set of tests, one on soft clay and the other on improved clay and examined the effects of soil improvement on the performance of piles under cyclic loading. Their results indicated that the soil improvement reduced the lateral deflection and enhanced the lateral resistance under low/ medium and high load levels. Wang et al. (2018) conducted a centrifuge study to investigate different OWT foundation systems, including monopile, GBF and gravel and steel wheeled foundations, installed in sand deposit and subjected to lateral monotonic and cyclic loading. Based on the centrifuge test results, they proposed a logarithmic relationship for the accumulation of lateral deformation with the number of load cycles, i.e.

$$\frac{y_N}{y_1} = 1 + b \ln (N) \qquad (7\text{-}1)$$

where y_1 and y_N are deflection at first and N cycles, respectively, and parameter b ranges from 0.36 to1.6 depending on foundation type, load intensity, and soil type (Wang et al., 2018). They concluded that HF system had higher stiffness and that gravel wheel and steel wheel footings

performed better than monopile in resisting the lateral loads Cherchia (2014) suggested that the hybrid foundation could have a considerable cost advantage because the diameter and length of the pile would be reduced and the plate may be cast onshore and moored to the required location, and the material weight could be significantly lower than that of monopile. He conducted centrifuge tests at 50 g on two hybrid foundations, underfins and skirted GBF, installed in medium dense sand and compared their behavior with that of monopiles. The lateral load was applied at e/D of 2 using a hydraulic jack with roller bearing to eliminate eccentricity. The experimental results demonstrated that under serviceability limits (6mm), the response of the hybrid systems was similar to that of monopile. However, the monopile exhibited higher stiffness under monotonic and cyclic loads at ultimate lateral load, and the response of the hybrid foundations was almost twice that of the monopile (almost 50mm). It is well known that pile capacity is affected by the loading eccentricity. For instance, Klinkvort and Hededal (2014) conducted 10 centrifuge tests on rigid monopiles in very dense sand to evaluate the effects of load eccentricity on the pile response. They reported that the load eccentricity affected the pile lateral ultimate load capacity which continued to decrease with increasing the eccentricity, but beyond 15D this change on the lateral ultimate capacity was less pronounced. This is in line with Brom's (1964a and 1964b) method which shows decreasing capacity as eccentricity increases.

7.3 Centrifuge Experimental Programme

Two foundation options installed in cohesive soil are studied and compared in a centrifuge testing program. Namely, a monopile (MP) of L/D ratio of 4.4 and D of 3.3 cm and a hybrid foundation (HF) with plate diameter (W) of 5cm and length of penetration (Lp) of 10cm. The aim from these tests are:

1- Establish MP and H.F lateral ultimate capacity (H_u)

2- Compare behavior of two models at given loads

3- Use results of centrifuge testing to calibrate/verify numerical models for further studies

A 4 cm sand layer was placed at the bottom of the tub and covered with a filter paper. Kaolin clay was mixed with water at 1:1 and poured over the filter paper in the 500 mm diameter tub and left to settle down. Afterwards the tub was loaded to the Centre for Energy and Infrastructure Ground (CEIG) facility 4 m diameter beam centrifuge. Models were tested in two different tubs (tub1 and2) under laterally applied monotonic loading. In both tubs, clay bed was consolidated until 70g with sand surcharge of 72 kPa (at 70g). Consolidation was achieved in stages moving from 10g to 70g over a period of 15 minutes to allow for equalisation of pore pressure. Subsequently, the sand was scrapped off and the models were installed at 1g (wished in place). This practice is reported in other studies (Kong et al., 2021; Hong et al., 2017; Zhang et al., 2011). All instrumentations were calibrated to ensure their accuracy and functionality. Since wind turbines are subjected to vertical-horizontal-moment (VHM) loading, it was necessary to have vertical load applied, hence weights representing 20% of the vertical capacity were mounted on top of these models. Each model was pushed to failure under laterally applied load from a load-controlled actuator. The clay profile was probed for shear strength, OCR and moisture content and unit weight determination.

The pneumatic solenoid valve actuator was capable of providing cyclic and monotonic loading. It has a capacity of 375N generated at 7Bars of input air pressure (Bayton et al., 2018). The eccentricity of loading was 115 mm for both models to produce equivalent eccentricity for both tests. A rigid frame system was fabricated to carry load actuator and laser sensors. Two laser

sensors (Baumer OADM 12) were placed halfway from tub center to record consolidation data while the other two sensors were mounted on the rigid frame system and held opposite to tower face at 100 mm vertical distance to record lateral displacement and rotation. Both test models were instrumented with half bridge strain gauges (at 2cm/1.5cm intervals for MP and HF, respectively) to monitor bending moment evolution with lateral loading while offering compensation for heat generated strains. Special epoxy coating was used to protect strain gauges from water damage. Water table was kept all times at or slightly above clay surface to avoid desiccation. Figure 7-2 shows the tub and headwork while Table 7-1 presents tests information.

Table 7-1 Tests matrix

Test ID	Foundation	Description	e, mm
T4	Monopile	Mono. Lateral load	120
T5	Monopile	Mono. Lateral load	120
T8	Hybrid foundation	Mono. Lateral load	115
T12	Hybrid foundation	Mono. Lateral load	115

Figure 7-1 Tub and headwork before spinning

7.3.1 *Model foundations*

The test models were a monopile of a length (L) of 14.3cm 4 and a diameter (D_p) of 3.3 cm and a hybrid foundation with a plate diameter (W) of 5cm and L_p/W of 2, where L_p is length of pile. The prototype equivalents are a 10 m deep pile with D_p of 2.31m and a 3.5m plate with 7m pile of 1.54m in diameter. The eccentricity of loading above mudline was 8.4 m and 5.88 m in prototype for both models to produce equivalent eccentricity for both tests. The test models were fabricated from acrylic material with E value of 2.9GPa. The lateral load testing was conducted at 70g. Tables 7-2 and 7-3 present model information. Figure 7-3 shows elevation views of the tested models.

Table 7-2 Monopile foundations details

	Properties	Model (N=70g)
Tower	**L,m**	0.1
	D_t, m	0.033
	t_t,m	0.003
	Material	**Acrylic**
	Added weight, grams	**87**
Monopile	**L_p, m**	0.143
	D_p,m	0.033
	EA, kN	2613.8
	Material	**Acrylic**

Table 7-3 Hybrid foundation details

	Properties	Model (N=70g)
Tower	**L,m**	0.1
	D_t, m	0.028
	t_t,m	Solid
	Material	Acrylic
	Added weight, grams	**150**
Monopile	**L_p, m**	0.1
	D_p,m	0.022
	t_p,m	0
	Material	Acrylic
	N	50
	M_t/M_{plate}	1.29693962
Plate	**W, m**	0.05
	t, m	0.0145
	Material	Acrylic

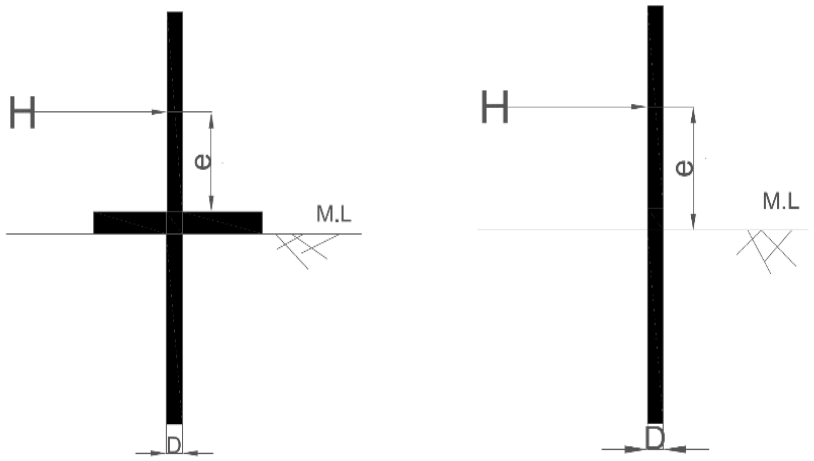

Figure 7-2 cross section of tested models

7.3.2 *Model soil*

Speswhite Kaoline clay by Imery's was used in preparing the test bed. The engineering properties of Speswhite Kaoline are well known in literature and is widely used for centrifuge studies (e.g., Alnuaim,2014; Lau, 2015). Clay was mixed with water at 1 to 2 ratio using a Winkworth mixer to ensure full saturation, homogeneity and ease of placement. A 4 cm sand layer was placed at the bottom of the tub and inundated with 2L of water and covered with a filter paper. Afterward, the Kaolin slurry was carefully scooped inside the tub to avoid air entrapment and placed in the 500 mm diameter tub until height of 44cm from the base, a 3 cm of sand layer weighing 6kg was placed over the clay layer. Afterwards the tub was loaded to the 4 m diameter beam centrifuge. Consolidation was achieved through spinning the centrifuge to 70g over a period of 15 minutes to allow for equalisation of stresses and pore pressure. The depth of the intended clay layer after consolidation is more than 24 cm to avoid boundary effects underneath the monopile.

7.3.3 *Test package arrangement and objectives*

Tests arrangements were carefully planned to maximize benefit of centrifuge setup and allow efficient and quick maneuvers between tests. Two test tubs were prepared, one for each model following the same procedure to produce similar soil profiles. In both tub-1 and tub-2, clay bed was consolidated until 70g with sand surcharge of 73 kPa. The consolidation stage started after installing the headworks constituting of 4 beam channels supporting the actuators and laser sensors, moving in stages from 1g until 70g in 15 minutes interval and left for 72 hours for primary consolidation completion. The centrifuge was stopped afterwards and the sand layer was removed for installation of models at 1g. All instrumentations were calibrated to ensure their accuracy and functionality. Both models were instrumented with half bridge foil strain gauges to obtain bending moment (B.M) data with 2 laser sensors at 100 vertical distance to detect lateral deflection and rotation. Figure 7-4 shows calibration process of strain gauges applied on the tested monopile. Stresses applied were small enough to assume residual strains were zero.

Figure 7-3 MP strain gauge calibration process

The load was applied using a pneumatic actuator which is rigidly attached to the headwork beams to ensure alignment with model foundations and ensure load is fully transferred to the foundations. The rate of lateral loading was estimated based on the following equation to produce undrained response (Hong et al.,2017).

$$V\ (\text{mm/sec}) = \frac{20 * C_h}{B} \tag{7-2}$$

where C_h is the soil lateral coefficient of consolidation, taken as C_v in this study, while B is the width of the foundation. For MP, B was taken as D while for HF B was taken as average diameter between plate width and pile diameter. In order to realistically simulate the vertical load of the prototype OWT foundation, weights representing 20% of the vertical capacity were mounted on top of these models. Figure 7-5 shows a plan view of tub and locations of test models. Models were placed more than 7D from each other to eliminate interaction with another test zone of influence (Zhang et al., 2017; Hong et al., 2017). Figures 7-6 and 7-7 show cross-sections of the

models and their instrumentations. Figures 7-8 and 7-9 show a plan and side views of test package from a mock-up test while Figure 7-10 presents the predicted sample height versus g level based on one dimensional consolidation theory and measured profile height at the end of primary consolidation.

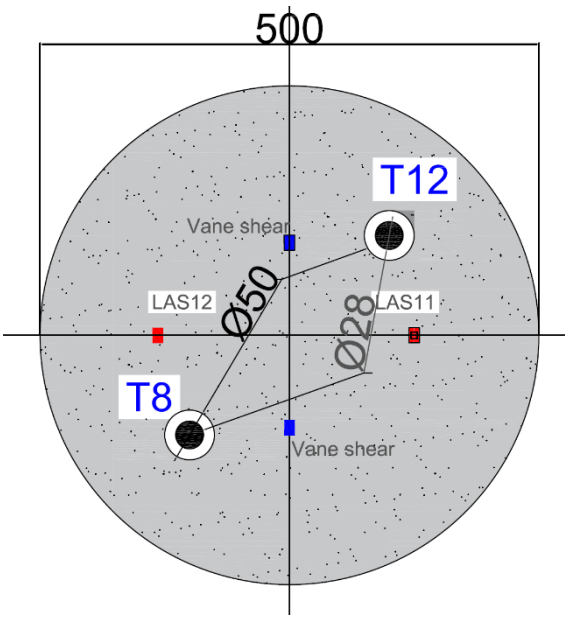

Figure 7-4 Top view and tests locations

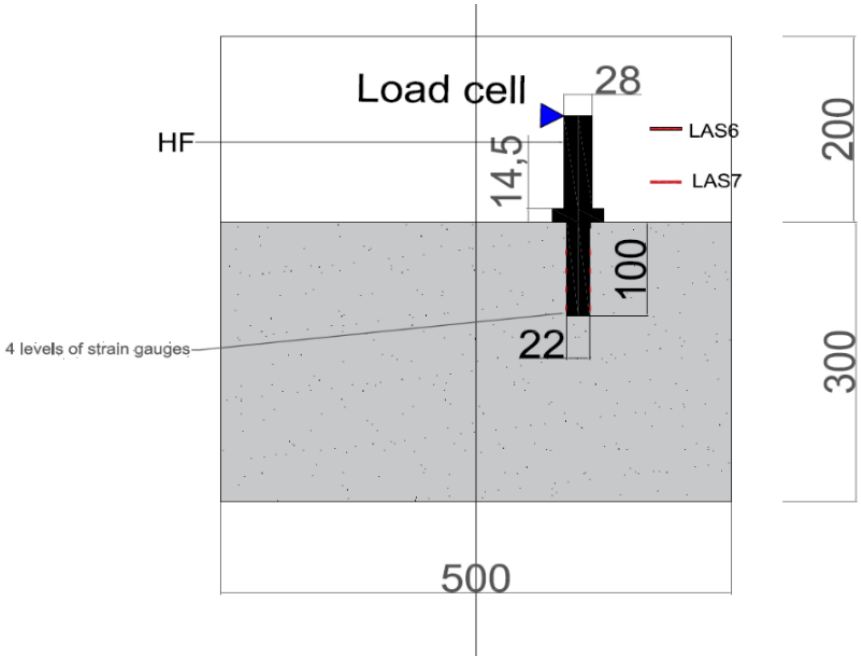

Figure 7-5 Cross section of H.F showing instrumentations

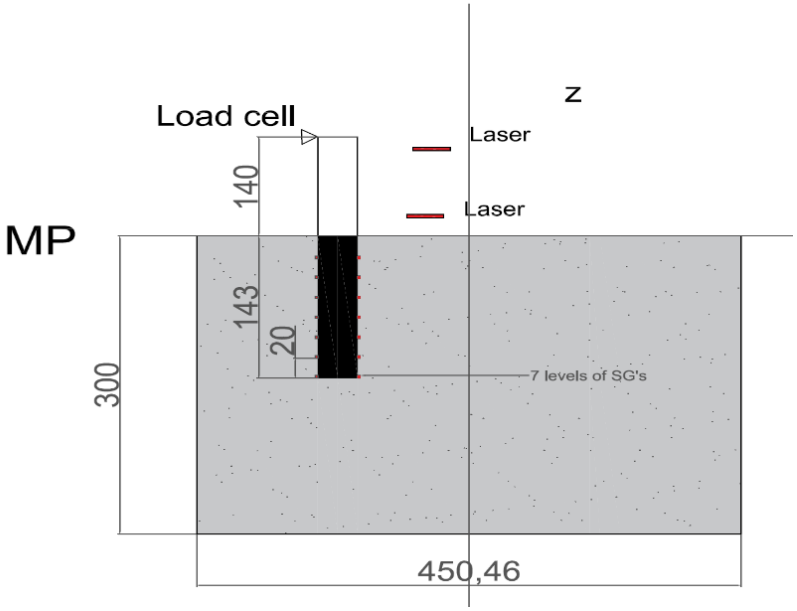

Figure 7-6 Cross section of MP showing instrumentations

Figure 7-7 View of the mockup setup showing SMC pnumatic actuator, settlement target pads and load cell

Figure 7-8 close up image showing pneumatic actuator and hybrid foundation with laser sensors

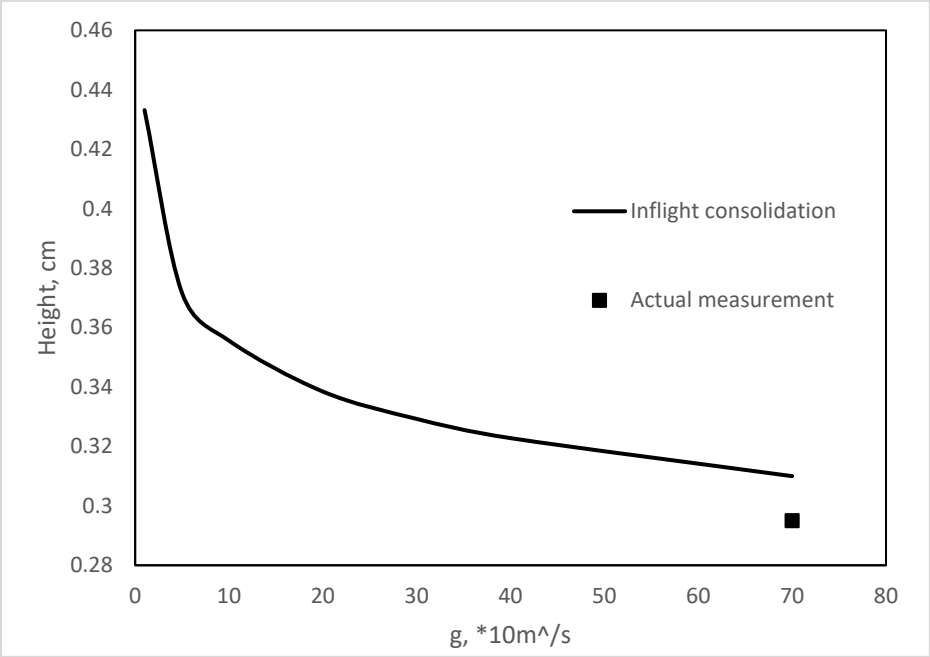

Figure 7-9 Settlement versus g level

7.4 Results

7.4.1 *Consolidation and Shear strength profile*

Inflight consolidation indicated a soft soil with average compression index of 0.49 and rebound index of 0.09. The inflight consolidation data indicated that the coefficient of consolidation, C_v, of the clay layer was 8E-7 m^2/s using Taylor's method. Shear Vane tests conducted at 1g indicated the undrained shear strength, S_u, was between 7 and 20 kPa at the surface and the bottom of the tub, respectively. Difference in measured S_u data are within 15% which is acceptable. The results from 1g were mapped to 50g based on the SHANSEP approach, the S_u and overconsolidation ratio, OCR, at 70g varied from 12-22 to 27-0.4 at the surface to the base of the tub, respectively.

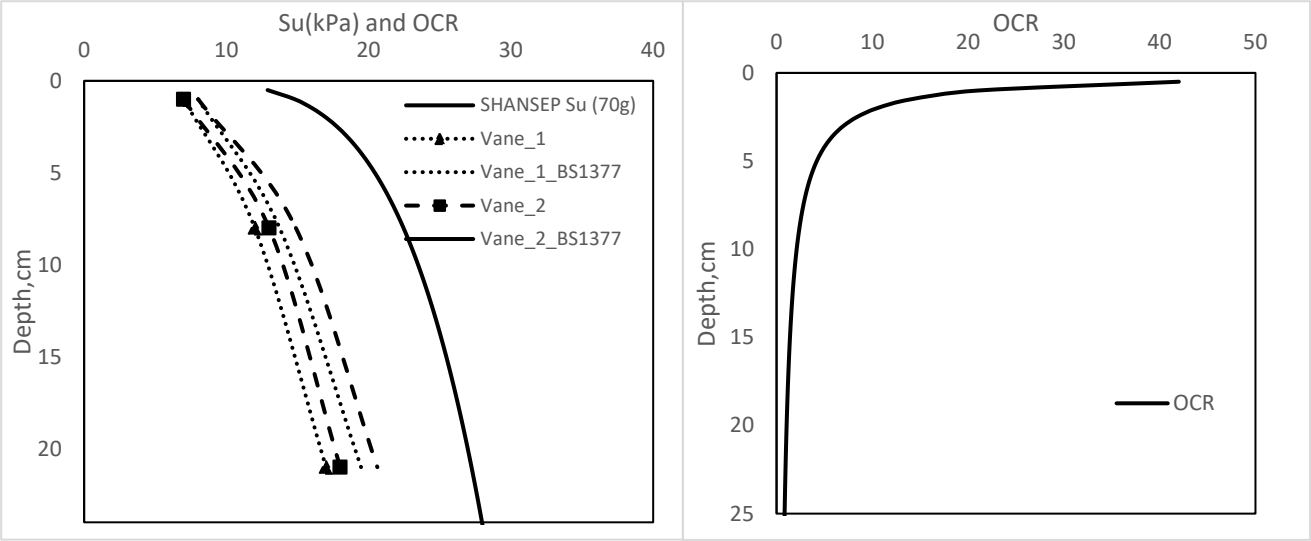

Figure 7-10 Mapped Shear strength and OCR profiles at 70g based on 1g data

The capacity was taken as the highest reached value. In all tests, the load deflection curve showed a hyperbolic shape, i.e., increasing initially linearly at small deflection and showing yielding as displacement increased. This is typical behavior for most foundations and is a result of soil elastoplastic response (Chen and Xu, 2016). The results can be fit to a hyperbolic curve of the form (Kulhawy and Chen, 1995):

$$H = \frac{y_o}{a+by_o} \tag{7-3}$$

Where H is the applied lateral load, yo is the measured deflection, a and b are the reciprocal of the initial stiffness and ultimate capacity

At small displacements, the soil experienced small strains which meant the response was purely in the elastic region. As the load progressed, the strain level increased around the foundations giving rise to plastic deformation and decreased stiffness response which eventually led to plastic flow at ultimate loads. Monopile and Hybrid Foundation lateral ultimate capacity,

H_u, values were between 42 and 57 N for monopile and from 38 to 6 for the hybrid foundation all happening at a deflection of 3.5 mm and 8mm, respectively (Figure 7-12). This variation in capacity is attributed to load rate and consolidation effects. Test T5 was done after conducting T4 which likely resulted in stiffer soil profile due to consolidation and reconsolidation happening between each test. Test 12, however, was conducted after T8 and showed smaller capacity. This can be a result of installation effects and contacts between plate and mudline. The initial stiffness values were 77.6 N/mm and 47 N/mm for MP and HF, respectively. Although the MP showed stiffer response, the HF system, with smaller diameter and lesser embedment, continued to offer resistance at higher mobilized lateral loading. This improvement in lateral response with the hybrid foundation is believed to be from the plate-soil-pile interaction. It is believed that this interaction of the plate with the pile increased both the stiffness and the lateral capacity of the hybrid foundation. It is known that the soil shear strength is stress dependent, with lateral load being applied at eccentricity, part of the plate experience increased stresses leading to increased shear resistance not only at the plate soil level but also at the pile shaft. Stiffness increase, although not high as the H_u, can also be indicative of HF performance at serviceability loads.

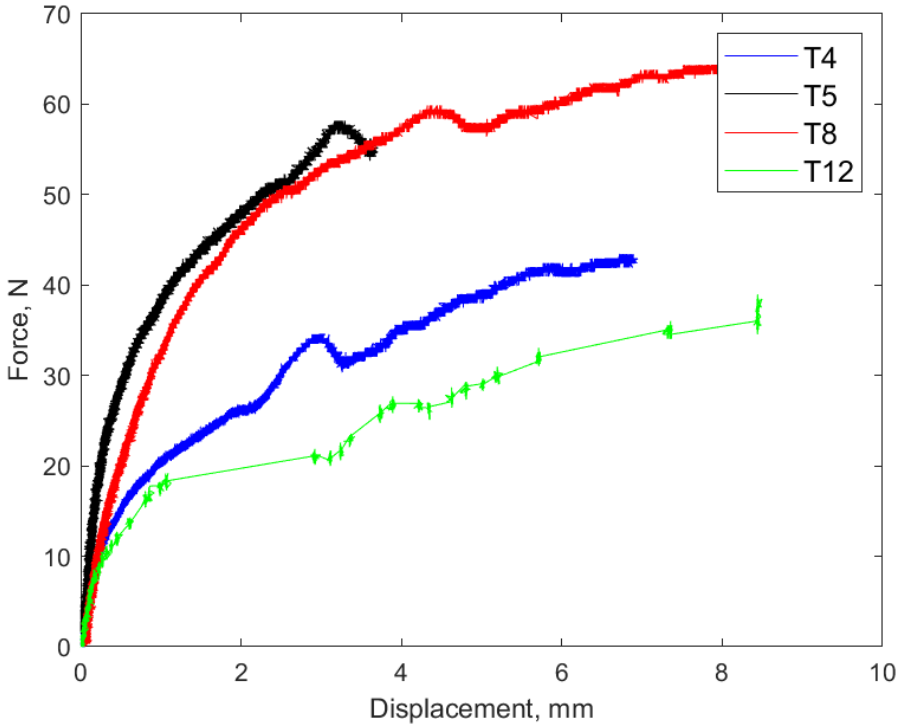

Figure 7-11 Load-displacement curves

7.4.2 *Discussion of results*

The monopile was loaded at 120 mm eccentricity above mudline with the load-controlled Solenoid actuator. The strain rate of loading for MP inferred from load displacement curve and the load time graph indicated the time factor, T_v, value is between 0.03 and 0.05 which falls within range of undrained loading. As the lateral loading proceeds, the pile face moves towards the soil it generates pressure on the soil both from pure shearing at pile edges and a combination of shear and compressive loading. This pressure is transferred to the soil pushing it outwards forming a gap with increased loading behind the pile. Under such high rate of loading pore pressure is generated giving raise to undrained behaviour. This is believed to be a worst-case scenario as offshore wind turbines are typically exposed to low-speed wind loads for most of their lifetime with few major storm loads (Yu et al. 2019). These wave and wind loads can fall between drained and undrained

loading therefore increasing the soil strength and stiffness with time. Having higher rigidity of the MP compared to the soil meant can be classified as either flexible or rigid depending on the pile's relative rigidity compared to the soil. Poulos and Hull (1989) defined upper bound and lower bound values of E_pI_p/E_sL^4 for flexible and rigid pile as being 0.0025 and 0.208, respectively, where E_p ,I_P, Es and L are the Young's modulus and second moment of inertia, soil stiffness and pile's length (Hong et al., 2017). Assuming the E_s value is $400S_u$, the pile has E_pI_p/E_sL^4 value of 0.109 which is within the above limits classifying the used pile as semi-rigid. Figure 7-13 shows the B.M versus depths diagrams under different load levels from Test T4 (blue line in Figure 7-12). It can be observed the pile rotation and tilting is uniform across the height and the bending moment shows no sign of rotation and zero toe bending which is the typical behavior of rigid piles (Zhang et al. (2011), Wang et al. (2015), Byrne et al. (2015), Lau (2015), Lai et al. (2020)).

The hybrid foundation was loaded at 120mm eccentricity above mudline with the load-controlled solenoid actuator. The strain rate of loading for HF inferred from load displacement curve and the load time graph indicated the time factor, T_v, value is between 0.03 and 0.05 which also falls within range of undrained loading. As the lateral loading proceeded, the plate rotated about its axis generating restoring moments from the soil pressure and increasing pressure in front of pile face, all contributing to resisting applied lateral loads. Under such high rate of loading pore pressure is generated giving raise to undrained behaviour. Repeated applied loading may cause differential settlement underneath the plate and scouring. In order to avoid these conditions, it is important to have the plate penetrates through the mudline to prevent separation from taking place, although this is out of the scope of this work.

Figure 7-13 shows the B.M diagram for HF (Test T8, red line in Figure 7-12) under different loads. It can be observed from the bending moment diagram that the pile shows no sign of flexing

and zero toe bending which is the typical behavior of rigid piles (Zhang et al. (2011), Wang et al. (2015), Byrne et al. (2015), Lau (2015), Lai et al. (2020)). Figure 7-13 shows that at higher loading conditions, the HF showed smaller or similar bending moment to MP, which can be viewed as a benefit of the system by cutting the pile size and minimizing steel use, this resulted from positive interaction of the plate absorbing some of the shear transferred loads to hybrid foundation's pile.

A key point for the OWT structures is serviceability and therefore we compare the evolution of rotation with applied loading. Since the capacities of the systems are close to one another, they were normalized from 0-1P where P denote maximum reached load. Figure 7-14 shows that as the load progressed the MP and HF rotations picks up at similar rates. However, at normalized loading of 0.3 the MP and HF seem to behave similarly.

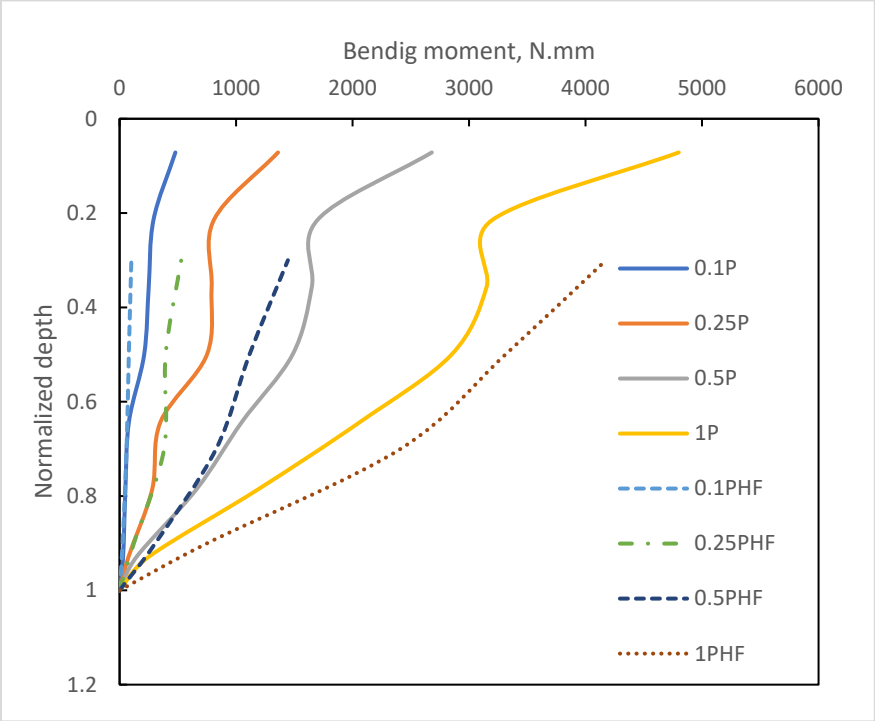

Figure 7-12 Bending moment profiles for HF and MP

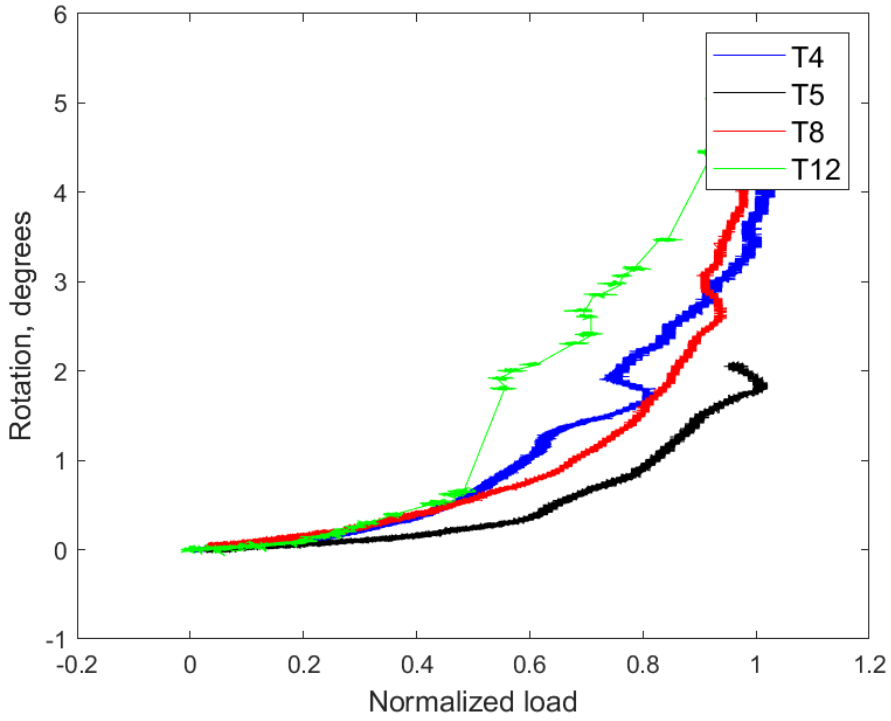

Figure 7-13 rotation evolution with load

7.5 Conclusions

The monotonic lateral behaviour of test models of MP and HF systems has been investigated through a centrifuge study. The two test models were pushed to failure laterally and their lateral ultimate capacity and response under working conditions were examined. The models were tested at 70g in an OC kaolin clay under undrained loading condition, a few conclusions were drawn:

1- H.F of L_p/W of 2 offered similar capacity to MP at reduced L_p and pile diameter

2- Bending moment indicated rigid behavior for all models with no flexing due to high EI_p/E_s values used

3- At higher lateral loads, H.F pile experienced similar BM as MP due to interaction of plate with soil and pile (SSI). This indicates HF can be advantageous in resisting lateral loads with improved distribution of stresses rendering efficient use of structural materials

4- This SSI improved foundation response to lateral loading through distribution of loading into shear loads underneath plate, passive soil pressure in front of pile and through imparted resisting moment from plate

5- At same load, MP offered increase stiffness response and less rotation at M.L compared to HF. This is due to weak soil conditions underneath plate, Stiffer HF response is expected with stiff clay sites. This can be beneficial when pile driving is an issue and smaller piles are more practical.

7.6 Co-Authorship Statement

Scaling of work was done by the candidate himself under supervision of Prof. Hesham El-Naggar and Prof. Timothy Newson. Dr. Jonathan A. All data calibration was done by candidate with under supervision of Dr. Jonathan Black. Dr. Jonathan carried out much of the rest of work because of Covid-19 impact on labs which meant candidate could not stay in UK to finish rest of the work. The candidate is truly thankful for Dr. Jonathan for his help.

7.7 References

Alnuaim, A. M. (2014). Performance of micropiled raft in sand and clay-centrifuge and numerical studies.(School of Graduate and Postdoctoral Studies, University of Western Ontario, 2014).

Abdelkader, Ahmed Mohamed Reda, Investigation of Hybrid Foundation System for Offshore Wind Turbine (Scholarship@Western). 2016.

API, 1993. Recommended practice for planning, designing, and Constructing fixed offshore platforms. API, RPT2A-WSD. American Petroleum Institute (API), Washington, D.C.

Bayton, S. ., Black, J. ., & Klinkvort, R. . (2018). Centrifuge modelling of long term cyclic lateral loading on monopiles. In *Physical Modelling in Geotechnics* (1st ed., pp. 689–694). Routledge. https://doi.org/10.1201/9780429438660-103

Black, J., Baker, N. & Ainsworth, A. 2014. Establishing a 50 g-ton geotechnical centrifuge at the University of Sheffield. Proceedings of the 8th International Conference on Physical Modelling in Geotechnics. Perth, Aus.

Cherchia, M. (2016). Centrifuge modeling of hybrid foundations for offshore wind turbines.

El-Marassi M. Investigation of hybrid monopile-footing foundation systems subjected to combined loading: The University of Western Ontario; 2011.

Kong, Zhu, J., Long, Y., Zhu, B., Yang, Q., Gao, Y., & Chen, Y. (2021). Centrifuge modelling on monotonic and cyclic lateral behaviour of monopiles in kaolin clay. Géotechnique, 1–14. https://doi.org/10.1680/jgeot.19.P.402

Lau, B. (2015). Cyclic behaviour of monopile foundations for offshore wind turbines in clay. ProQuest Dissertations Publishing.

Lai, Y., Wang, L., Hong, Y., & He, B. (2020). Centrifuge modeling of the cyclic lateral behavior of large-diameter monopiles in soft clay: Effects of episodic cycling and reconsolidation. *Ocean Engineering*, *200*, 107048– https://doi.org/10.1016/j.oceaneng.2020.107048

Lombardi, D., Bhattacharya, S., & Muir Wood, D. (2013). Dynamic soil–structure interaction of monopile supported wind turbines in cohesive soil. Soil Dynamics and Earthquake Engineering (1984), 49, 165–180. https://doi.org/10.1016/j.soildyn.2013.01.015

Ng, C. W. W. (2014). The state-of-the-art centrifuge modelling of geotechnical problems at HKUST. *Journal of Zhejiang University. A. Science*, *15*(1), 1–21. https://doi.org/10.1631/jzus.A1300217

Powrie, W., and Daly, M. P. (2007). "Centrifuge modeling of embedded retaining walls with stabilizing bases." Geotechnique, 57(6), 485–497.

Wang, X., Zeng, X., Yang, X., & Li, J. (2018). Feasibility study of offshore wind turbines with hybrid monopile foundation based on centrifuge modeling. *Applied Energy, 209*, 127-139. doi:10.1016/j.apenergy.2017.10.107

Wang, Z., Hong, Y., Ng, C. W. W., Wang, L. Z., Mašín, D., & He, B. (2017). Cyclic lateral response and failure mechanisms of semi-rigid pile in soft clay: Centrifuge tests and numerical modelling. *Canadian Geotechnical Journal, 54*(6), 806-824. doi:10.1139/cgj-2016-035

Zhang, White, D., & Randolph, M. (2011). Centrifuge Modeling of the Cyclic Lateral Response of a Rigid Pile in Soft Clay. Journal of Geotechnical and Geoenvironmental Engineering, 137(7), 717–729. https://doi.org/10.1061/(ASCE)GT.1943-5606.0000482

Y. Hong, B. He, L.Z. Wang, Z. Wang, C.W.W. Ng, and D. Mašín. Cyclic lateral response and failure mechanisms of semi-rigid pile in soft clay: centrifuge tests and numerical modelling. Canadian Geotechnical Journal (2017).

Chapter 8: Conclusions and Future Work Recommendations

8.1 Summary and Recommendations for Future Research

This thesis investigated a novel hybrid foundation option to support offshore wind turbines (OWTs) in clayey beds. The considered system was compared to the typically used monopile (MP) using Finite Element Method and centrifuge testing. For all FEM models, a typical 5MW turbine dimension was chosen as the superstructure and the effects of foundation geometry and soil profile were studied. The lateral ultimate capacity at eccentricity representative of that encountered in medium depth water is established for both systems. Comparison at service loading considered effects of foundation geometry and soil type on the recorded bending moment, shear force, foundation displacement at mudline and tower tip rotations. The stiffness properties were also established using three spring stiffness analogy which were then followed by free vibration testing to establish the dynamic performance of both systems and link the observed behavior with recorded stiffness properties. This was concluded with monotonic lateral loading of models representing the two systems in an OC clay bed in centrifuge environment at 70g.

8.1.1 *Summary of thesis findings*

The following conclusions maybe drawn from the thesis findings:

8.1.1.1 Ultimate capacity and serviceability

- The normalized ultimate capacity versus normalized stiffness of MP showed three distinct slopes, the normalized ultimate capacity was observed to increase significantly for E_p^*/E_{50} values less than 984 for all L/D ratio. At normalized stiffness values of more than 984, the effects of increasing the stiffness for a given L/D ratio was small for L/D ratios less than 6 and was considerable for higher L/D ratio

- The normalized lateral ultimate capacity increase against L/D ratio was dependent on the normalized stiffness (E_p^*/E_{50}) values. At large E_p^*/E_{50} values, the piles behaved as rigid piles and cubic growth of normalized lateral ultimate capacity was observed for L/D ratios considered herein. As normalized stiffness (E_p^*/E_{50}) values decrease below 1200, the effects of L/D ratio on lateral ultimate capacity diminish around L/D values of 5-8.
- The normalized ultimate capacity of hybrid foundation was found to be independent on the pile diameter, hence it was normalized against GBF values for each soil.
- Increase in L_p/W gave substantial increase in lateral capacity of H.F for all soils considered. However, it was noticed that for Clay profiles 3-6 increasing the L_p/W from 1 to 2 did not results in improvement on the lateral capacity because the structural capacity of the pile was reached.
- Decreasing/increasing pile length compare to MP30 resulted in small decrease/increase of maximum bending moment of around 3%. However, the hybrid systems saw substantial reduction in maximum bending moments of around 35-40% compared to MP30. This added contribution of plate can therefore reduce steel used for foundation which is beneficial.
- Maximum shear force was related to pile's length and varied from 20-30% when pile length was increased against MP30. Adding a plate and using smaller pile resulted in increase of maximum shear force. This is believed to be attributed to restoring forces acting below the plate adding additional pressures against the pile.
- Increasing pile length in profile 1(rigid behavior) resulted in pronounced decrease in tower tip displacement for all depths considered. The amount of reduction of tower tip

displacement was around 20% compared to MP30. For all other profiles, the increase in shear strength resulted in the critical depth of pile being reduced and therefore increase in stiffness beyond 40 m penetration was minimal. For Clay profiles 2,3,4,5 and 6 the decrease of tower tip displacement was 12.2, 3.16, 1.2, 0.9, and 0.29% when increasing pile length from 40 to 80.

8.1.1.2 Stiffness properties

- The normalized stiffness parameters versus normalized foundation stiffness showed almost linear increase in normalized stiffness values for all L/D ratio, unlike the normalized lateral ultimate capacities which showed a plateau for normalized stiffness values less than 2000. This is because the difference in applied lateral loads which, in the case of lateral ultimate capacity, caused structural failure in piles thereby reducing normalized capacity
- For the normalized horizontal stiffness for MP, η_L, the normalized stiffness values ceased to increase after L/D ratio of 11.67
- For the normalized coupling stiffness for MP, $\eta_{LR/RL}$, the normalized stiffness value ceased to increase after L/D ratio of 10
- For normalized coupling stiffness for MP, η_R, the normalized stiffness values ceased to increase after L/D ratio of 8
- The normalized lateral stiffness properties of hybrid foundations increase against Lp/W ratios and the increase rate was dependent on the clay shear strength. At small shear strength values, considerable increase in relative stiffness was obtained because of the addition of hybrid foundation pile. This is in line with normalized lateral ultimate capacity

findings which showed the capacity, and hence the stiffness of this foundation option is dependent on the foundation plate diameter and is insensitive to the pile' length

- The normalized horizontal stiffness for HF, η_L, the normalized stiffness values increased with increasing L_p/W ratio, however, at different rates. They showed highest increase for clay 1 and least increase for clay6. For clays from 2 to 6, the increase in the normalized stiffness between Lp/W 1 and 2 was smaller than the increase in clay 1. These findings are in line with lateral ultimate capacity findings where the normalized lateral ultimate capacity of this system showed little to no improvement when increasing the Lp/W ratio mainly because the structural capacity of the hybrid foundation pile hindered any further gain in lateral load resistance.
- The normalized coupling stiffness for HF, $\eta_{LR/RL}$, showed similar trends as in η_L
- For normalized coupling stiffness for HF, η_R, the normalized stiffness values increased for all Lp/W; however, the increase was observed to be at a decaying rate as the soil shear strength increased. Similar findings of increase in stiffness, although small, beyond Lp/W of 1 were observed, unlike normalized lateral ultimate capacity which is attributed to range of applied forces being within structural capacity of hybrid system pile and therefore no plateau was reached.

8.1.1.3 Dynamic performance

- The dynamic response of OWTs is dependent on the foundation's flexibility. For soft soils, the foundation geometry showed significant effects while for stiff soils the response was dependent on the soil properties.

- The natural frequency was impacted by L/D ratio for clays 1-4. For clays 5 and 6 no observed effects were noticed when changing the MP penetration
- The 1st natural frequency can be less than half of that obtained assuming rigid foundation. The maximum difference was obtained for the case of L/D of 3.33 in clay 1 were the 1st natural frequency was only 48% of the $F_{F.B}$.
- For clay 2, 3 and 4, a plateau was reached where the first natural frequency did not change beyond. This L/D ratio was found to be between 5-6.67
- The effect of foundation compliance on the 1st natural frequency was of lesser extent for the cases of HF.
- The maximum reduction of 1st natural frequency compared to fixed base for HF/GBF happened for GBF and HF with Lp/W of 1 in clay 1 and 2. In those cases there was a 40% reduction from foundation flexibility
- The change of Lp/W resulted in increase in fn1 for the cases of clay 1 and 2 only, for other soil profiles the effect of Lp/W on the 1st natural frequency is negligible
- The change in clay type resulted in increase of the ratio of $f_{n1}/f_{F.B}$, the lowest ratio was 0.6 for clay 1 and 2. For clay 3 and 4, this ratio was 0.8. For clay 5 and 6, the soil compliance has no effects on the fixed base 1st natural frequency and the foundation can be represented as a rigid foundation.

8.2 Recommendations for Future Work

This section provides a series of recommendations for future studies on the hybrid foundation option for OWT. The recommendations are divided into two parts: (i) Finite Element Modelling and (ii) Model testing.

8.2.1 *Finite element modelling*

This research evaluated the response of the hybrid foundation system in different clayey bed using normalization where applicable. It is recommended to carry out similar work on clayey soil and sandy soil to address the following:

- Employ different eccentricities to establish the effects of load eccentricity on the considered system lateral ultimate capacity in clayey beds and best fit the results to form a complete set of graphs that can be readily used for preliminary analyses
- Employ different eccentricities to establish the effects of load eccentricity on the considered system lateral ultimate capacity in sandy soils and best fit the results to form a complete set of graphs that can be readily used for preliminary analyses
- Establish the three spring stiffness properties of the considered systems and their effects on the 1st natural frequency in sand
- Establish a degradation model that can capture the long-term performance of both models in clay and sand

8.2.2 *Model testing*

This research evaluated the response of the hybrid foundation system in an OC clayey bed using centrifuge tests. It is recommended to carry out similar work on clayey soil to address the following:

- Evaluate the effects of different Lp/W ratios on the lateral ultimate capacity and stiffness properties

- Evaluate the long-term performance applying 100k and more cyclic lateral loading to evaluate degradation of stiffness properties
- Conduct snap tests in between cyclic loadings episodes to evaluate 1st natural frequency change and provide best fit equations
- Employ different W/D ratio to observe the effects of plate diameter and pile diameter on the lateral ultimate capacity

8.3 References

Abdelkader, Ahmed Mohamed Reda, Investigation of Hybrid Foundation System for Offshore Wind Turbine (Scholarship@Western). 2016.

API, 1993. Recommended practice for planning, designing, and Constructing fixed offshore platforms. API, RPT2A-WSD. American Petroleum Institute (API), Washington, D.C.

Association EWE. The European Offshore Wind Industry‑Key Trends and Statistics 2016; January; 2017.

Bentley, K.J. and El Naggar, M.H., 2000. Numerical analysis of kinematic response of piles. Canadian Geotechnical Journal, Vol. 37, No. 6, pp. 1368-1382

Black, J., Baker, N. & Ainsworth, A. 2014. Establishing a 50 g-ton geotechnical centrifuge at the University of Sheffield. Proceedings of the 8th International Conference on Physical Modelling in Geotechnics. Perth, Aus.,

Bowles, J. E. (1996). *Foundation analysis and design*. New York: McGraw-Hill.

Broms, B. B. (1964b). Lateral Resistance of Piles in Cohesive Soils. Journal of the Soil Mechanics and Foundations, **90**(2): 27-64.

Byrne, B.W. and Houlsby, G.T. (2003) “Foundations for Offshore Wind Turbines”, Philosophical Transactions of the Royal Society of London, Series A, Vol. 361, December, pp 2909-2930.

Byrne B. W., McAdam R., Burd H. J., Houlsby G. T., Martin C. M., Zdravković L., Taborda D. M. G., Potts D. M., Jardine R. J., Sideri M., Schroeder F. C., Gavin K., Doherty P., Igoe

D., Muir Wood A., Kellahave D. and Skov Gretlund J. 2015a. New design methods for large diameter piles under lateral loading for offshore wind applications. *Proceedings of Third International Symposium on Frontiers in Offshore Geotechics* 1, 705-710.

Byrne B. W., McAdam R., Burd H. J., Houlsby G. T., Martin C. M., Gavin K., Doherty P., Igoe D., Zdravković L., Taborda D. M. G., Potts D. M., Jardine R. J., Sideri M., Schroeder F. C., Muir Wood A., Kellahave D. and Skov Gretlund J. 2015b. Field testing of large diameter piles under lateral loading for offshore wind applications. *Proceedings of XVI European Conference on Soil Mechanics and Geotechnical Engineering*, Edinburgh, 1255-1260.

Byrne. Foundations for Offshore Wind Turbines (2013). Presentation. University of Oxford.

El-Marassi M., Elnaggar, M.H, Newson, T. and Stone, K. Numerical modelling of the performance of a hybrid monopiled-footing foundation. GeoEdmonton, 2008.

El-Marassi M. Investigation of hybrid monopile-footing foundation systems subjected to combined loading: The University of Western Ontario; 2011.

Jackson, F. A (2016). Assessment of earthquake site amplification and application of passive seismic methods for improved site classification in the greater vancouver region, british columbiaScholarship@Western.

Jonkman, J. M., Musial, W. D., & National Renewable Energy Laboratory (U.S.). (2010). *Offshore code comparison collaboration (OC3) for IEA task 23 offshore wind technology and deployment.* (No. 5000-48191.;5000-48191;). Golden, Colo: National Renewable Energy Laboratory.

Kramer, S. L. (1996). *Geotechnical earthquake engineering*. Upper Saddle River, N.J: Prentice Hall.

Malhotra, S. "Design and Construction of Offshore Wind Turbine Foundations," Wind Turbines, pp. 231-264.

Ng, C. W. W. (2014). The state-of-the-art centrifuge modelling of geotechnical problems at HKUST. *Journal of Zhejiang University. A. Science*, *15*(1), 1–21. https://doi.org/10.1631/jzus.A1300217

Poulos, H. G. (2016). Tall building foundations: Design methods and applications. *Innovative Infrastructure Solutions, 1*(1), 1-51. doi:10.1007/s41062-016-0010-2

Poulos, H. G. and Hull, T. (Role of analytical geomechanics in foundation engineering. Foundation engineering : current principles and practices. pp. 1578-1606 (1989). ILL item# 112694.

TOYOSAWA, Y., ITOH, K., KIKKAWA, N., YANG, J.-J., & LIU, F. (2013). Influence of model footing diameter and embedded depth on particle size effect in centrifugal bearing capacity tests. *Soils and Foundations*, *53*(2), 349–356. https://doi.org/10.1016/j.sandf.2012.11.027

Rahman, M. (1984). Wave diffraction by large offshore structures: An exact second-order theory. *Applied Ocean Research, 6*(2), 90-100. doi:10.1016/0141-1187(84)90046-4.

Wang, X., Zeng, X., Yang, X., & Li, J. (2018). Feasibility study of offshore wind turbines with hybrid monopile foundation based on centrifuge modeling. *Applied Energy, 209*, 127-139. doi:10.1016/j.apenergy.2017.10.107

Wang, Z., Hong, Y., Ng, C. W. W., Wang, L. Z., Mašín, D., & He, B. (2017). Cyclic lateral response and failure mechanisms of semi-rigid pile in soft clay: Centrifuge tests and numerical modelling. *Canadian Geotechnical Journal, 54*(6), 806-824. doi:10.1139/cgj-2016-035

Zhu, B., Zhu, Z., Li, T., Liu, J., & Liu, Y. (2017). Field Tests of Offshore Driven Piles Subjected to Lateral Monotonic and Cyclic Loads in Soft Clay. *Journal of Waterway, Port, Coastal, and Ocean Engineering*, *143*(5), 5017003–. https://doi.org/10.1061/(ASCE)WW.1943-5460.0000399

Westwood, A. Offshore wind statistics. barriers to wind. refocus, 2004, 5, (5), 20. (2005). Fuel and Energy Abstracts, 46(4), 248-248. doi:10.1016/S0140-6701(05)81686-8

Y. Hong, B. He, L.Z. Wang, Z. Wang, C.W.W. Ng, and D. Mašín. Cyclic lateral response and failure mechanisms of semi-rigid pile in soft clay: centrifuge tests and numerical modelling. Canadian Geotechnical Journal (2017).